Université de Montpellier
École doctorale GAIA

Mémoire d'Habilitation à Diriger des Recherches

Contrôle génétique de traits bénéfiques pour l'amélioration de la tolérance au stress hydrique

Présenté par Alexandre GRONDIN

UMR DIADE (232), Diversité Adaptation et Développement des plantes
Institut de Recherche pour le Développement, Université de Montpellier

Je déclare avoir respecté, dans la conception et la rédaction de ce mémoire d'HDR, les valeurs et principes d'intégrité scientifique destinés à garantir le caractère honnête et scientifiquement rigoureux de tout travail de recherche, visés à l'article L.211-2 du Code de la recherche énoncés par la Charte nationale de déontologie des métiers de la recherche et la Charte d'intégrité scientifique de l'Université de Montpellier. Je m'engage à les promouvoir dans le cadre de mes activités futures d'encadrement de recherche.

Remerciements

Une des joies du métier de chercheur est la richesse des rencontres que l'on peut faire sur son chemin. J'ai eu le privilège de rencontrer des personnes de nombreux horizons. Je suis aujourd'hui riche de nos discussions scientifiques et amicales. Nombreux sont ceux qui m'ont apporté leur conseils, leur soutien et une camaraderie franche parfois dès la première poignée de main. Alors bien sûr les chemins divergent, mais les souvenirs et la gratitude restent. Je ne pourrais, sans en oublier, nommer toutes ces personnes qui ont rendu cette vie de voyages loin de chez moi et de mes proches plus joyeuse et agréable. Alors à toutes et tous avec qui j'ai pu partager un bout de chemin lors de mes séjours à Montpellier, aux Philippines, en Inde, aux États-Unis, au Sénégal et ailleurs, je vous remercie du fond du cœur. J'espère que, sans lire votre nom, vous saurez vous reconnaitre. J'espère aussi que vous pourrez trouver dans ces mots, qui n'expriment malheureusement que très partiellement ma pensée, toute ma gratitude et mon amitié.

Quelques personnes à nommer néanmoins qui ont eu un rôle majeur dans mon parcours et ma construction scientifique. D'abord, Christophe Maurel et Lionel Verdoucq qui m'ont accordé leur confiance dès le Master, préparé pour le concours de l'école doctorale, soutenu pendant ma thèse et mis en contact avec Amelia Henry à l'IRRI. *Christophe et Lionel, vous avez façonné le chercheur que je suis aujourd'hui, merci pour cet apprentissage.* Merci à Amelia Henry et Inez Slamet-Loedin qui m'ont offert mon premier contrat de post-doc. *Merci Amelia pour ta confiance toujours, ton enthousiasme et ton amitié*. Travailler à l'IRRI a été une expérience extraordinaire qui m'a ouvert les yeux sur le monde et permis de prendre conscience de certains des grands enjeux actuels pour l'agriculture. Merci à Harkamal Walia qui m'a offert mon deuxième contrat de post-doc. J'ai surement été au-dessous des espérances mais j'ai aussi beaucoup appris de ces moments plus délicats. Merci à Doan Luu, Mikael Lucas, Soazig Guyomarc'h, Antony Champion et Pascal Gantet qui m'ont apporté un soutien essentiel lors de la préparation du concours IRD. Merci à Vincent Vadez dont le travail et la vision scientifique est pour moi une source d'inspiration perpétuelle. Enfin, un merci tout particulier à Laurent Laplaze qui depuis ma candidature et mon intégration à l'IRD m'apporte tant d'un point de vue scientifique et humain. *Laurent, quel plaisir d'interagir avec toi au quotidien au labo et en dehors, merci pour tout !*

Merci à encore à Laurent Laplaze, Antony Champion et Vincent Vadez d'avoir accepté de relire ce manuscrit. Merci aux membres du jury qui ont accepté de l'évaluer.

Enfin merci à mes parents, à toute ma famille, et à Ronald et Ruurd pour tous les bons moments de détente.

Table des matières

1. Curriculum vitae

Alexandre Grondin

Né le 29 mars 1983 à Saint-Denis de la Réunion (974)

Chargé de Recherche Classe Normale à l'Institut de Recherche pour le Développement (IRD)

Membre de l'équipe *Cereal Root Systems* (*CERES*) co-dirigée par Laurent Laplaze (DR1 IRD) et Pascal Gantet (PR UM)
UMR Diversité Adaptation et Développement des Plantes
911 Avenue Agropolis, 34394 Montpellier Cedex 5, France

- **Diplômes et formation**

2011 Doctorat, Biologie Intégrative des Plantes, Montpellier SupAgro, France
2007 Master, Biologie Fonctionnelle des Plantes, Université de Montpellier, France
2005 Licence, Physiologie Végétale, Université de Montpellier, France

- **Parcours professionnel**

Septembre 2018 – Septembre 2022
Expatriation au Centre d'Étude Régional pour l'Amélioration de l'Adaptation à la Sécheresse (CERAAS), Thiès, Sénégal
Contrôle génétique de traits racinaires contribuant à la tolérance au stress hydrique chez le mil

Depuis mai 2017
Chargé de Recherche Classe Normale, IRD Montpellier, France
Contrôle génétique de traits racinaires bénéfiques pour la nutrition hydro-minérale chez les céréales, équipe Cereal Root Systems

Mai 2015 – Avril 2017
Post-doctorant, Université de Nebraska-Lincoln, Etats-Unis
Identification de gènes impliqués dans la tolérance au stress hydrique chez le riz, Department of Agronomy and Horticulture

Aout 2012 – Avril 2015
Post-doctorant, Institut de Recherche International sur le Riz (IRRI), Philippines
Identification de gènes impliqués dans la tolérance au stress hydrique chez le riz, Crop and Environmental Science Division

Novembre 2011 – Juillet 2012
Professeur contractuel de l'Education Nationale, Rectorat de La Réunion, France
Introduction aux Sciences de la Vie et de la Terre, Collège de Trois-Bassins

Octobre 2007 – Mai 2011
Étudiant en thèse, Montpellier SupAgro, France
Fonction des aquaporines dans les mouvements stomatiques chez *Arabidopsis thaliana*, Laboratoire de Biochimie et Physiologie Moléculaire des Plantes, équipe Aquaporines

Mars 2006 – Juillet 2006, puis Janvier 2007 – Juillet 2007
Master Biologie Fonctionnelle des Plantes, Université de Montpellier, France
Étude structure-fonction de l'aquaporine PIP2;1 chez *Arabidopsis thaliana*, Laboratoire de Biochimie et Physiologie Moléculaire des Plantes, équipe Aquaporines

- **Encadrements d'étudiants en Master et Thèse**

J'ai eu l'occasion de participer à l'encadrement direct d'une dizaine d'étudiants en Master 1 et Master 2 de l'Université de Montpellier et de l'Université Cheikh Anta Diop de Dakar, et en parcours à l'IUT Montpellier-Sète. Parmi les étudiants de Master 2, Pablo AFFORTIT et Gagnon PENASSOU ont postulé au concours de l'école doctorale GAIA et obtenu une bourse pour continuer en thèse. Je présente ci-dessous uniquement les thèses auxquelles j'ai directement contribué à l'encadrement à des degrés divers.

-Gagnon PENASSOU (en cours – début 2023)
50% encadrement avec Laurent LAPLAZE et Antony CHAMPION (Directeur de thèse)
Contrôle génétique de la vigueur précoce et de l'efficience de la transpiration chez le riz
École doctorale GAIA avec financement IRD (obtenu au concours ED GAIA)

Gagnon est togolais et a obtenu un Master 2 Biotechnologies et Amélioration des Plantes Tropicales (BAPT) à l'UM. Son projet de thèse consiste à valider au champ un locus à caractère quantitatif (QTL) identifié comme contrôlant la vigueur précoce et l'efficience de la transpiration chez le riz à travers l'utilisation de populations biparentales. Il tentera également de caractériser au laboratoire par une approche de génétique fonctionnelle un gène candidat sous-jacent à ce QTL, qui a pu être ciblé grâce à son travail de Master 2.

-Hien Linh TRAN (2022-2025)
33% encadrement avec Hoang Thi GIANG et Pascal GANTET
Étude de la contribution de traits racinaires anatomiques au contenu en ion dans les grains chez le riz par une approche de génétique d'association
École doctorale GAIA avec co-financement Ambassade de France au Vietnam et l'*Agricultural Genetics Institute* (*AGI*) de Hanoï au Vietnam

Linh est de nationalité vietnamienne et a effectué son Master au Japon à l'Université de Nagaoka (parcours *Bioengineering*). Linh a réalisé en début de thèse un gros travail de phénotypage de l'anatomie racinaire chez un panel de diversité de riz vietnamien. Elle a également étudié la diversité du contenu en 17 ions dans le grain chez ce même panel. Elle étudie le déterminisme génétique des traits anatomiques racinaires et du contenu en ion dans le grain dans ce panel et les liens potentiels entre les caractéristiques racinaires et la qualité

du grain. Linh est basée pour une moitié du temps à l'*AGI* et l'autre moitié à l'IRD de Montpellier et devrait soutenir sa thèse au premier trimestre 2025.

-Princia Aurore Biawallys NAKOMBO-GBASSAULT (en cours – début 2021)
25% encadrement avec Ephrem KOSH-KOMBA, Laurent LAPLAZE (co-directeur) et Yves VIGOUROUX
Identification des déterminants génétiques contrôlant la nutrition minérale chez le mil et contribution de traits racinaires dans ces processus
École doctorale GAIA avec co-financement Ambassade de France en Centrafrique et IRD (ARTS)

Princia est une étudiante centrafricaine et a effectué son stage de Master 2 Amélioration des Plantes et Ingénierie végétale MÉditerranéennes et Tropicales (APIMET) dans l'équipe *CERES* sous la direction de Laurent LAPLAZE et Yves VIGOUROUX. Son travail de Master qui s'est poursuivi en thèse a consisté à valider un QTL et le rôle d'un gène candidat sous-jacent dans le contrôle de la croissance racinaire chez le mil à travers, respectivement, la caractérisation de population recombinante et une approche de génétique fonctionnelle. Des incohérences dans l'identité génétique de la population recombinante et les difficultés rencontrées pour la mise en œuvre de la transgénèse chez le mil nous ont poussé à réorienter le sujet vers l'identification des déterminants génétiques contrôlant la nutrition minérale chez le mil et la contribution de traits racinaires dans ces processus. Sa thèse est réalisée entre l'IRD (75% de son temps) et l'Université de Bangui. Elle a effectué un séjour de trois mois au Sénégal en 2022. Elle devrait soutenir sa thèse au deuxième trimestre 2025.

-Pablo AFFORTIT (en cours – début 2021)
50% encadrement avec Laurent LAPLAZE
Contrôle de l'anatomie racinaire chez le mil et étude de son implication dans la tolérance au stress hydrique
École doctorale GAIA avec financement MESR (obtenu au concours ED GAIA)

Pablo a réalisé son stage de Master 1 sous ma supervision au Laboratoire Commun de Microbiologie à Dakar où il a travaillé sur le rôle des aquaporines dans le contrôle de l'efficience de la transpiration chez le mil. Il a ensuite réalisé son stage de Master 2 BAPT dans l'équipe DYNADIV de l'UMR DIADE sur le développement d'approches de génétique d'association pour l'identification de déterminants génétiques contrôlant l'efficience de la transpiration chez le riz. Son travail de thèse consiste à identifier des traits racinaires bénéfiques pour la tolérance au stress hydrique chez le mil, d'identifier le déterminisme génétique de ces traits et de mieux comprendre leur signification physiologique, en particulier pour le contrôle de l'hydraulique de la plante. Il devrait soutenir sa thèse au deuxième semestre 2024.

Articles publiés :
En lien direct avec les activités de sa thèse :
Affortit P., Ahmed M.A., **Grondin A.**, Delzon S., Carminati A. & Laplaze L. (2023) Keep in touch : the soil – root hydraulic continuum and its role in drought resistance in crops. *Journal of Experimental Botany* erad312.

En lien avec son stage de Master 2 :
Affortit P.*, Effa-Effa B.*, Ndoye M.S., Moukouanga D., Luchaire N., Cabrera-Bosquet L., … **Grondin A.*** (2022) Physiological and genetic control of transpiration efficiency in African rice, Oryza glaberrima Steud. *Journal of Experimental Botany* 73, 5279–5293.
*co-premier Auteurs, *Auteur pour correspondance

En lien avec son stage de Master 1 :
Grondin A.*, **Affortit P.**, Tranchant-Dubreuil C., de la Fuente-Cantó C., Mariac C., Gantet P., … Laplaze L. (2020) Aquaporins are main contributors to root hydraulic conductivity in pearl millet [Pennisetum glaucum (L) R. Br.]. *Plos One* 15, e0233481.
*Auteur pour correspondance

-Joseph OVWEMUVWOSE (2021 – arrêt de la thèse le 12 juin 2022)
25% encadrement avec Eric NATIVEL, Vincent VADEZ (Co-directeur) et Christophe GOZE-BAC (Co-directeur)
Utilisation de la résonance magnétique nucléaire pour la mesure de la transpiration et le flux de carbone vers les racines chez le mil
École doctorale GAIA avec financement IRD (ARTS) et LabEx NUMEV (UM)

Joseph est de nationalité Nigériane et a obtenu un Master à l'Université de Nottingham (GB). Son travail de thèse s'est inscrit dans la continuité de projets réalisés en collaboration avec le laboratoire Charles Coulomb de l'UM et le CIRAD pour le développement d'un appareil de résonance magnétique nucléaire portable mesurant les flux d'eau de manière non destructive dans la base de la tige de mil et sorgho *in naturae*. Joseph a décidé d'arrêter ce projet pour se réorienter vers une nouvelle thèse à l'*Impérial College* de Londres.

-Mame Sokathil NDOYE (en cours – début 2021)
25 % encadrement avec Mikael LUCAS, Laurent LAPLAZE (Co-directeur) et Abdala Gamby DIEDHIOU (Co-directeur)
Identification de traits racinaires améliorant la tolérance du mil à la sécheresse à l'aide du modèle Open SimRoot
École doctorale Biotechnologie Végétale et Microbienne de l'Université Cheikh Anta Diop de Dakar (UCAD) avec financement USAID-Sorghum and Millet Innovation Lab dans le cadre du projet GenMil hébergé au Centre d'Etude Régional pour l'Amélioration de l'Adaptation à la Sécheresse (CERAAS)

Sokhatil est de nationalité sénégalaise et a obtenu un Master en Biomathématiques et Bioinformatique à l'UCAD. Avant de commencer sa thèse, elle a été impliquée dans le travail portant sur l'étude des déterminants génétiques contrôlant la vigueur précoce et l'efficience de la transpiration chez *O. glaberrima*. Son travail de thèse consiste à développer un modèle structure-fonction de la racine du mil sur le formalisme du modèle OpenSimRoot développé pour le maïs. Elle est basée au CERAAS au Sénégal et effectue des séjours réguliers à Montpellier à travers des financements IRD et de l'Ambassade de France au Sénégal. Sokhatil devrait soutenir sa thèse au cours du premier semestre 2024.

Article publiés :

Affortit P., Effa-Effa B., **Ndoye M.S.**, Moukouanga D., Luchaire N., Cabrera-Bosquet L., … **Grondin A.*** (2022) Physiological and genetic control of transpiration efficiency in African rice, Oryza glaberrima Steud. *Journal of Experimental Botany* 73, 5279–5293.
*Auteur pour correspondance

Ndoye M.S., Burridge J., Bhosale R., **Grondin A.** & Laplaze L. (2022) Root traits for low input agroecosystems in Africa : Lessons from three case studies. *Plant, Cell and Environment* 45, 637–649.

-Branly EFFA-EFFA (2017-2020)
50 % encadrement avec Laurent LAPLAZE et Pascal GANTET
Effets de la symbiose mycorhizienne sur le transport d'eau racinaire et la résistance au stress hydrique chez le riz
École doctorale GAIA avec financement du Centre National de la Recherche Scientifique et Technologique (CENAREST) du Gabon

Branly est de nationalité gabonaise. Il a obtenu un Master Biotechnologies Végétales et Microbiennes à l'UCAD. La thèse de Branly s'est inscrite dans la continuité de projets déjà initiés par Laurent LAPLAZE en collaboration avec l'UCAD et l'AfricaRice portant sur l'étude de l'impact de la symbiose mycorhizienne dans les agrosystèmes rizicoles au Sénégal. Elle avait pour ambition d'identifier les déterminants génétiques contrôlant le caractère bénéfique de cette symbiose dans un panel de riz *Oryza glaberrima*. Malgré un gros travail d'optimisation, nous n'avons pas réussi à trouver une condition permettant la colonisation des racines de riz par le champignon de manière robuste vis-à-vis de l'environnement. L'étude portant sur la mycorhization n'a pu être publiée. Une partie du travail de Branly portant sur l'étude des déterminants génétiques contrôlant la vigueur précoce et l'efficience de la transpiration dans ce même panel a néanmoins été publiée en 2022. Il a soutenu sa thèse le 16 décembre 2020. Il est actuellement chercheur titulaire au CENAREST (Gabon).

Articles publiés :
Affortit P.*, **Effa-Effa B.***, Ndoye M.S., Moukouanga D., Luchaire N., Cabrera-Bosquet L., … **Grondin A.*** (2022) Physiological and genetic control of transpiration efficiency in African rice, Oryza glaberrima Steud. *Journal of Experimental Botany* 73, 5279–5293.
*co-premier Auteurs, *Auteur pour correspondance

Mbodj D.*, **Effa-Effa B.***, Kane A., Manneh B., Gantet P., Laplaze L., … **Grondin A.*** (2018) Arbuscular mycorrhizal symbiosis in rice: Establishment, environmental control and impact on plant growth and resistance to abiotic stresses. *Rhizosphere* 8, 12–26.
*co-premier Auteurs, *Auteur pour correspondance

- **Encadrements directs de CDD, post-docs**

-Sebastián ARENAS JIMENEZ
Post-doctorant IRD, Janvier 2022 – Décembre 2023
Étude de la plasticité racinaire adaptative chez le mil
Financement projet PlastiMil (ANR JCJC, Porteur : Alexandre Grondin)

Sebastián est de nationalité colombienne et a obtenu sa thèse en science biologiques à l'Université Nationale Autonome de Mexico (UNAM). Son travail de post-doctorat a consisté à identifier si des traits racinaires et le contenu en ions dans les feuilles étaient sous le contrôle de l'interaction génotype x environnement (G x E) chez le mil. Il a également étudié l'utilité de différents indices de plasticité pour la détection, par génétique d'association, de QTL capturant la variance expliquée par le G x E, et ceci en comparaison avec des approches de détection de QTL multi-environnements.

-Awa FAYE

Post-doctorante CERAAS, Juillet 2020 – Décembre 2022
Identification de traits racinaires bénéfiques pour la tolérance au stress hydrique chez le mil
Financement projet Anatomics (Royal Society, Porteurs : Malcolm BENNETT et Ndjido KANE)

Awa est de nationalité sénégalaise et a obtenu une thèse à l'UCAD en biologie végétale. Son travail de post-doctorat au CERAAS a consisté à adapter chez le mil, des méthodes de phénotypage haut-débit au champ en condition de stress hydrique. Awa a contribué à la mise en place, au suivi, à la récolte des données et à l'analyse des données de deux essais au champ réalisées en 2021 et 2022 sur un panel de 160 lignées de mil cultivé en condition irriguée et de stress hydrique. Après son post-doctorat au CERAAS, Awa a réalisé post-doctorat en Allemagne sur des aspects de modélisation des cultures.

-Romaric HALLOT

Technicien IRD, Janvier 2023 – Novembre 2023
Mise en place d'un protocole de transformation *in vitro* de *Setaria italica*
Financement projets CIWA (USAID-Innovation Lab for Crop Improvment, Porteurs : Marème BELKO et Ndjido KANE) et PlastiMil (ANR JCJC, Porteur : Alexandre Grondin)

Romaric a obtenu un BTS en Biotechnologies au Lycée Mermoz de Montpellier et a intégré notre équipe afin de continuer un travail entamé depuis 2020 sur la mise en place de protocoles de transformation et d'édition du génome chez les mils (*Pennisetum glaucum* ou mil à chandelle ou mil, et *Setaria italica* ou millet). Ces espèces s'avèrent très récalcitrantes et malgré l'existence de protocoles dans la littérature, nos essais ont été infructueux. Romaric continuera sur un contrat de technicien dans notre équipe jusqu'en 2026, mais en se focalisant sur un projet visant à casser la barrière de fertilité entre *O. glaberrima* et *O. sativa* à travers des approches d'édition du génome.

-Jeannot NDIONE

Technicien CERAAS, Septembre 2018 – Décembre 2022
Soutien aux activités de phénotypage racinaire au champ au Sénégal
Financement IRD dédié au recrutement de personnel local et projet ICARUS (ANR MOPGA, PI : Vincent VADEZ)

Jeannot est sénégalais et basé au CERAAS. Il a apporté un appui technique sur l'optimisation des protocoles de phénotypage racinaire, les essais en ombrière pour la multiplication des graines du panel de mil, ainsi que le suivi des essais au champ, des activités de phénotypage et de récoltes du mil. Jeannot est toujours agent technique au CERAAS.

-Aida DIENG
Technicienne CERAAS, Avril 2023 – Décembre 2023
Suivi d'un essai au champ sur un panel de diversité de mil et activités de phénotypage associées
Financement IRD dédié au recrutement de personnel local et projet ICARUS (ANR MOPGA, Porteur : Vincent VADEZ)

Aida a eu la charge plus spécifique de suivre au quotidien au Centre National de la Recherche Agronomique (CNRA) de Bambey (lieux des parcelles expérimentales) toutes les activités concernant l'essai au champ réalisé en 2022 sur un panel de 160 lignées de mil, du semi jusqu'à la saisie des données, en passant par le phénotypage racinaire et la mesure des caractéristiques agro-morphologiques et la récolte. Aida est toujours agent technique au CNRA de Bambey.

-Tening DIOUF
Technicienne CERAAS, Mars 2021 – Septembre 2021
Suivi d'un essai au champ sur un panel de diversité de mil et activités de phénotypage associées
Financement IRD dédié au recrutement de personnel local

Comme Aida, Tening a suivi au quotidien toutes les activités concernant l'essai au champ réalisé en 2021 sur le panel de 160 lignées de mil. Tening poursuit actuellement une thèse sur l'influence des fumiers organiques et minéraux sur l'intensification durable de la culture du maïs au Sénégal.

- **Principaux projets de recherche financés**

-ANR SorDrought
Characterization of new physiological traits to support breeding for post-flowering drought tolerance in sorghum.
2024-2027, 840 k€
Porteur : Laurent LAPLAZE
Impliqué dans le phénotypage et l'étude du déterminisme génétique de traits racinaires et d'efficience d'utilisation de l'eau

-ANR PlastiMil
Root plasticity in pearl millet.
2021-2025, 287 k€
Porteur : Alexandre GRONDIN
Impliqué dans la conceptualisation, la mise en place des protocoles, l'analyse, l'interprétation et la gestion des données

-EPPN IonoMil
Roles of root traits on leaf mineral composition for improved drought tolerance in pearl millet – a combined ionomics and root phenotyping approach.
2021, montant non communiqué
Porteur : Alexandre GRONDIN

Impliqué dans la conceptualisation, la collecte des feuilles au champ, l'analyse, l'interprétation et la gestion des données

-Royal Society Anatomics

Anatomics in pearl millet: improving yield and drought tolerance of a major dietary staple food in the Sahel.
2019-2022, 209 k£
Porteurs : Malcolm BENNETT et Ndjido KANE
Impliqué dans la mise au point des protocoles, la mise en place et la gestion des essais et des activités de phénotypage, l'analyse, l'interprétation et la gestion des données

-USAID-SMIL GenMil

Genetic enhancement of pearl millet for yield, biotic and abiotic stress tolerance in West Africa
2019-2024, 1100 k$
Porteur : Ndjido KANE
Impliqué dans la conceptualisation, le phénotypage racinaire au champ et le développement du modèle FSPM racine de mil

-EPPN MycoRice

Effects of mycorrhizal inoculation on drought tolerance of African rice – from physiological traits to QTL identification
2019, Prise en charge complète d'une expérience sur la plateforme PhénoArch
Porteurs : Ricardo AROCA and Alexandre GRONDIN
Impliqué dans la conceptualisation, la mise en place et la gestion des essais et des activités de phénotypage, l'analyse, l'interprétation et la gestion des données

-ANR RootAdapt

Root traits for adaptation of pearl millet to future climate in West Africa
2018-2022, 536 k€
Porteur: Laurent LAPLAZE
Impliqué dans la mise en place et la gestion des essais au champ et des activités de phénotypage, les analyses transcriptomiques, et l'analyse et l'interprétation des données

-ANR MasteRoot

Determination of master regulatory genes controlling crown root development for cereals water deficit tolerance engineering
2018-2021, 411 k€
Porteur : Pascal GANTET
Impliqué dans le choix des gènes à étudier et l'interprétation des données de phénotypage de plantes transgéniques pour la tolérance à la sécheresse

- **Activités d'enseignements/Formations**

-Module HAA905V – Approches Intégrées en Amélioration des Plantes pour les Masters Biotechnologie et Amélioration des Plantes Tropicales (BAPT), Plantes et Sciences Microbiologiques pour l'Agroenvironnement (IDIL) et Management de l'Expérimentation

Végétale (MEV) de l'UM. Participation aux travaux dirigés et au jury de l'examen oral en 2017 et depuis 2022 (15h / an).

-Module Génétique des Populations et Génétique d'Association pour le Master BIOVEM de l'UCAD. Co-responsable du module depuis 2020, impliqué dans l'organisation et la gestion des enseignements, les cours (2 h / an) et travaux dirigés (4 h / an), les travaux pratiques (40h / an) et l'examen depuis 2019.

-Intervenant dans deux formations sur les « Méthodologies de Phénotypage Racinaire » au CERAAS en mars 2018 et sur « La Technologie CRISPR : Théorie, Législation et Pratiques » au CERAAS en mai 2023.

- **Conférences**

Je participe à au moins une conférence internationale par an (en France ou à l'étranger), avec proposition de présentation sous forme d'oral, ou à défaut sous forme d'un poster.
J'ai été invité à deux conférences :
-*Gordon Conference on Salt and Water Stress in Plants* du 22/05/2022 au 27/05/2022 à Les Diablerets en Suisse. J'y ai présenté les travaux relatifs au contrôle génétique de traits liés à l'utilisation de l'eau chez le riz Africain.
-*UK Rice Research Conference meeting*, *Linking UK and European Rice Research* du 07/02/23 au 08/02/23 à Cambridge. J'y ai là aussi présenté les travaux relatifs au contrôle génétique de traits liés à l'utilisation de l'eau chez le riz Africain.

- **Évaluation d'articles et rôle d'éditeur associé**

J'évalue environ une dizaine d'articles par an pour les journaux *Journal of Experimental Botany*, *BMC Genomics*, *Environmental and Experimental Botany*, *Scientific Reports*, *Plant and Soil*, *New Phytologist*, *Plant Physiology*, *Annals of Botany*, *Plant, Cell & Environment*. J'ai également été Éditeur associé pour le journal *Frontiers in Plant Science*, dans la section spéciale *Plant Abiotic Stress* en 2022.

J'évalue également régulièrement des projets de recherche pour l'*Israël Research Foundation* et *The United States – Israël Binational Agricultural Research and Development Fund*.

2. Publications scientifiques

- **Articles scientifiques**

23 articles internationaux, 1,547 citations, H-Index :13 (au 26 novembre 2023)
* Auteur pour correspondance

(23) Vadez V, **Grondin A**, Chenu K, Henry A, Laplaze L, Millet EJ, Carminati A. 2023. Context-dependent water-related traits determine crop production under drought. *Nature Reviews Earth & Environment*, *accepted*

(22) Fuente C. de la, **Grondin A.**, Sine B., Debieu M., Belin C., Hajjarpoor A., … Laplaze L. (2023) Glutaredoxin regulation of primary root growth confers early drought stress tolerance in pearl millet. *eLife* 12:RP86169.

(21) Affortit P., Ahmed M.A., **Grondin A.**, Delzon S., Carminati A. & Laplaze L. (2023) Keep in touch : the soil – root hydraulic continuum and its role in drought resistance in crops. *Journal of Experimental Botany* erad312.

(20) Vadez V., Pilloni R., **Grondin A.**, Hajjarpoor A., Belhouchette H., Brouziyne Y., … Bossuet J. (2023) Water use efficiency across scales: from genes to landscapes. *Journal of Experimental Botany*. erad052

(19) Affortit P., Effa-Effa B., Ndoye M.S., Moukouanga D., Luchaire N., Cabrera-Bosquet L., … **Grondin A.*** (2022) Physiological and genetic control of transpiration efficiency in African rice, Oryza glaberrima Steud. *Journal of Experimental Botany* 73, 5279–5293.

(18) Burridge J.D., **Grondin A.** & Vadez V. (2022) Optimizing Crop Water Use for Drought and Climate Change Adaptation Requires a Multi-Scale Approach. *Frontiers in Plant Science* 13.

(17) de la Fuente Cantó C., Diouf M.N., Ndour P.M.S., Debieu M., **Grondin A.**, Passot S., … Laplaze L. (2022) Genetic control of rhizosheath formation in pearl millet. *Scientific Reports* 12, 1–13.

(16) Ndoye M.S., Burridge J., Bhosale R., **Grondin A.** & Laplaze L. (2022) Root traits for low input agroecosystems in Africa : Lessons from three case studies. *Plant, Cell and Environment* 45, 637–649.

(15) Chevallier T., Loireau M., Courault R., Chapuis-Lardy L., Desjardins T., Gomez C., … Chotte J.L. (2020) Paris climate agreement: Promoting interdisciplinary science and stakeholders' approaches for multi-scale implementation of continental carbon sequestration. *Sustainability (Switzerland)* 12.

(14) Grondin A.*, Affortit P., Tranchant-Dubreuil C., de la Fuente-Cantó C., Mariac C., Gantet P., … Laplaze L. (2020) Aquaporins are main contributors to root hydraulic conductivity in pearl millet [Pennisetum glaucum (L) R. Br.]. *Plos One* 15, e0233481.

(13) Campbell M.T., **Grondin A.**, Walia H. & Morota G. (2020) Leveraging genome-enabled growth models to study shoot growth responses to water deficit in rice. *Journal of Experimental Botany* 71, 5669–5679.

(12) Faye A., Sine B., Chopart J.-L., **Grondin A.**, Lucas M., Diedhiou A.G., … Laplaze L. (2019) Development of a model estimating root length density from root impacts on a soil profile in pearl millet (Pennisetum glaucum (L.) R. Br). Application to measure root system response to water stress in field conditions. *Plos One* 14, e0214182.

(11) Nguyen K. Le, **Grondin A.**, Courtois B. & Gantet P. (2019) Next-Generation Sequencing Accelerates Crop Gene Discovery. *Trends in Plant Science* 24, 263–274.

(10) Debieu M., Sine B., Passot S., **Grondin A.**, Akata E., Gangashetty P., … Laplaze L. (2018)

Response to early drought stress and identification of QTLs controlling biomass production under drought in pearl millet. *PLoS ONE* 13, 1–19.

(9) Mbodj D., Effa-Effa B., Kane A., Manneh B., Gantet P., Laplaze L., … **Grondin A.*** (2018) Arbuscular mycorrhizal symbiosis in rice: Establishment, environmental control and impact on plant growth and resistance to abiotic stresses. *Rhizosphere* 8, 12–26.

(8) Grondin A., Dixit S., Torres R., Venkateshwarlu C., Rogers E., Mitchell-Olds T., … Henry A. (2018) Physiological mechanisms contributing to the QTL qDTY3.2 effects on improved performance of rice Moroberekan x Swarna BC2F3:4 lines under drought. *Rice* 11, 1–17.

(7) Rodrigues O., Reshetnyak G., **Grondin A.**, Saijo Y., Leonhardt N., Maurel C. & Verdoucq L. (2017) Aquaporins facilitate hydrogen peroxide entry into guard cells to mediate ABA- and pathogen-triggered stomatal closure. *Proceedings of the National Academy of Sciences of the United States of America* 114.

(6) Henry A., Wehler R., **Grondin A.**, Franke R. & Quintana M. (2016) Environmental and physiological effects on grouping of drought-Tolerant and susceptible rice varieties related to rice (Oryza sativa) root hydraulics under drought. *Annals of Botany* 118.

(5) Grondin A., Mauleon R., Vadez V. & Henry A. (2016) Root aquaporins contribute to whole plant water fluxes under drought stress in rice (Oryza sativa L.). *Plant, Cell and Environment* 39, 347–65.

(4) Dixit S., **Grondin A.**, Lee C.-R., Henry A., Olds T.-M. & Kumar A. (2015) Understanding rice adaptation to varying agro-ecosystems: trait interactions and quantitative trait loci. *BMC genetics* 16, 86.

(3) Grondin A., Rodrigues O., Verdoucq L., Merlot S., Leonhardt N. & Maurel C. (2015) Aquaporins contribute to ABA-triggered stomatal closure through OST1-mediated phosphorylation. *Plant Cell* 27.

(2) Postaire O., Tournaire-Roux C., **Grondin A.**, Boursiac Y., Morillon R., Schäffner A.R. & Maurel C. (2010) A PIP1 aquaporin contributes to hydrostatic pressure-induced water transport in both the root and rosette of Arabidopsis. *Plant physiology* 152, 1418–30.

(1) Verdoucq L., **Grondin A.** & Maurel C. (2008) Structure-function analysis of plant aquaporin AtPIP2;1 gating by divalent cations and protons. *The Biochemical journal* 415, 409–416.

- **Chapitre d'ouvrage**

Grondin A*, Bhosale R, Atkinson JA, Faye A, Jones DH, Benson E, Burridge J, Sine B, Vadez V, Pridmore T, Wells DM, Laplaze L, Kane NA, Bennett MJ (2022) High-throughput root phenotyping: Opportunities and challenges for the adaptation of arid and semi-arid crops to future climates. *In Crop Adaptation and Improvement for Drought-Prone Environments*. Editors: Kane A, Foncéka D, Dalton TJ *New Prairie Press* 258-282

- **Articles de vulgarisation scientifique**

Grondin A, Guyomarc'h S, Laplaze L, (2022) Le système racinaire des plantes : de l'ombre à la lumière
https://www.encyclopedie-environnement.org/vivant/racines-plantes/
Encyclopédie de l'environnement, v18-03-2022.

Laplaze L, **Grondin A**, Cournac L (2022) Root traits enhance the agroecological transition. Les Dossiers d'Agropolis International, n°26 Transformations agroécologiques pour des systèmes alimentaires durables : Panorama de la recherche France-CGIAR.

Grondin A, Laplaze L, Kane NA (2021) Le système racinaire pour l'amélioration de la productivité et de la résilience du mil dans un contexte d'agriculture à faibles intrants, n°3 Jokko Sciences pour le Développement, Bulletin d'information semestriel de la Représentation de l'IRD au Sénégal.

3. Thématique de recherche et objectifs

3.1 Contexte

- **Vers un changement des systèmes agricoles**

Les années 1960s ont été marquées par le début de ce que l'on appelle la révolution verte, qui correspond à des décennies de forte augmentation du rendement des céréales (Evenson and Gollin, 2003). Ces progrès ont été rendu possibles par l'amélioration variétale, l'utilisation intensive d'intrants et l'optimisation de pratiques culturales. Cette augmentation de la production a eu des effets indéniables sur la baisse du prix des céréales ainsi que sur l'augmentation de la sécurité alimentaire et le développement économique. Néanmoins, de grandes disparités géographiques existent dans l'impact qu'a pu avoir la révolution verte. L'Afrique a peu profité de ces innovations contrairement à l'Asie par exemple. De plus, l'intensification des cultures céréalières a eu des conséquences environnementales indésirables, comme la dégradation des sols, la pollution des eaux sous-terraines par le lessivage des fertilisants chimiques et des produits phytosanitaires, et le déclin de la biodiversité. Ce modèle agricole basé sur l'utilisation importante d'intrants participe également à l'émission de gaz à effet de serre qui contribuent aux changements climatiques. La riziculture inondée contribue par exemple à 15-20 % des émissions de méthane anthropiques (Hirt *et al.*, 2023). Cela questionne sur la durabilité de ces systèmes de culture qui sont aujourd'hui encore majoritaires.

Les piliers qui ont fait le succès de la révolution verte sont aujourd'hui confrontés à de nombreux défis. D'une part, les rendements n'augmentent plus à un rythme qui permettrait de suivre l'augmentation prédite de la population mondiale. Cela peut s'expliquer par la réduction du gain génétique qui tend à atteindre ses limites chez les grandes cultures. D'autre part, la disponibilité en intrants est menacée. La ressource en certains engrais n'est par exemple pas infinie et leur prix peut grandement varier en fonction de la conjoncture internationale. L'utilisation de l'eau et sa répartition entre usages agricoles, domestiques et industriels fait l'objet de tensions fortes liées au caractère moins prévisible de l'accès à cette ressource causé par les changements climatiques. De fait, les changements climatiques souvent accompagnés d'évènements extrêmes (fortes températures, sécheresses…) affectent le rendement des céréales qui n'y sont pas adaptées. Le stress hydrique représente la contrainte abiotique majeure affectant le rendement des céréales (source FAO ; https://www.fao.org/resources/digital-reports/disasters-in-agriculture/en/). Il est donc nécessaire d'adapter les céréales à ces nouvelles contraintes et de faire évoluer l'agriculture vers des systèmes de culture durable.

Développer des variétés plus frugales et résilientes tout en maintenant la productivité nécessite de repenser l'amélioration variétale pour mieux prendre en compte les contextes climatiques locaux, explorer plus en profondeur la diversité génétique pour identifier et des réponses adaptatives, et mieux comprendre dans quels contextes ces réponses seraient les

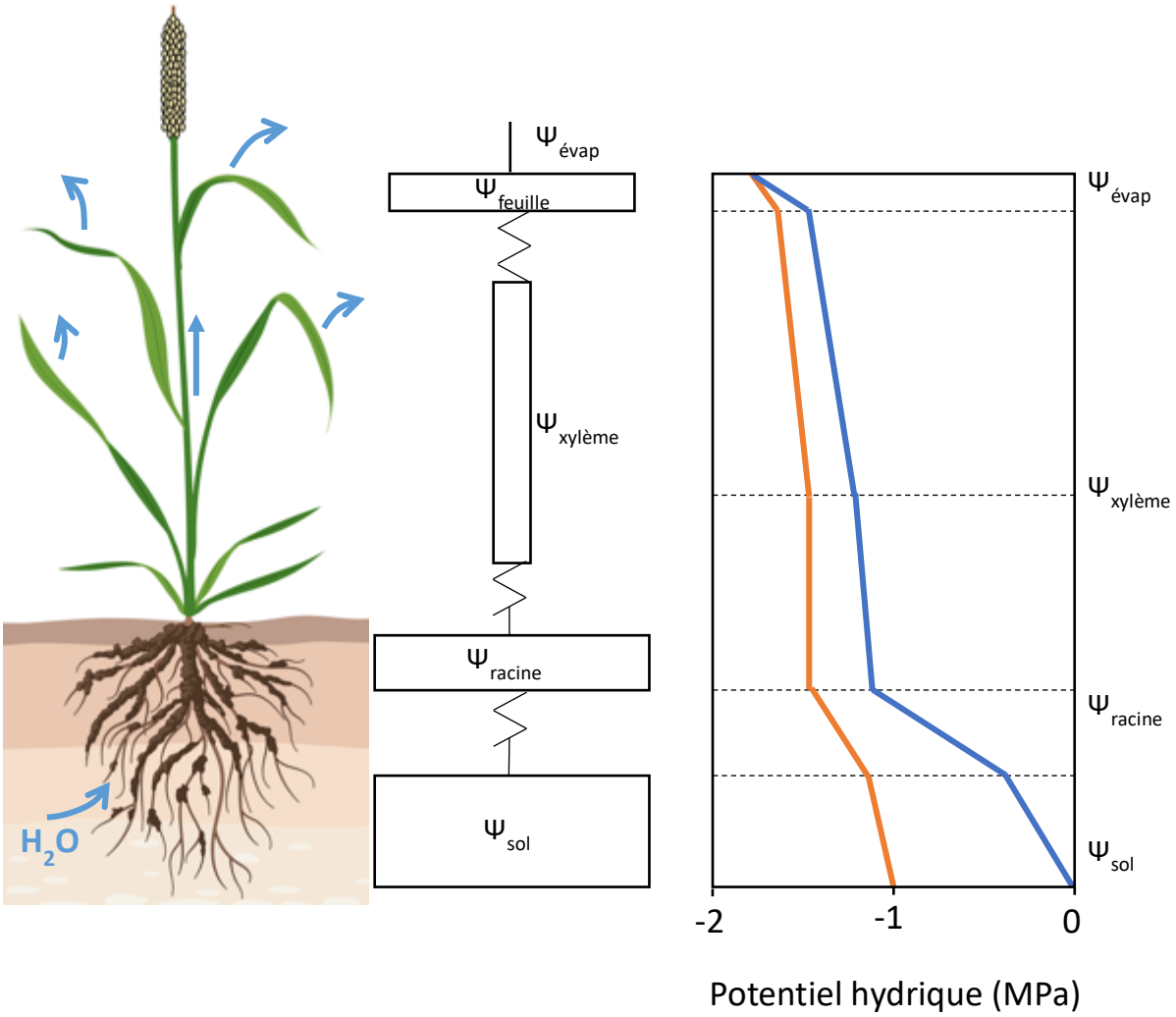

Figure 1 : Modèle du transport d'eau chez les plantes. La plante est représentée par différents compartiments (la racine, le xylème et les feuilles avec les sites d'évaporation au niveau de la chambre sous-stomatique) ayant des potentiels hydriques (Ψ) différents. Des résistances existent entre le sol et l'interface avec la racine, entre les tissus racinaires et les vaisseaux conducteurs du xylème, et entre le xylème et les feuilles au niveau des sites d'évaporation. Des plantes cultivées en condition bien irriguée (bleu) ou en condition de stress hydrique (orange) peuvent avoir le même potentiel hydrique foliaire en cas de comportement isohydrique. Figure reproduite à partir de la Figure 1 de Tardieu et al, 2017.

plus bénéfiques. Les espoirs d'une deuxième révolution verte reposent sur des innovations technologiques telles que le séquençage à haut-débit pour l'exploration de la diversité génétique, l'intelligence artificielle pour l'exploration de la diversité phénotypique, ou l'édition des génomes pour accélérer la sélection.

- **La gestion de la ressource en eau comme cible pour améliorer la tolérance des céréales au stress hydrique**

L'eau circule du sol vers les racines puis les parties aériennes pour être évaporée lors de la transpiration sous forme de vapeur dans l'atmosphère au niveau des stomates (Tardieu *et al.*, 2017). Dans un sol irrigué, l'ouverture des stomates crée un gradient de potentiel hydrique entre l'atmosphère plus sèche, la plante et le sol plus humide qui induit l'entrée de l'eau dans la plante par les racines (Figure 1). Lors d'un assèchement de l'air ou du sol, si les flux d'eau issues des racines ne sont plus capables d'égaler la demande des parties aériennes, le potentiel hydrique foliaire commence à chuter. Les plantes commencent alors à fermer leurs stomates pour réduire la transpiration. Cela permet le maintien de potentiels hydriques foliaires acceptables pour le maintien du métabolisme et éviter la cavitation dans les vaisseaux du xylème. En contrepartie, la fermeture stomatique réduit l'entrée du CO_2 dans la plante, l'assimilation photosynthétique et la production de biomasse.

Une grande variabilité génétique inter- et intra-spécifique a pu être observée dans la réponse de la transpiration à l'environnement hydrique du sol ou de l'atmosphère. En réponse à l'asséchement du sol, des plantes isohydriques fermeront leur stomates à des potentiels hydriques du sol relativement élevés prévenant une chute trop importante du potentiel hydrique foliaire (Tardieu and Simonneau, 1998). Cette stratégie relève d'un comportement conservatif permettant une économie de l'eau du sol qui peut s'avérer bénéfique en cas de stress hydrique intense (Tardieu *et al.*, 2018). D'autres plantes anisohydriques fermeront leurs stomates à des potentiels hydriques du sol plus faibles autorisant une chute plus importante du potentiel hydrique foliaire (Tardieu and Simonneau, 1998). Cette stratégie plus à risque mais où la plante continue à produire de la biomasse est considérée comme plus adaptée pour des cas de stress hydriques modérés (Tardieu *et al.*, 2018). Cette classification iso/anisohydrique est néanmoins loin d'être stricte et ces comportements peuvent varier chez une même plante en fonction du type de sol ou en fonction de leur stade de développement (Hochberg *et al.*, 2018; Abdalla *et al.*, 2022).

L'assèchement de l'air et l'augmentation de la demande évaporative qui s'en suit peut également induire la fermeture stomatique. Au cours d'une journée sèche et chaude, certaines plantes peuvent restreindre leur transpiration lorsque la pression de vapeur d'eau dans l'air dépasse un certain seuil et cela même dans des conditions où la ressource en eau dans le sol n'est, *a priori*, pas limitante (Vadez *et al.*, 2014). Ce mécanisme appelé restriction de la transpiration à la demande évaporative (Figure 2) a généralement lieu en milieu de journée et domine la régulation de l'ouverture stomatique par la lumière (Kholová *et al.*,

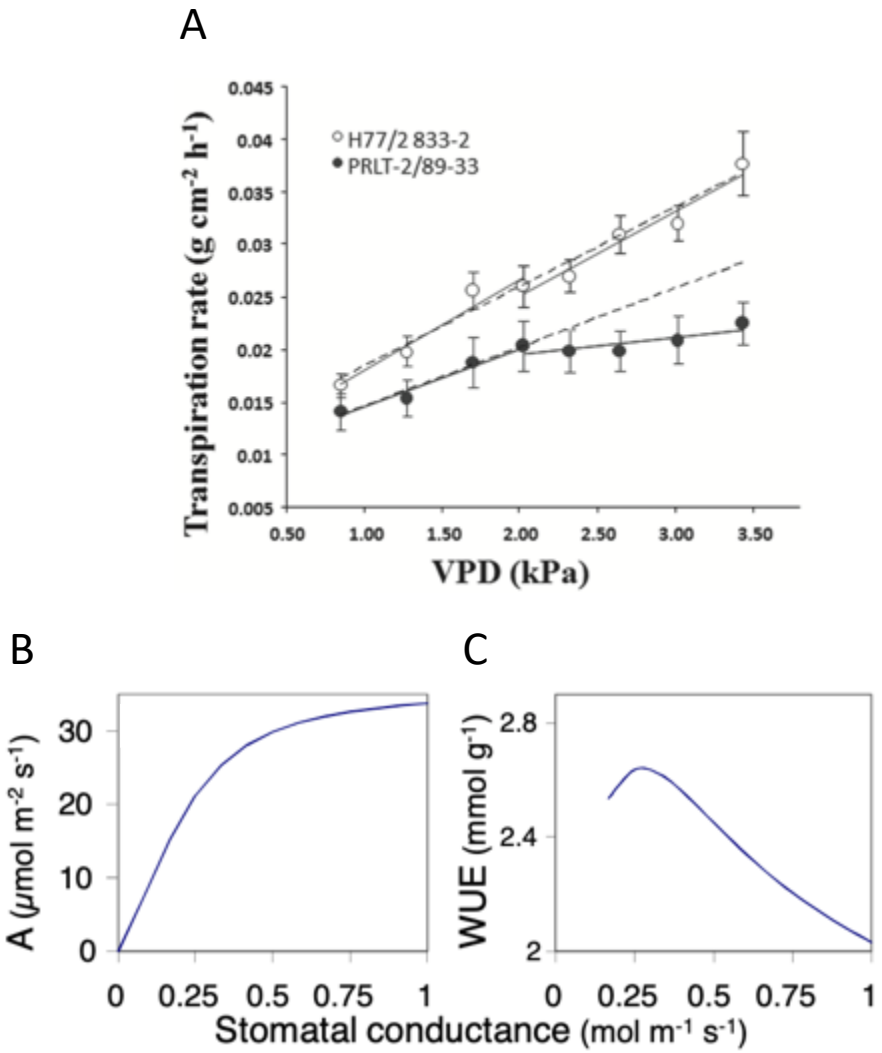

Figure 2 : Optimisation de l'efficience d'utilisation de l'eau par la stratégie de restriction de la transpiration en réponse à la demande évaporative. A: En comparaison avec le génotype H77/2833-2, le génotype PRLT-2/89-33 réduit sa transpiration en réponse à l'augmentation de la demande évaporative ici représentée par la VPD (Vapour Pressure Deficit). Issue de Vadez et al., 2014 (Figure 2). B: Non-linéarité de la relation entre la conductance stomatique et l'assimilation photosynthètique (A). Issue de Tardieu, 2022 (Figure 3a). C: Effets de la réduction de la conductance stomatique sur l'efficience d'utilisation de l'eau (WUE). Issue de Tardieu 2022 (Figure 3b).

2010). Cette stratégie peut être considérée comme conservative. Néanmoins, elle se met en place uniquement pendant les heures les plus chaudes de la journée où la fixation du carbone est faible par rapport à l'eau utilisée. Elle a donc un impact limité sur la production de biomasse mais un impact très fort sur l'économie d'eau (Vadez *et al.*, 2014). De plus, la relation entre la conductance stomatique et l'assimilation en carbone pour la photosynthèse n'est pas linéaire (Figure 2). Dans la partie non-linéaire, cela implique une réduction plus faible de l'assimilation par rapport à la réduction de la perte en eau induisant une augmentation de l'efficience d'utilisation de l'eau (Tardieu, 2022). Cette stratégie de restriction de la transpiration en réponse à la demande évaporative a été associée à une meilleure efficience d'utilisation de l'eau et une meilleure tolérance à la sécheresse chez des céréales comme le maïs, le blé, le mil ou le sorgho (Kholová *et al.*, 2010; Gholipoor *et al.*, 2013; Medina *et al.*, 2019; Choudhary *et al.*, 2020). Plus précisément, la restriction de la transpiration en réponse à la demande évaporative s'avère être particulièrement efficace pour la tolérance à un stress hydrique terminal, où l'économie d'eau réalisée pendant la phase végétative permet d'assurer le remplissage des grains.

Les plantes peuvent donc mettre en place différentes stratégies afin de répondre où prévenir l'apparition d'un stress hydrique. Ces stratégies seront plus ou moins efficaces en fonction du stress auquel elles seront confrontées. Améliorer la tolérance d'une céréale face au stress hydrique nécessite donc la caractérisation précise de l'environnement pédoclimatique dans lequel elle se développe afin de mieux définir le type de stress encouru (à quel moment du cycle ? à quelle intensité ? à quelle fréquence ?) et l'impact de ce stress sur les rendements. Des modèles de culture ont été développés afin de mieux caractériser les types de stress hydrique affectant les plantes dans certains environnements (aussi appelé « *envirotyping* »). Ces modèles permettent de mieux comprendre les effets de différentes stratégies d'utilisation de l'eau sur la performance des céréales dans un environnement, et cela en lien avec les pratiques agronomiques (Chenu *et al.*, 2017). Les mécanismes physiologiques qui sous-tendent la gestion de l'eau par la plante à travers la régulation de la transpiration sont néanmoins complexes et encore peu pris en compte dans ces modèles. Une meilleure compréhension de ces mécanismes et de leurs effets dans différents scénarios de stress est nécessaire pour élargir le spectre de tolérance des céréales au stress hydrique.

- **Mécanismes physiologiques impliqués dans le contrôle de l'hydraulique des plantes**

Pour mieux caractériser les mécanismes associés au stress hydrique, il s'agit de mieux définir ce stress. Récemment, une définition basée sur la régulation des processus hydrauliques au cours du stress a été proposée (Vadez et al, 2023, accepté). Une plante soumise à un stress hydrique entrerait ainsi différentes phases en fonction de d'intensité de stress (Figure 3) : dans la première phase, la transpiration de plantes stressées ne change pas par rapport à des plantes non stressées et les processus de développement ne sont pas affectés ; dans la deuxième phase, les flux d'eau dans les racines et à travers la plante ne permettent plus de

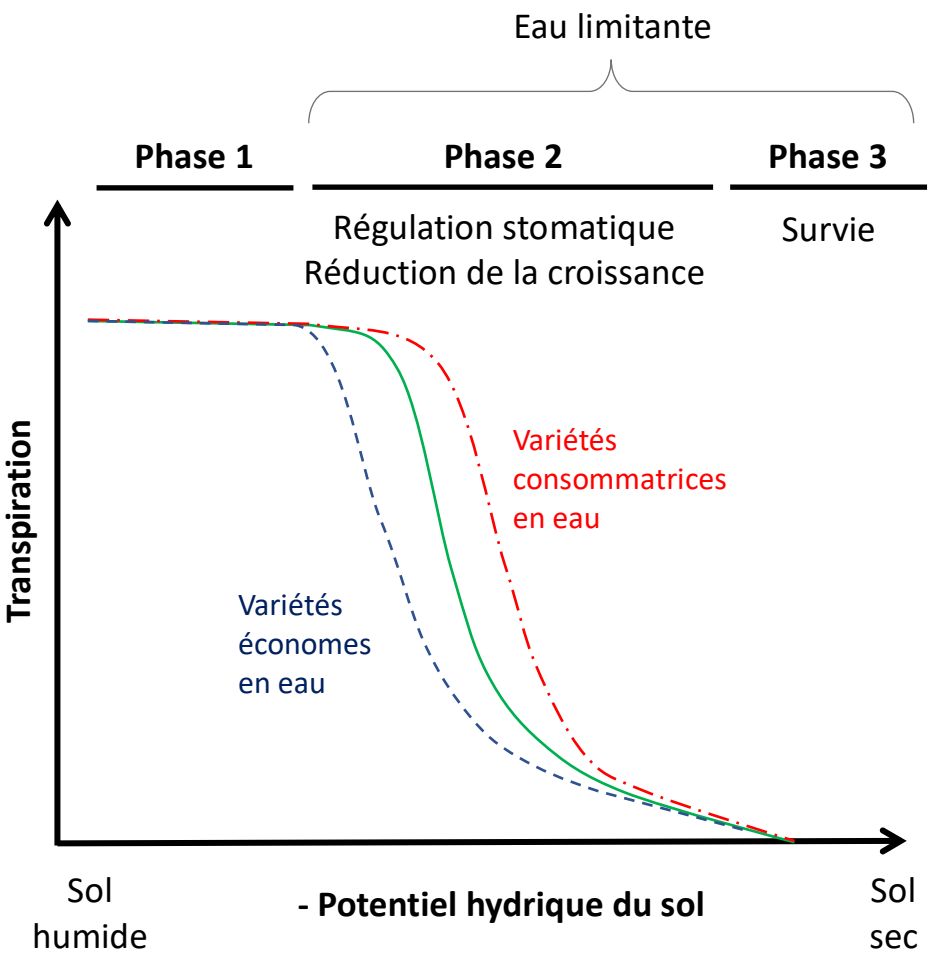

Figure 3 : Réponse de la transpiration à la chute du potentiel hydrique du sol au cours d'un stress hydrique. Durant la phase 1 la croissance n'est pas limitée. Durant la phase 2, l'eau est limitante et la plante réduit sa transpiration pour ajuster l'offre à la demande en eau. Durant la phase 3, la plante ne peut plus extraire l'eau du sol et entre en mode de survie qui amène à sa dessiccation complète si cette phase se prolonge. Les plantes économes en eau ont un comportement isohydrique conservateur au prix de la fixation du carbone. Les plantes consommatrices en eau ont une stratégie anisohydrique à plus haut risque. La trajectoire verte correspondrait à la réponse de plantes mettant en place des mécanismes de restriction de la transpiration en réponse à la demande évaporative. Elles seraient plus économes en eau que les plantes anisohydriques et seraient capables de maintenir une plus forte croissance que les plantes isohydriques dans la phase 2. Figure adaptée de Vadez et al., 2023 (accepté).

supporter la transpiration. La transpiration diminue graduellement grâce à la fermeture stomatique pour égaler les capacités d'offre en eau. Cela induit également un ralentissement de la croissance ; dans la troisième phase, les racines ne peuvent plus extraire d'eau du sol, la conductance stomatique est à son minimum et la croissance s'arrête. La plante entre alors en phase de survie. Dans la première phase, la plante pourra mettre en place des mécanismes qui permettent de compenser la réduction de l'eau dans le sol afin de maintenir l'offre sans affecter la transpiration. Cela peut passer par une augmentation de l'activité des aquaporines dans la racine. Dans la deuxième phase, ces mécanismes pourront s'intensifier et des mécanismes de tolérance pourront être mis en place afin d'optimiser l'utilisation de la quantité d'eau qui devient limitante. Dans la troisième phase de survie, les mécanismes mis en jeu relèvent plus généralement de processus liés à l'ajustement osmotique ou de détoxification d'espèces réactives de l'oxygène pour le maintien de la turgescence des cellules et des fonctions métaboliques respectivement (Vadez et al, 2023, accepté). Le modèle de compensation hydrique entre l'offre et la demande implique que différents maillons du continuum sol-plante-atmosphère pouvant représenter des résistances pour l'acquisition, le transport et l'utilisation de l'eau influenceraient la tolérance au stress hydrique au cours de la phase 2. Les mécanismes présentés par la suite ciblent l'amélioration de la tolérance à cette phase de stress hydrique.

Le sol représente un premier degré de résistance. En effet, des d'études récentes montrent que dans un sol qui s'assèche, la conductivité hydraulique chute de manière drastique et le gradient de potentiel hydrique autour des racines devient alors une source de résistance majeure (Abdalla *et al.*, 2021). Une forte densité de poils absorbants participerait à limiter la chute du potentiel hydrique matriciel du sol dans la rhizosphère au cours d'un stress hydrique et donc au maintien de la continuité hydrique (Carminati *et al.*, 2017). La rhizodéposition, i.e. la déposition par la plante de molécules carbonées dans le sol à travers l'exsudation ou la mort cellulaire, contribue à changer les propriétés physico-chimiques de la rhizosphère (Figure 4; de la Fuente Cantó *et al.*, 2020). Le mucilage en particulier, composé de polysaccharides possédant des propriétés hydrophiles, augmenterait l'humidité du sol autour de la racine et participerait à maintenir la continuité hydraulique sol-racine lors d'un stress hydrique (Benard *et al.*, 2019). De fait, la rhizodeposition contribue à la formation d'un manchon racinaire (i.e., sol adhérent aux racines) qui a été associé à une meilleure tolérance au stress hydrique chez le blé, l'orge ou *Setaria italica* (George *et al.*, 2014; Basirat *et al.*, 2019; Liu *et al.*, 2019).

La manière dont les racines se développent et s'agencent dans le sol impacte l'accès à la ressource en eau (Figure 4). Des expériences de pressurisation combinées à de la modélisation hydraulique sol-plante montrent que des surfaces racinaires plus larges permettent de maintenir la transpiration plus longtemps en condition de stress hydrique chez la tomate (Abdalla *et al.*, 2021). La capacité de capture d'eau n'est néanmoins pas homogène entre les différents types racinaires, celle-ci ayant principalement lieu dans les zones apicales

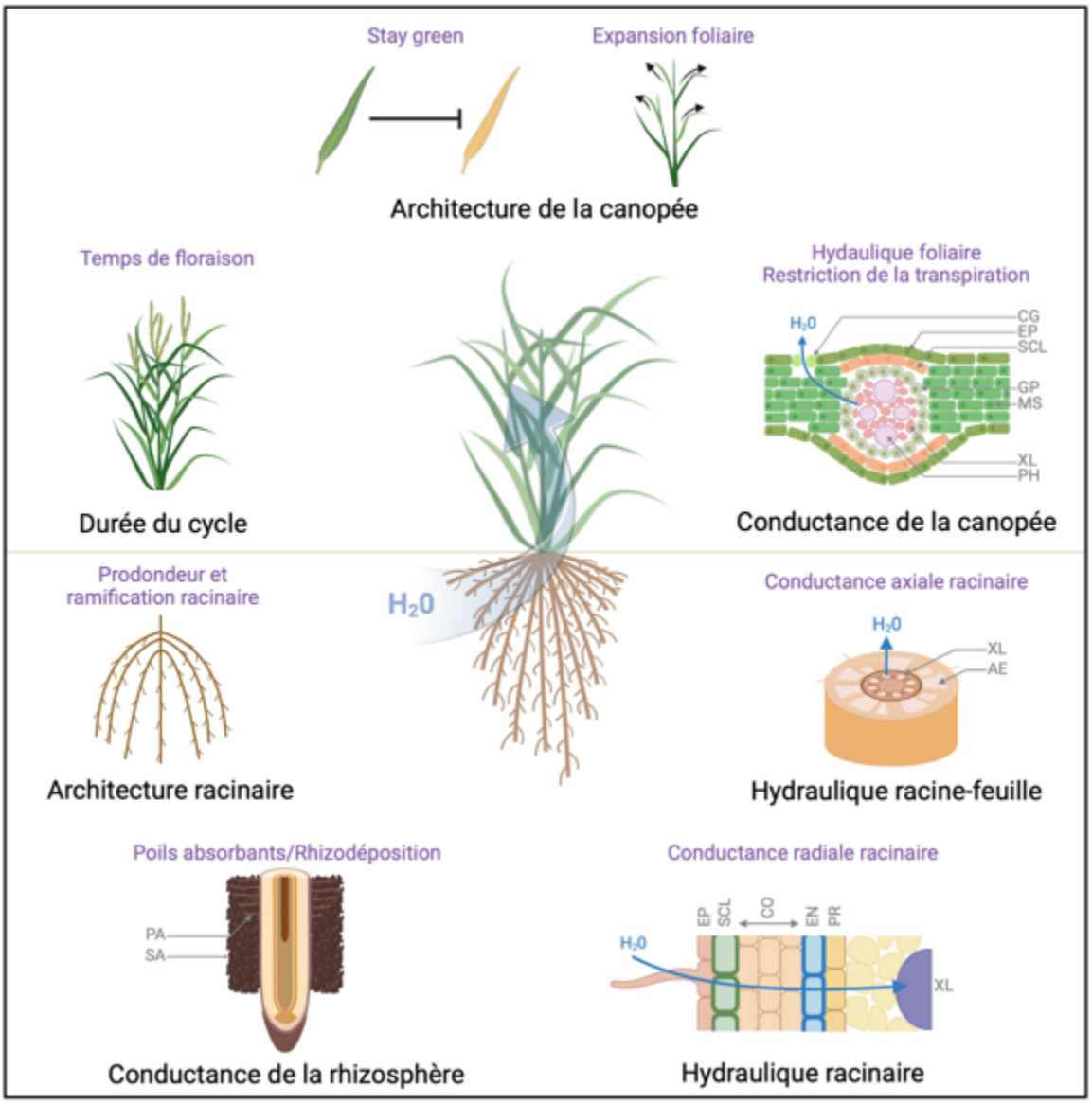

Figure 4 : Processus (en noir) et traits morphologiques et physiologiques associés (en violet) dans le hydraulique continuum sol-plante-atmosphère. PA: poils absorbant; SA: sol adhérent aux racines; EP: épiderme; SCL: sclérenchyme; CO: cortex; EN: endoderme; PR: pericycle; XL; xylème; AE: aérenchyme; PH: phloème; MS: mésophylle; GP: gaine perivasculaire; CG: cellule de garde. Figure adaptée de Vadez et al., 2023 (accepté).

peu lignifiées des racines et au niveau des racines latérales (Zwieniecki *et al.*, 2003; Henry *et al.*, 2012; Cai *et al.*, 2022). La répartition des racines dans les différents horizons de sol peut ainsi également influencer l'accès à la ressource en eau. Des systèmes racinaires plus profond permettent par exemple au riz, au maïs et au blé de mieux tolérer le stress hydrique (Uga *et al.*, 2013; Lynch, 2018; Bacher *et al.*, 2023). Ce caractère a reçu beaucoup d'attention dans la littérature mais ne représente pas une solution miracle car son efficacité dépend du type de sol et de la disponibilité de l'eau en profondeur. De plus, les contreparties de ce caractère sur la nutrition minérale et en particulier la nutrition en phosphore restent floues.

La capacité des racines à transporter l'eau, i.e. la conductance hydraulique racinaire peut également être limitante pour les flux d'eau dans la plante (Vadez, 2014). La conductance hydraulique racinaire se décompose en conductance radiale où l'eau circule du sol vers les vaisseaux conducteurs, et en conductance axiale où l'eau circule au travers des vaisseaux du xylème vers les parties aériennes (Figure 4). L'anatomie de la racine influence donc le transport de l'eau dans la racine. La formation de barrières pariétales (Calvo-Polanco *et al.*, 2021) ou d'aérenchymes (Ranathunge *et al.*, 2003) ont un effet inhibiteur sur la conductance radiale. Les aquaporines, des canaux à eau présents dans les membranes lipidiques, régulent la conductance hydraulique radiale (Maurel *et al.*, 2015). Chez la vigne, des cultivars anisohydriques cultivés en condition de stress hydrique montrent une forte augmentation de la conductance hydraulique racinaire au cours de la journée en comparaison avec des cultivars isohydriques, qui a pu être reliée à l'expression plus forte d'une aquaporine de la membrane plasmique (Vandeleur *et al.*, 2009). Chez la tomate, la surexpression d'une aquaporine présente sur le tonoplaste permet de changer le comportement isohydrique de plantes sauvages vers un comportement anisohydrique chez les plantes transgéniques (Sade *et al.*, 2009). L'augmentation du diamètre des vaisseaux du xylème a quant à elle un effet activateur sur la conductance axiale (Rishmawi *et al.*, 2023). Chez le blé, une réduction de la surface des vaisseaux du xylème a été associée à une limitation de l'utilisation de l'eau et une meilleure tolérance au stress hydrique (Richards and Passioura, 1989).

La demande en eau dépend de la capacité des parties aériennes à évaporer cette eau dans l'atmosphère. Cette dernière dépend notamment de la surface foliaire, de la densité des stomates et du contrôle de leur ouverture (Figure 4). Des plantes de sorgho surexprimant des transporteurs d'auxine de type *PIN-FORMED* (*PIN1*, *2* et *4*) montrent une réduction de la taille de leur canopée. En réduisant leur demande en eau, ces plantes sont capables de maintenir leur transpiration plus longtemps durant un stress hydrique (Borrell *et al.*, 2022). D'ailleurs, une réponse rapide au stress hydrique chez de nombreuses céréales comme le maïs ou le riz consiste à réduire l'expansion foliaire pour atteindre ces mêmes objectifs d'économie en eau (Tardieu *et al.*, 2011). Au-delà de la morphologie des parties aériennes, des effecteurs endogènes peuvent influencer le fonctionnement stomatique pour moduler la transpiration. Des plantes de vigne anisohydriques montrent par exemple une conductance hydraulique

foliaire et des mouvements stomatiques relativement peu sensibles à l'acide abscissique par rapport à des plantes isohydrique (Coupel-Ledru *et al.*, 2016).

Le maintien du continuum sol-plante-atmosphère découle donc de nombreux processus en interactions à différents niveaux d'organisation de la plante, et ceci, en interaction avec l'environnement (Klein *et al.*, 2020; Strock and Lynch, 2020; Burridge *et al.*, 2022). Ces interactions doivent être prises en compte pour mieux comprendre les contreparties ou synergies de différents assemblages phénotypiques sur l'utilisation de l'eau dans différents scénarios de stress hydrique.

- **La plasticité phénotypique pour l'adaptation au stress hydrique**

Identifier le contrôle génétique de traits constitutifs améliorant la tolérance au stress hydrique est utile pour l'amélioration, mais n'est pas idéal dans le cas où ces derniers impliquent une contrepartie sur le rendement en condition irriguée. Des traits plastiques ont des états phénotypiques qui changent en fonction de l'environnement (Figure 5). Ces changements sont considérés comme adaptatifs s'ils sont associés au maintien des caractères agronomiques d'intérêt dans le nouvel environnement. Au contraire, la plasticité est considérée comme mal-adaptive si elle a un effet négatif sur les caractères agronomiques d'intérêt dans le nouvel environnement (Schneider, 2022). Idéalement, un caractère adaptatif en condition de sécheresse mais non adaptatif en condition irriguée serait plastique pour ne se manifester qu'en condition de stress hydrique. Considérons l'exemple d'un environnement à sols profonds où les pluies sont suffisamment abondantes en début de cycle pour humidifier le sol en profondeur, mais où un stress hydrique pendant la phase de floraison peut impacter les rendements de façon aléatoire d'une année sur l'autre. Une réponse plastique de croissance racinaire en profondeur durant le stress hydrique pourrait être adaptative dans cet environnement. En effet, elle permettrait un plus grand accès à l'eau au cours du stade critique de remplissage des grains. Néanmoins, au moins trois conditions devraient être réunies pour obtenir un effet adaptatif : un sol profond, des pluies abondantes en début de cycle et une sécheresse terminale. Les environnements dans lesquels la plasticité a des effets adaptatifs sont donc spécifiques. Cette plasticité pourra avoir des effets neutres ou mal-adaptifs dans d'autres environnements. De fait, la sélection variétale a privilégié des caractères constitutifs à effets stables sur les rendements à travers différents environnements, tandis que les mécanismes de plasticité ont été contre-sélectionnés (Figure 5; Welcker *et al.*, 2022). Mieux exploiter la plasticité adaptative représente donc un levier intéressant pour améliorer la tolérance au stress hydrique dans certains types d'environnement.

D'un point de vue évolutif, il est possible d'envisager que certaines plantes aient pu développer, en fonction de leur environnement, des réponses plastiques leur permettant de mieux tolérer le stress hydrique. Ainsi, l'expression de certains traits plastiques serait

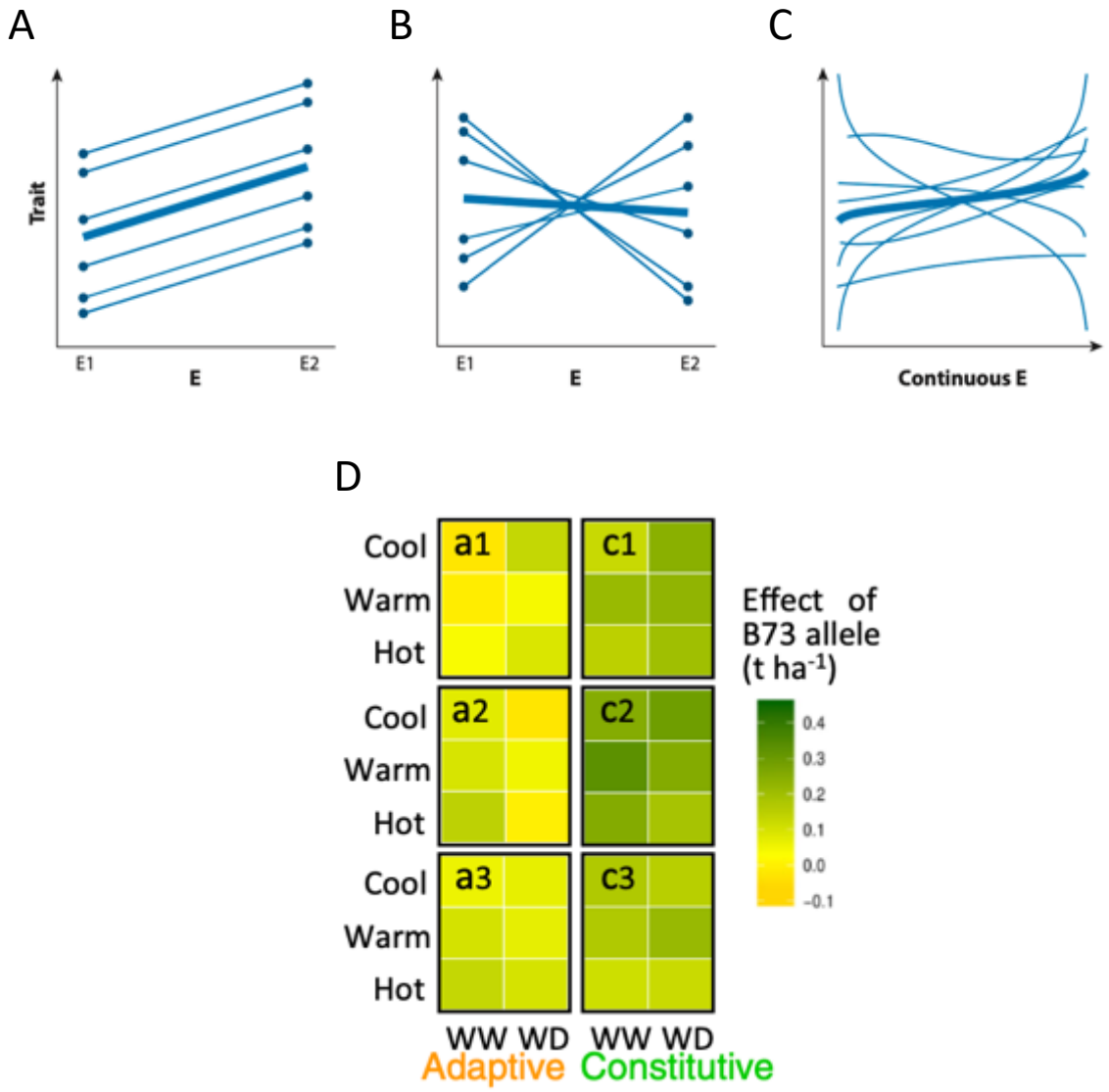

Figure 5 : Traits plastiques et effets sur les rendements chez le maïs. A-C: Une droite/courbe fine représente la variation d'un trait pour un génotype entre l'environnement 1 (E1) et l'environnement 2 (E2). La droite/courbe épaisse représente la réponse moyenne de tous les génotypes. Issues de Des Marais et al., 2013. A: Réponse plastique sans interaction entre le génotype et l'environnement. B: Réponse plastique avec interaction entre le génotype et l'environnement. C: Réponse plastique continue avec interaction entre le génotype et l'environnement. D: Effet des allèles a1, a2, a3, c1, c2 et c3 sur le rendement de la variété de maïs B73 cultivée en condition irriguée (WW) ou de stress hydrique (WD) dans différents environnements (cool, warm, hot). Les allèles a1, a2 et a3 contrôlent des traits plastiques tandis que les traits c1, c2 et c3 contrôlent des traits constitutifs. a1: associé à la synthèse d'ABA; a2: associé à la conductance stomatique; a3: associé à la tolérance aux fortes températures; c1: associé à l'architecture de la canopée; C2 et c3: associés au temps de floraison. Issue de Welcker et al., 2023 (Figure 9a).

contrôlée par l'interaction entre la génétique et l'environnement (G x E). Les racines qui se développent dans le sol, un environnement ou les ressources fluctuent de manière spatiale et temporelle, sont particulièrement plastiques. Par exemple, les racines d'*Arabidopsis thaliana* auront tendance à orienter leur croissance vers des zones plus humides du sol (hydrotropisme ; Shkolnik *et al.*, 2018). Le développement des racines latérales sera également privilégié dans des zones en contact avec un sol plus humide (« *hydropatterning* » ; Bao *et al.*, 2014; Orosa-Puente *et al.*, 2018). Chez *Setaria viridis*, le stress hydrique induit un arrêt du développement des racines coronaires (Sebastian *et al.*, 2016). Chez le mil, un développement racinaire plus profond a pu être observé en condition de stress hydrique (Faye *et al.*, 2019). Par ailleurs, des études récentes ont montré qu'il existe une grande diversité intra-spécifique dans la plasticité des traits racinaires architecturaux et anatomiques en réponse au stress hydrique chez le maïs et le riz (Sandhu *et al.*, 2016; Kadam *et al.*, 2017; Schneider *et al.*, 2020*a*,*b*). Ces études ont tenté d'identifier le contrôle génétique de la plasticité racinaire par des approches de génétique d'association. Néanmoins, un doute subsiste sur le fait que ces associations, supposées contrôler l'interaction G x E, soient réellement indépendantes du contrôle génétique du trait dans une condition donnée. De plus, le caractère adaptatif de ces réponses plastiques reste à démontrer.

- **Les racines, grandes oubliées de la sélection variétale**

Les racines se développent pour la grande majorité dans le sol ce qui limite grandement nos capacités à les observer et à étudier leur fonctions. De fait, l'étude des racines a souvent été réalisée hors-sol. Ces systèmes sont parfois très éloignés des conditions agronomiques et les mécanismes observés en condition contrôlée ont rarement pu être validés en condition agronomique. Il existe des méthodes de phénotypage de l'architecture, de l'anatomie et des fonctions racinaires en condition semi-agronomique et agronomique (Grondin *et al.*, 2022). Ces méthodes restent néanmoins peu applicables en sélection car elles sont sujettes à des débits de mesures relativement faibles, peuvent être peu accessibles et coûteuses, et sont peu représentatives du système global. Les racines ont donc été négligées en sélection variétale et l'amélioration de leurs fonctions hydrauliques représente un réel levier d'amélioration de la tolérance au stress hydrique. S'il reste encore difficile pour des sélectionneurs de concevoir des programmes de sélection ciblés sur des traits racinaires, des avancements récents en phénotypage et modélisation permettent d'envisager des approches de « *pre-breeding* ».

Phénotypage de l'architecture et de l'anatomie racinaire

Différentes méthodes existent afin de phénotyper des traits d'architecture racinaire en condition contrôlée (aéroponie, hydroponie, pots ou rhizotrons ; Atkinson *et al.*, 2019). Ces méthodes sont généralement limitées à l'étude de plantes jeunes. Les méthodes utilisées au champ permettent d'étudier des plantes plus matures (Figure 6). Elles diffèrent selon leur rapidité d'exécution, leur degré de technicité, les parties du système racinaire observées mais

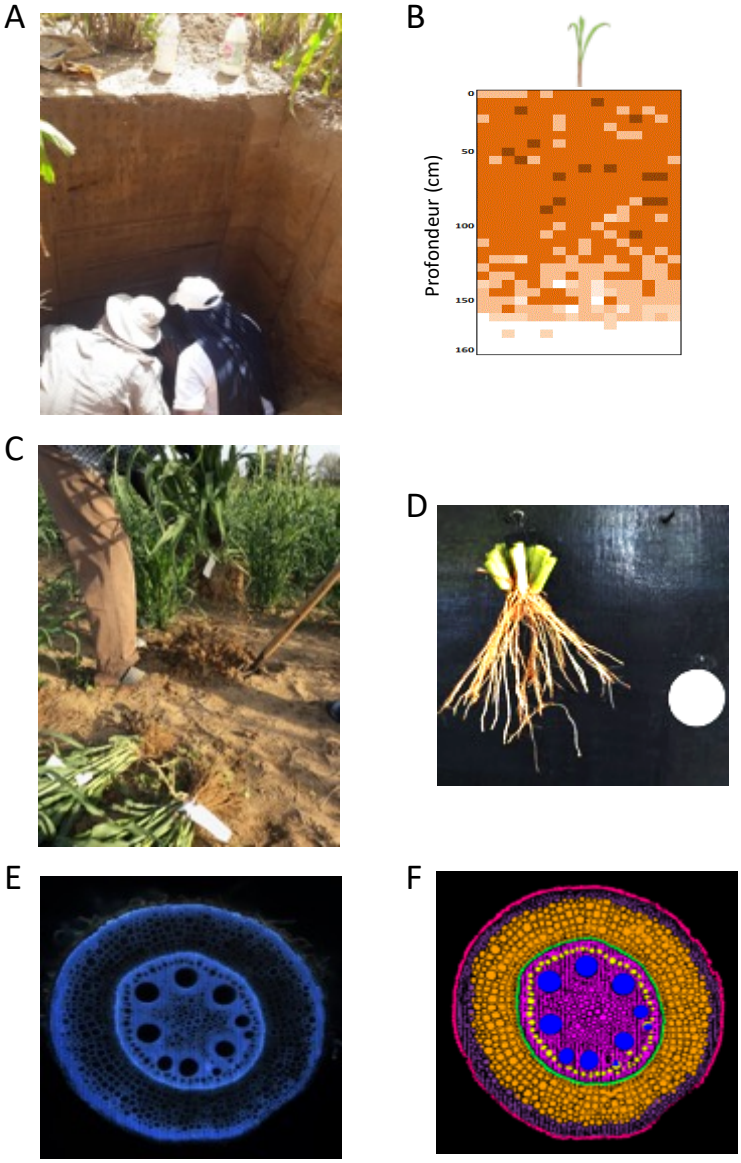

Figure 6 : Méthodes de phénotypage de l'architecture et de l'anatomie racinaire au champ. A: Tranchée de sol et comptage d'impact racinaires. Source: Laurent Laplaze. B: Modélisation de la densité de racinaire dans un profil de sol en fonction du nombre d'impact. Source: Awa Faye. C: Prélèvement racinaire par la méthode de *shovelomics*. Source: Jimmy Burridge. D: Imagerie de l'architecture racinaire après lavage de racines prélevées par *shovelomics*. Source: Alexandre Grondin. E: Imagerie de l'anatomie racinaire par tomographie à ablation laser (LAT). Image Darren Wells. F: Segmentation de tissus anatomiques sur images LAT. Source: Darren Wells.

toutes ne permettent qu'une observation partielle des racines (Grondin *et al.*, 2022). La méthode de comptage d'impacts sur une tranchée permet d'estimer par modélisation la densité de longueur racinaire (Chopart and Siband, 1999). Cette méthode permet l'observation la plus complète au champ des architectures racinaires. Elle est néanmoins difficile à mettre en œuvre. A l'inverse, la *shovelomics* (« pelle » - omique en français) est une méthode simple rapide mais peu résolutive. En effet, elle consiste à déterrer le système racinaire dans sa partie superficielle (20-30 premier cm) et à étudier des traits d'architecture comme l'angle racinaire, le nombre de racines ou la ramification racinaire (Trachsel *et al.*, 2011). La mesure de ces traits est néanmoins très robuste et certains peuvent représenter des proxys pour la mesure d'autres traits non mesurés (Burridge *et al.*, 2016; Schneider *et al.*, 2020*b*). Chez le maïs, la mesure de l'angle racinaire pourrait par exemple représenter un proxy de la profondeur racinaire (Schneider *et al.*, 2021). Plus récemment, la *shovelomics* a été utilisée pour l'étude de l'anatomie racinaire à haut-débit à l'aide d'une méthode de tomographie après ablation laser (LAT ; Strock *et al.*, 2022). La méthode LAT consiste à sectionner et à capturer une image d'une section transversale de la racine en utilisant l'auto-fluorescence des tissus de manière quasi-simultanée. La segmentation des images pour la quantification des traits anatomiques peut ensuite être rapidement effectuée par des logiciels exploitant l'intelligence artificielle (Hall and Lanba, 2019).

Phénotypage de l'hydraulique racinaire

Les capacités de transport d'eau du système racinaire sont traditionnellement mesurées par pressurisation des racines et mesure du flux de sève exsudé au niveau de la tige après décapitation des parties aériennes. Cette méthode a été très utilisée afin de déterminer la contribution des aquaporines dans la conductivité hydraulique racinaire (Postaire *et al.*, 2010). Elle permet de mesurer la capacité intrinsèque du système racinaire à transporter l'eau mais ne reflète pas la contribution de ce système dans le continuum sol-plante-atmosphère. D'autres méthodes comme l'imagerie neutron permettent de mesurer la capture d'eau à l'interface sol-racine. Cette méthode consiste à soumettre un échantillon à un faisceau à neutron. Le signal non absorbé est ensuite récolté à l'aide d'un scintillateur et converti en lumière qui sera capturée par une caméra (Cai *et al.*, 2022). Cette méthode, encore peu utilisée car techniquement difficile à mettre en œuvre, a permis de caractériser les racinaires responsables de la capture d'eau chez le maïs (Ahmed *et al.*, 2018). Au champ, une technologie permettant de mesurer le contenu en eau du sol à travers sa résistance électrique représente un proxy pour la capture d'eau par les racines (Bacher *et al.*, 2023). Comme l'imagerie neutron, elle est difficile à mettre en œuvre.

La mesure des flux d'eau dans le continuum sol-plante-atmosphère consiste plus simplement à mesurer, par gravimétrie, la perte en eau d'un pot où pousse une plante dans un sol humide. Cette méthode est basée sur le principe de fonctionnement d'un lysimètre (Figure 7). Elle utilise des tubes PVC installés au champ et dont la taille et l'espacement permet à la plante de croitre dans un volume d'air et de sol comparable à celui qu'elle pourrait explorer en plein

A

B

C

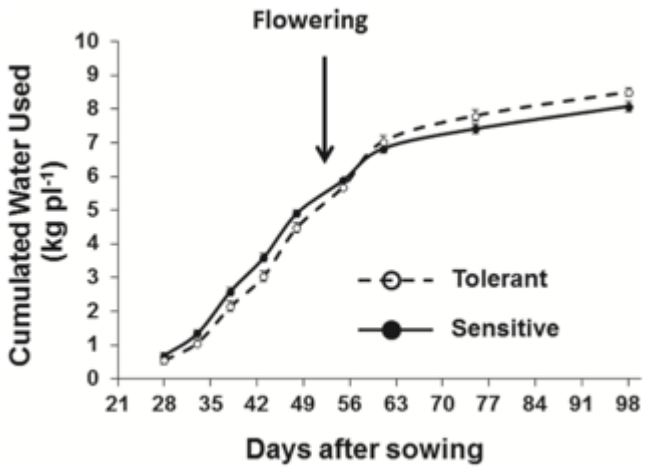

Figure 7 : Utilisation de lysimétres en condition semi-agronomique pour la mesure de l'utilisation de l'eau. A-B: Lysimètres en cours de pesée sur la plateforme lysimétrique de l'ICRISAT. Issues de Vadez et al., 2014 (Figure 1). C: Mesure de la quantité d'eau utilisée cumulée au cours du cycle chez une variété de pois chiche tolérante au stress hydrique et une variété de pois chiche sensible au stress hydrique. La variété tolérante utilise moins d'eau pendant sa phase végétative et plus d'eau pendant sa phase reproductive. Cette réponse serait liée à la stratégie de restriction de la transpiration en réponse à la demande évaporative. Issue de Vadez et al., 2014 (Figure 5).

champ (Vadez *et al.*, 2014). La mesure de la perte en eau des pots permet de mesurer l'eau transpirée par la plante depuis l'état de plantule jusqu'à la maturité. Cette méthode permet également de mesurer avec précision et sur la durée du cycle l'efficience de la transpiration qui est le ratio entre la biomasse et l'eau totale transpirée. L'efficience de la transpiration représente l'efficience de l'utilisation de l'eau à l'échelle de la plante entière. Elle est une alternative à la mesure de l'efficience d'utilisation de l'eau par la discrimination isotopique du carbone. Elle est également plus intégrative que la mesure instantanée de l'efficience d'utilisation intrinsèque de l'eau (assimilation en carbone / transpiration ; Vadez *et al.*, 2014). Des systèmes similaires utilisant des pots plus petits où le suivi de la dynamique de croissance des parties aériennes est possible par imagerie existent en serre (Cabrera-Bosquet *et al.*, 2016) ou au champ (Vadez *et al.*, 2015).

Modélisation du développement et des fonctions racinaires

Le fonctionnement des racines intègre un ensemble de caractéristiques architecturales, anatomiques et fonctionnelles dans un espace de sol où les ressources peuvent être fluctuantes. Des approches empiriques ont permis de mettre en évidence des interactions entre traits en condition de stress hydrique (Klein *et al.*, 2020). Néanmoins, le nombre limité de traits et d'environnements étudiés affecte la bonne compréhension de ces interactions. La modélisation permet de prédire les effets de traits multiples dans un grand nombre de scénarios. Les effets prédits sur les processus physiologiques sont néanmoins limités au niveau d'intégration pris en compte par le modèle. Des modèles structure-fonction ont été développés pour étudier l'effet de l'anatomie racinaire sur l'hydraulique à l'échelle cellulaire. MECHA (Couvreur *et al.*, 2018) ou GRANAR (Heymans *et al.*, 2020) permettent d'étudier la modulation de l'hydraulique d'un ou plusieurs tissus sur la conductance radiale. A un niveau d'intégration supérieur, des modèles considèrent l'architecture racinaire pour prédire l'hydraulique de la racine. Ces modèles sont moins résolutifs d'un point de vue anatomique car la conductance radiale n'y est pas considérée à l'échelle de la cellule. Ils permettent néanmoins de prédire l'effet de la ramification, du diamètre des racines ou de la taille des vaisseaux sur la conductance d'un système racinaire (Boursiac *et al.*, 2022). Le modèle *OpenSimRoot* est un modèle de ce type qui intègre en plus un modèle de sol (Figure 8; Postma *et al.*, 2017). Ce modèle est également capable de simuler la croissance des parties aériennes grâce à un module de partition du carbone. Il permet ainsi de prédire, en fonction du type de sol et de sa quantité en eau et en nutriments, l'effet de différents types d'architecture sur la nutrition hydrominérale et la croissance des parties aériennes (Ajmera *et al.*, 2022; Schäfer *et al.*, 2022).

Des modèles de culture qui capturent à la fois les informations agronomiques et physiologiques ont été mis au point chez certaines céréales comme le maïs (APSIM *maize* ; Hammer *et al.*, 2010), le sorgho (APSIM *sorghum* ; Ravi Kumar *et al.*, 2009) ou le blé (*SiriusQuality* ; Martre *et al.*, 2006). Ils permettent de simuler le développement, la croissance et les rendements en grain en fonction de l'environnement pédoclimatique de culture et des

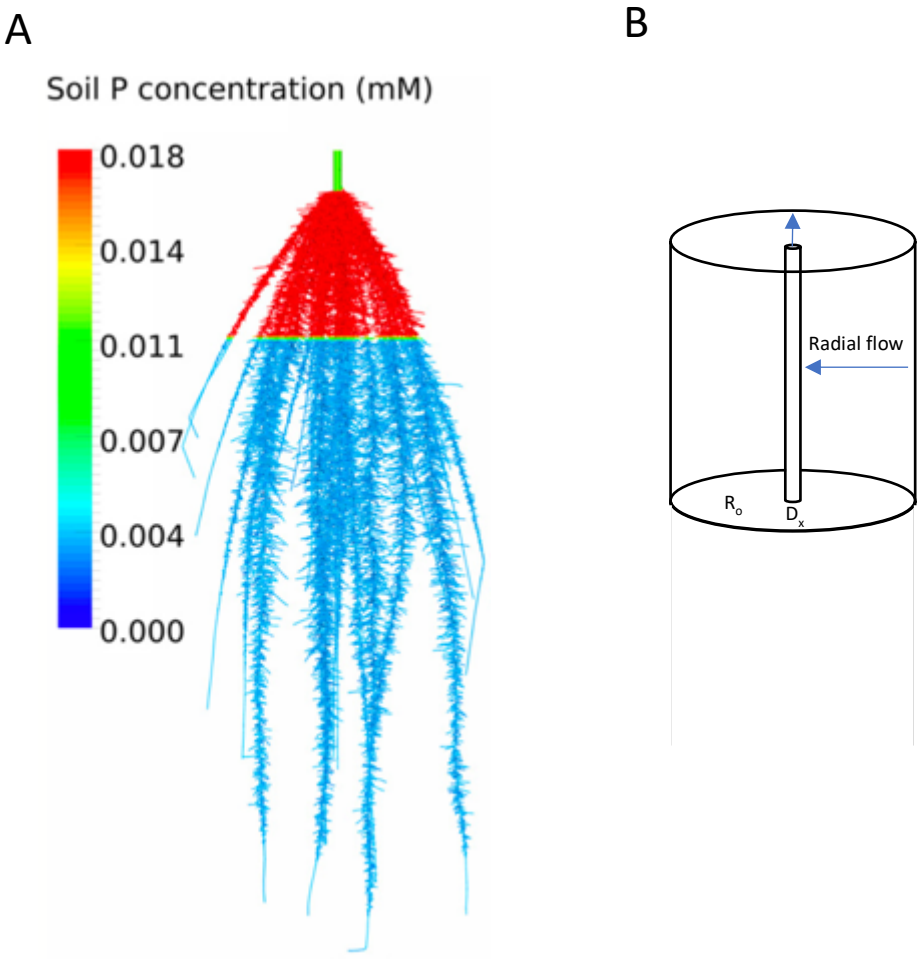

Figure 8 : Modèle *OpenSimRoot* pour la modélisation des fonctions racinaires. A: simulation de l'architecture raicinaire d'une plante de maïs dans un sol où la disponibilité du phosphore (P) est élevée en surface. Issue de Postma et al., 2017 (Figure 5). B: Représentation schématique de la modélisation continue à travers un segment de racine pour l'acquisition et du transport de phosphore dans le modèle *OpenSimRoot*. R_o: rayon de la racine; D_x: diamètre du xylème. Reproduction à partir de Postma et al., 2017 (Figure 4b).

pratiques agronomiques. Chez le sorgho, APSIM a par exemple été utilisé afin de simuler l'effet de différentes stratégies d'utilisation de l'eau sur la résilience des rendements à des stress hydriques imposés à différent stades du développement (Kholová *et al.*, 2014). Chez le blé, l'utilisation d'APSIM a suggéré que l'augmentation de la densité racinaire en profondeur permettrait un meilleur accès à l'eau au stade de floraison et une meilleure résilience du rendement en condition de stress hydrique (Manschadi *et al.*, 2006). Ces prédictions ont pu être confirmées au champ (Kirkegaard *et al.*, 2007). Ces modèles doivent néanmoins encore être améliorés pour mieux prendre en compte des caractéristiques physiologiques plus fines (Jarvis *et al.*, 2022). Ils ne prennent par exemple pas en compte le fonctionnement hydraulique racinaire. Combiner des modèles structure-fonction du système racinaire avec des modèles de culture représente un enjeux majeur pour mieux comprendre les mécanismes physiologiques impliqués dans le contrôle de l'utilisation de l'eau en condition de stress hydrique (Chenu *et al.*, 2017).

3.2 Objectifs de mes recherches

- **Problématique**

De nombreuses études ont permis de décrypter les réponses moléculaires et hormonales des plantes en condition de stress hydrique (Todaka *et al.*, 2015; Liu *et al.*, 2023). D'autres études ont décrit des mécanismes physiologiques qui seraient impliqués dans la tolérance à ce stress et ont identifié le contrôle génétique de certains de ces mécanismes (Langridge and Reynolds, 2015). On peut néanmoins se demander quel a été l'impact de ces recherches sur la sélection de variétés améliorées pour la tolérance au stress hydrique. Partant du principe que la tolérance au stress hydrique est particulièrement complexe, la sélection a été principalement guidée par la sélection directe pour le rendement en condition de stress hydrique (Swamy *et al.*, 2013). Certains de ces QTL identifiés pour le maintien du rendement en condition de stress hydrique peuvent colocaliser avec des QTL contrôlant des mécanismes de tolérance à ce stress. Chez le mil par exemple, des QTL contrôlant des traits associés à l'économie en eau du sol co-localisent avec un QTL majeur associé au rendement sous stress hydrique terminal (Kholová *et al.*, 2012). De plus, certains QTL identifiés comme contrôlant des traits cibles peuvent déjà être présents dans la majorité du matériel élite. C'est par exemple le cas du QTL *DRO1* contrôlant la profondeur racinaire chez le riz (A. Henry communication personnelle). On peut néanmoins citer au moins trois exemples où une sélection ciblée sur des traits a permis d'améliorer la tolérance au stress hydrique dans des contextes spécifiques : des QTL contrôlant la capacité à retarder la senescence des feuilles après la floraison (*stay green*) chez le sorgho (Harris *et al.*, 2007), (2) des QTL contrôlant la conservation de l'eau dans le sol via des mécanismes de restriction de la transpiration chez le maïs (Cooper *et al.*, 2014; Messina *et al.*, 2015), et (3) des QTL contrôlant la taille du métaxylème chez le blé (Richards and Passioura, 1989). Ces exemples représentent des preuves de concept de l'utilité des traits adaptatifs pour la sélection. Il est donc utile et nécessaire d'identifier de nouveaux traits adaptatifs impliqués dans l'adaptation des céréales aux stress et les déterminants génétiques

qui les contrôlent. Ces recherches fondamentales mais à but appliquées permettront d'appuyer et de guider la sélection.

L'effet variable que peut avoir les QTL contrôlant des traits adaptatifs représente néanmoins un frein pour leur prise en compte par la sélection variétale (Welcker *et al.*, 2022). En fonction de l'environnement, un caractère adaptatif pour le stress hydrique pourra avoir des effets positifs ou négatifs sur les rendements. Par exemple, une stratégie conservative et constitutive consistant à réduire la densité stomatique pour économiser l'eau engendrera une baisse de la biomasse en absence de stress (Dunn *et al.*, 2019). Une meilleure compréhension de la plasticité adaptative en réponse au stress hydrique et des contextes dans lesquels ces mécanismes pourraient avoir un effet bénéfique est nécessaire. Cela implique la mise en place d'expérimentations au plus proche des conditions agronomiques, dans différents environnements et sur un matériel génétique facilement utilisable par les sélectionneurs. L'enjeux actuel consiste également à développer des nouvelles méthodologies permettant de mieux appréhender les fonctions racinaires d'acquisition et de transport d'eau dans l'hydraulique de la plante entière.

Mon parcours m'a amené à m'intéresser dès mes stages de Master à l'hydraulique des plantes à travers l'étude de la fonction des aquaporines. Au cours de ces stages, j'ai étudié la régulation affectant l'activité de l'aquaporine PIP2;1 d'*A. thaliana* par des approches moléculaires et biochimiques. Au cours de ma thèse, j'ai étudié le rôle de cette aquaporine dans les mouvements stomatiques. La signification physiologique de la régulation de son activité par la phosphorylation dans le contexte de la fermeture stomatique en réponse à l'ABA a été étudiée par une approche de génétique fonctionnelle. J'ai effectué un post-doctorat à l'IRRI où j'ai développé mes compétences en termes de phénotypage au champ et commencé à mieux appréhender le rôle des racines dans la tolérance au stress hydrique. Au cours d'un deuxième post-doctorat à l'Université de Nebraska-Lincoln, j'ai continué à caractériser la réponse du riz au stress hydrique. Je me suis familiarisé avec des méthodes d'étude d'expression des gènes (séquençage des ARN), de phénotypage haut-débit en plateforme et de génétique (*Genome Wide Association Studies*, GWAS). En tant que chargé de recherche à l'IRD, j'étudie plus précisément le développement et le rôle des racines dans le contrôle de l'hydraulique de la plante entière et de sa gestion de la ressource en eau. Mes recherches s'effectuent, autant que faire se peut, dans un contexte de stress hydrique appliqué au champ ou assimilé.

L'objectif général de mon parcours de recherche a consisté à identifier et mieux comprendre des mécanismes développementaux ou physiologiques liés à l'hydraulique des plantes. De la compréhension fondamentale des processus hydrauliques dans la cellule de garde, j'ai tenté au fil des années d'orienter mes recherches vers l'amélioration variétale pour une meilleure tolérance des céréales au stress hydrique, avec un focus particulier sur les racines (Figure 9). Ainsi, j'ai contribué à répondre aux questions suivantes :

(1) Quels sont les traits d'architecture, d'anatomie ou fonctionnels racinaires et aériens permettant d'améliorer de la tolérance au stress hydrique et dans quels contextes ?
(2) Comment ces traits interagissent-ils entre eux et peuvent-ils avoir des effets synergiques pour l'amélioration de la tolérance au stress hydrique ?
(3) Ces traits sont-ils contrôlés par l'interaction G x E et si oui, dans quels contextes sont-ils adaptatifs ?
(4) Quels sont les déterminants génétiques contrôlant ces traits et sont-ils utilisables pour la sélection ?
(5) Comment ces traits affectent l'hydraulique des plantes et l'utilisation de l'eau ainsi que son efficience à travers le contrôle de la transpiration ?

- **Stratégie**

(1) Quels sont les traits d'architecture, d'anatomie ou fonctionnels racinaires et aériens permettant d'améliorer de la tolérance au stress hydrique et dans quels contextes ?

Il s'agit d'exploiter la diversité génétique pour des traits racinaires et aériens impliqués dans l'hydraulique et de mettre en lien ces traits avec la résilience du rendement en grain sous stress hydrique. Ces approches consistent à mettre au point des protocoles de phénotypage de traits racinaires dans de larges panels, à déployer des méthodes statistiques pour l'analyse des données et à mettre en association ces données.

(2) Comment ces traits interagissent-ils entre eux et peuvent-ils avoir des effets synergiques pour l'amélioration de la tolérance au stress hydrique ?

Il s'agit ici de développer et d'utiliser des modèles structure-fonction du système racinaire qui permettent de simuler les effets de traits multiples sur les fonctions racinaires et la production de biomasse. La comparaison des effets de combinaisons de traits sur la production de biomasse renseigne sur l'additivité, la synergie ou au contraire sur l'antagonisme entre traits.

(3) Ces traits sont-ils contrôlés par l'interaction G x E et si oui, dans quels contextes sont-ils adaptatifs ?

La réponse des traits à l'environnement est étudiée par le calcul d'indices de plasticité qui renseignent sur la variabilité du trait en fonction de l'environnement. Les traits étudiés pour leur plasticité sont ceux dont la variance est significativement contrôlée par l'interaction G x E, i.e. dont la réponse est différente entre les génotypes. La plasticité est mise en lien avec la résilience du rendement en grain sous stress hydrique pour identifier la plasticité adaptative.

(4) Quels sont les déterminants génétiques contrôlant ces traits et sont-ils utilisables pour la sélection ?

Des approches de génétique d'association sont utilisées afin d'identifier des QTL contrôlant les traits intéressants (1) et leur plasticité (3). Des gènes candidats dans ces régions QTL sont

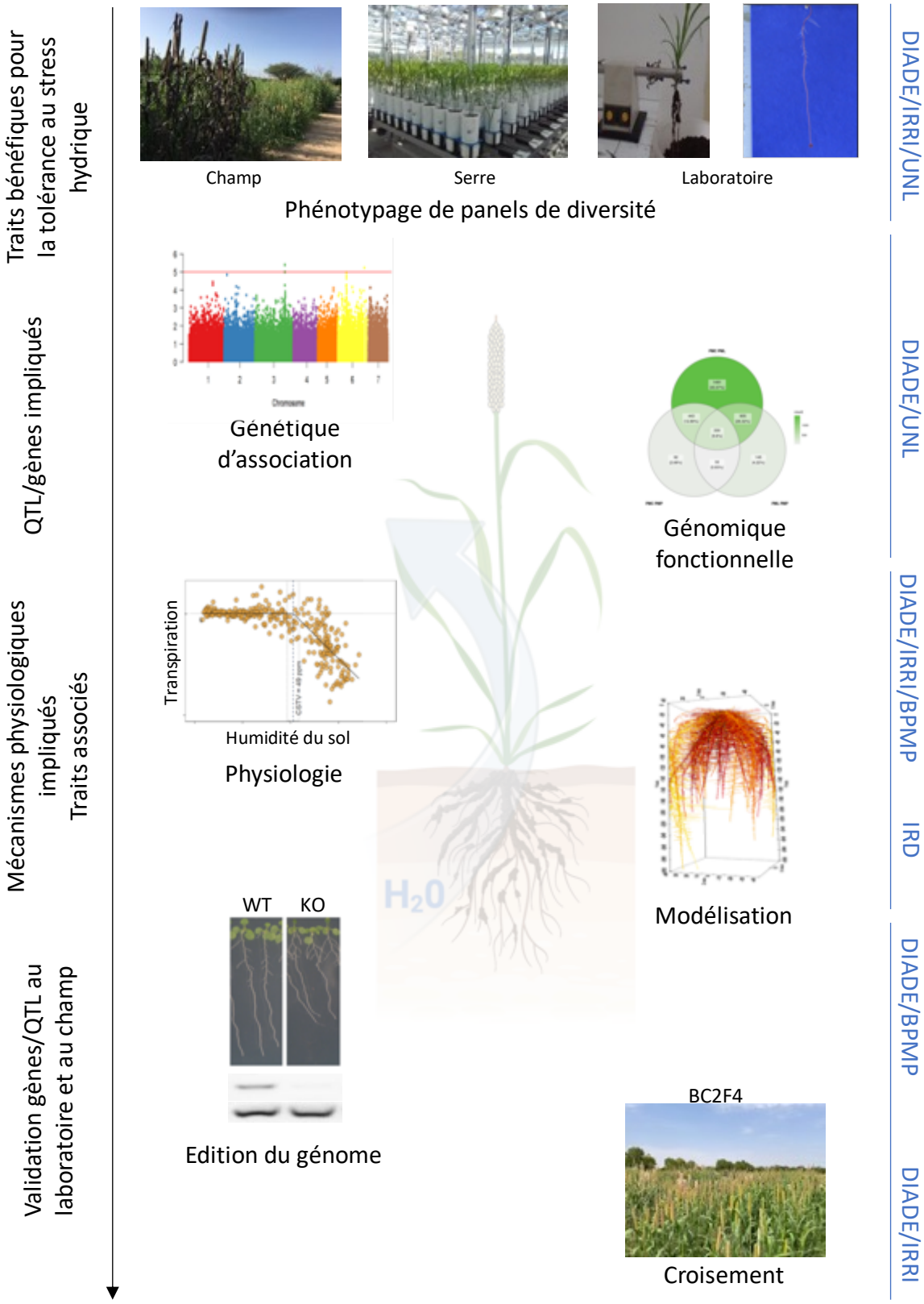

Figure 9 : Schéma des approches et des compétences acquises dans mon parcours de recherche, le fil conducteur étant une meilleure compréhension de l'hydraulique des plantes. DIADE: UMR DIversité Adaptation et DEveloppement des plantes; IRRI: International Rice Research Institute; UNL: University Nebraska-Lincoln; BPMP: UMR Biochimie & Physiologie des Plantes.

identifiés. Les analyses génétiques sont souvent couplées à des analyses d'expression des gènes afin de mieux cibler le gène candidat sous-jacent. Le gène candidat le plus intéressant peut faire l'objet d'une validation fonctionnelle afin de mieux comprendre les mécanismes physiologiques et moléculaires impliqués.

(5) *Comment ces traits affectent l'hydraulique des plantes et l'utilisation de l'eau ainsi que son efficience à travers le contrôle de la transpiration ?*

Le rôle de traits identifiés en (1), (2) et (3) dans l'hydraulique de la plante est étudié dans des sous-panels d'haplotype, de lignées recombinantes ou mutantes présentant des contrastes pour ces traits. Cela consiste généralement à mesurer la conductance hydrique racinaire, le statut hydrique des feuilles ou l'utilisation de l'eau et son efficience.

- **Modèles d'étude et enjeux**

Dans mon parcours, j'ai travaillé sur différentes espèces : *A. thaliana*, le riz (*O. sativa* et *O. glaberrima*) et le mil (*Pennisetum glaucum*). Mes travaux se concentrent actuellement sur le riz et le mil. Le riz *O. sativa* est la céréale modèle adaptée aux agrosystèmes tropicaux humides. Le riz *O. glaberrima* est plus adapté aux climats chauds et secs et représente une source intéressante d'allèles pour la tolérance aux stress abiotiques. Ce modèle riz permet la combinaison d'études génétiques et de génomique fonctionnelle pour la découverte de gènes important pour l'adaptation à au stress hydrique. Le mil est une céréale adaptée aux climats tropicaux arides. Il constitue un modèle pour une meilleure compréhension de l'adaptation des céréales à la sécheresse. Ces modèles ont donc leurs propres spécificités et les avancées bénéficient à l'un et l'autre grâce au transfert de technologies et à l'intégration des connaissances vers une compréhension globale des mécanismes de tolérance au stress hydrique. L'espère modèle *A. thaliana* reste aussi utilisée pour ses ressources génétiques qui permettent une première confirmation rapide de la fonction de gènes candidats de riz ou mil, et la caractérisation fine des mécanismes moléculaires impliqués (généralement au travers de collaborations).

Vers une culture du riz plus durable

Le riz est l'aliment de base pour plus de la moitié de la population mondiale. En Afrique de l'Ouest, le riz est devenu la céréale la plus consommée. Plusieurs pays de la sous-région, dont le Sénégal, développent des politiques visant à l'autosuffisance pour cette céréale. La riziculture en condition inondée est l'agrosystème le plus productif. Pourtant, ce système demande une grande quantité d'eau et engendre une importante production de gaz à effets de serre. Tout l'enjeu pour la riziculture consiste à faire sa transition d'un système de culture inondé anaérobie vers un système de culture irrigué ou pluvial aérobie tout aussi productif, cela afin de faire face à la raréfaction de la ressource en eau et de répondre aux objectifs d'une agriculture plus durable. Cela nécessite le développement de variétés mieux adaptées à la condition aérobie et au semis direct, i.e. plus vigoureuse pour mieux lutter contre les adventices, plus efficaces à transporter et utiliser l'eau et plus tolérantes face au stress

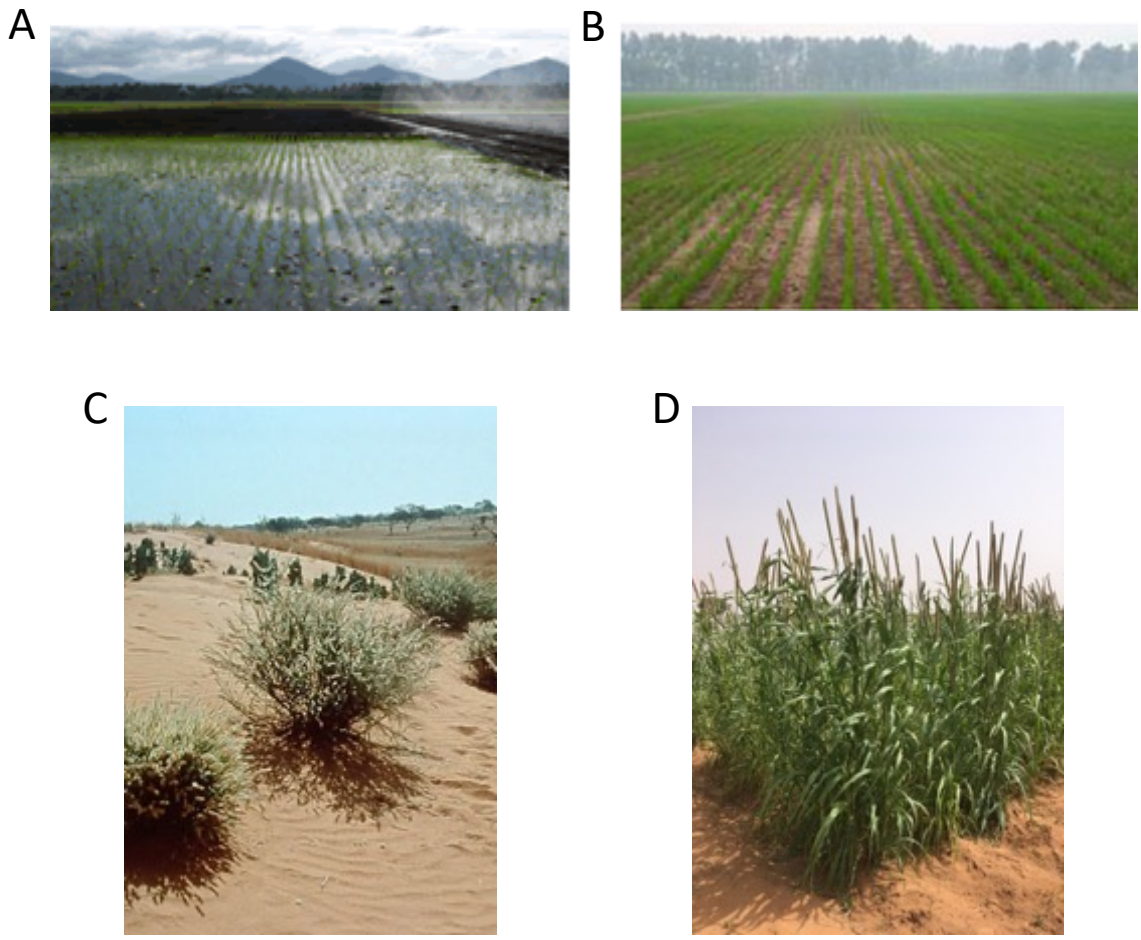

Figure 10 : Images de riz et mils. A: Culture du riz en condition inondée anaérobie. Image *Rice Knowledge Bank*. B: Culture du riz en condition aérobie. Source: *Rice Knowledge Bank.* C: Mils sauvages. Source: Yves Vigouroux. D: Variétés de mil améliorées cultivées à la station ICRISAT de Sadoré au Niger. Source: Alexandre Grondin.

hydrique (Figure 10). Nos études sont ciblées sur une meilleure compréhension de ces mécanismes.

Vers une culture du mil capable de mieux gérer la ressource en eau du sol
Le mil est une céréale importante pour la sécurité alimentaire dans les zones arides et semi-arides en Afrique et en Inde, où il représente une source importante de micronutriments et de protéines. Cette céréale est particulièrement tolérante au stress hydrique et aux fortes températures mais son rendement peut être fortement affecté par ce stress (Figure 10). Le mil est une céréale particulièrement plastique. L'enjeux est d'identifier la stratégie d'utilisation de l'eau la plus adaptée pour cette céréale en fonction du type de stress qu'elle peut subir. Le rôle des racines dans les mécanismes d'acquisition et de transport d'eau et de régulation de la transpiration en réponse à la demande évaporatoire représente notre cible d'étude.

- **Collaborations**

Tout au long de ma carrière, mes travaux ont bénéficié de collaborations nationales et internationales. Mes travaux de thèse ont été réalisés en collaboration avec Nathalie Leonhardt au CEA Cadarache et mes travaux de post-doctorat ont impliqué Vincent Vadez à l'ICRISAT en Inde, Philip Benfey à l'Université de Duke aux États-Unis et Bettina Berger du *Plant Accelerator* à l'Université d'Adélaïde en Australie. Dans l'équipe CERES, j'ai profité d'un réseau de collaborations en France et à l'international qui avait été tissé avant mon arrivée et que je contribue à compléter (Figure 11). Il me permet d'envisager des approches multidisciplinaires qui vont au-delà de mes compétences propres, d'avoir accès à des outils innovants, et de remplir nos objectifs de recherche pour la durabilité et le développement.

Au sein de notre UMR, nous avons des collaborations fortes avec l'équipe DYNADIV, Yves Vigouroux et Philippe Cubry en particulier, qui nous apportent un soutien essentiel dans le domaine de la génétique du mil et du riz. Ils nous appuient pour la génération des données de génotypage et ont mis au point les scripts GWAS que nous utilisons. En France nous avons établis des collaborations avec certaines équipes du CIRAD de l'UMR AGAP qui travaillent sur des thématiques de recherche proche des nôtres. Nous collaborons par exemple avec l'équipe Développement adaptatif du riz et du sorgho que coordonne Christophe Perrin et qui s'intéresse aux processus de développement racinaire chez le riz. Pour mieux comprendre les mécanismes photosynthétiques potentiellement impliqués dans la vigueur précoce chez le riz nous avons entrepris une collaboration avec Anja Krieger-Liszkay de l'Institut des sciences du vivant Frédéric Joliot. Nous avons également initié une collaboration avec l'équipe Génétique et innovation variétale dirigée par David Pot afin d'identifier des traits racinaires pour la tolérance du sorgho au stress hydrique. Plus récemment, nous avons établi une collaboration avec Vincent Segura de l'équipe Diversité et Adaptation de la vigne qui est spécialiste en génétique quantitative et nous apporte un appui pour l'identification de QTL de G x E. Sur ces

approches nous collaborons également avec Mélisande Blein-Nicolas de l'équipe Biologie de l'Adaptation et Systèmes en Évolution (BASE) et Renaud Rincent de l'équipe Génétique Quantitative et Méthodologie de la Sélection (GQMS) qui font toutes les deux parties de l'UMR Génétique Quantitative et Évolution - Le Moulon (GQE). Dans cette même UMR, nous apportons aussi un soutien pour le phénotypage racinaire à l'équipe Génomique Évolutive et Adaptation des plantes Domestiquées (GEvAD) dirigée par Maud Tenaillon qui étudie le rôle des racines dans l'adaptation de la culture de maïs et de haricot en association. Pour le développement d'outils de mesure innovants de l'hydraulique des plantes nous collaborons avec les physiciens Christophe Goze-Bac et Eric Nativel du Laboratoire Charles Coulomb de l'Université de Montpellier.

A l'international, nous entretenons des collaborations fortes avec Malcolm Bennett et Darren Wells de l'Université de Nottingham au Royaume-Uni qui nous apportent un appui sur le phénotypage racinaire (LAT notamment). Nous collaborons avec Jeongmin Choi du *Crop Science Center* à l'Université de Cambridge sur les effets de la symbiose mycorhizienne chez le riz. Nous collaborons également avec Jonathan Lynch de l'Université de Penn State aux États-Unis sur la modélisation structure-fonction du système racinaire et Hannah Schneider du *Leibniz Institute of Plant Genetics and Crop Plant Research* (IPK) en Allemagne sur les aspects de plasticité racinaire. Nous avons aussi des liens précieux avec les centres internationaux, Prakash Gangashetty et Mohammaed Riyazaddin à l'ICRISAT, Amelia Henry et Damien Platten à l'IRRI, Baboucarr Manneh à l'AfricaRice, qui nous fournissent du matériel génétique, nous apportent un appui sur l'expérimentation au champ et un lien direct avec les sélectionneurs.

Enfin et surtout, ma mission de chercheur à l'IRD m'amène à développer des collaborations fortes avec des universités et centres de recherche de pays situés en zone tropicale et subtropicale. Au Sénégal, nous collaborons de manière pérenne avec Aboubacry Kane et Abdala Gamby Diedhiou du Département de Biologie Végétale de l'UCAD sur des projets cherchant à caractériser les effets de la symbiose endomycorhizienne sur la tolérance à la sécheresse chez le riz. J'ai été expatrié 4 ans à l'ISRA-CERAAS de Thiès où j'ai eu des collaborations proches avec des sélectionneurs dont Ghislain Kanfany (maintenant à l'Université Gaston Berger de St-Louis) pour le mil et Cyril Diatta pour le sorgho, des physiologistes dont Bassirou Sine, des génomiciens dont Ndjido Kane et des agronomes dont Aliou Faye. Ces collaborations nous permettent de réaliser des expérimentations au champ, d'avoir accès à des ressources génétiques et de mieux comprendre les contextes et enjeux locaux à prendre en compte dans nos recherches. Nous collaborons aussi avec l'AGI à Hanoi sur la caractérisation des déterminants contrôlant l'anatomie racinaire dans une collection de riz vietnamienne.

- France

- Grande-Bretagne

- Allemagne

- États-Unies

- Sénégal

- Vietnam

- Centre CGIAR

Figure 11 : Collaborations avec les Universités et Instituts de recherche en France et à l'étranger.

4. Activités de recherche (2005-2023)

4.1 Fonction des aquaporines dans l'hydraulique des plantes

Les aquaporines sont des canaux facilitant la diffusion de l'eau et d'autres petites molécules neutres au travers des membranes biologiques (Figure 12; Maurel *et al.*, 2015). Les plantes supérieures possèdent une trentaine d'isoforme d'aquaporine qui se répartissent en cinq sous-familles : les *Plasma Membrane Intrinsic Proteins* (PIP), les *Tonoplast Intrinsic Proteins* (TIP), les *Nodulin26-like Intrinsic Proteins* (NIP), les *Small Intrinsic Proteins* (SIP) et les *uncharacterized (X) Intrinsic Proteins* (XIP ; Maurel *et al.*, 2015).

Les PIP, présentes sur les membranes plasmiques, sont les isoformes les plus étudiées et un rôle pour ces protéines dans de nombreux processus physiologiques a pu être démontré. Dans les racines, elles contribuent significativement au transport radial de l'eau depuis les cellules de l'épiderme jusqu'aux vaisseaux du xylème (Figure 12; Postaire *et al.*, 2010). Dans les feuilles, elles participent aux flux d'eau des cellules de la gaine périvasculaire jusqu'aux cellules du mésophylle en contact avec la chambre sous-stomatique (Postaire *et al.*, 2010). Plus récemment, leur rôle dans le transport et la signalisation de l'H_2O_2 a pu être démontré (Rodrigues *et al.*, 2017). Les PIP sont aussi impliquées dans le transport de CO_2 et facilitent la diffusion de ce dernier des espaces intercellulaires du mésophylle foliaire vers les sites d'action de la Rubisco dans les choloroplastes (Ermakova *et al.*, 2021). La fonction des PIP est régulée de façon transcriptionnelle et post-traductionnelle par le stress hydrique, notamment à travers des signaux hormonaux impliquant l'acide abscissique et l'auxine (Maurel *et al.*, 2015).

Je me suis intéressé à la fonction des aquaporines dans le transport d'eau, à l'échelle de la protéine (travail de Master), de la cellule (travail de thèse), de l'organe et de la plante entière (travail de post-doc jusqu'à maintenant). Ces travaux ont abouti à la publication de 6 articles dont trois articles en premier auteur.

- **Fonctionnalité de la protéine *At*PIP2;1**

L'activité de transport d'eau des PIP est contrôlée par le pH, le calcium et la phosphorylation (Johansson *et al.*, 1998; Gerbeau *et al.*, 2002; Tournaire-Roux *et al.*, 2003; Maurel *et al.*, 2008). La caractérisation de la structure tridimensionnelle de l'aquaporine PIP2;1 d'épinard a permis de décrypter les mécanismes moléculaires impliqués dans ces régulations (Törnroth-Horsefield *et al.*, 2006). Le modèle structure-fonction a décrit le mouvement de la boucle cytosolique D de la protéine comme contrôlant l'ouverture du pore des PIP et a suggéré le rôle de certains résidus pour la stabilisation de cette boucle dans un état ouvert ou fermé (Figure 13; Törnroth-Horsefield *et al.*, 2006).
Nous avons entrepris de valider fonctionnellement ces prédictions au cours de mes stages de Master réalisés sous la direction de Lionel Verdoucq et Christophe Maurel dans l'équipe

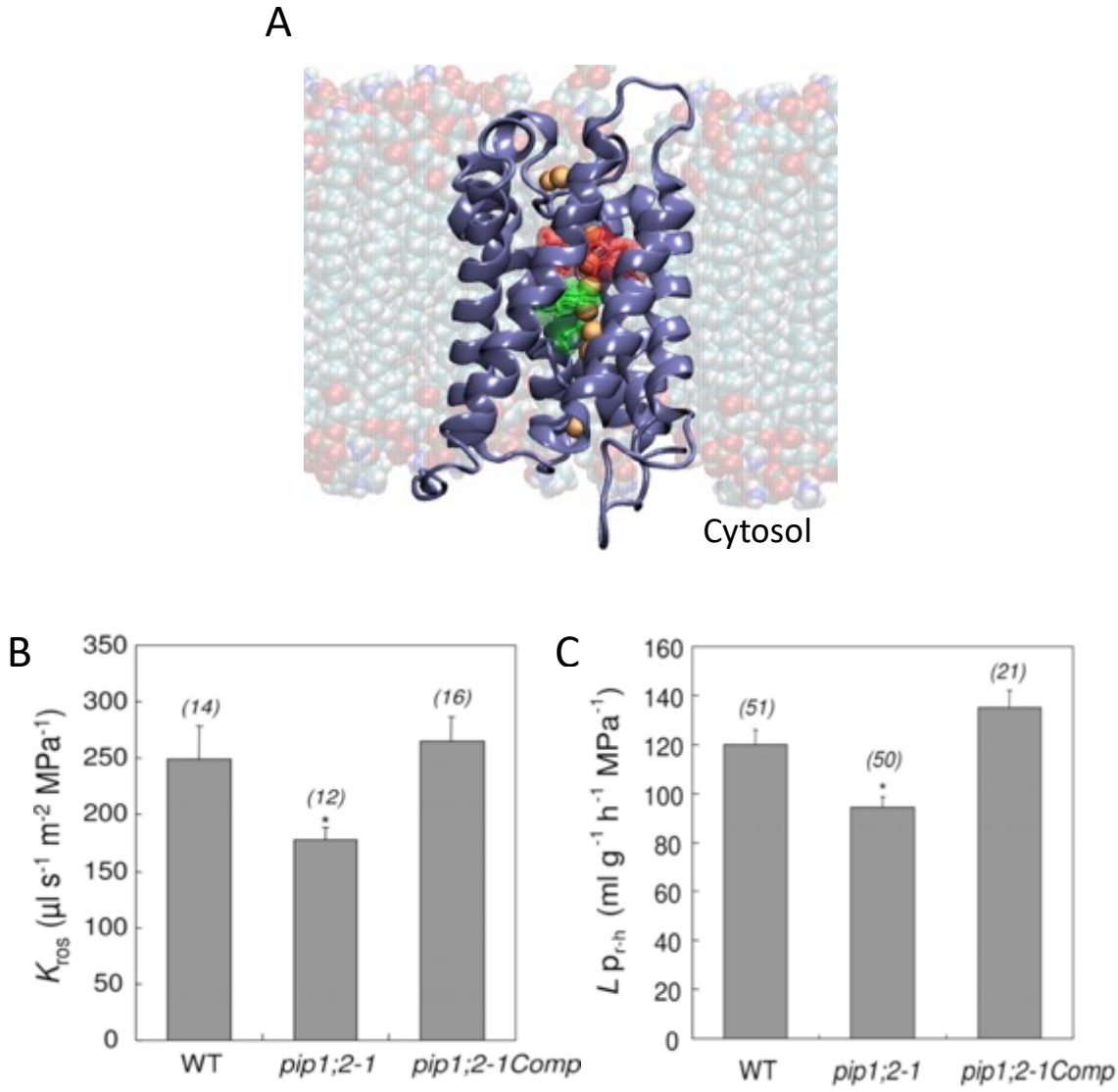

Figure 12 : Structure tridimensionnelle d'une aquaporine et fonction dans le transport d'eau. A: Aquaporine PIP2;1 d'épinard (violet) enchâssée dans la membrane plasmique. Les résidus responsables du filtre de sélectivité sont colorés en rouge et vert. Les molécules d'eau sont représentées en jaune. Issue de Maurel et al., 2008 (Figure 1). B-C: Conductivité hydraulique de la rosette (B, Kros) et de la racine (C, Lpr-h) de plantes d'*A. thaliana* sauvages (WT), mutantes pertes de fonction pour l'aquaporine PIP1-2 (*pip1;2-1*) et mutantes *pip1;2-1* complémentées par le gène *PIP1;2*. Issues de Postaire et al., 2011 (Figures 3 et 8).

aquaporines de l'UMR B&PMP. La stratégie a consisté à produire des protéines PIP2;1 d'*A. thaliana* sauvages où mutantes sur des sites prédits comme important pour sa régulation et d'étudier leur perméabilité en protéoliposomes à l'aide d'un spectrophotomètre à flux interrompu.

La surexpression chez *P. pastoris*, a permis de produire en quantité suffisante certaines formes d'PIP2;1. La perméabilité des protéoliposomes reconstitués avec la protéine PIP2;1 sauvage mesurée à différents pH et concentrations en calcium a permis de confirmer l'effet inhibiteur de ces effecteurs et d'affiner la gamme de sensibilité de la protéine. Ces mêmes expérimentations menées sur les formes mutantes ont permis de clarifier les mécanismes moléculaires impliqués dans la stabilisation du pore en configuration fermée lors de la baisse du pH. La protonation d'une histidine de la boucle D stabilise le pore dans une configuration fermée à travers la formation de ponts salins avec un glutamate et une asparagine de l'extrémité N-terminale. Ces mêmes résidus glutamate et asparagine sont capables de fixer le calcium ainsi que d'autres cations divalents comme manganèse ou le cadmium. Cela stabilise la boucle D en configuration fermée à travers la formation de ponts salins entre le glutamate de l'extrémité N-terminale, une arginine située sur la boucle B et l'histidine de la boucle D. De façon intéressante, la mutation de l'arginine ne modifie pas la sensibilité au pH indiquant que ce résidu est spécifiquement impliqué dans la réponse aux cations divalents. Ces résultats ont permis d'identifier des formes mutantes de PIP2;1 utiles pour mieux comprendre la signification physiologique de sa régulation par ces différents effecteurs dans la plante. L'ensemble de ces résultats a fait l'objet d'une publication dans la revue *Biomechical Journal* (Verdoucq *et al.*, 2008).

- **Fonction des aquaporines dans le contrôle des mouvements stomatiques chez *A. thaliana***

Les mouvements stomatiques sont dus à des changements de volume important des cellules de garde. L'ouverture est associée à un influx d'eau et au gonflement des cellules de garde. La fermeture est associée à un efflux d'eau et à la perte de turgescence des cellules de garde (Maurel *et al.*, 2016; Jezek and Blatt, 2017). Un rôle des aquaporines avait été proposé dans ces processus mais n'avait jamais été démontré. Mon travail de thèse a consisté à mieux comprendre la fonction des aquaporines PIP1;2 et PIP2;1 dans le fonctionnement stomatique chez *A. thaliana*. Les mouvements stomatiques de mutants *pip1;2* et *pip2;1* ont été étudiés en réponse à différents stimuli sur des épidermes isolés, en comparaison avec ceux de plantes sauvages. Ces expérimentations ont montré les mutants *pip1;2* et *pip2;1* ne montraient pas de défaut d'ouverture stomatique en réponse à la lumière et à de fortes concentrations de CO_2. De plus, aucun défaut de fermeture stomatique en réponse à l'obscurité n'a été observé. Par contre, ces mutants montrent un défaut de fermeture stomatique en réponse à l'ABA. Ces résultats suggérent qu'PIP1;2 et PIP2;1 participent spécifiquement à l'efflux d'eau des cellules de garde en réponse à l'ABA. Toutes ces mesures ont été réalisées au CEA Cadarache en collaboration avec Nathalie Leonhardt.

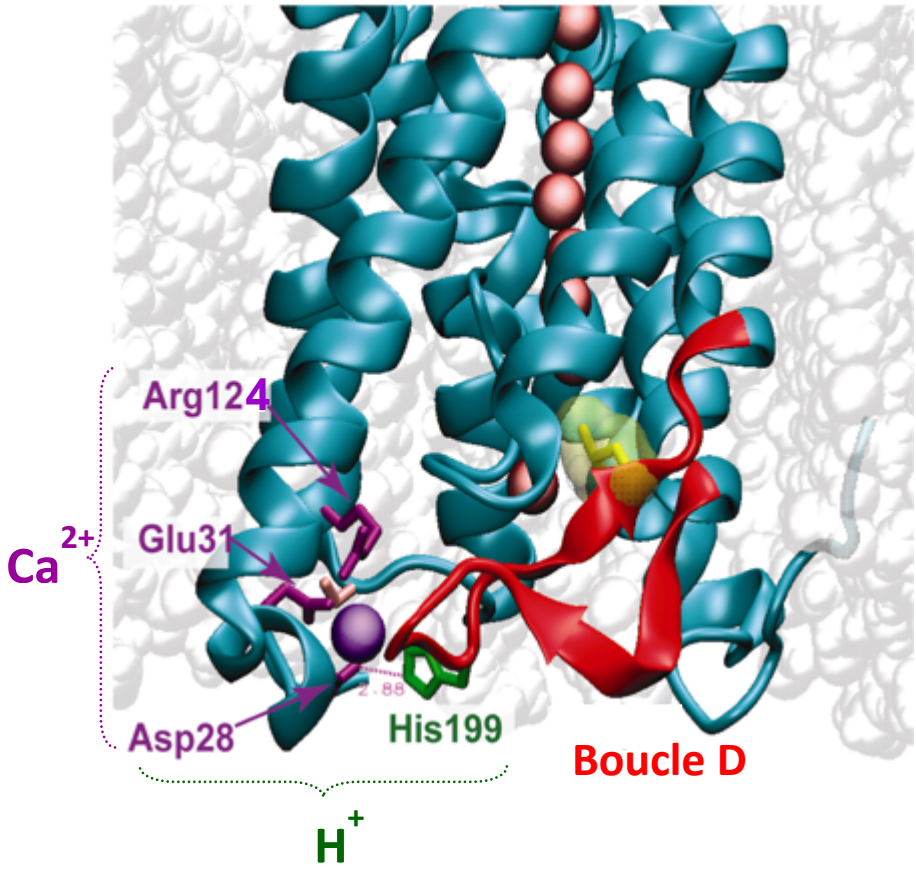

Figure 13 : Mécanismes de régulation de l'activité de l'aquaporine PIP2;1 d'épinard par le pH et les ions divalents. La boucle D est représentée en rouge. Les molécules d'eau sont représentées à l'intérieur du pore. Le calcium est représentée en violet. Issue de Maurel et al., 2008 (Figure 3b).

Afin d'étudier si l'ABA était capable d'induire un changement de l'activité de transport d'eau de PIP1;2 et PIP2;1, des mesures de perméabilité hydrique de protoplastes de cellules de garde ont été réalisées. Pour cela, j'ai bénéficié de l'aide de Raphael Morillon (CIRAD) qui avait mis au point une méthode de mesure de la perméabilité hydrique de protoplastes de cellules du mésophylle chez *A. thaliana* par imagerie sous microscope après un choc osmotique. Ces mesures ont montré que la perméabilité à l'eau de protoplastes de cellule de garde sauvage était induite en réponse à l'ABA. Cette réponse est perdue chez les mutants *pip1;2* et *pip2;1*, suggérant que l'augmentation de la perméabilité des cellules de garde en réponse à l'ABA est médiée par une activation de PIP1;2 et PIP2;1 (Figure 14).

La fermeture stomatique induite par l'ABA implique la production d'espèces réactives de l'oxygène (ROS) et notamment d'H_20_2 dans les parois des cellules de garde par l'effet combiné de NADPH oxydase (RbohF et RbohD) et de superoxide dismutase (Kwak *et al.*, 2003; Wang *et al.*, 2016). L'entrée d'H_20_2 dans les cellules de garde constitue un signal pour la poursuite de la cascade de signalisation induisant la fermeture stomatique. Des études suggéraient que PIP2;1 serait perméable à l'H_2O_2 (Dynowski *et al.*, 2008). Nous avons émis l'hypothèse selon laquelle PIP2;1 faciliterait le transfert d'H_2O_2 dans la cellule de garde lors de la fermeture stomatique en réponse à l'ABA. L'utilisation d'un marqueur fluorescent a permis de montrer que l'accumulation des ROS à l'intérieur des cellules de garde du mutant *pip2;1* était fortement perturbée en réponse à l'ABA. Ces résultats ont suggéré un rôle pour PIP2;1 dans le transport et la signalisation H_2O_2 médié par l'ABA conduisant à la fermeture stomatique. Olivier Rodrigues a, au cours de sa thèse, confirmé le rôle de PIP2;1 dans le transport et la signalisation H_2O_2 lors de la fermeture stomatique en réponse à la Flagellin22, une molécule simulant l'attaque d'un pathogène. Dans ce travail, un senseur fluorescent Hyper spécifique de l'H_2O_2 a été utilisé (Rodrigues *et al.*, 2017).

Open Stomata 1 (OST1/SnRK2.6) est une protéine kinase centrale pour la signalisation ABA dans la cellule de garde (Hsu *et al.*, 2021). Le site de phosphorylation en position 121 de PIP2;1 possède une séquence consensus reconnue par OST1 (Sirichandra *et al.*, 2010). Nous avons émis l'hypothèse que PIP2;1 pourrait, au cours de la cascade de signalisation ABA, être activée à la suite de sa phosphorylation par OST1. Olivier Rodrigues a montré qu'OST1 est en effet capable de phosphoryler PIP2;1 *in vitro* et d'activer son activité en ovocytes de xénope. De plus, l'expression d'une forme mutante de PIP2;1 déficiente vis-à-vis de la phosphorylation de la Serine 121 dans un fond mutant *pip2;1* est incapable de complémenter le phénotype du mutant, contrairement à la forme sauvage et à une forme mutante mimant une phosphorylation constitutive. L'ensemble des résultats montrent donc que la fermeture stomatique en réponse à l'ABA nécessite une augmentation de la perméabilité à l'eau et à l'H_2O_2 des cellules de garde induite par l'activation de PIP2;1 suite à sa phosphorylation par OST1 (Figure 14). Cette étude, qui a apporté les premières évidences du rôle des aquaporines

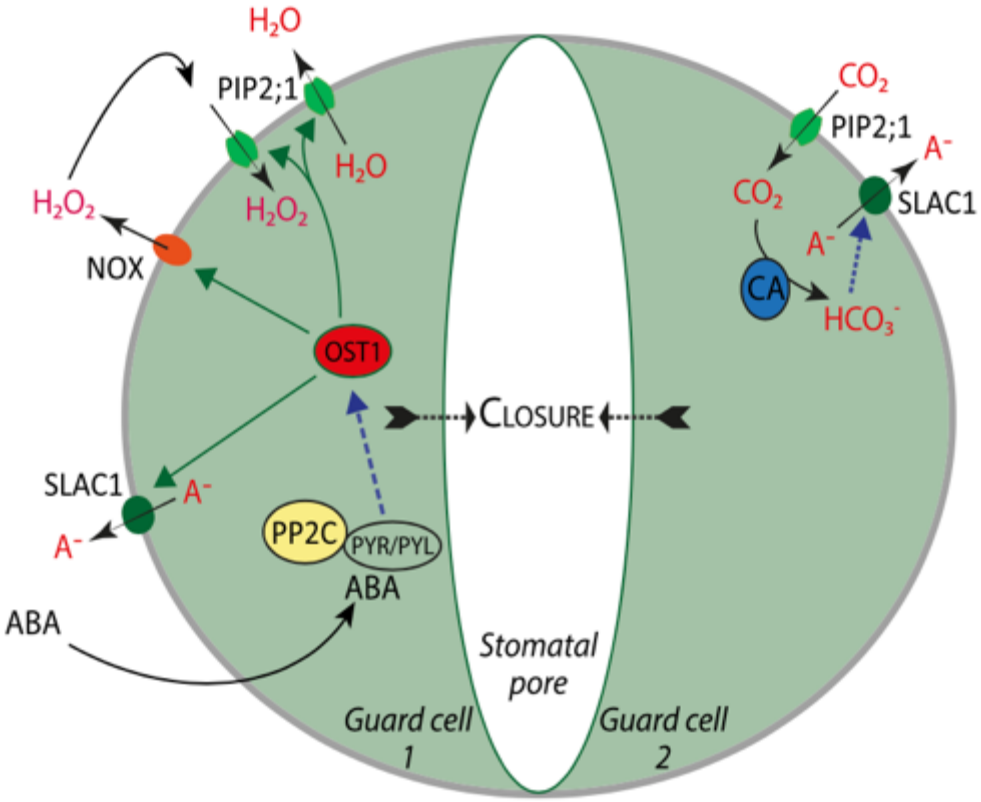

Figure 14 : Schéma simplifié de l'implication des aquaporines dans la fermeture stomatique induite par l'ABA et le CO_2 chez *A. thaliana*. En réponse à l'ABA, l'aquaporine PIP2;1 est activée après phosphorylation par OST1. PIP2;1 facilite l'entrée d'H_2O_2 dans la cellule de garde et l'efflux d'eau. PIP2;1 serait également impliquée dans l'entrée de CO2 et la formation, en coopération avec la β-Carbonic Anhydrase 4 (CA), de bicarbonate. L'augmentation de bicarbonate dans la cellule de garde active SLAC1, un canal ionique nécessaire pour la fermeture des cellules de garde, *via* CA (Wang et al., 2016). Issue de Maurel et al., 2016.

dans le fonctionnement stomatique, a été publiée dans la revue *The Plant Cell* (Grondin *et al.*, 2015).

- **Rôle des aquaporines dans le contrôle de la transpiration chez le riz**

L'expression des aquaporines est sous le contrôle du rythme circadien. Au cours de la journée, l'expression des aquaporines dans les racines et la conductivité hydraulique racinaire augmentent avec l'augmentation de la transpiration (Maurel *et al.*, 2015). Chez le maïs, l'oscillation de l'expression des aquaporines et la conductivité hydraulique racinaire augmentent plus fortement chez des plantes cultivées en condition de stress hydrique en comparaison avec des plantes cultivées en condition irriguée (Caldeira *et al.*, 2014). Cela permettrait d'augmenter les capacités de transport d'eau des racines pour augmenter la capture d'eau lorsque le sol s'assèche (Caldeira *et al.*, 2014). Un effet inverse de l'ABA sur l'expression des aquaporines et le transport d'eau dans les racines a néanmoins pu être observé chez d'autres espèces (Maurel *et al.*, 2015). Chez le riz, peu de données étaient disponibles quant au rôle des aquaporines dans la modulation du transport d'eau racinaire en condition de stress hydrique. Certaines études avaient montré qu'un stress osmotique induisait une augmentation de l'expression des aquaporines (Guo *et al.*, 2006; Lian *et al.*, 2006) alors que d'autres suggéraient qu'un stress hydrique en sol induisait un comportement inverse (Henry *et al.*, 2012).

Au cours de mon post-doctorat à l'IRRI, j'ai entrepris de mieux comprendre le rôle des aquaporines dans l'hydraulique de la plante entière en condition de stress hydrique chez le riz. J'ai étudié la contribution des aquaporines au transport d'eau racinaire et au maintien de la transpiration en condition de stress hydrique dans le panel *OryzaSNP*. Les effets de l'azide (un inhibiteur d'aquaporine) sur la conductivité hydrique racinaire, l'exsudation spontanée au niveau de tiges excisées (proxy de la conductance osmotique) et la transpiration ont été étudiés sur des plantes cultivées en sol. Une augmentation de la contribution des aquaporines à la conductivité hydraulique racinaire et à la conductance osmotique a pu être observée en condition de stress hydrique, suggérant un rôle des aquaporines pour le maintien des flux d'eau dans ces conditions. De façon paradoxale, le stress hydrique induit une réduction de l'expression des aquaporines et aucune corrélation n'a pu être observée entre la contribution des aquaporines et l'abondance en transcrits des PIP. Ces résultats ont mis en évidence les limites des études d'expression pour la prédiction de la fonction des aquaporines dans le transport d'eau. Ces dernières sont en effet particulièrement stables dans les membranes (Martínez-Ballesta *et al.*, 2018) et finement régulées de manière post-traductionnelle (Maurel *et al.*, 2015).

La contribution des aquaporines de la racine dans l'hydraulique de la plante entière a pu être mise en évidence par l'annihilation complète du rétablissement du potentiel hydrique foliaire de plantes stressées après re-irrigation avec une solution d'azide. Nos résultats suggèrent que

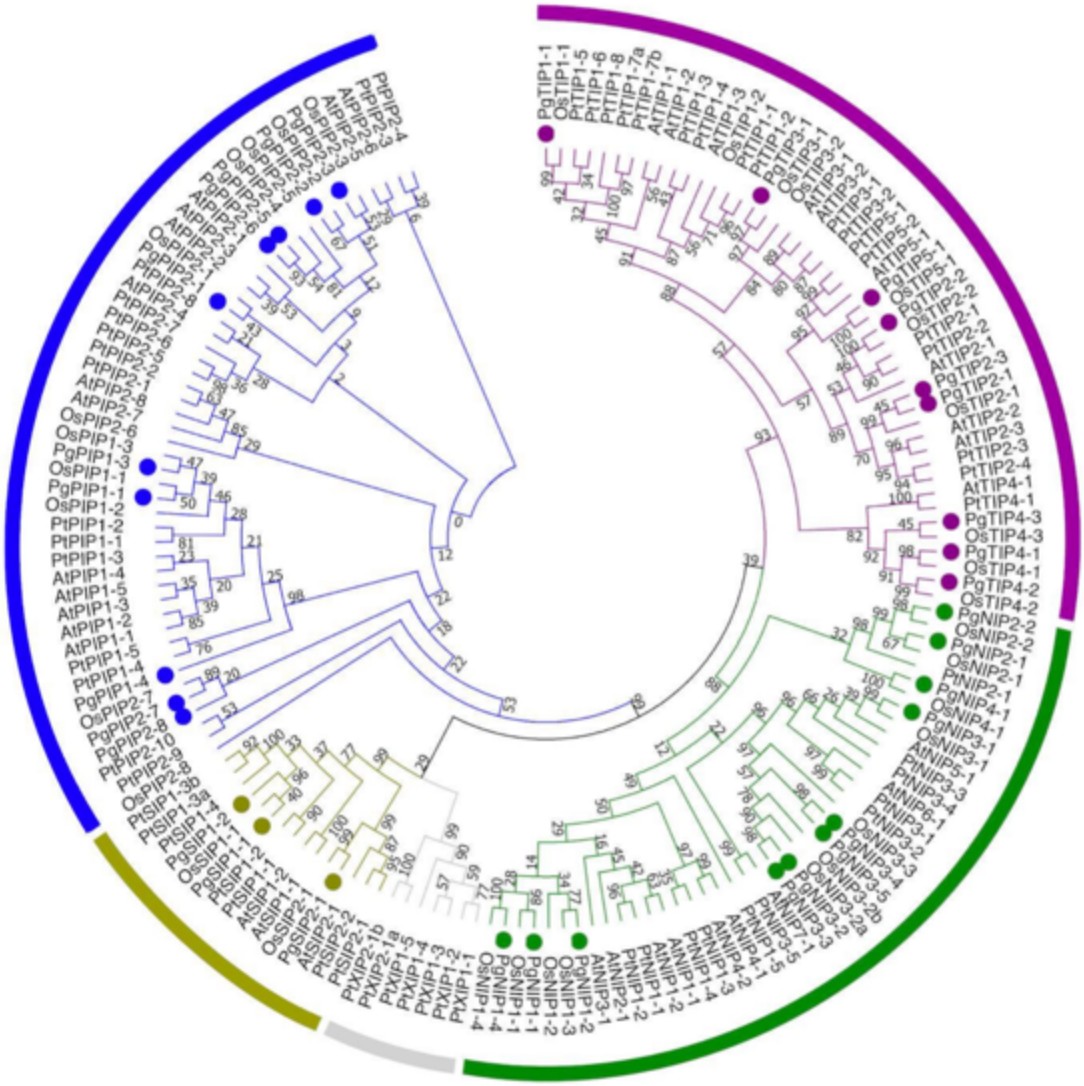

Figure 15 : Arbre phylogénétique des aquaporines de mil et lien avec les isoformes retrouvées chez *A. thaliana*, *O. sativa* et *Populus trichocarpa*. Les aquaporines de mil (*Pennisetum glaucum*) sont illustrées par un cercle de couleur. Issue de Grondin et al., 2020 (Figure 2).

les aquaporines contribuent à hauteur de 20-30 % aux flux d'eau racinaire permettant de soutenir la transpiration en condition irriguée. De plus, le maintien de la transpiration au cours de l'asséchement du sol est positivement corrélé à la contribution des aquaporines dans la conductivité hydrique racinaire. Ces résultats suggèrent que, chez le riz comme chez d'autres espèces, l'augmentation du transport d'eau racinaire via la fonction des aquaporines est associée à un comportement de type anisohydrique. Ce travail, réalisé en collaboration avec Vincent Vadez à l'ICRISAT, a été publié dans la revue *Plant, Cell and Environment* (Grondin *et al.*, 2015).

- **Rôle des aquaporines dans le contrôle de l'efficience de la transpiration chez le mil**

Une meilleure efficience de la transpiration a été associée à une restriction de la transpiration à la demande évaporative chez certaines espèces dont le mil (Vadez *et al.*, 2013). Cette réponse a également été associée à la fonction des aquaporines dans la racine (Reddy *et al.*, 2017). Nous avons entrepris de mieux comprendre le lien entre le transport d'eau racinaire médiée par les aquaporines et l'efficience de la transpiration à travers l'étude de deux variétés de mil contrastées pour leur efficience de la transpiration. Le génotype à faible efficience de la transpiration a montré une plus forte conductance hydraulique racinaire liée à une plus forte contribution des aquaporines en comparaison avec le génotype à forte efficience. La re-annotation des aquaporines dans le génome complet du mil (Varshney *et al.*, 2017) a permis d'identifier 33 aquaporines dont dix font parties de la sous-famille des PIP (Figure 15). L'étude de l'expression des PIP a montré que la sous-famille des PIP1 sont les plus exprimées chez le mil. En particulier, PIP1;3 et PIP1;4 sont significativement plus exprimées chez le génotype de mil montrant une plus faible efficience de la transpiration. Ces résultats montrent que les aquaporines participeraient chez le mil, comme chez d'autres espèces, aux ajustements des capacités de transport d'eau racinaire pour maintenir la transpiration lors de l'augmentation de la demande évaporative. Ils ont permis de préciser les PIP potentiellement mises en jeu dans ces mécanismes. Ces travaux, réalisés avec un étudiant en Master 1 (Pablo Affortit), ont été publiés dans le revue *PLOS ONE* (Grondin *et al.*, 2020).

4.2 Contrôle génétique de traits aériens influençant l'utilisation de l'eau

Améliorer la vigueur précoce du riz représente un enjeu majeur pour améliorer sa compétitivité face aux adventices dans des agrosystèmes aérobie. En contrepartie, la forte vigueur induira une augmentation de la quantité en eau requise par la plante qui pourrait, dans des environnements où l'eau viendrait à manquer en début de cycle, précipiter l'apparition d'un stress hydrique de début de cycle. L'efficience de la transpiration est généralement associée à la tolérante au stress hydrique. Améliorer l'efficience de la transpiration chez des plantes à forte vigueur constituerait alors un avantage. Néanmoins, l'efficience de la transpiration a également pu être associée à des réductions de biomasse

quand elle est liée à une réduction de la conductance stomatique plutôt qu'à une augmentation de l'assimilation photosynthétique. Le mécanisme de restriction de la transpiration en réponse à la demande évaporative permet d'améliorer l'efficience de la transpiration tout en limitant les effets négatifs sur la production de biomasse. Aucune corrélation n'a par exemple pu être observée entre l'efficience de la transpiration et la production de biomasse chez des espèces au métabolisme C3 (arachide) et C4 (sorgho et mil) cultivées en condition irriguée dans des climats arides à forte demande évaporative (Vadez *et al.*, 2014). Au cours de mon post-doctorat à l'Université du Nebraska-Lincoln et dans mes recherches à l'IRD, je me suis intéressé au lien entre vigueur précoce, utilisation de l'eau et efficience d'utilisation de l'eau chez le riz. Ces travaux ont abouti à la publication de deux articles.

- **Lien entre vigueur précoce et utilisation de l'eau en condition de stress hydrique**

Les plateformes lysimétriques de phénotypage à haut-débit permettent des mesures simultanées de la dynamique de croissance et de l'utilisation de l'eau chez un grand nombre de génotype. Nous avons utilisé une plateforme de ce type afin de mieux comprendre les interactions entre vigueur précoce et tolérance au stress hydrique, et les déterminants génétiques qui les contrôlent, chez *Oryza sativa*. Un panel de riz séquencé a été mis en culture au *Plant Accelerator* à Adelaïde en condition irriguée et de stress hydrique appliqué au stade végétatif. La dynamique de croissance des parties aériennes, la dynamique d'utilisation de l'eau et le point d'inflexion de la croissance en fonction de la quantité d'eau du sol ont été mesurés pour chaque génotype. Ces données ont été utilisées pour modéliser la dynamique de croissance des parties aériennes en réponse à l'assèchement du sol dans ce panel sur la base du modèle de croissance de Gompertz (Winsor, 1932). Nous avons pu montrer qu'une forte vigueur initiale est associée à un point d'inflexion plus rapide de la croissance dans la condition de stress hydrique. De façon intéressante, la corrélation négative entre la capture d'eau et le point d'inflexion observé en début de croissance s'inverse pour devenir positive après le point d'inflexion. Le modèle de croissance a ensuite été implémenté par des informations sur le profil allélique des différents génotypes afin d'inférer l'effet des marqueurs génétiques sur les différents paramètres du modèle. Pour cela, une approche de statistique Bayesienne basée sur celle développée par Onogi *et al.* (2016) a été utilisée. Des associations contrôlant potentiellement le taux de croissance et le point d'inflexion de la croissance liée au stress ont pu être identifiées. L'analyse GWAS conventionnelle sur le point d'inflexion de la surface foliaire a permis d'identifier une association proche d'un gène codant pour l'aquaporine *OsPIP1;1*.

Cette étude où j'ai principalement contribué au phénotypage, à l'analyse des données, à l'analyse génétique, et uniquement de façon marginale à la modélisation, a été publié dans la revue *Journal of Experimental Botany* (Campbell *et al.*, 2020). Elle a permis de montrer qu'une forte vigueur précoce n'est pas forcément incompatible avec une utilisation parcimonieuse

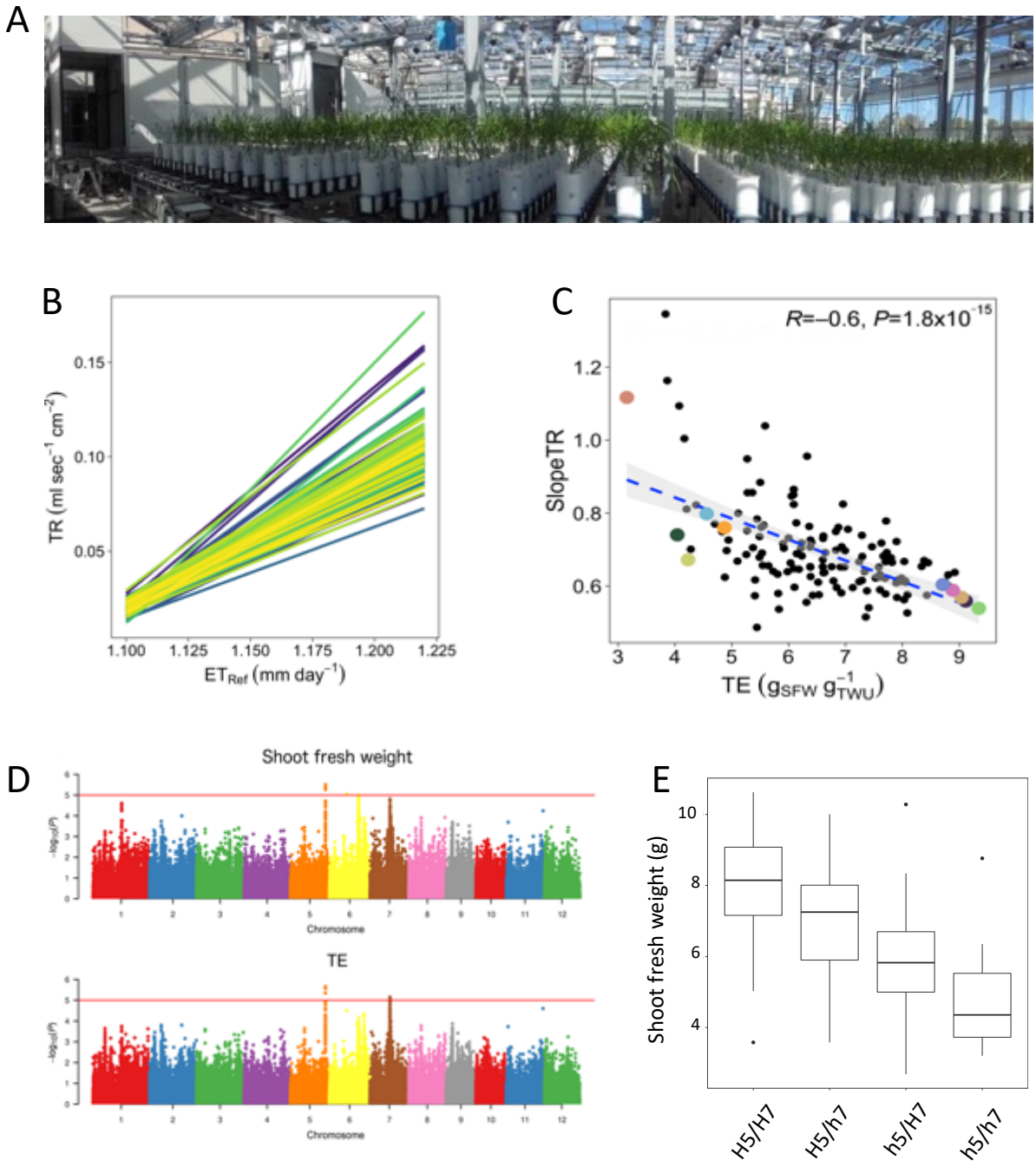

Figure 16 : Contrôle de la vigueur précoce et de l'efficience de la transpiration chez le le riz africain *O. glaberrima*. A: Plantes du panel de diversité en culture dans la serre de la plateforme PhenoArch (Institut Agro Montpellier). B: Réponse de la transpiration (TR) à la demande évaporative (ETref: évapotranspiration de référence) dans le panel. C: Lien entre efficience de la transpiration (TE) et pente de la réponse de la transpiration à la demande évaporative (SlopeTR). C: Manhattan plots pour la biomasse à 30 jours (*Shoot fresh weight*) comme proxy de la vigueur précoce et pour l'efficience de la transpiration (*TE*). E: Effets de la variation allélique pour les SNP les plus significatifs situés aux associations sur les chromosomes 5 et 7. H: haplotype fort. H: haplotype faible. Issues de Affortit et al., 2022 (Figures 2 et 4).

de l'eau si des mécanismes de mitigation de la croissance foliaire se mettent en place tôt lors de l'apparition du stress hydrique. Ces mécanismes qui impliqueraient la fonction des aquaporines permettraient de rester compétitif face aux adventices en maintenant la croissance durant la période de stress hydrique.

- **Lien entre vigueur précoce et efficience de la transpiration en condition irriguée**

Le riz africain, *O. glaberrima*, a été domestiqué dans le delta interne du Niger à partir d'un ancêtre sauvage *O. barthii* adapté aux conditions sahéliennes, et de façon indépendante au riz asiatique *O. sativa* (Cubry *et al.*, 2018). Le riz africain possède une tolérance accrue aux stress abiotiques et un spectre de résistance plus large face aux stress abiotiques. *O. glaberrima* représente donc une ressource en allèles intéressants pour l'amélioration de la tolérance au stress hydrique (Wang *et al.*, 2014). Un panel de diversité composé de 163 accessions de riz africain adaptées à des agrosystèmes différents a été séquencé et est disponible à l'IRD. Ce panel est composé d'accessions provenant principalement d'Afrique de l'Ouest, mais de régions contrastées en termes de température et de précipitation. Il a été utilisé pour l'identification de QTL pour la tolérance à la salinité (Meyer *et al.*, 2016), le temps de floraison (Cubry *et al.*, 2020), l'architecture de la panicule (Ntakirutimana *et al.*, 2023), la fluorescence de la photosynthèse (Robson *et al.*, 2023) ou la résistance au *Rice yellow mottle virus* (Thiémélé *et al.*, 2010).

Dans ce panel, nous avons entrepris d'étudier les variations de vigueur précoce et d'efficience de la transpiration, ainsi que les liens physiologiques et génétiques entre ces deux caractères. La dynamique de production de biomasse et d'utilisation de l'eau a été mesurée sur une plateforme lysimétrique haut-débit en condition bien irriguée (PhenoArch à Montpellier SupAgro ; Figure 16). La biomasse a été mesurée à 30 jours et a été considérée comme un proxy de la vigueur précoce . La quantité d'eau totale utilisée pour produire cette biomasse a servi pour le calcul de l'efficience de la transpiration. Le taux de transpiration quotidien a également été mesuré. La pente de la réponse de la transpiration à la demande évaporative a été mesurée comme un indice de restriction de la transpiration. Nos résultats ont montré une forte corrélation positive entre la biomasse et l'eau totale utilisée. De façon intéressante, une corrélation négative et significative a été observée entre la pente de la réponse de la transpiration à la demande évaporative et l'efficience de la transpiration (Figure 16). Cela indique que des génotypes plus efficients transpirent moins lorsque la demande évaporative augmente. Ces résultats ont été confirmés dans un sous-panel de génotype présentant des biomasses contrastés. Dans ce sous-panel, une corrélation positive et significative a été observée entre le ratio de biomasse racinaire et aérienne, et la réponse de la transpiration à la demande évaporative. Cela suggère que des accessions avec une plus faible surface racinaire en rapport avec leur surface aérienne sont celles capables de plus restreindre leur transpiration.

A

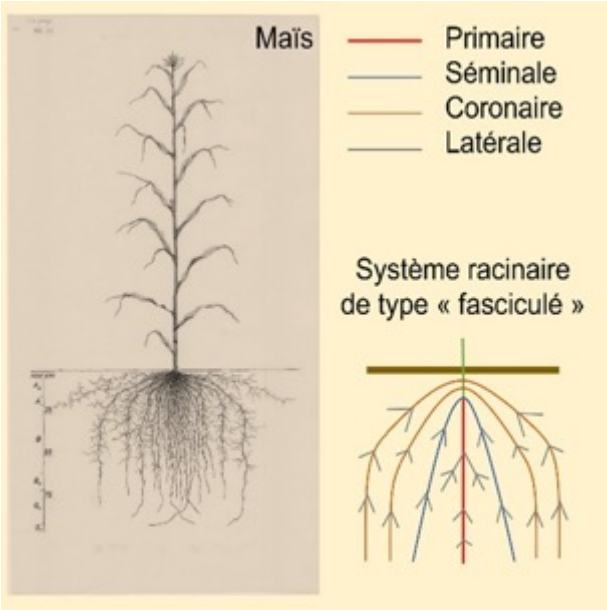

B

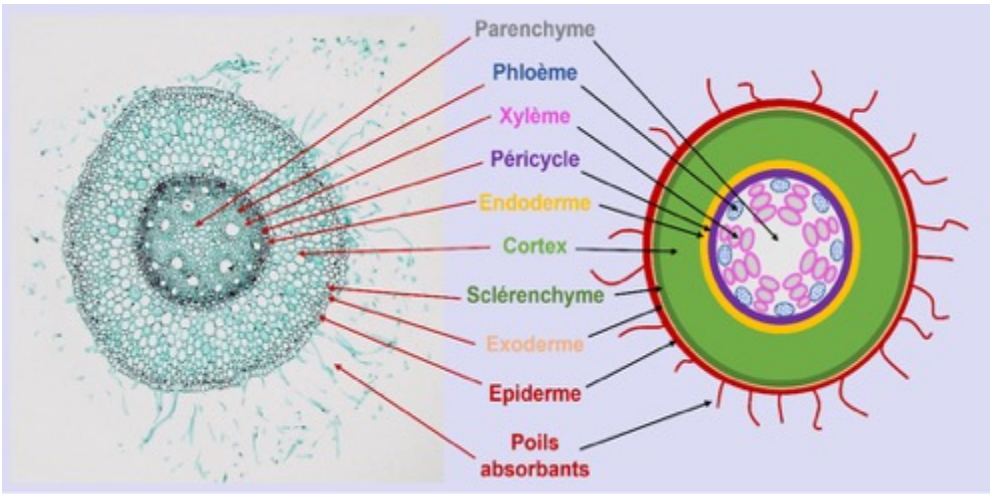

Figure 17 : Architecture et anatomie racinaire chez le maïs. A: Schéma du système racinaire de type fasciculé de maïs avec leurs différents types de racines. B: Organisation anatomique typique d'une racine de maïs avec les différents tissus racinaires. Issues de Grondin et al 2023 (https://www.encyclopedie-environnement.org/vivant/racines-plantes/).

Des GWAS ont permis d'identifier différentes associations contrôlant ces caractères (Figure 16). En particulier, nous avons identifié deux associations significatives sur les chromosomes 5 et 7 pour la vigueur précoce et l'efficience de la transpiration. L'association observée sur le chromosome 5 co-localise avec un QTL déjà identifié chez *O. sativa* contrôlant la vigueur précoce. L'étude du déséquilibre de liaison entre les marqueurs a permis de délimiter la région QTL sur le chromosome 5 à environ 100 kb. Cette région contient 23 gènes dont un code pour une farnesyl-diphosphate synthase 1 (FPS1). FPS1 est impliqué dans la formation d'isopropénoïdes précurseurs en autres d'hormones impliquées dans la croissance, d'antioxydants et de plastoquinones (Manzano *et al.*, 2016). Les plastoquinones sont impliquées dans la chaine de transfert d'électron lors de la photosynthèse (Havaux, 2020). Le QTL sur le chromosome 7, qui est en interaction avec celui sur le chromosome 5, contient des gènes codant des aquaporines PIP (Figure 16). D'autres associations intéressantes ont été identifiées pour la réponse de la transpiration à la demande évaporative.

L'ensemble de ces résultats confirment que, chez le riz, la vigueur précoce peut être associée à une meilleure efficience de la transpiration par la mise en place du mécanisme de restriction de la transpiration en réponse à la demande évaporative. Des déséquilibres de surface entre racines et parties aériennes influençant l'hydraulique pourraient jouer un rôle dans ces mécanismes. Les résultats de cette étude, réalisée en collaboration avec l'UCAD et l'AfricaRice, ont été publiés dans la revue *Journal of Experimental Botany*. Pablo Affortit, étudiant en Master que j'encadrais pour ce travail en est le premier auteur tandis que je suis dernier auteur et auteur pour correspondance (Affortit *et al.*, 2022).

4.3 Contrôle génétique de traits racinaires influençant l'acquisition et le transport d'eau

Le maïs, le riz et le mil possèdent un système racinaire de type fasciculé, caractérisé par une racine embryonnaire et surtout de très nombreuses racines coronaires qui se développent à partir de la base de la tige (Figure 17; Rebouillat *et al.*, 2009; Passot *et al.*, 2016). Ces racines portent des racines latérales de différents types qui contrastent notamment par leur taux de croissance (Passot *et al.*, 2018). L'organisation anatomique des leurs racines contient de l'extérieur vers l'intérieur : l'épiderme avec les poils absorbants qui sont en contact avec le sol, le sclérenchyme dont les parois cellulaires sont plus ou moins lignifiées, le cortex pouvant contenir des cavités aérifères appelées aérenchymes, l'endoderme dont les cellules sont entourées de lignine et de subérine constituant une barrière pariétale, puis au centre, la stèle qui contient les vaisseaux du xylème et du phloème (Figure 17; Atkinson *et al.*, 2019). Il a pu être montré, de façon empirique ou par la modélisation, que la modulation du nombre de ces traits architecturaux et anatomiques influence la tolérance au stress hydrique. Des QTL et gènes contrôlant certains de ces traits ont pu être identifiés dans des populations biparentales ou à travers l'utilisation de panels de diversité. Si certains de ces QTL ont été validés au champ en condition de stress hydrique, la connaissance fine des mécanismes

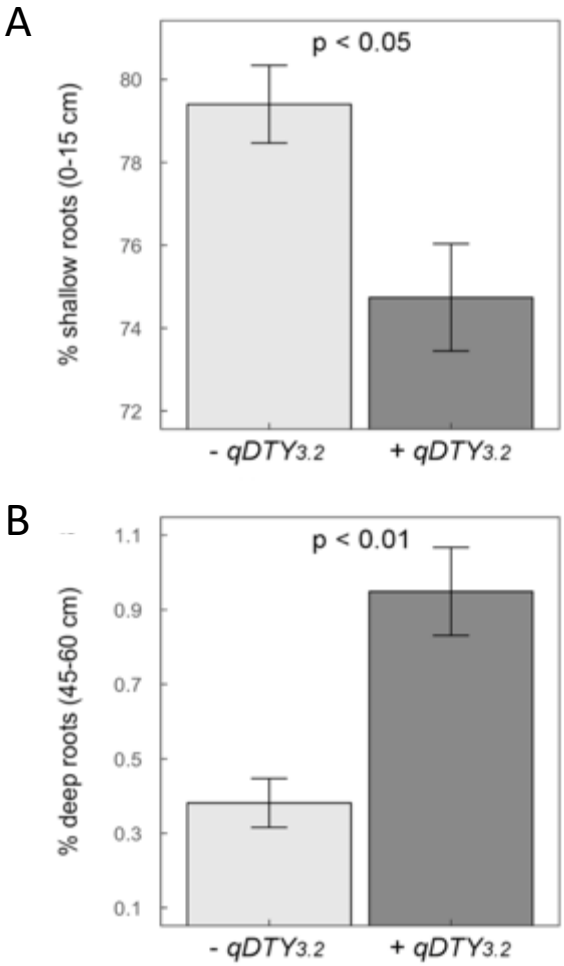

Figure 18 : Effet du QTL de rendement *qDTY$_{3.2}$* sur la profondeur racinaire chez le le riz *O. sativa*. Les masses racinaires de 37 lignées recombinantes BC2F4 possédant le QTL et 18 lignées BC2F4 ne possédant pas le QTL ont été utilisées pour calculer le pourcentage de racines dans la partie superficielle du sol (0-15 cm; A) et dans la partie profonde (45-60 cm; B). Issus de Grondin et al., 2018 (Figure 5).

physiologiques impliqués, notamment en termes d'hydraulique à l'échelle de la plante entière reste souvent peu claire. L'enjeu consiste à comprendre comment ces traits influencent, en interaction avec d'autres traits, les capacités d'acquisition et de transport d'eau racinaire en lien avec la demande des parties aériennes en condition irriguée et de stress hydrique.

Dans mon parcours, j'ai eu l'occasion d'utiliser différentes stratégies afin d'étudier l'utilité de traits racinaires en condition de stress hydrique dans différents types de matériel végétal et en utilisant différentes méthodes de phénotypage. Pour certains traits identifiés comme bénéfiques, j'ai contribué à mieux caractériser les mécanismes physiologiques impliqués et à identifier leur contrôle génétique. J'ai également participé au développement de méthodes de phénotypage au champ et de modélisation pour une meilleure compréhension des fonctions racinaires dans un sol et à l'échelle de la plante entière.

- **Caractérisation de traits racinaires impliqués dans la tolérance au stress hydrique chez les céréales**

Architecture racinaire et capture d'eau chez le riz

La stratégie de sélection pour l'amélioration de la tolérance au stress hydrique du riz adoptée à l'IRRI était basée sur la sélection directe pour le rendement en grain en condition de stress (Swamy and Kumar, 2013). L'idée était ensuite d'identifier les mécanismes physiologiques sous-jacents à ces QTL de rendement sous stress afin de pyramider des QTL qui pourraient agir de manière complémentaire. Dans ce cadre, j'ai participé à caractérisation physiologique d'une population BC2F4 issue d'un croisement entre la variété Moroberekan et Swarna. Nous avons montré que certains QTL contrôlant des traits physiologiques co-localisent avec le QTL de rendement en grain sous stress ($qDTY_{3.2}$). L'étude plus précise d'un sous-panel de lignées BC2F4 a montré que l'amélioration de la tolérance au stress hydrique apportée par le QTL de rendement était en partie liée à un développement racinaire plus profus et profond (Figure 18). L'augmentation de la profondeur racinaire chez les lignées permettrait une meilleure capture d'eau du sol en profondeur et améliorerait la tolérance au stress hydrique. Ces résultats ont été publiés dans *BMC Genetics* (Dixit *et al.*, 2015) et *Rice* (Grondin *et al.*, 2018).

Anatomie et nutrition hydro-minérale chez le riz et le mil

Les traits anatomiques racinaires et leur contrôle génétique ont généralement été moins étudiés que les traits d'architecture racinaire. La technologie LAT permet aujourd'hui d'élargir les capacités d'études de l'anatomie à des grand panels de diversité. Cette méthode a par exemple été utilisée pour l'étude de l'anatomie racinaire dans un panel de diversité de maïs et permis d'identifier le gène *bHLH121* comme régulateur de la formation d'aérenchyme (Schneider *et al.*, 2023). La formation d'aérenchyme a été associée à la tolérance au stress hydrique non pas à cause de leur effet sur le transport d'eau, mais car ils réduisent le coût métabolique des tissues racinaires et par la même l'efficience métabolique de l'exploration du sol (Lynch, 2018; Schäfer *et al.*, 2022). D'autres traits anatomiques comme l'épaisseur des

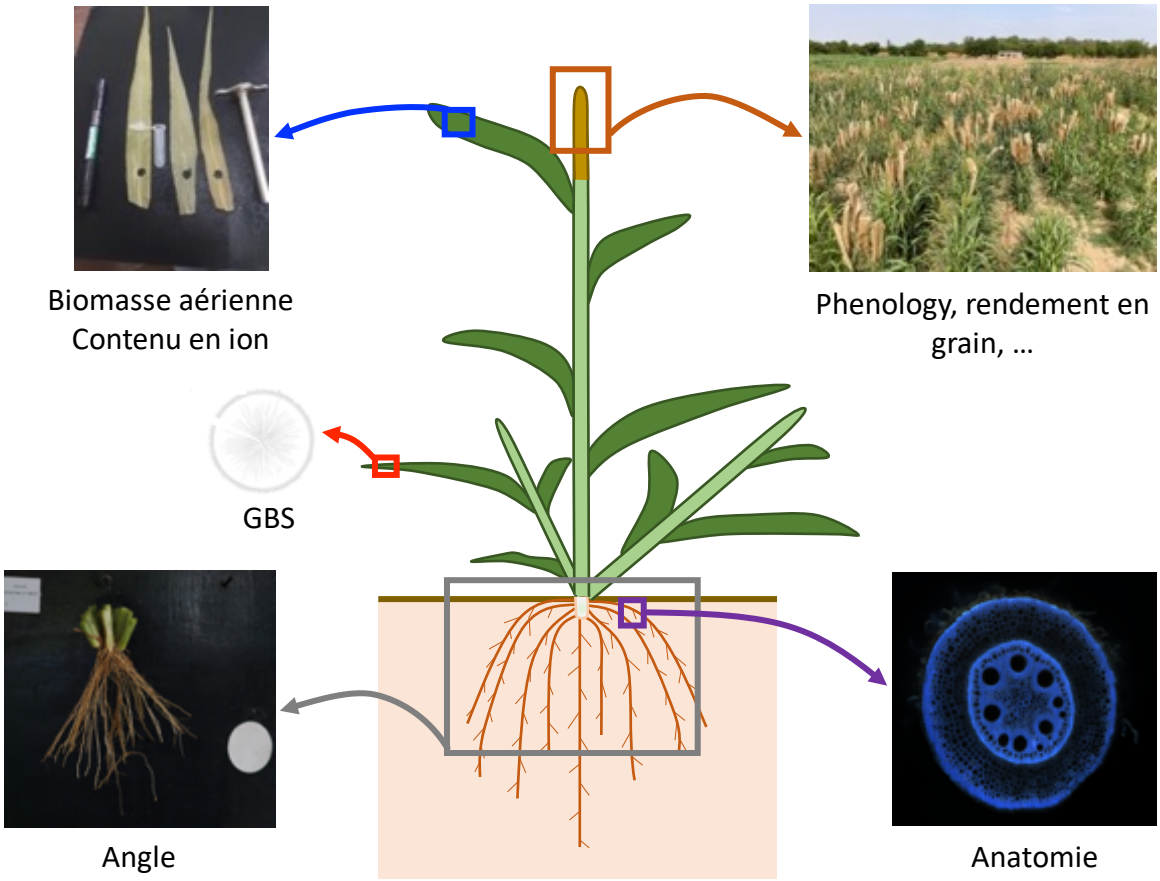

Figure 19 : Génotypage et phénotypage d'un panel de mil au champ au Sénégal pendant les saisons sèches 2021 et 2022. Les plantes ont été cultivées en condition irriguée et de stress hydrique végétatif. Les mêmes lots de graines ont été utilisés pour les deux années. Les mêmes plantes ayant servi pour le phénotypage racinaire ont été utilisées pour la mesure de la biomasse aérienne et du contenu en grain. Sources: Alexandre Grondin et Darren Wells (anatomie).

barrières pariétales ou la taille des vaisseaux du xylème influencent l'hydraulique racinaire mais aussi la nutrition minérale (Schoppach *et al.*, 2014; Calvo-Polanco *et al.*, 2021).

Nous avons entrepris d'étudier la diversité des traits anatomiques et leur rôle potentiel dans la tolérance au stress hydrique dans un panel de diversité de mil au champ au Sénégal en collaboration avec nos collègues de l'Université de Nottingham et de l'ISRA (Figure 19). Ce panel composé de 160 lignées séquencées a été cultivé en condition irriguée et de stress hydrique appliqué au stade végétatif pendant deux années consécutives. Le stress a été appliqué 3 semaines après semis par arrêt de l'irrigation pendant 3 semaines, après quoi l'irrigation a été rétablie jusqu'à la récolte. Les racines du nœud 4 ont été prélevées après 6 semaines de culture dans les deux conditions hydriques (i.e., à la fin de la période de stress). Une image anatomique de ces racines a été obtenue par LAT et les caractéristiques anatomiques ont été mesurées à l'aide du logiciel d'intelligence artificielle RootScan en collaboration avec nos collègues de l'Université de Nottingham. Sur ces mêmes plantes, un échantillon de la dernière feuille ligulée a été prélevé afin d'étudier son contenu en ion. Les plantes restantes dans la parcelle ont été cultivées en condition irriguée jusqu'à maturité afin de mesurer les paramètres agro-morphologiques à la récolte. Enfin, ces lignées ont été re-séquencées par *Genotyping By Sequencing* (*GBS*) afin de s'assurer de leur identité génétique et les mêmes lots de graine ont été utilisés pour les deux années d'essai au champ.

L'analyse des données à l'aide d'outils statistiques a permis de nettoyer et de corriger les différentes variables pour les effets spatiaux dans le champ. D'une manière générale, une large variabilité et une bonne héritabilité (> 0.5) ont été observées pour les différents traits étudiés. Un effet significatif du stress hydrique a pu être observé sur les traits anatomiques, de quantité en ions et agronomiques, avec pour certaines un effet significatif de l'interaction G x E. C'est par exemple le cas pour la surface des vaisseaux du xylème. De façon intéressante, la surface de ces vaisseaux est significativement positivement corrélée avec un index de tolérance du rendement en grain sous stress sur les deux années. Ces résultats indiquent que chez le mil, dans des conditions où le stress est appliqué au stade végétatif, des plantes avec des surfaces de vaisseaux du xylème plus grandes sont globalement plus tolérantes au stress hydrique en termes de maintien du rendement en grain. Ces résultats vont à l'encontre d'observations précédentes selon lesquelles des plantes montrant des surfaces de vaisseaux du xylème plus faibles seraient plus tolérantes au stress hydrique (Richards and Passioura, 1989). Ces différences pourraient s'expliquer par le type de stress imposé qui influencerait les effets bénéfiques ou non de la surface des vaisseaux xylème sur le maintien des rendements. Nous étudions actuellement l'hypothèse selon laquelle une stratégie consistant à maintenir les capacités de transport d'eau racinaire à travers une plus grande surface des vaisseaux du xylème permettrait à la plante de mil de maintenir sa transpiration et sa croissance plus longtemps au cours d'un stress hydrique végétatif. Afin d'explorer cette hypothèse, l'évolution de la transpiration en réponse à l'asséchement du sol est étudiée en détail dans un sous-panel de lignées contrastées pour la surface des vaisseaux du xylème (Figure 20). Ces

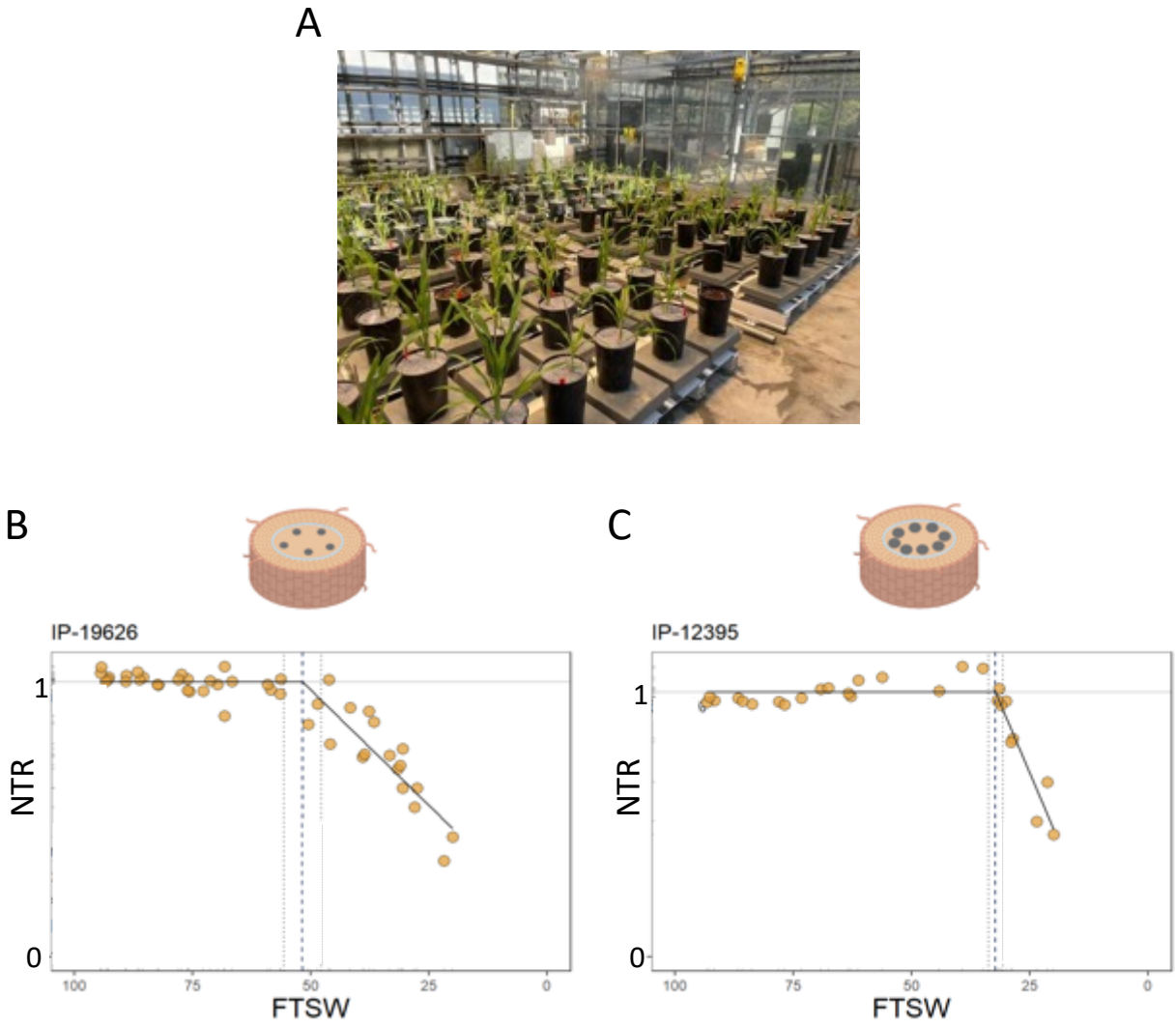

Figure 20 : Réponse de la transpiration à l'assèchement du sol chez des lignées de mil contrastées pour la surface des vaisseaux du xylème. A: Plantes de mil contrastées pour la surface des vaisseaux du xylème cultivées sur une plateforme lysimètrique à l'IRD de Montpellier. B-C: Evolution de la transpiration en réponse à l'assèchement du sol chez deux lignées de mil avec une plus faible (IP-19626) et plus forte (IP-12395) surface des vaisseaux du xylème. FTSW: fraction d'eau transpirable du sol (plus la FTSW diminue, moins la plante est capable d'extraire de l'eau du sol). NTR: taux de transpiration normalisée par rapport à la transpiration de plantes du même génotype cultivées en condition irriguée. Source : Pablo Affortit.

études incluent également une description précise des réponses des parties aériennes. Le contrôle génétique de la surface ces vaisseaux du xylème est également étudié par GWAS. Ce travail fait l'objet de la thèse de Pablo Affortit.

En parallèle, nous étudions le déterminisme génétique contrôlant les traits anatomiques dans une population de riz *O. sativa* vietnamienne séquencée en collaboration avec nos collègues de l'AGI au Vietnam. Un essai au champ a été réalisé avec 182 accessions issues de ce panel en condition inondée au Vietnam où des racines coronaires ont été prélevées. L'anatomie de ces racines a été étudiée par microscopie à épifluorescence. Un logiciel de reconnaissance semi-automatique des tissus racinaires a été utilisé pour la mesure des traits anatomiques (Lartaud *et al.*, 2015). Comme chez le mil, l'analyse des données a montré une grande variabilité et une bonne héritabilité pour les différentes traits. Avec l'hypothèse selon laquelle certains traits anatomiques pourraient indirectement influencer la composition en ions désirables et indésirables dans les grains, nous avons échantillonné des grains de riz issus de plantes cultivées lors de ce même essai au champ. La composition en ions des grains de riz brun et blanc a été étudiée. L'étude des liens entre traits anatomiques et composition en ion des grains est en cours. Ces données permettront d'identifier des traits anatomiques intéressants pour la nutrition hydrominérale. Les déterminants génétiques contrôlant ces traits seront ensuite étudiés par GWAS. Ce travail fait l'objet de la thèse de Hien Linh Tran.

- **Caractérisation de gènes candidats contrôlant la croissance racinaire**

Les approches de génétique d'association permettent d'identifier de potentiels QTL contrôlant des traits bénéfiques pour la tolérance au stress hydrique. L'étape suivante d'identification du gène candidat sous-jacent responsable de la variation du caractère représente un défi majeur. Cibler un gène parmi plusieurs gènes présents dans un QTL consiste à : (i) étudier l'annotation fonctionnelle des gènes et du lien potentiel avec le caractère étudié, (ii) étudier l'expression des gènes candidats chez des haplotypes (génotypes dont la combinaison d'allèles en déséquilibre de liaison dans la région QTL diffère), et (iii) étudier le polymorphisme et son effet sur les séquences promotrices ou codantes. Le ou les gènes sélectionnés peuvent ensuite faire l'objet d'une validation par une approche de génétique fonctionnelle. La démocratisation de l'édition du génome par CRISPR-Cas9 permet d'envisager la validation fonctionnelle de gènes chez les céréales, moyennant l'existence d'un protocole de transgénèse efficace pour l'espèce considérée.

Au cours de mon post-doctorat à l'Université du Nebraska-Lincoln, j'ai travaillé sur un QTL contrôlant la biomasse racinaire (Figure 21). Ce QTL a été identifié par GWAS dans un panel de 383 accessions de riz *O. sativa* cultivées en serre en condition semi-hydroponique. Ce QTL co-localise avec une région qui avait précédemment été identifiée comme contrôlant la biomasse racinaire dans un population biparentale (Horii *et al.*, 2006). Des haplotypes pour ce QTL ont été sélectionnés et les différences de biomasse racinaire ont été validées en sol. L'étude fine de l'architecture racinaire a montré que la réduction de biomasse était liée à une

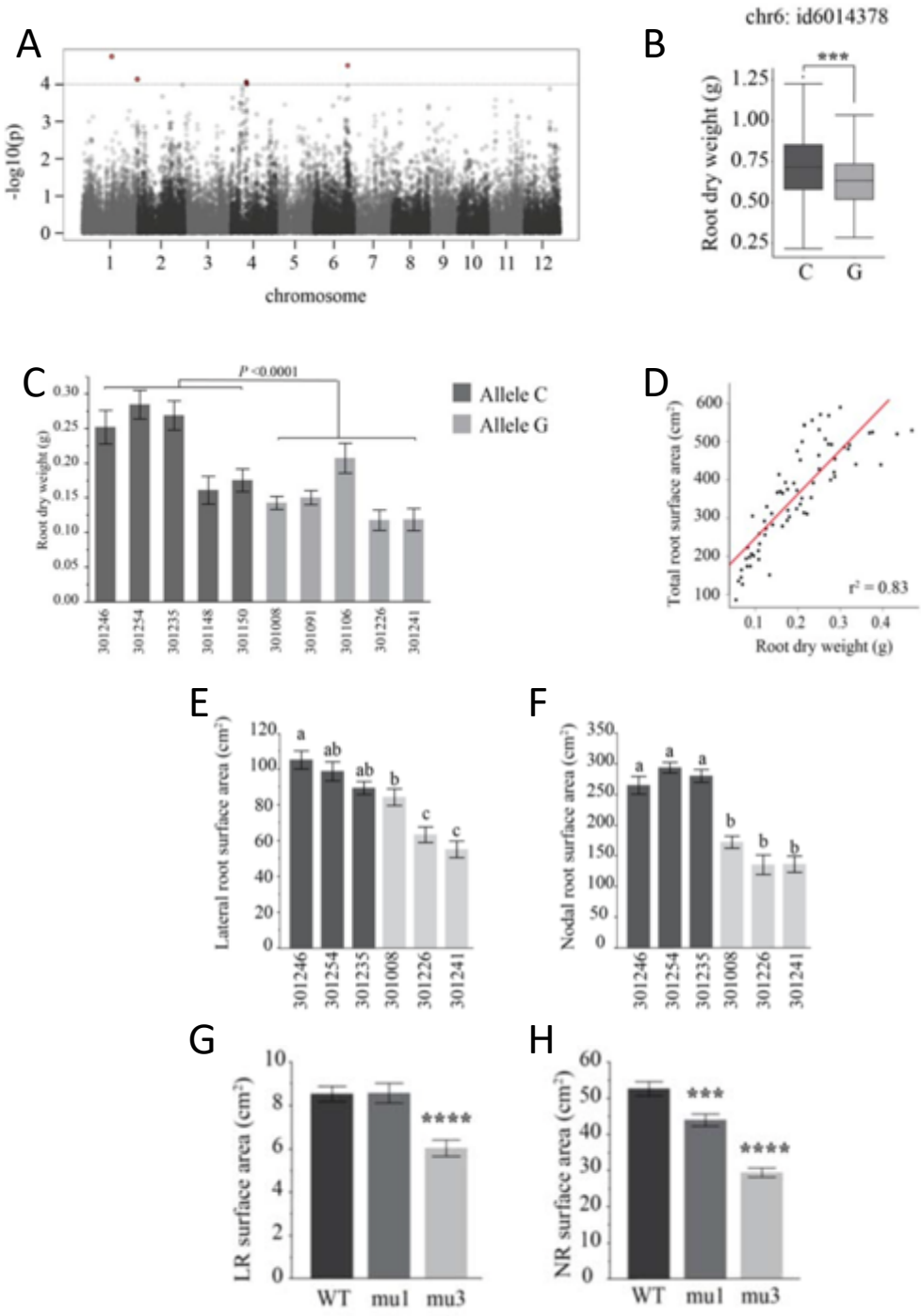

Figure 21 : Rôle de RDW6 dans la croissance racinaire chez le riz. A: Manhattan plot pour la biomasse racinaire dans un panel de riz *O. sativa*. B: Effet de l'allèle au SNP significatif sur le chromosome 6 sur la biomasse racinaire. C: Biomasse racinaire chez une sélection d'haplotypes pour l'association sur le chromosome 6. D: Relation entre la biomasse racinaire et la surface racinaire totale chez les haplotypes. E et F: Surface totale des racines latérales et des racines nodales chez les haplotypes, respectivement. G-H: Surface totale des racines latérales (LR) et nodales (NR) chez des plantes de riz sauvages (WT) et des plantes mutantes invalidées pour le gène *RDW6* (mu1 et mu3). Issues de Saluja et al., en préparation.

réduction significative de la surface des racines coronaires. L'étude de l'expression des gènes chez ces haplotypes dans les feuilles et les racines a montré l'expression différentielle d'un gène dont la fonction était inconnue (*LOC_Os06g44034*) mais qui contenait une séquence précurseur du microARN156j. Cette famille de microARN est connue pour réguler différents processus développementaux chez les plantes (Wang *et al.*, 2019). Ce gène a été nommé *Root Dry Weight 6* (*RDW6*). Il est significativement plus exprimé chez les haplotypes montrant une forte biomasse et serait donc un régulateur positif de la biomasse racinaire. L'édition de ce gène par CRISPR-Cas9 (insertion d'un codon stop dans le premier exon et délétion du précurseur du microARN) induit une réduction significative de la biomasse à travers une réduction de la surface des racines coronaires et latérales. La comparaison de l'expression des gènes entre les lignées mutantes et sauvages suggère que ce gène serait impliqué, entre autres, dans des voies de régulations hormonales. Un article regroupant l'ensemble de ces résultats dont je suis co-premier auteur a été soumis à la revue *Plant Physiology* mais a été rejeté avec modifications majeures. L'article est encore en attente d'être publié.

Chez le mil, j'ai travaillé sur la caractérisation de QTL contrôlant la croissance de la racine primaire et l'exsudation racinaire. Le mil possède la caractéristique d'avoir une racine primaire qui croit rapidement en profondeur au cours des stades précoces de son développement (Passot *et al.*, 2016). Il avait été proposé que ce trait pourrait être bénéfique pour l'établissement de la plante, en particulier en condition de stress hydrique en début de cycle. L'étude de la croissance de la racine primaire dans un panel de diversité de mil séquencé a montré que ce trait était héritable et présentait une grande variabilité génotypique (Figure 22). Des lignées contrastées pour ce trait ont été cultivées en condition de stress hydrique au stade plantule au champ au Sénégal. Nous avons ainsi montré que la croissance de la racine primaire était positivement corrélée à des indices de tolérance au stress comme la capacité des feuilles à rester photosynthétiquement active. Des analyses GWAS ont identifié une association significative contrôlant ce caractère sur le chromosome 1. Cette association a été confirmée par *Bulk Segregant Analysis* dans une population F2 issue d'un croisement entre deux lignées contrastées pour la croissance de la racine primaire. Dans la région du QTL, un gène codant une glutaredoxine nommée *PgGRXC9* dont l'homologue le plus proche chez *A. thaliana* est *ROXY19*, a été identifié. *PgGRXC9* est exprimée dans l'épiderme et la stèle des apex racinaires et dans la zone d'élongation. Ce gène est significativement plus fortement exprimé dans des lignées de mil présentant une forte croissance racinaire. Chez *A. thaliana*, la mutation du gène *ROXY19* induit, comme chez les haplotypes de mil pour le gène *PgGRXC9*, une réduction de la croissance de la racine primaire. Ces résultats suggèrent que *Pg*GRXC9 est un régulateur positif de la croissance de la racine primaire chez le mil, un caractère important pour son adaptation au stress hydrique de début de cycle. Un article reprenant ces résultats dont je suis co-premier auteur a été publié dans la revue *elife* (Fuente *et al.*, 2023). Une approche similaire mais sans validation fonctionnelle a été réalisée pour le caractère d'exsudation racinaire et les résultats ont été publiés dans la revue *Scientific Reports* (de la Fuente Cantó *et al.*, 2022).

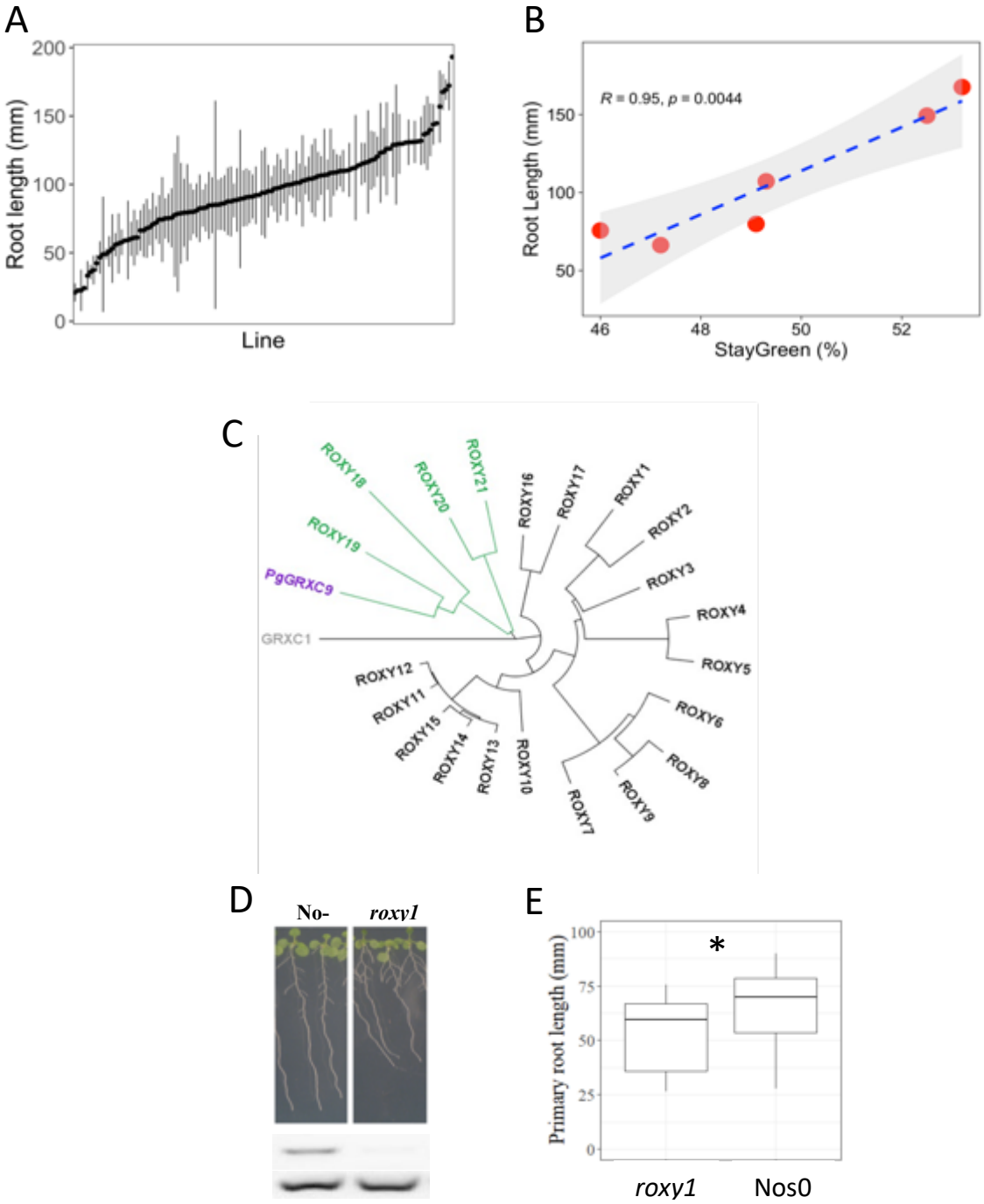

Figure 22 : Contrôle de la croissance racinaire par une glutaredoxine chez le mil et *A. thaliana*. A: Variation pour la longueur racinaire dans un panel de diversité de mil. B: Corrélation entre la longueur racinaire de plantes de mil et leur capacité à garder une activité photosynthétique en condition de stress hydrique (*Stay green*). B: Arbre phylogénétique montrant la proximité entre les glutaredoxines chez le mil et *A. thaliana*. D: Images de plantes sauvages (No-0) et des plantes mutantes pertes de fonction pour le gène *ROXY19* à 17 jours après semis. E: Croissance racinaire chez les plantes sauvages et mutantes *roxy19*. Issues de Fuente et al., 2023 (Figures 1 et 4).

- **Développement d'outils d'analyse et de mesure des racines et de leurs fonctions hydriques**

Phénotypage racinaire du mil au champ

Le phénotypage au champ est laborieux et les méthodes existantes sont souvent basées sur un compromis entre le débit et la précision. Parmi les différentes méthodes existantes, le comptage d'impacts racinaires sur une tranchée est une méthode à faible débit mais qui permet d'avoir une mesure relativement précise de la densité de longueur racinaire dans un profil de sol (Chopart and Siband, 1999). Cette méthode nécessite une étape de calibration afin de développer un modèle permettant de prédire la densité de longueur en fonction du comptage d'impact. En collaboration avec nos collègues de l'ISRA, nous avons développé un modèle pour le mil. Ce modèle a été utilisé afin d'étudier la croissance racinaire de variétés de mil en condition irrigué et de stress hydrique. Nous avons montré que les variétés étudiées réorientent leur croissance racinaire vers des horizons de sol plus profonds en condition de stress hydrique. Ce travail a été publié dans la revue *PLOS ONE* (Faye *et al.*, 2019).

Mesure des contenus en eau et des flux d'eau dans la base de la tige

La résonance magnétique nucléaire (RMN) a été appliquée pour l'imagerie (IRM) des plantes et la mesure de la compartimentation et des flux d'eau (Scheenen *et al.*, 2000, 2007). Si l'IRM requiert de gros équipements, la RMN à bas champ a été envisagée pour réaliser des mesures hydrauliques de plantes dans leur environnement naturel. Un appareil RMN portable bas champ pour la mesure des contenus et flux d'eau chez les céréales a été développé au Laboratoire Charles Coulomb (L2C) de l'Université de Montpellier (Figure 23). Chez le sorgho, des signaux RMN mesurés dans la tige en condition irriguée et de stress hydrique sont associés à l'asséchement du sol et à la chute de la conductance stomatique (Sidi-Boulenouar *et al.*, 2019). Ils ont été assimilés à un proxy de la mesure du contenu en eau dans la tige. En collaboration avec nos collègues du L2C, nous avons souhaité continuer le développement de cet appareil pour mieux comprendre la signification physiologique de ces signaux. Notre hypothèse est que ces derniers pourraient être plus largement associés à la transpiration. Cet appareil de RMN portable pourrait alors permettre la mesure dynamique de la transpiration au champ. Joseph Ovwemuvwose, a commencé mais arrêté sa thèse sur ce sujet.

Modèle structure-fonction du système racinaire chez le mil

Le modèle structure-fonction *OpenSimRoot* a été initialement développé pour le maïs mais a depuis été adapté à d'autres espèces comme le riz (Postma *et al.*, 2017; Ajmera *et al.*, 2022). Il permet d'étudier l'effet de la modulation de traits racinaires sur la production de biomasse aérienne dans différents types de sol. En collaboration avec des collègues de *Penn State University* et de l'ISRA, nous avons entrepris d'adapter le modèle *OpenSimRoot* au mil (Figure 24). Une caractérisation phénotypique fine du développement et de la croissance racinaire d'une lignée de mil élite (Souna 3) a été réalisée, et ces mesures ont permis le développement d'un modèle *OpenSimRoot* de mil. Le sol a été paramétré selon les caractéristiques d'un sol

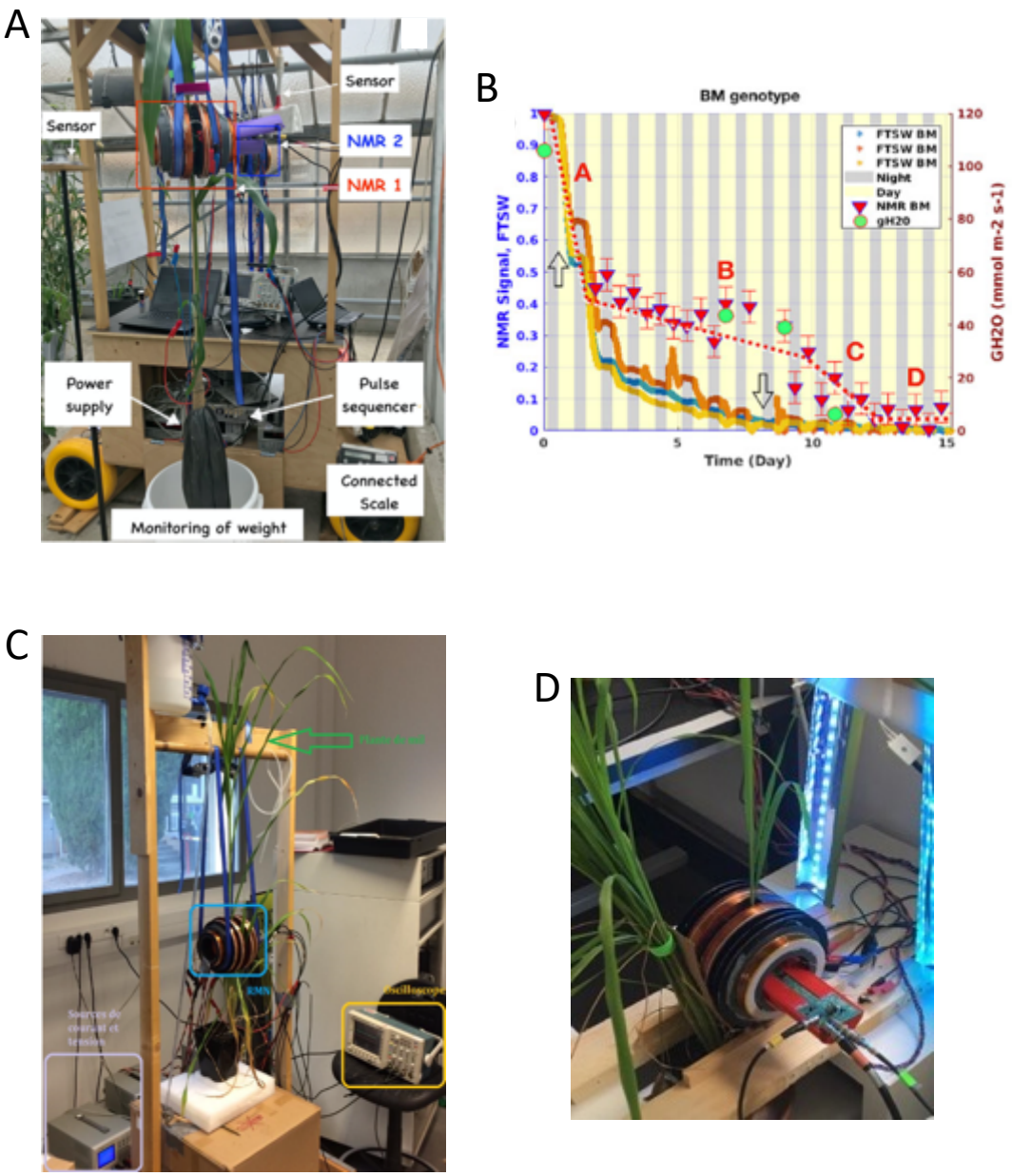

Figure 23 : Mesure des contenus en eau par résonance magnétique nucléaire bas champ. A: Prototype permettant de mesurer les contenus en eau dans la base de tige de sorgho. Issue de Sidi-Boulenouar et al., 2019 (Figure 1b). B: Le signal RMN a été mesuré chez trois plantes au cours de l'asséchement du sol suivi par la mesure de la fraction d'eau transpirable (FTSW). Le signal RMN correspond aux triangles rouges. Les cercles verts correspondent à la mesure de la conductance stomatique (en mmol m-2 s-1) à l'aide d'un poromètre. Issue de Sidi-Boulenouar et al., 2019 (Figure 2a). C: Etude des signaux RMN chez une plante de mil. Source: Eric Nativel. D: étude des signaux RMN chez une plante de riz. Source: Alexie Técher.

sableux typique d'un environnement sahélien. Les impacts racinaires et la biomasse aérienne prédits dans un sol non limitant ont été comparés avec des mesures empiriques réalisées au champ. Cela nous a permis de valider le modèle. Ce modèle est actuellement utilisé pour tester l'impact de différents traits racinaires sur la production de biomasse en condition de carence en phosphore. Ce travail fait l'objet du travail de thèse de Mame Sokhatil Ndoye.

Étude de la plasticité racinaire chez le mil

La plasticité adaptative implique la mise en jeu de mécanismes où le génotype interagit avec l'environnement pour l'expression de certains phénotypes bénéfiques pour l'adaptation de la plante au nouvel environnement. Des études suggèrent que cette plasticité pourrait être contrôlée par des déterminants génétiques qui sont indépendants du contrôle du phénotype dans un environnement donné (Kusmec *et al.*, 2017; Monforte, 2020). Ces gènes contrôleraient ainsi la transition d'un état phénotypique à l'autre. L'identification de déterminants génétiques contrôlant ces transitions n'est pas triviale car elle nécessite de dissocier le contrôle du trait dans un environnement de son contrôle en réponse à différents environnements. Des modèles GWAS multi-environnements couplés à des analyses de génétique quantitative permettent de quantifier la part de variance que peut capturer des associations. Ceci permet d'identifier des QTLs plus susceptibles de capturer les effets G x E, et donc des gènes impliqués dans la plasticité (van Eeuwijk *et al.*, 2010). Une approche alternative consiste à identifier des traits contrôlés par l'interaction G x E, à calculer des indices de plasticité pour ces traits, et à utiliser ces indices dans des approches GWAS (Laitinen and Nikoloski, 2019). Ces indices de plasticité peuvent être calculés selon plusieurs méthodes basées sur des concepts statistiques différents (Valladares *et al.*, 2006; Elias *et al.*, 2016; Reckling *et al.*, 2021; Schneider, 2022). Nous avons entrepris d'identifier des traits racinaires plastiques en réponse au stress hydrique chez le mil, et les déterminants génétiques qui les contrôlent (Figure 25). Pour cela, nous utilisons le jeu de données anatomiques obtenu au champ au Sénégal en condition irriguée et de stress hydrique. Nous avons identifié des traits contrôlés par l'interaction G x E et calculé leur plasticité en utilisant plusieurs méthodes. En parallèle, et en collaboration avec nos collègues de l'UMR GQE et de l'IPK, nous avons utilisé des méthodes de génétique quantitative afin d'étudier la capacité des différentes méthodes à capturer des associations expliquant l'interaction G x E. Un indice de plasticité en particulier représente la pente de la régression entre la valeur du trait dans différents environnements pour chaque génotype et un index environnemental (Finlay and Wilkinson, 1963). Les associations GWAS pour cette indice capturent avec une grande efficacité des associations pouvant expliquer l'interaction G x E. Ce travail a fait l'objet du post-doctorat de Sebastian Arenas.

Transgénèse chez le mil et S. italica

L'édition des gènes candidats sous-jacent des QTL fait partie intégrante de nos approches. Elle permet de valider le rôle du gène dans le contrôle du trait considéré. Elle permet également d'étudier finement les acteurs moléculaires impliqués et les mécanismes

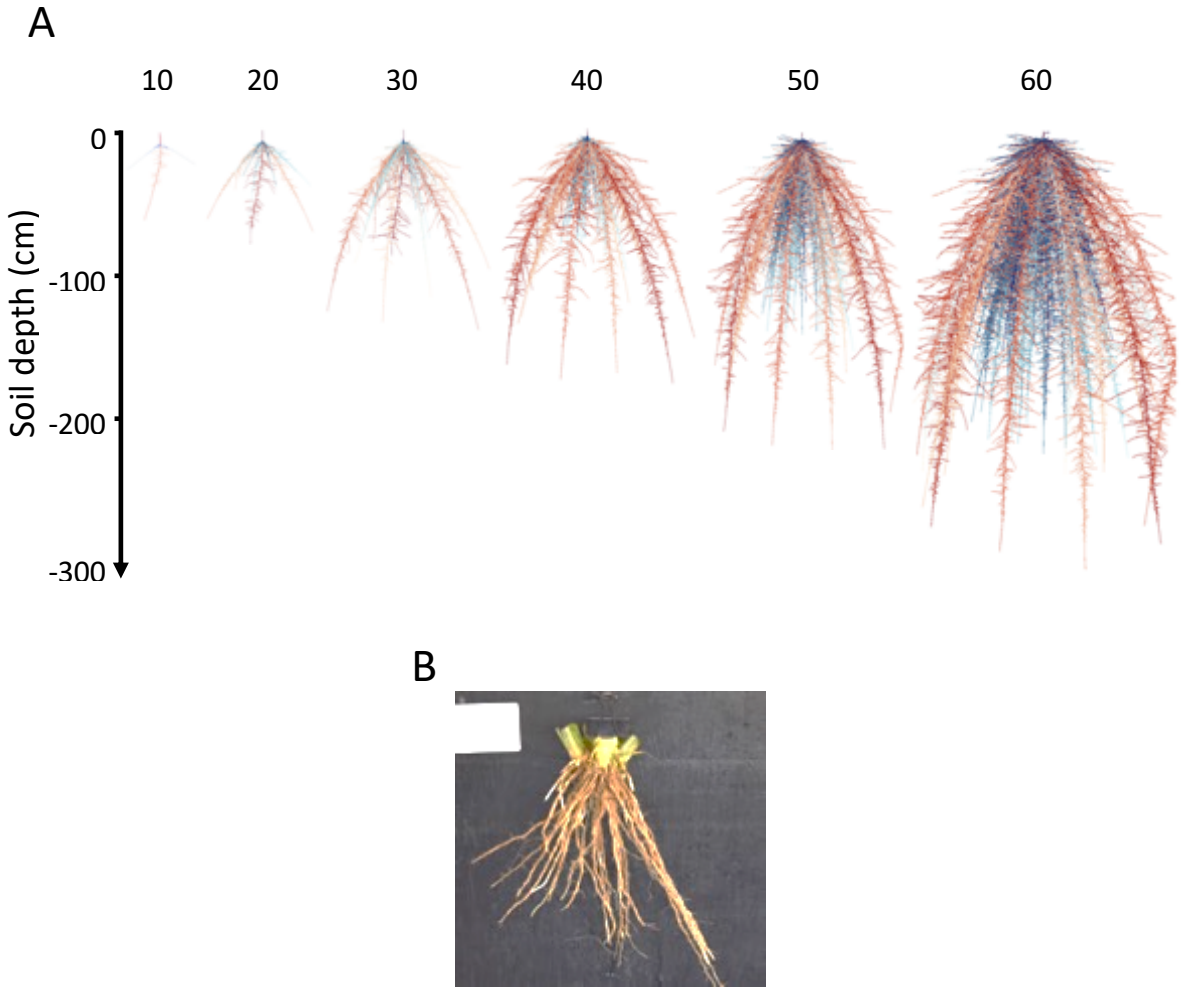

Figure 24 : Simulations de l'architecture racinaire d'une plante de mil Souna3 au cours du temps à l'aide du modèle *OpenSimRoot*. A: Simulations réalisées en condition optimale d'eau et de nutriment dans le sol. Source: Sokhatil Ndoye. B: Image d'un système racinaire de mil Souna3 prélevé par la méthode de *shovelomics* à 42 jours après semis. Source: Alexandre Grondin. DAS: Days after sowing.

physiologiques associés. Nous disposons au laboratoire de protocoles utilisés en routine pour la transformation de *O. sativa* et *O. glaberrima*, mais pas pour le mil. Des protocoles pour la transformation du mil existent dans la littérature (Jha *et al.*, 2011). Nous avons ainsi tenté d'adapter ces protocoles à la lignée de mil TIFT23DB, i.e. celle utilisée pour le séquençage du génome complet. Ces tentatives se sont avérées infructueuses. Nous avons choisi *S. italica* comme alternative. En effet, cette espèce est génétiquement très proche du mil et des protocoles pour sa transformation existent (Santos *et al.*, 2020; Sood *et al.*, 2020; Liang *et al.*, 2022). Nous avons tenté de transformer six accessions de *S. italica* sans succès. Ce travail, initié par Jean-Rémy Brossier (2020-2022), a été poursuivi par Romaric Hallot (2022-2023).

4.4 Bilan

Au cours des années, mon travail de recherche s'est orienté de l'étude des mécanismes hydrauliques à l'échelle de la cellule vers l'étude de ces mécanismes l'échelle de la plante entière dans un contexte de stress hydrique. Avec cette vision plus intégrée, améliorer la tolérance au stress hydrique d'une céréale revient à élaborer des stratégies qui lui permettent d'utiliser avec la plus grande efficacité possible l'eau qu'elle a à sa disposition pendant la durée de son cycle pour produire du grain. Mon travail a contribué à identifier et à mieux comprendre ces différentes stratégies de gestion de la ressource en eau. Il me permet de prendre la mesure des interactions multiples entre traits racinaires et aériens pour la mise en place de ces stratégies. Il m'apporte la conviction qu'une meilleure compréhension de ces interactions à l'échelle de la plante entière dans son environnement est indispensable pour guider la sélection.

Les études portant sur la caractérisation de traits racinaires adaptatifs pour la tolérance au stress hydrique doivent mieux prendre en compte l'impact de ces traits dans le continuum hydraulique sol-plante-atmosphère. Il parait également important de mieux comprendre l'effet de l'environnement sur ces traits, et si leur effet adaptatif est conservé entre différents environnements. Enfin, une bonne compréhension des interactions entre traits adaptatifs ou non est importante afin de définir les assemblages les plus efficaces pour la bonne gestion de l'eau. Cela nécessite le développement d'outils permettant d'explorer la diversité pour l'identification de traits adaptatifs et une meilleure compréhension des interactions G x E contrôlant ces traits. Le développement de modèles permettant de mieux explorer les combinaisons de traits dans le continuum hydraulique et leurs effets sur les rendements dans des environnements et des contraintes hydriques précises est aussi nécessaire. Le déploiement de ces connaissances en sélection sera facilité par l'étude de matériel végétal élite où l'effet de QTL finement caractérisés contrôlant des traits adaptatifs pourra être rapidement testé. Toutes ces considérations vont bien au-delà de mes domaines de compétence et de recherche. Certaines pourront néanmoins être prises en compte dans le projet de recherche que je propose par la suite.

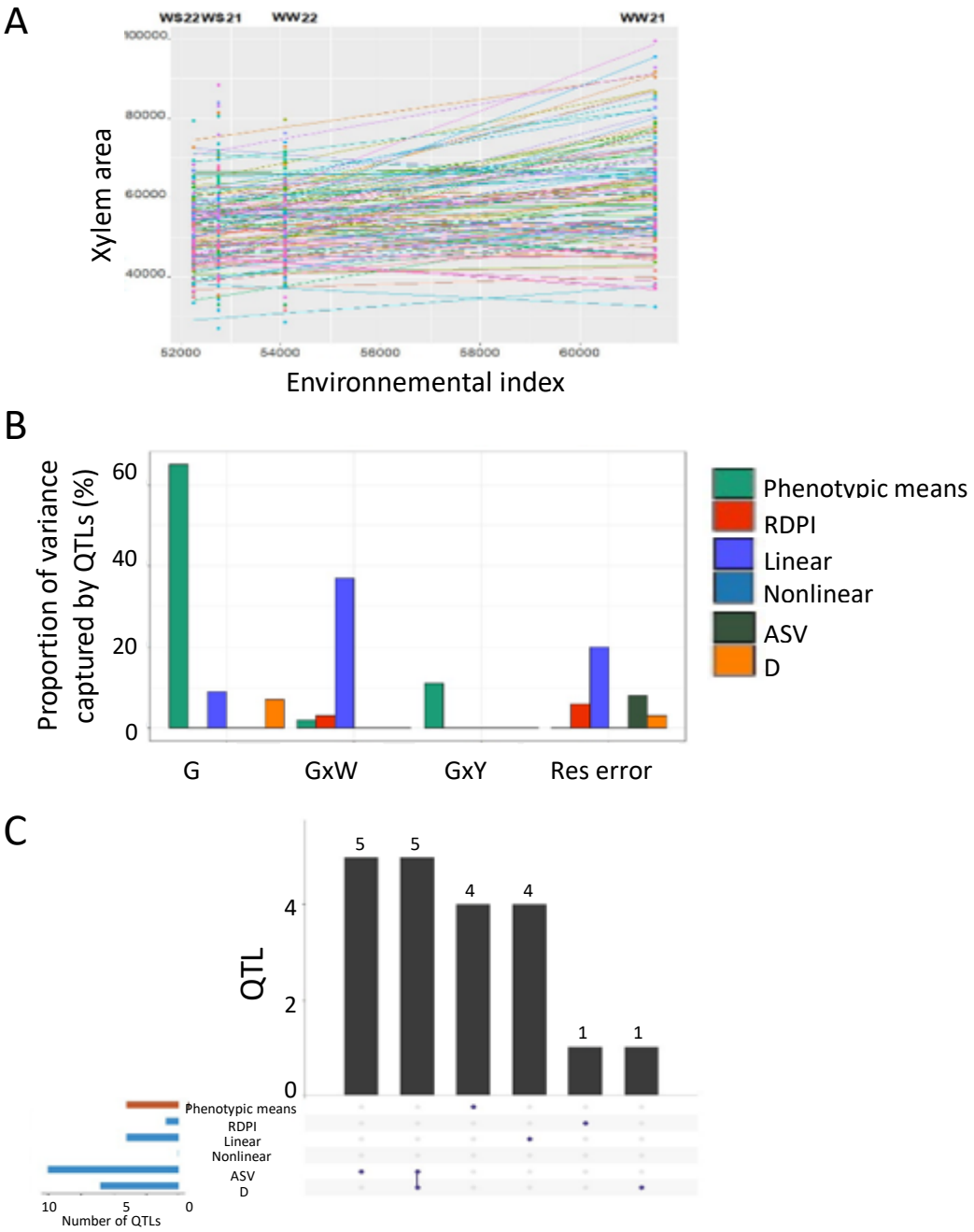

Figure 25 : Contrôle génétique de la plasticité des vaisseaux du xylème chez le mil. A: Mesure de la plasticité à l'aide de la méthode de Finlay-Wilkinson. La variation du phénotype pour chaque génotype est mesurée en considérant un index environnemental pour les quatre environnements : WW21 (irriguée 2021), WW22 (irriguée 2022), WS21 (stress hydrique 2021), WS22 (stress hydrique 2022). B: La proportion de variance capturée par les QTLs identifiés par GWAS à partir de différents indices de plasticité a été mesurée. Phenotypic means: moyenne de la surface des vaisseaux du xylème par traitement. RDPI: *relative distance plasticity* (Valladares et al., 2006). Linear: pente de la relation linéaire de Finlay-Wilkinson. Nonlinear: résidues de la relation linéaire. ASV: *AMMI stability index* (Elias et al., 2016). D: *Distance of the interaction principal component point to its origin in space* (Elias et al., 2016). G: composante génétique; GxW: interaction entre génétique et traitement. GxY: interaction entre génétique et année. Res error: erreur résiduelle. C: Diagramme Upset. Source: Sebastian Arenas.

5. Projets de recherche

5.1 Axe 1 : Contribution à la durabilité des agrosystèmes rizicoles

La riziculture inondée est très demandeuse en eau qui tend à se raréfier. Elle représente aussi une source importance d'émission de méthane qui tend à réchauffer l'atmosphère. La transition de la riziculture vers des agrosystèmes moins gourmands en eau et plus durables représente donc un enjeu majeur. Cela passe notamment par le développement de la culture en condition aérobie qui reste néanmoins moins productrice que la riziculture inondée et plus sujette au stress hydrique. Des stratégies d'amélioration agronomique et variétale sont nécessaires pour son expansion. Favoriser la mise en place de la symbiose mycorhizienne représente une voie d'amélioration agronomique. Augmenter la vigueur précoce et les capacités de transport d'eau ainsi que l'efficience de la transpiration représente une voie d'amélioration variétale. Certains agrosystèmes, de bas-fond notamment, ont cependant vocation à rester inondés. Dans ces conditions, limiter l'émission de méthane par la plante dans l'atmosphère représente une voie pour limiter leur impact climatique. Par la suite, je décris plusieurs projets en collaboration, partiellement financés où faisant l'objet de demandes de financement, qui proposent des approches pour améliorer la culture du riz dans les agrosystèmes aérobies.

- **Axe 1.1 : Traits anatomiques pour l'amélioration de la nutrition hydrominérale**

Les aérenchymes influenceraient positivement la croissance racinaire et la nutrition minérale mais auraient un effet négatif sur le transport d'eau radial dans la racine et la colonisation de ces dernières par les champignons endomycorhiziens à arbuscules (CMA ; Lynch *et al.*, 2021; Galindo-Castañeda *et al.*, 2022). La taille des vaisseaux du xylème influence quant à elle la conductance hydraulique axiale et de fait les capacités de transport d'eau des systèmes racinaires (Rishmawi *et al.*, 2023). Chez le riz, le rôle de ces traits dans la nutrition hydrominérale et la colonisation des racines par les CMA reste flou. De plus, les déterminants génétiques contrôlant ces traits restent élusifs. Des QTL potentiellement impliqués dans le contrôle de traits anatomiques ont été proposés (Kadam *et al.*, 2017) mais ils n'ont pas été validés et les gènes candidats sous-jacents n'ont pas été identifiés.

Dans le cadre d'une collaboration avec Hoang Thi Giang de l'AGI au Vietnam, nous avons avec Pascal Gantet (équipe CERES ; UMR DIADE) initié le phénotypage de l'anatomie racinaire dans un panel de riz *O. sativa* composé d'accessions vietnamiennes séquencées. Ce travail est partiellement financé par l'AGI et l'Ambassade de France au Vietnam à travers la bourse de thèse de Hien Linh Tran (2022-2025). Linh Tran a mesuré les traits anatomiques dont la surface des aérenchymes et des vaisseaux du xylème dans ce panel sur de racines issues de plantes cultivées au Vietnam en condition inondée. Les résultats préliminaires suggèrent qu'il existe une grande diversité pour ces deux traits, et que ces variations sont héritables. Ces résultats ont permis l'identification d'accessions contrastées pour ces traits. **Dans ce panel,**

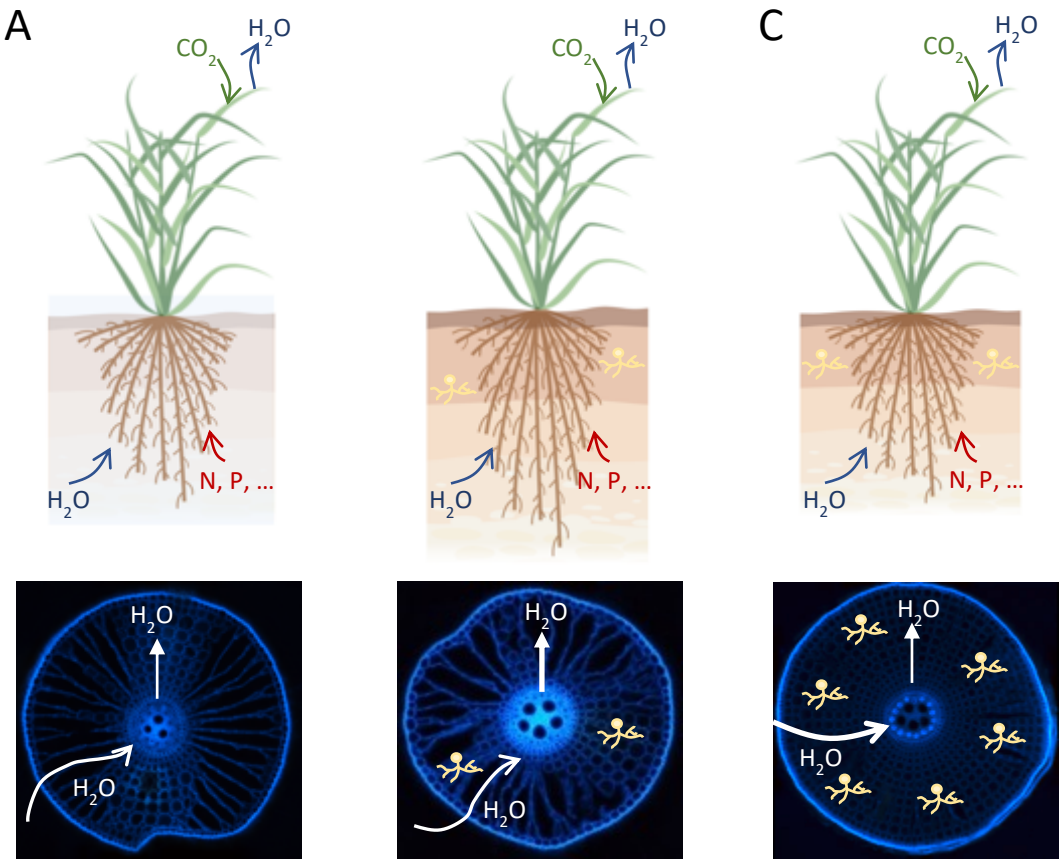

Figure 26 : Effets hypothétiques de l'anatomie racinaire sur le transport d'eau et l'infection des racines par les mycorhizes. A: Plante de riz cultivée en condition inondée sans infection des racines par les mycorhizes. B: Plante de riz cultivée en condition aérobie montrant une plus grande proportion d'aérenchymes et de surface des vaisseaux du xylème, mais un plus faible taux d'infection par les mycorhizes. C: Plante de riz cultivée en condition aérobie montrant une plus faible proportion d'aérenchymes et de surface du xylème, et un plus fort taux d'infection par les mycorhizes. Sources images anatomiques: Hien Linh Tran.

nous ambitionnons d'étudier (i) l'impact des aérenchymes sur le transport d'eau racinaire et la colonisation des racines par les CMA (Figure 26), (ii) l'impact de la surface des vaisseaux du xylème sur le transport et l'efficience d'utilisation de l'eau, (iii) leurs effets sur la tolérance au stress hydrique et (iv) les QTL/gènes contrôlant ces traits.

Impact des aérenchymes sur le transport d'eau et la symbiose mycorhizienne en condition aérobie et de stress hydrique

Des accessions contrastées pour la surface des aérenchymes mesurée en condition inondée seront sélectionnées. Celles avec des surfaces foliaires homogènes et provenant de l'agrosystèmes aérobie seront privilégiées. La surface des aérenchymes sera étudiée en condition aérobie afin de s'assurer du maintien des contrastes dans cette condition. Une dizaine d'accessions montrant des contrastes pour la surface des aérenchymes dans les racines coronaires et latérales seront cultivées en condition irriguée aérobie et de stress hydrique végétatif sur une plateforme lysimétrique à l'IRD de Montpellier après inoculation ou non par des CMA. Le stress hydrique sera appliqué après 4 semaines pour laisser le temps à la symbiose de se mettre en place. Cette phase d'établissement du stress hydrique sera suivie par un arrêt de l'irrigation pendant 3 semaines. La transpiration et la surface foliaire seront suivies en réponse à la demande évaporative et en réponse au stress hydrique. A la récolte, la surface racinaire, la surface des aérenchymes dans les racines et le taux de mycorhization seront mesurés et mis en lien avec la dynamique de la transpiration, la biomasse et l'efficience de la transpiration. Un système de pot à pression sera également utilisé afin de mesurer la conductivité hydraulique racinaire chez ces plantes cultivées dans les différentes conditions étudiées. Des études ont pu faire un lien entre la mycorhization et la fonction des aquaporines racinaires (Aroca *et al.*, 2007). Un inhibiteur d'aquaporine sera utilisé afin d'étudier si leur contribution aux flux d'eau racinaire est modifiée par la mise en place de la symbiose mycorhizienne. Ce travail devrait nous permettre d'identifier les bénéfices ou contreparties de la présence d'aérenchymes, et les mécanismes de compensation éventuels, sur le transport d'eau dans la racine. Ce travail sera réalisée en collaboration avec Abdala Gamby Diedhiou de l'UCAD, les sélectionneurs de l'AfricaRice et Jeongmin Choi du *Crop Science Center* à l'Université de Cambridge. Jeongmin Choi a une forte expertise dans le domaine de la symbiose mycorhizienne et maitrise les protocoles permettant de favoriser sa mise en place et ses effets. Ce travail est financé par un projet Agropolis et inclura des accessions de riz *O. glaberrima*. En effet, le riz Africain, plus tolérant au stress hydrique et adapté aux conditions de culture aérobie, pourrait montrer des réponses originales par rapport au riz asiatique. De plus, nous avons initié une collaboration avec Christophe Perrin et Camila Rebelledo (UMR AGAPi ; CIRAD) pour le montage d'un projet commissionné par la fondation *Methane Hub* qui pourrait permettre de financer ces approches. L'étude du rôle des aérenchymes dans la diffusion de méthane en condition inondée pourra également être envisagée en collaboration avec Ando Radanielson et Amelia Henry à l'IRRI.

Impact de la surface des vaisseaux du xylème sur l'utilisation de l'eau en condition aérobie et de stress hydrique

Des accessions contrastées pour la surface des vaisseaux du xylème en condition inondée seront sélectionnées, et comme pour les aérenchymes, le phénotype sera confirmé en condition aérobie. Une dizaine d'accessions montrant des contrastes pour la surface du xylème en condition aérobie, et avec des surfaces foliaires relativement homogènes, seront sélectionnées. Ces plantes seront mises en culture sur la plateforme lysimétrique de l'IRD en condition irriguée aérobie pour la mesure de leurs capacité d'extraction d'eau, de la réponse de la transpiration à la demande évaporative et de l'efficacité de la transpiration. Ces résultats seront mis en lien avec la surface des vaisseaux du xylème et l'architecture racinaire. Ces pots sont néanmoins d'une capacité réduite et peu adaptés à l'étude du stress hydrique terminal (post-floraison). Dans des lysimètres de plus grand volume disponibles au CERAAS au Sénégal, les effets de la surface des vaisseaux du xylème sur l'utilisation de l'eau, l'efficience de la transpiration et la production de grain en condition aérobie et de stress hydrique végétatif et terminal seront étudiés chez les accessions de ce sous-panel. Cela permettra de définir si ce trait est intéressant pour l'amélioration de la culture du riz en condition aérobie et la tolérance au stress hydrique. Cette approche, qui n'est pas encore financée, sera réalisée en collaboration avec les sélectionneurs de l'AfricaRice au Sénégal et de l'AGI au Vietnam. Elle pourra être initiée dans le cadre de la thèse de Hien Linh Tran à Montpellier et être approfondie dans le cadre du projet commissionné par la fondation *Methane Hub*.

Identification de gènes candidats contrôlant la formation des aérenchymes et du xylème

Des approches GWAS seront mises en œuvre afin d'identifier des régions du génome associées à la formation des aérenchymes et la taille des vaisseaux du xylème. Si les approches physiologiques précédentes révèlent un intérêt de ces traits pour l'adaptation de la culture du riz à la condition aérobie et au stress hydrique, des croisements entre accessions adaptées à des écosystèmes aérobies et contrastées pour ces deux traits seront réalisés. Les populations biparentales issues des croisements serviront pour la validation des QTL. Des lignées recombinantes dans la région des QTL et contrastées pour la formation des aérenchymes et des vaisseaux du xylème serviront pour étudier l'effet de ces traits pour l'amélioration des rendements en condition aérobie et de stress hydrique au champ. Des gènes dont l'annotation fonctionnelle sera en lien avec le trait étudié seront édités par CRISPR-Cas9 et feront l'objet d'une caractérisation fonctionnelle. L'approche GWAS sera initiée par Hien Linh Tran.

Résultats attendus

- Caractérisation de l'effet des aérenchymes et de la surface des vaisseaux du xylème sur les capacités de transport d'eau, l'efficience de la transpiration et la tolérance au stress hydrique chez le riz
- Influence des aérenchymes sur la mise en place de la symbiose mycorhizienne et impacts sur la croissance et la tolérance du riz au stress hydrique

- Identification de QTL/gènes contrôlant les aérenchymes et la surface des vaisseaux du xylème

• Axe 1.2 : Vigueur précoce pour la lutte contre les adventices et lien avec l'efficience de la transpiration

La vigueur précoce améliore la compétitivité du riz face aux adventices qui sont un facteur limitant pour les rendements dans les agrosystèmes aérobies. Une étude récente a montré que la capacité des feuilles à créer un ombrage au sol était le principal facteur expliquant une meilleure compétitivité du riz face aux adventices (Huber *et al.*, 2023). En limitant la lumière incidente sur le sol, la vigueur précoce permet également de limiter l'évaporation de l'eau du sol et améliore l'efficience de l'irrigation du champ (Vadez *et al.*, 2023). Nous avons mis en évidence que la vigueur précoce était associée à une meilleure efficience de la transpiration chez *O. glaberrima*. Ce mécanisme est lié à la restriction de la transpiration potentiellement causée par des diminutions de surfaces d'acquisition d'eau dans les racines (Affortit *et al.*, 2022). Deux QTL localisés sur le chromosome 5 et 7 contrôlant la vigueur précoce et l'efficience de la transpiration ont été identifiés (Affortit *et al.*, 2022). Ces QTL fonctionnent en interaction et contiennent, entre autres, le gène *Farnesyl diphosphate synthéthase 1* (*FPS1*) sur le chromosome 5 et un cluster de gène codant des aquaporines PIP sur le chromosome 7. FPS1 est une enzyme importante de la voie de biosynthèse des isoprénoïdes précurseurs de caroténoïdes, plastoquinones, ubiquinones, stérols et hormones végétales (Manzano *et al.*, 2016). Le gène *FPS1* est exprimé dans les feuilles et les racines alors que les gènes *PIP* sont principalement exprimés dans les racines chez le *O. sativa* et *A. thaliana* (source : Plant eFP, BAR). Chez *A. thaliana*, l'état de réduction des plastoquinones dans la chaine de transport d'électron lors de la photosynthèse influence le développement racinaire et améliore la tolérance au stress hydrique (Leverne *et al.*, 2023). Nous avons émis l'hypothèse que le gène *FPS1* pourrait être impliqué, à travers son rôle dans la biosynthèse d'isoprénoïdes, dans des mécanismes photosynthétiques, antioxydatifs ou hormonaux influençant la vigueur précoce.

Dans le cadre d'une collaboration avec Anja Krieger-Liszkay de l'Institut des sciences du vivant Frédéric Joliot, et avec Antony Champion et Laurent Laplaze (Équipe CERES ; UMR DIADE), nous avons entrepris de mieux caractériser la fonction du gène *FPS1*. Ce travail est partiellement financé par l'IRD à travers la bourse de thèse de Gagnon Penassou (2023-2026). Le travail de Master 2 de Gagnon Penassou a permis de montrer des différences d'expression significatives du gène *FPS1* entre haplotype fort et haplotype faible pour le QTL sur le chromosome 5 (Figure 27). Son travail a également mis en évidence un défaut de biomasse aérienne et une plus faible efficience de la transpiration chez un mutant perte de fonction d'*A. thaliana* pour le gène *FPS1*. Nous avons initié l'édition du gène *FPS1* et des trois autres gènes de la famille des *FPS* chez *O. sativa* et *O. glaberrima* par CRISPR-Cas9. **Nous ambitionnons de continuer la caractérisation des QTL contrôlant la vigueur précoce et l'efficience de la transpiration avec l'objectif de (i) valider la fonction du gène *FPS1* dans le**

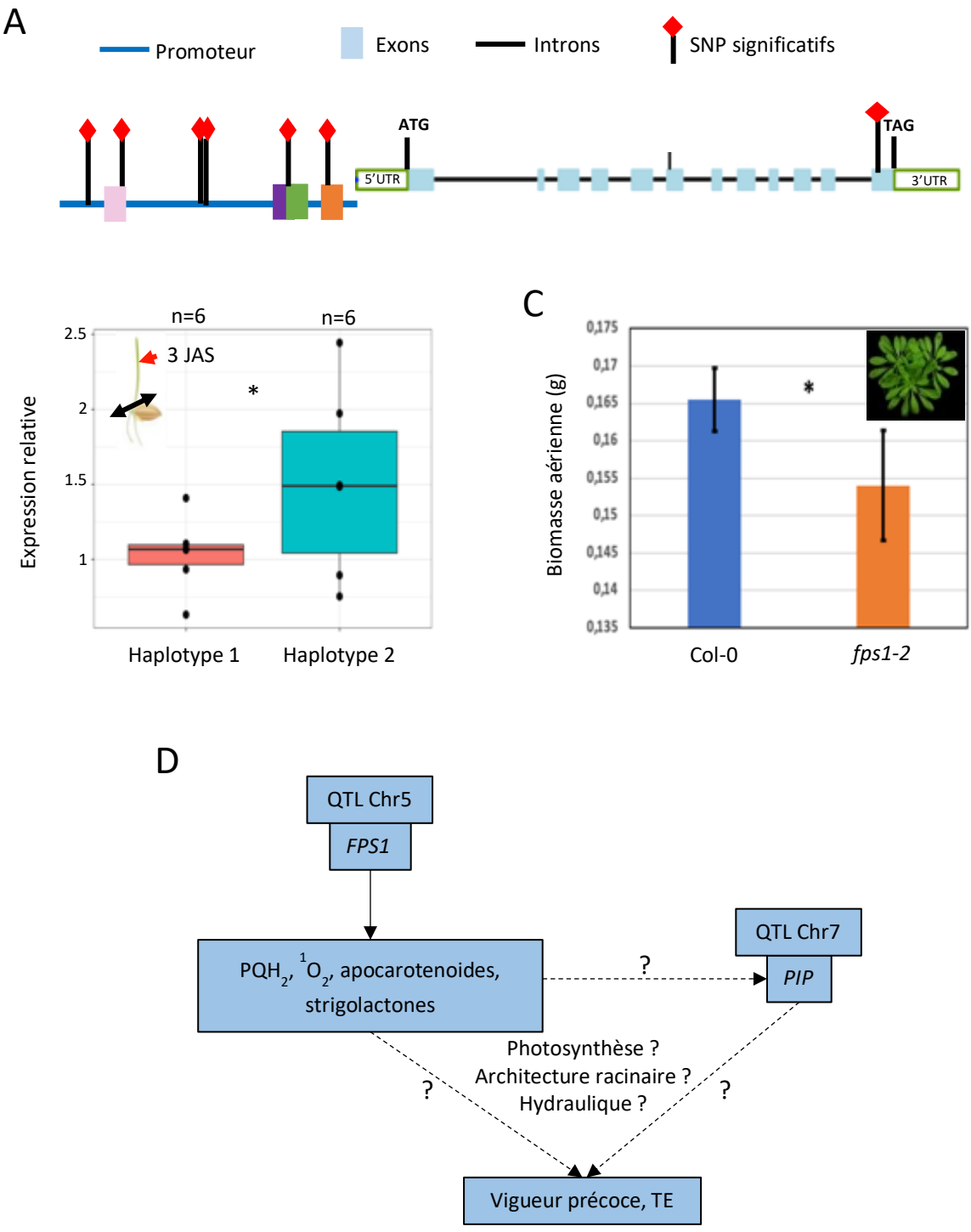

Figure 27 : Rôle potentiel du gène *FPS1* dans le contrôle de la vigueur précoce et de l'efficience de la transpiration. A: L'approche GWAS a permis d'identifier plusieurs SNPs significatifs localisés dans des régions régulatrices du promoteur de *FPS1*. B: L'expression de *FPS1* est significativement plus élevée dans les feuilles à 3 jours après semis chez 6 génotypes de l'haplotype 2 montrant une plus forte vigueur précoce. C: Des plantes mutantes pertes de fonction pour le gène *FPS1* chez *A. thaliana* montrent un défaut de biomasse aérienne à 48 jours après semis. D: Modèle d'action hypothétique de FPS1 en interaction avec des aquaporines PIP situées dans le QTL sur le chromosome 7 pour le contrôle de la vigueur précoce et de l'efficience de la transpiration. Source : Gagnon Penassou.

contrôle de la vigueur précoce et de l'efficience de la transpiration chez *A. thaliana* et le riz, (ii) de mieux comprendre les liens entre la vigueur et hydraulique de la plante et les effets sur l'efficience de la transpiration, et (iii) d'étudier leurs effets sur l'amélioration de la compétitivité du riz, de son efficience de la transpiration et des rendements en grain en condition de culture aérobie. Un projet qui permettra de financer une partie de ces travaux a été déposé à l'ANR (Porteur : Anja Krieger-Liszkay).

Validation du gène FPS1 dans le contrôle de la vigueur précoce et de l'efficience de la transpiration - lien avec la biosynthèse de plastoquinones et autres dérivés d'isoprénoïdes

Des mutants pour le gène *fps1* seront produits dans un fond génétique *O. sativa* et *O. glaberrima* afin de valider sa fonction chez les deux espèces. Chez *A. thaliana*, un certain degré de redondance a pu être observé entre les deux gènes appartenant à la famille des *FPS* (Manzano *et al.*, 2016). Nous réaliserons des mutants multiples des 4 gènes présents chez *O. sativa* et *O. glaberrima* à travers une approche CRISPR-Cas9. Nous tenterons également de complémenter le phénotype observé chez le mutant *fps1* d'*A. thaliana* par l'expression, chez ce mutant, du gène *FPS1* de riz. Les mutants *fps* d'*A. thaliana* et de riz seront étudiés pour leur vigueur précoce, leur architecture racinaire et leur efficience de la transpiration. Le fonctionnement de l'appareil photosynthétique, les quantités de plastoquinone, de certaines hormones, d'apocaroténoïdes et d'espèces réactives de l'oxygène seront mesurés dans les feuilles et les racines chez ces mutants en comparaison avec des plantes sauvages. L'expression des gènes par séquençage des ARN sera étudiée chez les mutants et les plantes sauvages dans les feuilles et les racines afin d'identifier les principaux réseaux de gènes mis en jeu. Nous étudierons l'existence de signaux aériens liés à *FPS1* qui contrôleraient la croissance racinaire. Pour cela, des greffes de parties aériennes de plantes mutantes d'*A. thaliana*, et potentiellement de riz, seront réalisées sur des systèmes racinaires sauvages, et vice versa. Ces approches ont été proposées dans le projet ANR soumis.

Rôle des aquaporines PIP en interaction avec le gène FPS1 pour le contrôle de la vigueur et de l'efficience de la transpiration

Le QTL contrôlant la vigueur précoce et l'efficience d'utilisation de l'eau situé sur le chromosome 7 contient quatre gènes d'aquaporine PIP dont certaines sont fortement exprimées dans les racines. Nous avons observé que les plantes à forte vigueur présentent une restriction de la transpiration en réponse à la demande évaporative. Cela suggère des limitations hydrauliques au niveau racinaire où l'offre ne serait plus capable de maintenir la demande lors de l'augmentation de la demande évaporative. Ces mécanismes pourraient être liés à des déséquilibres de surfaces racines/feuilles (Affortit *et al.*, 2022). Au-delà des surfaces, les aquaporines pourraient également participer à ces limitations hydrauliques dans les racines. Afin de tester cette hypothèse, différentes combinaisons de mutants pertes de fonction pour les gènes *PIP* présents dans le QTL sur le chromosome 7 seront produits. L'aquaporine PIP la plus exprimée sera également sur-exprimée dans la racine grâce à un promoteur racine spécifique (proR) chez une variété possédant des versions alléliques

associées à une plus forte biomasse et efficience d'utilisation de l'eau. Ces mutants et surexpresseurs seront cultivés, avec les plantes sauvages correspondantes, sur une plateforme lysimétrique à l'IRD pour la mesure de la réponse de la transpiration à la demande évaporative et l'efficience d'utilisation de l'eau. Des altérations dans ces phénotypes chez les mutants *pip* et proR:PIP permettront de valider la fonction de ces aquaporines dans le QTL et précisera leurs rôles dans le contrôle de l'hydraulique de la plante entière. Il s'avère que ce QTL sur le chromosome 7 est en interaction avec le QTL contenant le gène *FPS1* sur le chromosome 5. Le gène *FPS1* pourrait ainsi, à travers son rôle dans la biosynthèse des isoprénoïdes et molécules dérivées (dont l'acide abscissique), influencer l'hydraulique dans les racines à travers la régulation de l'expression et/ou la fonction des aquaporines. Si le rôle des PIP est confirmé, nous étudierons les interactions possibles entre la fonction de FPS1 et des PIP. Chez des mutants *fps1*, la dynamique d'expression des PIP sera étudiée au cours de l'augmentation de la demande évaporative sur une journée. Ces mutants seront cultivés en pot à pression pour la mesure de la conductivité hydraulique racinaire et la contribution des aquaporines sous différentes conditions de demande évaporative. Les résultats de l'approche précédente concernant le dosage des dérivés d'isoprénïodes renseigneront sur les voies de régulation des aquaporines via FPS1 qui pourraient être mises en jeu. D'autres mutants impliqués dans ces voies de signalisation pourront alors être testés pour affiner la compréhension de la signalisation mise en jeu (mutants de biosynthèse ou signalisation ABA par exemple). De plus, si l'hypothèse de signalisation longue distance est confirmée, des expériences de greffes entre mutants *fps1* et *pip* pourront être réalisées chez *A. thaliana*. Ce travail sera initié dans le cadre de la thèse de Gagnon Penassou.

Impact des QTL de vigueur précoce et d'efficience de la transpiration sur l'adaptation du riz à la culture en condition aérobie

Des lignées portant des versions alléliques fortes des QTL d'*O. glaberrima* pour la vigueur précoce et l'efficience de la transpiration dans un fond génétique *O. sativa* (*Chromosome Segment Substitution Lines*, CSSL) sont disponibles à l'IRRI. De plus, nous avons initié des croisements entre haplotypes forts et faibles d'*O. glaberrima* pour les deux QTL identifiés qui serviront pour la génération de lignées recombinantes contenant différentes combinaisons des QTL d'intérêt. La performance de ces lignées sera étudiée au champ en condition aérobie et de stress hydrique en comparaison avec des lignées issues des programmes de sélection de l'IRRI et de l'AfricaRice pour le semis direct et la culture en condition aérobie. Cela permettra d'évaluer l'intérêt de ces QTL pour la sélection. Ce travail sera initié dans le cadre de la thèse de Gagnon Penassou.

Résultats attendus

- Validation des gènes *FPS1* et *PIP* dans le contrôle de la vigueur précoce et de l'efficience de la transpiration chez le riz
- Identification des mécanismes de coordination entre croissance et hydraulique pour le contrôle de de l'efficience de la transpiration

- Validation de l'effet des QTL/gènes sur l'amélioration des rendements du riz en condition aérobie

5.2 Axe 2 : Contribution à l'amélioration de la tolérance au stress hydrique végétatif chez le mil

Le projet *Anatomics* avait pour but d'identifier des traits racinaires anatomiques associés à la tolérance au stress hydrique végétatif chez le mil et les déterminants génétiques qui les contrôlent. Ce projet a été réalisé en collaboration avec Malcolm Bennett, Darren Wells et Jonathan Atkinson à l'Université de Nottingham ; Awa Faye, Ndjido Kane et Bassirou Sine à l'ISRA ; et Laurent Laplaze et Vincent Vadez (Équipe CERES, UMR DIADE) ; et Philippe Cubry (Équipe Dynadiv, UMR DIADE). Nous avons acquis au cours de ce projet un large jeu de données multi-phénotypique et pluriannuel collecté au champ sur un panel de diversité du mil. Le projet ANR JCJC *PlastiMil* que je coordonne se base sur les données issues du projet *Anatomics* pour étudier les déterminants génétiques contrôlant la plasticité adaptative en réponse au stress hydrique. L'étude des traits anatomiques en lien avec la tolérance au stress hydrique est prise en charge par Pablo Affortit, étudiant en thèse financé par une bouse du Ministère de l'Enseignement et de la Recherche. Le rôle des traits racinaires dans la nutrition minérale fait l'objet de la thèse de Princia Nakombo-Gbassault, étudiante en thèse financée par l'IRD et l'Ambassade de France en République Centrafricaine. L'identification de traits plastiques adaptatifs est portée par Sébastian A. Jimenez, post-doctorant financé par le projet *PlastiMil*.

Une corrélation positive entre le maintien du rendement sous stress hydrique végétatif et la surface des vaisseaux du xylème a été mise en évidence dans ce jeu de données. Des résultats préliminaires obtenus par Pablo Affortit suggèrent que des plantes avec des surfaces de vaisseaux du xylème plus grandes seraient capables d'extraire de façon plus efficace l'eau et de maintenir la transpiration plus longtemps au cours de l'asséchement du sol. La surface racinaire et la surface foliaire pourraient co-varier avec la surface des vaisseaux du xylème formant un assemblage bénéfique pour l'extraction et l'utilisation de l'eau. Cette stratégie « dépensière » en eau se traduirait également par un retour plus rapide à une croissance optimale après re-irrigation du sol. Par ailleurs, l'étude de la réponse de la surface des vaisseaux du xylème au stress hydrique montre que ce trait est plastique et que cette plasticité est dépendante du génotype. En effet, l'interaction G x E contribue de manière significative à la variance de ce trait. Nous avons émis l'hypothèse qu'une augmentation de la taille des vaisseaux du xylème pourrait constituer une réponse adaptative au stress hydrique végétatif chez le mil. Sébastian Jimenez a utilisé plusieurs méthodes afin de mesurer des indices de plasticité. Il utilise une procédure mise en place Mélisande Blein-Nicolas, Renaud Rincent et Yacine Djabali (UMR GQE) pour étudier dans quelle mesure ces indices permettent l'identification par GWAS de marqueurs capturant la variance expliquée par l'interaction G x E (Djabali *et al.*, 2023). Des premières analyses suggèrent que la régulation

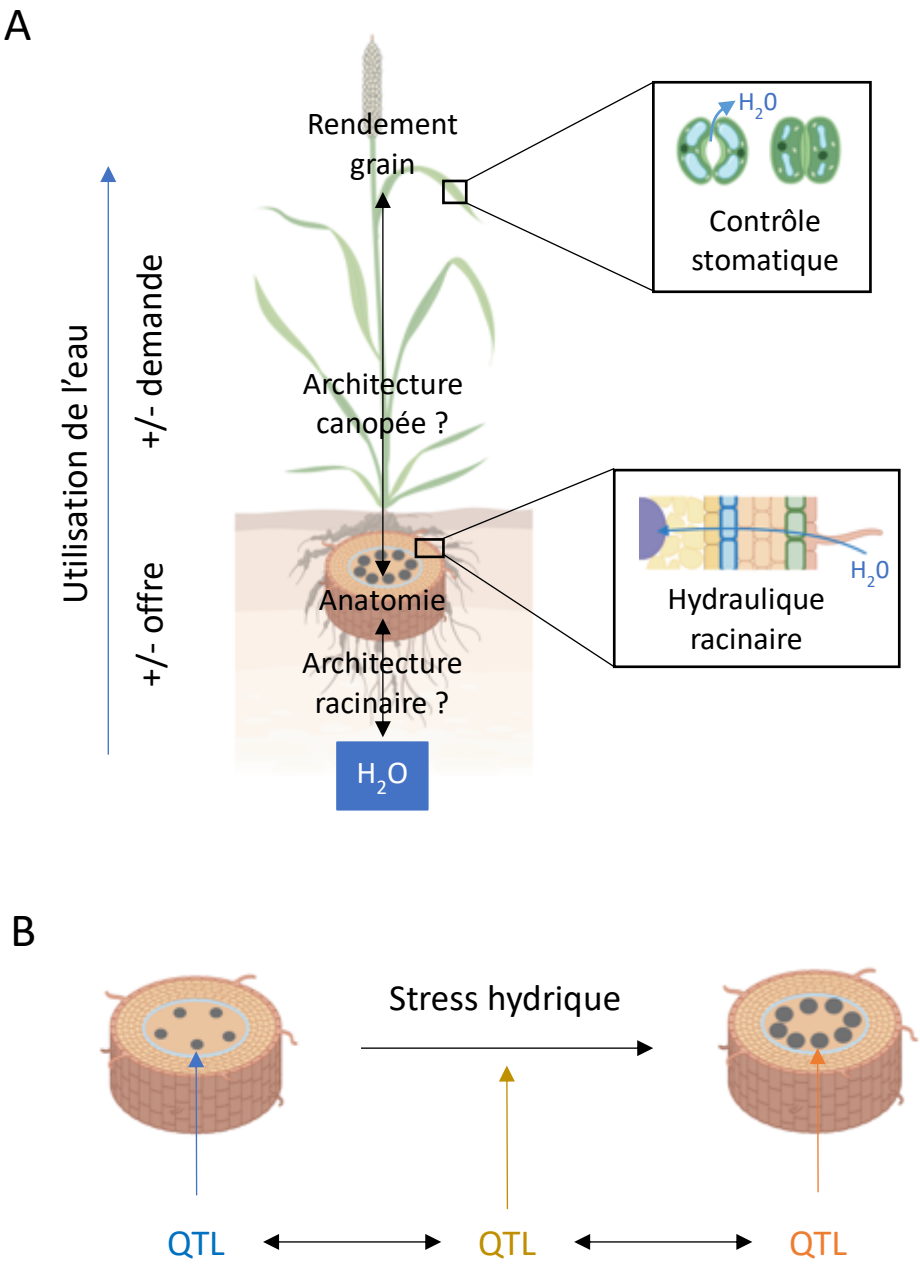

Figure 28 : Effets de la surface des vaisseaux du xylème sur la tolérance au stress hydrique végétatif chez le mil. A: Interactions possibles entre surface des vaisseaux du xylème et autres traits d'architecture racinaire et de la canopée pour le contrôle de l'utilisation de l'eau et du maintien du rendement. B: Modèle du contrôle génétique de la surface des vaisseaux du xylème et de sa plasticité.

génétique de la surface des vaisseaux du xylème dans une condition donnée serait partiellement indépendante de celle de sa plasticité (Figure 25). Le changement d'état de la surface des vaisseaux du xylème en réponse au stress hydrique serait donc sous contrôle génétique propre.

Nous continuerons, dans le cadre du projet *PlastiMil* et des collaborations existantes, à caractériser le rôle des vaisseaux du xylème et de sa plasticité dans l'hydraulique chez le mil et l'effet sur sa tolérance face au stress hydrique (Figure 28). **Nous avons ainsi pour objectifs (i) d'identifier des assemblages de traits propices à l'extraction d'eau pour la tolérance du mil à un stress hydrique végétatif, (ii) définir la plasticité de la surface des vaisseaux du xylème en réponse à différents types de stress hydrique et les conditions où cette plasticité aurait un effet adaptatif et (iii) d'identifier des QTL/gènes contrôlant la surface des vaisseaux du xylème et sa plasticité en réponse au stress hydrique.**

Assemblage de traits pour le maintien du continuum hydraulique sous stress hydrique

La surface des vaisseaux du xylème augmente la conductance hydraulique axiale dans la racine. L'augmentation de la taille des vaisseaux du xylème augmente aussi la vulnérabilité de ces derniers en condition de stress et peut causer des dommages hydriques pour la plante (Sun *et al.*, 2021). La vulnérabilité des vaisseaux du xylème dépendrait des capacités d'acquisition et de transport radial d'eau d'une part et de la demande évaporative d'autre part. L'effet bénéfique des vaisseaux du xylème sur la tolérance au stress hydrique végétatif dépendrait ainsi d'un assemblage de traits qui contribuerait au maintien du continuum hydraulique. Nous émettons l'hypothèse que cela passerait par des mécanismes de compensations liés soit à une augmentation des capacités d'absorption et/ou de la conductance radiale, soit à une diminution de la transpiration par la diminution de la surface foliaire et/ou de la conductance stomatique. Le sous-panel de lignées contrastées pour la surface des vaisseaux du xylème sera cultivé dans un système de rhizotrons en condition irriguée et de stress hydrique. Ce système permettra de suivre le développement racinaire et de mesurer les traits architecturaux comme la longueur et la densité des racines latérales avec précision. Ces lignées seront également cultivées dans des pots à pression en condition irriguée et de stress hydrique. Cela permettra la mesure à différentes heures de la journée de la conductivité hydraulique racinaire. Ces mesures seront réalisées en présence ou non d'un inhibiteur d'aquaporines afin d'étudier leur contribution aux flux d'eau. Ces lignées seront enfin cultivées sur la plateforme lysimétrique de l'IRD en condition irriguée et de stress hydrique. Dans cette expérience, la surface foliaire et la réponse de la transpiration à l'augmentation de la demande évaporative seront étudiées. Toutes ces données seront mises en relation avec la surface des vaisseaux du xylème et permettront d'identifier les co-variables associées à l'effet bénéfique de ce trait sur les capacités d'extraction d'eau de la plante. Ce travail initié au cours de la thèse de Pablo Affortit sera poursuivi par un stage de Master.

Caractérisation de la plasticité des vaisseaux du xylème en réponse au stress hydrique

La réponse plastique de la surface des vaisseaux du xylème observée au champ en condition de stress hydrique végétatif parait adaptative. Cette réponse pourrait néanmoins être non bénéfique dans d'autres conditions. Ainsi, il parait important de mieux caractériser cette plasticité, et ces effets associés, en réponse à différent types de stress hydrique. Un sous-panel composé de lignées avec des surfaces des vaisseaux du xylème relativement similaires mais qui contrastent pour sa plasticité sera sélectionné. Ces lignées seront mises en culture sur la plateforme lysimétrique de l'IRD dans différentes conditions de stress hydrique (faible à sévère). L'humidité du sol sera évaluée par la mesure de la fraction d'eau du sol transpirable par la plante (*Fraction of soil transpirable water*, FTSW), i.e. la différence entre la quantité d'eau maximale que peut contenir un volume de sol et la quantité d'eau restante dans ce volume de sol que la plante n'est plus capables d'extraire. Des plantes seront mises en culture dans des pots stabilisés à des FTSW à 100, 80, 60, 40 et 20 % pendant 4 semaines. La surface des vaisseaux du xylème des racines coronaires développées sur chaque nœuds sera mesurée à la base de la tige. La comparaison de la surface des vaisseaux du xylème entre nœuds et conditions de stress hydrique permettra de préciser la réponse plastique. La comparaison des taux de transpiration et des biomasses entre génotypes en lien avec la surface des vaisseaux du xylème, et leur plasticité, permettra d'étudier le rôle adaptatif de ces derniers dans les capacités d'extraction d'eau. Cette approche est financée par le projet *PlastiMil*. Nous avons déposé un projet pour l'obtention d'une bourse Raman-Charpak qui permettrait d'accueillir pendant 6 mois un étudiant indien, Vinay Sharma (ICRISAT), pour réaliser ce travail.

Contrôle génétique de la surface des vaisseaux du xylème et de leur plasticité

L'étude de la plasticité racinaire permettra de mieux définir les contrastes entre génotypes et racines sur différents nœuds pour la réponse plastique. Trois lignées avec des réponses plastiques contrastées seront sélectionnées : pas de plasticité, une réponse plastique adaptative (augmentation de la surface des vaisseaux du xylème *a priori*) et une plasticité mal-adaptive (réduction de la surface des vaisseaux du xylème *a priori*). Ces lignées seront cultivées en condition irriguée et dans deux conditions de FTSW induisant une réponse plastique modérée et forte. Les apex de la racine considérée seront prélevées au cours des premiers stades de son développement qui correspondent à la mise en place de la vasculature dans la stèle. L'échantillonnage consistera à prélever les racines dès apparition des premiers poils absorbants (zone de division + zone d'élongation). L'expression totale des gènes dans ces racines sera étudiée par séquençage des ARN. La comparaison de l'expression des gènes entre la condition irriguée et de stress hydrique permettra de sélectionner des gènes qui répondent au stress hydrique. La comparaison de l'expression des gènes entre lignées plastiques et non plastique permettra d'identifier des gènes spécifiquement impliqués dans la réponse plastique. Cette approche est financée par le projet *PlastiMil*.

Dans le panel entier, différentes approches seront utilisées pour identifier des régions du génome associées à la plasticité des vaisseaux du xylème par GWAS. Les moyennes de la surface du xylème en condition irriguée et stress hydrique serviront pour des approches

utilisant un modèle mixte multivarié (Boer *et al.*, 2007; Korte *et al.*, 2012), et des modèles de méta-analyse (Walsche *et al.*, 2023) en collaboration avec Vincent Ségura (UMR AGAPi). Les indices de plasticité serviront pour des analyses GWAS (simple et multi-locus ; Segura *et al.*, 2012). Les associations obtenues pour les différents modèles et les différentes variables utilisées (moyennes ou indices de plasticité) seront comparées. Des associations retrouvées entre modèles et capturant une importante part de la variance expliquée par l'interaction G x E seront sélectionnées. Dans ces régions, nous chercherons à identifier des gènes potentiellement impliqués dans la réponse plastique identifiés par séquençage des ARN. Ce travail a été initié par Pablo Affortit et Sebastian Arenas et sera poursuivi par un étudiant de Master. Une approche d'identification de gènes candidat à travers l'utilisation de l'intelligence artificielle pour une exploration en profondeur des connaissances présentes dans la littérature (articles scientifiques, bases de données publiques…) sera mise en œuvre en collaboration avec Pierre Larmande (équipe CERES, UMR DIADE) dans le cadre du projet ANR DIG-AI (Porteur : P. Larmande).

Afin de valider les QTL identifiées par GWAS, nous produirons des populations biparentales BC2F4 par des croisements réalisés entre lignées contrastées pour la surface des vaisseaux du xylème d'une part et pour leur plasticité d'autre part. Ces lignées recombinantes seront séquencées et des analyses QTL seront réalisées. Des lignées recombinantes dans la région du QTL ayant l'effet le plus fort seront identifiées et mises en culture au champ afin de valider l'effet adaptatif du QTL pour la tolérance au stress hydrique végétatif. Ces croisements pourront être réalisés en collaboration avec des sélectionneurs mil de l'ISRA ou de l'ICRISAT qui interviennent dans le projet *PlastiMil*.

Les gènes candidats potentiellement impliqués dans le contrôle de la surface des vaisseaux du xylème et leur plasticité feront l'objet d'une validation fonctionnelle. Nous n'avons pas réussi à mettre en place un protocole de transformation chez le mil. A défaut, des orthologues de ces gènes seront identifiés chez *A. thaliana* et *O. sativa* et leur analyse fonctionnelle sera réalisée. Si des mutants pour ces gènes ne sont pas déjà disponibles, ils seront produits par édition du gènome à l'aide de CRISPR-Cas9. Nous pourrons envisager de surexprimer de manière hétérologue les gènes candidats de mil contrôlant la plasticité chez *A. thaliana* et *O. sativa* afin d'étudier si cela induit ou altère une réponse plastique de la surface des vaisseaux du xylème. Ces approches de validation fonctionnelle sont en partie financées par le projet *PlastiMil* mais nécessiteront sur le long terme une recherche de nouveaux financements.

Résultats attendus

- Caractérisation des interactions hydrauliques entre vaisseaux du xylème et autres traits d'architecture et fonctionnels racinaire et aérien
- Norme de réaction pour la plasticité des vaisseaux du xylème en réponse au stress hydrique

- Identification de QTL/gènes contrôlant la surface des vaisseaux du xylème et leur plasticité adaptative en réponse au stress hydrique végétatif chez le mil

5.3 Axe 3 : Développement des capacités de phénotypage et de modélisation pour soutenir la sélection

Le phénotypage de plantes de façon simple, précise et rapide est fondamental pour la sélection. Les traits mécanistiques associés aux processus hydrauliques représentent une cible de choix pour la sélection de plante plus tolérantes au stress hydrique. Mieux comprendre ces traits passe par la prise en compte des différents assemblages de trait à l'échelle de la plante entière. Pourtant, les méthodes permettant de suivre ces traits et les processus hydrauliques associés sont souvent peu révélatrices de la vraie vie de la plante et ne sont pas adaptées au haut-débit. Les lysimètres représentent un bon moyen de mesurer des processus hydrauliques de façon non destructive à l'échelle de la plante entière. Certaines plateformes de phénotypage permettent de suivre de façon simultanée la perte en eau et la dynamique de croissance de la canopée de plantes cultivées en pot dans des conditions proches de celles du champ (Vadez *et al.*, 2015). Les mesures racinaires sont néanmoins difficiles à mettre en œuvre dans ces systèmes de culture. On peut également se demander l'effet que peut avoir ces pots sur le développement racinaire. De fait, il n'existe à ce jour aucune méthode permettant de phénotyper à haut-débit et de façon simultanée et robuste les traits mécanistiques racinaires, aériens et leurs effets sur les processus hydrauliques à l'échelle de la plante entière. Ainsi, le phénotypage de traits mécanistiques et fonctionnels constitue un frein pour l'analyse de la diversité, les approches génétiques et la sélection.

Les avancées technologiques permettront sans doute un jour de mesurer l'ensemble des traits d'une plante et les processus hydrauliques associés *in naturae*. En attendant, il existe des modèles de culture permettant de simuler des plantes entières mais qui prennent peu en compte la structure et le fonctionnement racinaire. Il existe également des modèles structure-fonction de la racine mais qui prennent peu en compte la structure de la canopée et le fonctionnement aérien. Combiner des modèles de culture avec des modèles structure-fonction racinaire permettrait d'améliorer les capacités de prédiction des fonctions hydrauliques à l'échelle de la plante entière, de mieux comprendre les assemblages de traits fonctionnant en synergie et d'élaborer des idéotypes. Coupler ces modèles à des modèles génétiques permettrait de prédire des phénotypes de plante et les fonctions associées pour l'hydraulique en fonction de leur génotype, donc de génotyper plutôt que de phénotyper (à condition de bien caractériser l'environnement sol et atmosphère). Cela permettrait aux sélectionneurs de développer *in silico* des schémas de sélection pour une meilleure combinaison d'allèle dans un environnement donné.

Le développement de modèles de culture prenant mieux en compte les traits mécanistiques racinaires nécessite des méthodes de phénotypage permettant de mesurer les systèmes

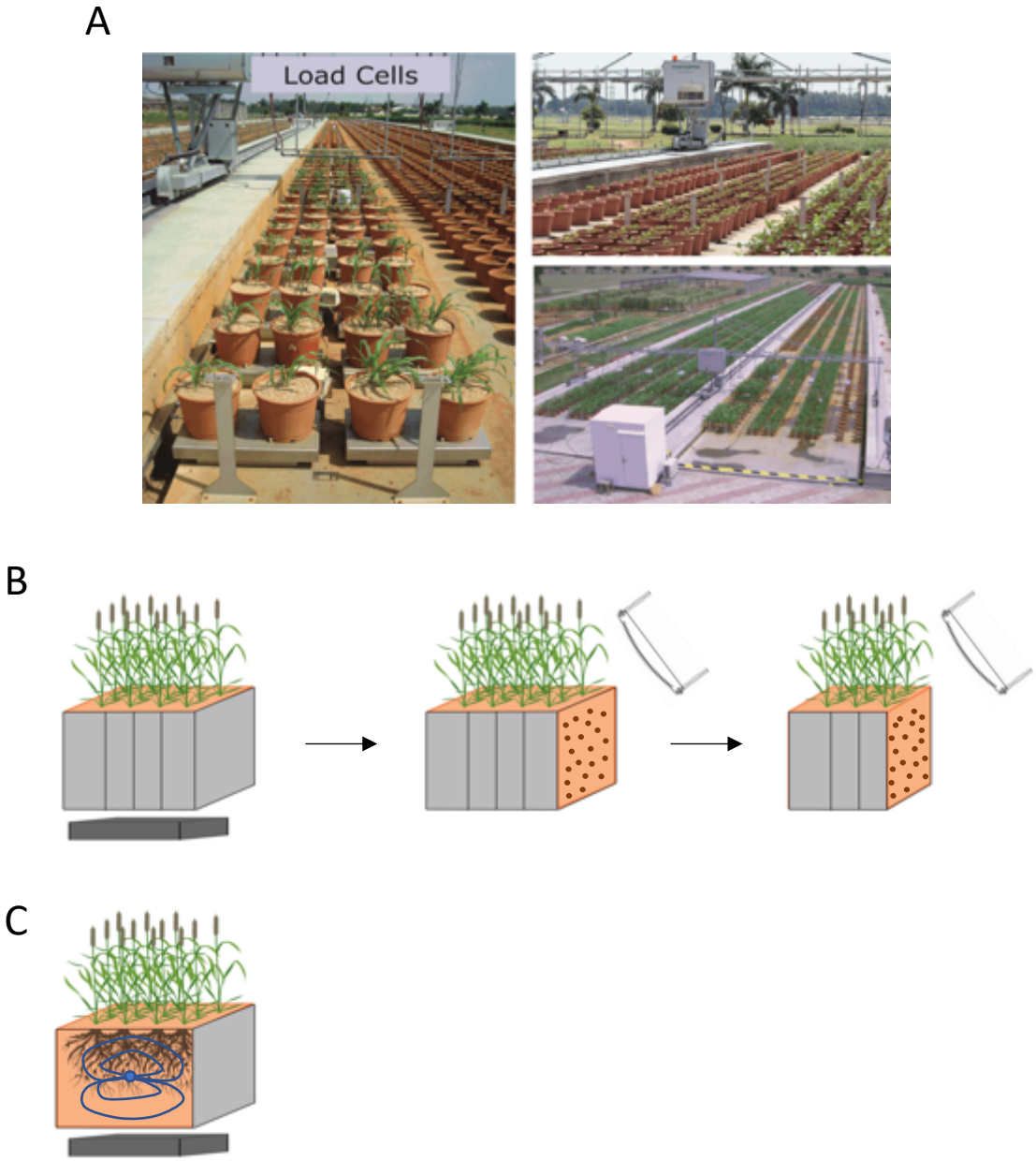

Figure 29 : Phénotypage de l'hydraulique des plantes en lien avec l'acquisition de l'eau par les racines et l'utilisation de l'eau par les parties aériennes en condition semi-agronomique. A: Plateforme LeasyScan à l'ICRISAT. Les plantes sont cultivées dans des pots sur des balances. Des scanners 3D permettent d'imager les parties aériennes. Issue de Vadez et al., 2015 (Figure 2). B: Un nouveau dispositif consisterait à utiliser, à la place des pots, des conteneurs représentant des parcelles. Ces derniers seraient toujours placés sur des balances. Certains conteneurs seraient manufacturés de façon à pouvoir réaliser des tranchées de sol pour le comptage d'impacts racinaires. C: D'autres conteneurs seraient équipés de sondes pour la mesure de la résistance électrique du sol.

racinaires, leur plasticité et leur fonctionnement hydrique en lien avec les parties aériennes et l'hydraulique de la plante entière. Ces méthodes n'ont pas vocation à être haut-débit. Combiner des méthodes existantes pourrait être envisagé (Figure 28). Par exemple, les pots des lysimètres pourraient être remplacés par des conteneurs représentant des parcelles placées sur des balances, où il serait possible de suivre la capture d'eau du sol par les racines à l'aide de sonde électrique (Bacher *et al.*, 2023). Un système de découpe du sol dans les conteneurs pourrait permettre de compter des impacts afin de mesurer la profondeur et la densité racinaire (Faye *et al.*, 2019). Le déplacement des conteneurs dans une chambre noire pourrait même permettre le comptage automatisé des impacts par spectroscopie à fluorescence (Wasson *et al.*, 2016). L'implémentation de la tomographie à ablation laser permettrait d'étudier en quasi-simultanée l'anatomie de ces racines (Strock *et al.*, 2019). En parallèle, des scanners seraient capables de se déplacer dans et au-dessus de la canopée pour suivre le développement des parties aériennes par l'imagerie 3D (Vadez *et al.*, 2015).

Le développement des modèles génétiques nécessite le phénotypage haut-débit des traits racinaires utilisés en modélisation et de leur plasticité en réponse à l'environnement hydrique et en interaction ou non avec le génotype. Des méthodes de phénotypage permettant de mesurer une partie de ces traits au champ dans différentes conditions hydriques existent. Pour d'autres traits, ils seront mesurés sur des plateformes et la validité des mesures au champ pourra être vérifiée dans des panels plus restreints. Des approches de génétique permettront de définir les allèles contrôlant ces traits et leur plasticité afin de prendre en compte les interactions avec l'environnement. Cela fait l'objet des activités développées dans l'Axe 1 et 2 de ce projet. J'ambitionne de contribuer au développement de ces capacités de phénotypage permettant d'ouvrir la voie vers l'amélioration des modèles de culture pour une meilleure prise en compte de la fonction des racines dans l'hydraulique à l'échelle de la plante entière. Le développement des capacités de phénotypage proposé dans cet Axe 3 pourrait être réalisé en collaboration avec l'ISRA au Sénégal. Ce projet n'est pas financé mais pourra être proposé, en collaboration avec des modélisateurs, généticiens et sélectionneurs, dans le cadre d'appels à projets Européen ou via d'autres bailleurs.

5.4 Conclusion

Ce projet propose de continuer l'identification et la caractérisation de traits bénéfiques pour l'adaptation de la culture du riz et du mil à la raréfaction de la ressource en eau. Il repose sur une vision du fonctionnement hydraulique des plantes basée sur des équilibres entre offre par les racines et demande par les parties aériennes. Il propose de mieux comprendre les traits importants pour la régulation de cette équilibre afin de définir les meilleures stratégies de gestion de la ressource en eau par la plante dans différents environnements de stress. Les activités proposées sont en partie financées sur le court terme et des projets ont été soumis ou sont en cours de construction pour le financement sur le plus long terme.

Ce travail a une visée appliquée. Il s'efforce de considérer les processus hydrauliques dans le fonctionnement de la plante entière dans un environnement proche des conditions agronomiques. Il utilise des approches de phénotypage, de physiologie et de modélisation pour étudier la variabilité et identifier des traits bénéfiques pour la régulation des équilibres hydriques. Il comprend également une part génétique importante qui a pour but de mieux caractériser les QTL identifiés. Ces approches ont néanmoins vocation à être encore affinées, sur les méthodes de phénotypage (Axe 3) mis en œuvre ou sur le matériel génétique utilisé. Ces dernières dépendent néanmoins des ressources disponibles chez les espèces étudiées. Le mil reste une espèce orpheline. Un nouveau projet financé par l'ANR et porté par Laurent Laplaze (*SorDrought*) propose de mobiliser de nouveaux traits physiologiques pour l'amélioration de la tolérance au stress hydrique terminal chez le sorgho. Ce projet, auquel je participe, sera réalisé en collaboration avec l'UMR AGAP Institut (AGAPi ; David Pot), l'ISRA/CERAAS (Bassirou Sine et Cyril Diatta), l'UMR BioGeCo (Sylvain Delzon) et deux compagnies privées (Patrice Jeanson à Eurosorgho et Philippe Dufour à RAGT2n). Il propose d'utiliser des populations de type *Backcross Nested Association Mapping* (BCNAM) de sorgho qui permettent l'identification de QTL et l'étude de traits associés dans un fond génétique homogène et élite. Le projet propose également la validation de gènes candidats associés aux QTL identifiés chez le sorgho, cette espèce étant relativement peu récalcitrante à la transformation *in vitro*.

Au final ce projet multi-espèce et pluridisciplinaire est ambitieux mais possible grâce à un travail collaboratif au sein de l'équipe CERES d'abord, au sein de l'UMR DIADE ensuite, et grâce aux nombreux liens scientifiques fructueux établis en France et à l'étranger. En particulier, nos collaborations avec l'ISRA/CERAAS au Sénégal et l'AGI au Vietnam nous donne accès à des terrains d'études privilégiés où les enjeux pour l'agriculture sont majeurs et les possibilités d'impacts multiples. Dans les années à venir, j'envisage une nouvelle période d'expatriation dont les contours restent encore à être définis en équipe.

6. Références

Abdalla M, Ahmed MA, Cai G, Wankmüller F, Schwartz N, Litig O, Javaux M, Carminati A. 2022. Stomatal closure during water deficit is controlled by below-ground hydraulics. Annals of botany **129**, 161–170.
Abdalla M, Carminati A, Cai G, Javaux M, Ahmed MA. 2021. Stomatal closure of tomato under drought is driven by an increase in soil–root hydraulic resistance. Plant Cell and Environment **44**, 425–431.
Affortit P, Effa-Effa B, Ndoye MS, *et al.* 2022. Physiological and genetic control of transpiration efficiency in African rice, Oryza glaberrima Steud. Journal of Experimental Botany **73**, 5279–5293.
Ahmed MA, Zarebanadkouki M, Meunier F, Javaux M, Kaestner A, Carminati A. 2018. Root type matters: Measurement of water uptake by seminal, crown, and lateral roots in maize. Journal of Experimental Botany **69**, 1199–1206.
Ajmera I, Henry A, Radanielson AM, Klein SP, Ianevski A, Bennett MJ, Band LR, Lynch JP. 2022. Integrated root phenotypes for improved rice performance under low nitrogen availability. Plant Cell and Environment **45**, 805–822.
Aroca R, Porcel R, Ruiz-Lozano JM. 2007. How does arbuscular mycorrhizal symbiosis regulate root hydraulic properties and plasma membrane aquaporins in Phaseolus vulgaris under drought, cold or salinity stresses? New Phytologist **173**, 808–816.
Atkinson JA, Pound MP, Bennett MJ, Wells DM. 2019. Uncovering the hidden half of plants using new advances in root phenotyping. Current Opinion in Biotechnology **55**, 1–8.
Bacher H, Montagu A, Herrmann I, Walia H, Schwartz N, Peleg Z. 2023. Stress-induced deeper rooting introgression enhances wheat yield under terminal drought. Journal of Experimental Botany **74**, 4862–4874.
Bao Y, Aggarwal P, Robbins NE, *et al.* 2014. Plant roots use a patterning mechanism to position lateral root branches toward available water. Proceedings of the National Academy of Sciences of the United States of America **111**, 9319–9324.
Basirat M, Mousavi SM, Abbaszadeh S, Ebrahimi M, Zarebanadkouki M. 2019. The rhizosheath: a potential root trait helping plants to tolerate drought stress. Plant and Soil **445**, 565–575.
Benard P, Zarebanadkouki M, Brax M, Kaltenbach R, Jerjen I, Marone F, Couradeau E, Felde VJMNL, Kaestner A, Carminati A. 2019. Microhydrological niches in soils: How mucilage and EPS alter the biophysical properties of the rhizosphere and other biological hotspots. Vadose Zone Journal **18**, 1–10.
Boer MP, Wright D, Feng L, Podlich DW, Luo L, Cooper M, Van Eeuwijk FA. 2007. A mixed-model quantitative trait loci (QTL) analysis for multiple-environment trial data using environmental covariables for QTL-by-environment interactions, with an example in maize. Genetics **177**, 1801–1813.
Borrell AK, Wong ACS, George-Jaeggli B, *et al.* 2022. Genetic modification of PIN genes induces causal mechanisms of stay-green drought adaptation phenotype. Journal of Experimental Botany **73**, 6711–6726.
Boursiac Y, Pradal C, Bauget F, Lucas M, Delivorias S, Godin C, Maurel C. 2022. Phenotyping and modeling of root hydraulic architecture reveal critical determinants of axial water transport. Plant Physiology **190**, 1289–1306.
Burridge JD, Grondin A, Vadez V. 2022. Optimizing crop water use for drought and climate change adaptation requires a multi-scale approach. Frontiers in Plant Science **13**, 824720.

Burridge J, Jochua CN, Bucksch A, Lynch JP. 2016. Legume shovelomics: High-Throughput phenotyping of common bean (*Phaseolus vulgaris* L.) and cowpea (*Vigna unguiculata* subsp, *unguiculata*) root architecture in the field. Field Crops Research **192**, 21–32.
Cabrera-Bosquet L, Fournier C, Brichet N, Welcker C, Suard B, Tardieu F. 2016. High-throughput estimation of incident light, light interception and radiation-use efficiency of thousands of plants in a phenotyping platform. New phytologist **212**, 269–281.
Cai G, Tötzke C, Kaestner A, Ahmed MA. 2022. Quantification of root water uptake and redistribution using neutron imaging: a review and future directions. Plant Journal **111**, 348–359.
Caldeira CF, Jeanguenin L, Chaumont F, Tardieu F. 2014. Circadian rhythms of hydraulic conductance and growth are enhanced by drought and improve plant performance. Nature Communications **5**, 1–9.
Calvo-Polanco M, Ribeyre Z, Dauzat M, *et al.* 2021. Physiological roles of Casparian strips and suberin in the transport of water and solutes. New Phytologist **232**, 2295–2307.
Campbell MT, Grondin A, Walia H, Morota G. 2020. Leveraging genome-enabled growth models to study shoot growth responses to water deficit in rice. Journal of Experimental Botany **71**, 5669–5679.
Carminati A, Passioura JB, Zarebanadkouki M, Ahmed MA, Ryan PR, Watt M, Delhaize E. 2017. Root hairs enable high transpiration rates in drying soils. New Phytologist **216**, 771–781.
Chenu K, Porter JR, Martre P, Basso B, Chapman SC, Ewert F, Bindi M, Asseng S. 2017. Contribution of crop models to adaptation in wheat. Trends in Plant Science **22**, 472–490.
Chopart JL, Siband P. 1999. Development and validation of a model to describe root length density of maize from root counts on soil profiles. Plant and Soil **214**, 61–74.
Choudhary S, Guha A, Kholova J, Pandravada A, Messina CD, Cooper M, Vadez V. 2020. Maize, sorghum, and pearl millet have highly contrasting species strategies to adapt to water stress and climate change-like conditions. Plant Science **295**, 110297.
Cooper M, Gho C, Leafgren R, Tang T, Messina C. 2014. Breeding drought-tolerant maize hybrids for the US corn-belt: Discovery to product. Journal of Experimental Botany **65**, 6191–6194.
Coupel-Ledru A, Lebon E, Christophe A, Gallo A, Gago P, Pantin F, Doligez A, Simonneau T. 2016. Reduced nighttime transpiration is a relevant breeding target for high water-use efficiency in grapevine. Proceedings of the National Academy of Sciences of the United States of America **113**, 8963–8968.
Couvreur V, Faget M, Lobet G, Javaux M, Chaumont F, Draye X. 2018. Going with the flow: Multiscale insights into the composite nature of water transport in roots. Plant Physiology **178**, 1689–1703.
Cubry P, Pidon H, Ta KN, *et al.* 2020. Genome wide association study pinpoints key agronomic QTLs in African rice *Oryza glaberrima*. Rice **13**, 1–12.
Cubry P, Tranchant-Dubreuil C, Thuillet AC, *et al.* 2018. The rise and fall of African rice cultivation revealed by analysis of 246 new genomes. Current Biology **28**, 1–9.
Dixit S, Grondin A, Lee C-R, Henry A, Olds T-M, Kumar A. 2015. Understanding rice adaptation to varying agro-ecosystems: trait interactions and quantitative trait loci. BMC genetics **16**, 86.
Djabali Y, Rincent R, Martin ML, Blein-Nicolas M. 2023. Plasticity QTLs specifically contribute to the genotype × water availability interaction in maize. Theoretical and Applied Genetics **136**, 228.

Dunn J, Hunt L, Afsharinafar M, Meselmani M Al, Mitchell A, Howells R, Wallington E, Fleming AJ, Gray JE. 2019. Reduced stomatal density in bread wheat leads to increased water-use efficiency. Journal of Experimental Botany **70**, 4737–4747.
Dynowski M, Schaaf G, Loque D, Moran O, Ludewig U. 2008. Plant plasma membrane water channels conduct the signalling molecule H2O2. The Biochemical journal **414**, 53–61.
van Eeuwijk FA, Bink MC, Chenu K, Chapman SC. 2010. Detection and use of QTL for complex traits in multiple environments. Current Opinion in Plant Biology **13**, 193–205.
Elias AA, Robbins KR, Doerge RW, Tuinstra MR. 2016. Half a century of studying genotype × Environment interactions in plant breeding experiments. Crop Science **56**, 2090–2105.
Ermakova M, Osborn H, Groszmann M, *et al.* 2021. Expression of a CO2-permeable aquaporin enhances mesophyll conductance in the C4 species *Setaria viridis*. eLife **10**, 1–16.
Evenson RE, Gollin D. 2003. Assessing the impact of the Green Revolution, 1960 to 2000. Science **300**, 758–762.
Faye A, Sine B, Chopart J-L, *et al.* 2019. Development of a model estimating root length density from root impacts on a soil profile in pearl millet (*Pennisetum glaucum* (L.) R. Br). Application to measure root system response to water stress in field conditions. Plos One **14**, e0214182.
Finlay KW, Wilkinson GN. 1963. The analysis of adaptation in a plant-breeding programme. Australian Journal of Agricultural Research. **14**, 742–754
Fuente C de la, Grondin A, Sine B, *et al.* 2023. Glutaredoxin regulation of primary root growth confers early drought stress tolerance in pearl millet. eLife **12:RP86169**.
Galindo-Castañeda T, Lynch JP, Six J, Hartmann M. 2022. Improving soil resource uptake by plants through capitalizing on synergies between root architecture and anatomy and root-associated microorganisms. Frontiers in Plant Science **13**, 1–15.
George TS, Brown LK, Ramsay L, White PJ, Newton AC, Bengough AG, Russell J, Thomas WTB. 2014. Understanding the genetic control and physiological traits associated with rhizosheath production by barley (*Hordeum vulgare*). New Phytologist **203**, 195–205.
Gerbeau P, Amodeo G, Henzler T, Santoni V, Ripoche P, Maurel C. 2002. The water permeability of Arabidopsis plasma membrane is regulated by divalent cations and pH. Plant Journal **30**, 71–81.
Gholipoor M, Choudhary S, Sinclair TR, Messina CD, Cooper M. 2013. Transpiration response of maize hybrids to atmospheric vapour pressure deficit. Journal of Agronomy and Crop Science **199**, 155–160.
Grondin A, Affortit P, Tranchant-Dubreuil C, de la Fuente-Cantó C, Mariac C, Gantet P, Vadez V, Vigouroux Y, Laplaze L. 2020. Aquaporins are main contributors to root hydraulic conductivity in pearl millet [*Pennisetum glaucum* (L) R. Br.]. Plos One **15**, e0233481.
Grondin A, Bhosale R, Atkinson JA, *et al.* 2022. High-throughput root phenotyping: Opportunities and challenges for the adaptation of arid and semi-arid crops to future climates. In: Kane NA, Foncéka D, Dalton T, eds. Crop Adaptation and Improvement for Drought-Prone Environments. Manhattan, KS: New Prairie Press, 258–282.
Grondin A, Dixit S, Torres R, Venkateshwarlu C, Rogers E, Mitchell-Olds T, Benfey PN, Kumar A, Henry A. 2018. Physiological mechanisms contributing to the QTL qDTY3.2 effects on improved performance of rice Moroberekan x Swarna BC2F3:4 lines under drought. Rice **11**, 1–17.
Grondin A, Rodrigues O, Verdoucq L, Merlot S, Leonhardt N, Maurel C. 2015. Aquaporins contribute to ABA-triggered stomatal closure through OST1-mediated phosphorylation. Plant Cell **27**, 1945–54.

Guo L, Zi YW, Lin H, Wei EC, Chen J, Liu M, Zhang LC, Li JQ, Gu H. 2006. Expression and functional analysis of the rice plasma-membrane intrinsic protein gene family. Cell Research **16**, 277–286.
Hall B, Lanba A. 2019. Three-dimensional analysis of biological systems via a novel laser ablation technique. Journal of Laser Applications **31**, 022602.
Hammer GL, Van Oosterom E, McLean G, Chapman SC, Broad I, Harland P, Muchow RC. 2010. Adapting APSIM to model the physiology and genetics of complex adaptive traits in field crops. Journal of Experimental Botany **61**, 2185–2202.
Harris K, Subudhi PK, Borrell A, Jordan D, Rosenow D, Nguyen H, Klein P, Klein R, Mullet J. 2007. Sorghum stay-green QTL individually reduce post-flowering drought-induced leaf senescence. Journal of Experimental Botany **58**, 327–338.
Havaux M. 2020. Plastoquinone in and beyond photosynthesis. Trends in Plant Science **25**, 1252–1265.
Henry A, Cal AJ, Batoto TC, Torres RO, Serraj R. 2012. Root attributes affecting water uptake of rice (*Oryza sativa*) under drought. Journal of Experimental Botany **63**, 4751–4763.
Heymans A, Couvreur V, LaRue T, Paez-Garcia A, Lobet G. 2020. GranAR, a computational tool to better understand the functional importance of monocotyledon root anatomy. Plant Physiology **182**, 707–720.
Hirt H, Al-Babili S, Almeida-Trapp M, *et al.* 2023. PlantACT! – how to tackle the climate crisis. Trends in Plant Science **28**, 537–543.
Hochberg U, Rockwell FE, Holbrook NM, Cochard H. 2018. Iso/Anisohydry: A plant–environment interaction rather than a simple hydraulic trait. Trends in Plant Science **23**, 112–120.
Horii H, Nemoto K, Miyamoto N, Harada J. 2006. Quantitative trait loci for adventitious and lateral roots in rice. Plant Breeding **125**, 198–200.
Hsu PK, Dubeaux G, Takahashi Y, Schroeder JI. 2021. Signaling mechanisms in abscisic acid-mediated stomatal closure. Plant Journal **105**, 307–321.
Huber M, Julkowska MM, Snoek LB, van Veen H, Toulotte J, Kumar V, Kajala K, Sasidharan R, Pierik R. 2023. Towards increased shading capacity: A combined phenotypic and genetic analysis of rice shoot architecture. Plants People Planet, 1–20.
Jarvis N, Larsbo M, Lewan E, Garré S. 2022. Improved descriptions of soil hydrology in crop models: The elephant in the room? Agricultural Systems **202**, 103477.
Jezek M, Blatt MR. 2017. The membrane transport system of the guard cell and its integration for stomatal dynamics. Plant Physiology **174**, 487–519.
Jha P, Shashi, Rustagi A, Agnihotri PK, Kulkarni VM, Bhat V. 2011. Efficient *Agrobacterium*-mediated transformation of *Pennisetum glaucum* (L.) R. Br. using shoot apices as explant source. Plant Cell, Tissue and Organ Culture **107**, 501–512.
Johansson I, Karlsson M, Shukla VK, Chrispeels MJ, Larsson C, Kjellbom P. 1998. Water transport activity of plasma membrane aquaporin PM28A is regulated by phosphorylation. The Plant cell **10**, 451–459.
Kadam NN, Tamilselvan A, Lawas LMF, *et al.* 2017. Genetic control of plasticity in root morphology and anatomy of rice in response to water deficit. Plant Physiology **174**, 2302–2315.
Kholová J, Hash CT, Kumar PL, Yadav RS, Kocová M, Vadez V. 2010. Terminal drought-tolerant pearl millet [*Pennisetum glaucum* (L.) R. Br.] have high leaf ABA and limit transpiration at high vapour pressure deficit. Journal of experimental botany **61**, 1431–40.
Kholová J, Murugesan T, Kaliamoorthy S, *et al.* 2014. Modelling the effect of plant water

use traits on yield and stay-green expression in sorghum. Functional Plant Biology **41**, 1019–1034.
Kholová J, Nepolean T, Tom Hash C, Supriya A, Rajaram V, Senthilvel S, Kakkera A, Yadav R, Vadez V. 2012. Water saving traits co-map with a major terminal drought tolerance quantitative trait locus in pearl millet [*Pennisetum glaucum* (L.) R. Br.]. Molecular Breeding **30**, 1337–1353.
Kirkegaard JA, Lilley JM, Howe GN, Graham JM. 2007. Impact of subsoil water use on wheat yield. Australian Journal of Agricultural Research **58**, 303–315.
Klein SP, Schneider HM, Perkins AC, Brown KM, Lynch JP. 2020. Multiple integrated root phenotypes are associated with improved drought tolerance. Plant Physiology **183**, 1011–1025.
Korte A, Vilhjálmsson BJ, Segura V, Platt A, Long Q, Nordborg M. 2012. A mixed-model approach for genome-wide association studies of correlated traits in structured populations. Nature Genetics **44**, 1066–1071.
Kusmec A, Srinivasan S, Nettleton D, Schnable PS. 2017. Distinct genetic architectures for phenotype means and plasticities in *Zea mays*. Nature Plants **3**, 715–723.
Kwak JM, Mori IC, Pei ZM, Leonhard N, Angel Torres M, Dangl JL, Bloom RE, Bodde S, Jones JDG, Schroeder JI. 2003. NADPH oxidase AtrbohD and AtrbohF genes function in ROS-dependent ABA signaling in arabidopsis. EMBO Journal **22**, 2623–2633.
de la Fuente Cantó C, Diouf MN, Ndour PMS, *et al.* 2022. Genetic control of rhizosheath formation in pearl millet. Scientific Reports **12**, 1–13.
de la Fuente Cantó C, Simonin M, King E, Moulin L, Bennett MJ, Castrillo G, Laplaze L. 2020. An extended root phenotype: the rhizosphere, its formation and impacts on plant fitness. Plant Journal **103**, 951–964.
Laitinen RAE, Nikoloski Z. 2019. Genetic basis of plasticity in plants. Journal of Experimental Botany **70**, 795–804.
Langridge P, Reynolds MP. 2015. Genomic tools to assist breeding for drought tolerance. Current Opinion in Biotechnology **32**, 130–135.
Lartaud M, Perin C, Courtois B, *et al.* 2015. PHIV-RootCell: A supervised image analysis tool for rice root anatomical parameter quantification. Frontiers in Plant Science **5**, 1–7.
Leverne L, Roach T, Perreau F, Maignan F, Krieger-Liszkay A. 2023. Increased drought resistance in state transition mutants is linked to modified plastoquinone pool redox state. Plant Cell and Environment **46**, 3737–3747.
Lian H-L, Yu X, Lane D, Sun W-N, Tang Z-C, Su W-A. 2006. Upland rice and lowland rice exhibited different PIP expression under water deficit and ABA treatment. Cell research **16**, 651–60.
Liang Z, Wu Y, Ma L, Guo Y, Ran Y. 2022. Efficient genome editing in *Setaria italica* using CRISPR/Cas9 and base editors. Frontiers in Plant Science **12**, 1–10.
Liu TY, Ye N, Song T, *et al.* 2019. Rhizosheath formation and involvement in foxtail millet (*Setaria italica*) root growth under drought stress. Journal of Integrative Plant Biology **61**, 449–462.
Liu S, Zenda T, Tian Z, Huang Z. 2023. Metabolic pathways engineering for drought or/and heat tolerance in cereals. Frontiers in Plant Science **14**, 1–32.
Lynch JP. 2018. Rightsizing root phenotypes for drought resistance. Journal of Experimental Botany **69**, 3279–3292.
Lynch JP, Strock CF, Schneider HM, Sidhu JS, Ajmera I, Galindo-Castañeda T, Klein SP, Hanlon MT. 2021. Root anatomy and soil resource capture. Plant Soil **466**, 21–63

Manschadi AM, Christopher J, Devoil P, Hammer GL. 2006. The role of root architectural traits in adaptation of wheat to water-limited environments. Functional Plant Biology **33**, 823–837.
Manzano D, Andrade P, Caudepón D, Altabella T, Arró M, Ferrer A. 2016. Suppressing farnesyl diphosphate synthase alters chloroplast development and triggers sterol-dependent induction of jasmonate- and Fe-related responses. Plant Physiology **172**, 93–117.
Martínez-Ballesta M del C, García-Gomez P, Yepes-Molina L, Guarnizo AL, Teruel JA, Carvajal M. 2018. Plasma membrane aquaporins mediates vesicle stability in broccoli. PLoS ONE **13**, 1–19.
Martre P, Jamieson PD, Semenov MA, Zyskowski RF, Porter JR, Triboi E. 2006. Modelling protein content and composition in relation to crop nitrogen dynamics for wheat. European Journal of Agronomy **25**, 138–154.
Maurel C, Boursiac Y, Luu D-T, Santoni V, Shahzad Z, Verdoucq L. 2015. Aquaporins in plants. Physiological Reviews **95**, 1321–1358.
Maurel C, Verdoucq L, Luu D-T, Santoni V. 2008. Plant aquaporins: membrane channels with multiple integrated functions. Annual review of plant biology **59**, 595–624.
Maurel C, Verdoucq L, Rodrigues O. 2016. Aquaporins and plant transpiration. Plant Cell and Environment **39**, 2580–2587.
Medina S, Vicente R, Nieto-Taladriz MT, Aparicio N, Chairi F, Vergara-Diaz O, Araus JL. 2019. The plant-transpiration response to vapor pressure deficit (VPD) in durum wheat is associated with differential yield performance and specific expression of genes involved in primary metabolism and water transport. Frontiers in Plant Science **9**, 1–19.
Messina CD, Sinclair TR, Hammer GL, Curan D, Thompson J, Oler Z, Gho C, Cooper M. 2015. Limited-transpiration trait may increase maize drought tolerance in the US corn belt. Agronomy Journal **107**, 1978–1986.
Meyer RS, Choi JY, Sanches M, *et al.* 2016. Domestication history and geographical adaptation inferred from a SNP map of African rice. Nature Genetics **48**, 1083–1088.
Monforte AJ. 2020. Time to exploit phenotypic plasticity. Journal of Experimental Botany **71**, 5295–5297.
Ntakirutimana F, Tranchant-Dubreuil C, Cubry P, Chougule K, Zhang J, Wing RA, Adam H, Lorieux M, Jouannic S. 2023. Genome-wide association analysis identifies natural allelic variants associated with panicle architecture variation in African rice, *Oryza glaberrima* Steud. G3: Genes, Genomes, Genetics **13**, 1–21.
Onogi A, Watanabe M, Mochizuki T, Hayashi T, Nakagawa H, Hasegawa T, Iwata H. 2016. Toward integration of genomic selection with crop modelling: the development of an integrated approach to predicting rice heading dates. Theoretical and Applied Genetics **129**, 805–817.
Orosa-Puente B, Leftley N, von Wangenheim D, *et al.* 2018. Root branching toward water involves posttranslational modification of transcription factor ARF7. Science **362**, 1407–1410.
Passot S, Gnacko F, Moukouanga D, *et al.* 2016. Characterization of pearl millet root architecture and anatomy reveals three types of lateral roots. Frontiers in plant science **7**, 829.
Passot S, Moreno-Ortega B, Moukouanga D, Balsera C, Guyomarc'h S, Lucas M, Lobet G, Laplaze L, Muller B, Guédon Y. 2018. A new phenotyping pipeline reveals three types of lateral roots and a random branching pattern in two cereals. Plant Physiology **177**, 896–910.
Postaire O, Tournaire-Roux C, Grondin A, Boursiac Y, Morillon R, Schäffner AR, Maurel C.

2010. A PIP1 aquaporin contributes to hydrostatic pressure-induced water transport in both the root and rosette of Arabidopsis. Plant Physiology **152**, 1418–1430.
Postma JA, Kuppe C, Owen MR, Mellor N, Griffiths M, Bennett MJ, Lynch JP, Watt M. 2017. OpenSimRoot: widening the scope and application of root architectural models. New Phytologist **215**, 1274–1286.
Ranathunge K, Steudle E, Lafitte R. 2003. Control of water uptake by rice (*Oryza sativa* L.): role of the outer part of the root. Planta **217**, 193–205.
Ravi Kumar S, Hammer GL, Broad I, Harland P, McLean G. 2009. Modelling environmental effects on phenology and canopy development of diverse sorghum genotypes. Field Crops Research **111**, 157–165.
Rebouillat J, Dievart A, Verdeil JL, Escoute J, Giese G, Breitler JC, Gantet P, Espeout S, Guiderdoni E, Périn C. 2009. Molecular genetics of rice root development. Rice **2**, 15–34.
Reckling M, Ahrends H, Chen TW, *et al.* 2021. Methods of yield stability analysis in long-term field experiments. A review. Agronomy for Sustainable Development **41**, 27.
Reddy PS, Tharanya M, Sivasakthi K, Srikanth M, Hash CT, Kholova J, Sharma KK, Vadez V. 2017. Molecular cloning and expression analysis of aquaporin genes in pearl millet [*Pennisetum glaucum* (L) R. Br.] genotypes contrasting in their transpiration response to high vapour pressure deficits. Plant Science **265**, 167–176.
Richards RA, Passioura JB. 1989. A breeding program to reduce the diameter of the major xylem vessel in the seminal roots of wheat and its effect on grain yield in rain-fed environments. Australian Journal of Agricultural Research **40**, 943–950.
Rishmawi L, Bauget F, Protto V, Bauland C, Nacry P, Maurel C. 2023. Natural variation of maize root hydraulic architecture underlies highly diverse water uptake capacities. Plant Physiology **192**, 2404–2418.
Robson JK, Ferguson JN, McAusland L, *et al.* 2023. Chlorophyll fluorescence-based high-throughput phenotyping facilitates the genetic dissection of photosynthetic heat tolerance in African (*Oryza glaberrima*) and Asian (*Oryza sativa*) rice. Journal of Experimental Botany **74**, 5181–5197.
Rodrigues O, Reshetnyak G, Grondin A, Saijo Y, Leonhardt N, Maurel C, Verdoucq L. 2017. Aquaporins facilitate hydrogen peroxide entry into guard cells to mediate ABA- and pathogen-triggered stomatal closure. Proceedings of the National Academy of Sciences of the United States of America **114**, 9200–9205.
Sade N, Vinocur BJ, Diber A, Shatil A, Ronen G, Nissan H, Wallach R, Karchi H, Moshelion M. 2009. Improving plant stress tolerance and yield production: Is the tonoplast aquaporin *Si*TIP2;2 a key to isohydric to anisohydric conversion? New Phytologist **181**, 651–661.
Sandhu N, Raman KA, Torres RO, Audebert A, Dardou A, Kumar A, Henry A. 2016. Rice root architectural plasticity traits and genetic regions for adaptability to variable cultivation and stress conditions. Plant Physiology, pp.00705.2016.
Santos CM, Romeiro D, Silva JP, Basso MF, Molinari HBC, Centeno DC. 2020. An improved protocol for efficient transformation and regeneration of *Setaria italica*. Plant Cell Reports **39**, 501–510.
Schäfer ED, Owen MR, Band LR, Farcot E, Bennett MJ, Lynch JP. 2022. Modeling root loss reveals impacts on nutrient uptake and crop development. Plant Physiology **190**, 2260–2278.
Scheenen TWJ, van Dusschoten D, de Jager PA, Van As H. 2000. Quantification of water transport in plants with NMR imaging. Journal of Experimental Botany **51**, 1751–1759.
Scheenen TWJ, Vergeldt FJ, Heemskerk AM, Van As H. 2007. Intact plant magnetic

resonance imaging to study dynamics in long-distance sap flow and flow-conducting surface area. Plant Physiology **144**, 1157–1165.
Schneider HM. 2022. Characterization, costs, cues and future perspectives of phenotypic plasticity. Annals of Botany **130**, 131–148.
Schneider HM, Klein SP, Hanlon MT, Kaeppler S, Brown KM, Lynch JP. 2020*a*. Genetic control of root anatomical plasticity in maize. Plant Genome **13**, 1–14.
Schneider HM, Klein SP, Hanlon MT, Nord EA, Brown KM, Warry A, Bhosale R, Lynch JP. 2020*b*. Genetic control of root architectural plasticity in maize. Journal of Experimental Botany **71**, 3185–3197.
Schneider HM, Lor VSN, Hanlon MT, *et al.* 2021. Root angle in maize influences nitrogen capture and is regulated by calcineurin B-like protein (CBL)-interacting serine/threonine-protein kinase 15 (*Zm*CIPK15). Plant Cell and Environment **45**, 837–853.
Schneider H, Lor VSN, Zhang X, *et al.* 2023. Transcription factor *bHLH121* regulates root cortical aerenchyma formation in maize. Proceedings of the National Academy of Sciences **120**, e2219668120.
Schoppach R, Wauthelet D, Jeanguenin L, Sadok W. 2014. Conservative water use under high evaporative demand associated with smaller root metaxylem and limited trans-membrane water transport in wheat. Functional Plant Biology **41**, 257–269.
Sebastian J, Yee M-C, Goudinho Viana W, *et al.* 2016. Grasses suppress shoot-borne roots to conserve water during drought. Proceedings of the National Academy of Sciences **113**, 8861–8866.
Segura V, Vilhjalmsson BJ, Platt A, Korte A, Seren U, Long Q, Nordborg M. 2012. An efficient multi-locus mixed model approach for genome-wide association studies in structured populations. Nature Genetics **44**, 825–830.
Shkolnik D, Nuriel R, Bonza MC, Costa A, Fromm H. 2018. MIZ1 regulates ECA1 to generate a slow, long-distance phloem-transmitted Ca2+ signal essential for root water tracking in Arabidopsis. Proceedings of the National Academy of Sciences of the United States of America **115**, 8031–8036.
Sidi-Boulenouar R, Cardoso M, Coillot C, *et al.* 2019. Multiscale NMR investigations of two anatomically contrasted genotypes of sorghum under watered conditions and during drought stress. Magnetic Resonance in Chemistry **57**, 749–756.
Sirichandra C, Davanture M, Turk BE, Zivy M, Valot B, Leung J, Merlot S. 2010. The arabidopsis ABA-activated kinase OST1 phosphorylates the bZIP transcription factor ABF3 and creates a 14-3-3 binding site involved in its turnover. PLoS ONE **5**, 1–13.
Sood P, Singh RK, Prasad M. 2020. An efficient *Agrobacterium*-mediated genetic transformation method for foxtail millet (*Setaria italica* L.). Plant Cell Reports **39**, 511–525.
Strock CF, Lynch JP. 2020. Root secondary growth: an unexplored component of soil resource acquisition. Annals of Botany **126**, 205–218.
Strock CF, Schneider HM, Galindo-Castañeda T, *et al.* 2019. Laser ablation tomography for visualization of root colonization by edaphic organisms. Journal of Experimental Botany **70**, 5327–5342.
Strock CF, Schneider HM, Lynch JP. 2022. Anatomics: High-throughput phenotyping of plant anatomy. Trends in Plant Science, 1–4.
Sun Q, Gilgen AK, Signarbieux C, Klaus VH, Buchmann N. 2021. Cropping systems alter hydraulic traits of barley but not pea grown in mixture. Plant Cell and Environment **44**, 2912–2924.
Swamy M, Ahmed HU, Henry A, *et al.* 2013. Genetic, physiological, and gene expression

analyses reveal that multiple QTL enhance yield of rice mega-variety IR64 under drought. PLoS ONE **8**, e62795.
Swamy BPM, Kumar A. 2013. Genomics-based precision breeding approaches to improve drought tolerance in rice. Biotechnology Advances **31**, 1308–1318.
Tardieu F. 2022. Different avenues for progress apply to drought tolerance, water use efficiency and yield in dry areas. Current Opinion in Biotechnology **73**, 128–134.
Tardieu F, Draye X, Javaux M. 2017. Root water uptake and ideotypes of the root system: whole-plant controls matter. Vadose Zone Journal **16**.
Tardieu F, Granier C, Muller B. 2011. Water deficit and growth. Co-ordinating processes without an orchestrator? Current Opinion in Plant Biology **14**, 283–289.
Tardieu F, Simonneau T. 1998. Variability among species of stomatal control under fluctuating soil water status and evaporative demand: modelling isohydric and anisohydric behaviours. Journal of Experimental Botany **49**, 419–432.
Tardieu F, Simonneau T, Muller B. 2018. The physiological basis of drought tolerance in crop plants: A scenario-dependent probabilistic approach. Annual Review of Plant Biology **69**, 733–759.
Thiémélé D, Boisnard A, Ndjiondjop MN, Chéron S, Séré Y, Aké S, Ghesquière A, Albar L. 2010. Identification of a second major resistance gene to Rice yellow mottle virus, RYMV2, in the African cultivated rice species, *O. glaberrima*. Theoretical and Applied Genetics **121**, 169–179.
Todaka D, Shinozaki K, Yamaguchi-Shinozaki K. 2015. Recent advances in the dissection of drought-stress regulatory networks and strategies for development of drought-tolerant transgenic rice plants. Frontiers in plant science **6**, 84.
Törnroth-Horsefield S, Wang Y, Hedfalk K, Johanson U, Karlsson M, Tajkhorshid E, Neutze R, Kjellbom P. 2006. Structural mechanism of plant aquaporin gating. Nature **439**, 688–694.
Tournaire-Roux C, Sutka M, Javot H, Gout E, Gerbeau P, Luu D-T, Bligny R, Maurel C. 2003. Cytosolic pH regulates root water transport during anoxic stress through gating of aquaporins. Nature **425**, 393–397.
Trachsel S, Kaeppler SM, Brown KM, Lynch JP. 2011. Shovelomics: High throughput phenotyping of maize (*Zea mays* L.) root architecture in the field. Plant and Soil **341**, 75–87.
Uga Y, Sugimoto K, Ogawa S, *et al.* 2013. Control of root system architecture by DEEPER ROOTING 1 increases rice yield under drought conditions. Nature genetics **45**, 1097–102.
Vadez V. 2014. Root hydraulics: The forgotten side of roots in drought adaptation. Field Crops Research **165**, 15–24.
Vadez V, Kholová J, Hummel G, Zhokhavets U, Gupta SK, Hash CT. 2015. LeasyScan: A novel concept combining 3D imaging and lysimetry for high-throughput phenotyping of traits controlling plant water budget. Journal of Experimental Botany **66**, 5581–5593.
Vadez V, Kholova J, Medina S, Kakkera A, Anderberg H. 2014. Transpiration efficiency: New insights into an old story. Journal of Experimental Botany **65**, 6141–6153.
Vadez V, Kholová J, Yadav RS, Hash CT. 2013. Small temporal differences in water uptake among varieties of pearl millet (*Pennisetum glaucum* (L.) R. Br.) are critical for grain yield under terminal drought. Plant and Soil **371**, 447–462.
Vadez V, Pilloni R, Grondin A, *et al.* 2023. Water use efficiency across scales: from genes to landscapes. Journal of Experimental Botany. erad052
Vadez V, Grondin A, Chenu K, Henry A, Laplaze L, Millet EJ, Carminati A. 2023. Context-dependent water-related traits determine crop production under drought. Nature Reviews Earth & Environment, *accepted*

Valladares F, Sanchez-Gomez D, Zavala MA. 2006. Quantitative estimation of phenotypic plasticity: Bridging the gap between the evolutionary concept and its ecological applications. Journal of Ecology **94**, 1103–1116.
Vandeleur RK, Mayo G, Shelden MC, Gilliham M, Kaiser BN, Tyerman SD. 2009. The role of plasma membrane intrinsic protein aquaporins in water transport through roots: Diurnal and drought stress responses reveal different strategies between isohydric and anisohydric cultivars of grapevine. Plant Physiology **149**, 445–460.
Varshney RK, Shi C, Thudi M, *et al.* 2017. Pearl millet genome sequence provides a resource to improve agronomic traits in arid environments. Nature Biotechnology **35**, 969–976.
Verdoucq L, Grondin A, Maurel C. 2008. Structure-function analysis of plant aquaporin *At*PIP2;1 gating by divalent cations and protons. The Biochemical journal **415**, 409–416.
Walsche A De, Vergne A, Rincent R, *et al.* 2023. metaGE : Investigating Genotype × Environment interactions through meta-analysis. bioRxiv, 1–20.
Wang C, Hu H, Qin X, Zeise B, Xu D, Rappel WJ, Boron WF, Schroeder JI. 2016. Reconstitution of CO2 regulation of SLAC1 anion channel and function of CO2-permeable PIP2;1 aquaporin as CARBONIC ANHYDRASE4 interactor. Plant Cell **28**, 568–582.
Wang C, Wang Q, Zhu X, Cui M, Jia H, Zhang W, Tang W, Leng X, Shen W. 2019. Characterization on the conservation and diversification of miRNA156 gene family from lower to higher plant species based on phylogenetic analysis at the whole genomic level. Functional and Integrative Genomics **19**, 933–952.
Wang M, Yu Y, Haberer G, *et al.* 2014. The genome sequence of African rice (*Oryza glaberrima*) and evidence for independent domestication. Nature Genetics **46**, 982–988.
Wasson A, Bischof L, Zwart A, Watt M. 2016. A portable fluorescence spectroscopy imaging system for automated root phenotyping in soil cores in the field. Journal of Experimental Botany **67**, 1033–1043.
Welcker C, Spencer NA, Turc O, *et al.* 2022. Physiological adaptive traits are a potential allele reservoir for maize genetic progress under challenging conditions. Nature Communications **13**, 1–13.
Winsor CP. 1932. The Gompertz curve as a growth curve. Proceedings of the National Academy of Sciences of the United States of America **18**, 1–8.
Zwieniecki MA, Orians CM, Melcher PJ, Holbrook NM. 2003. Ionic control of the lateral exchange of water between vascular bundles in tomato. Journal of Experimental Botany **54**, 1399–1405.

7. Annexes

Annexe 1. **Grondin A.**, Rodrigues O., Verdoucq L., Merlot S., Leonhardt N. & Maurel C. (2015) Aquaporins contribute to ABA-triggered stomatal closure through OST1-mediated phosphorylation. *Plant Cell* 27.
Cette publication résume mon travail de thèse. Elle est la première à avoir mis en évidence un rôle pour les aquaporines dans le fonctionnement stomatique chez *A. thaliana*.

Annexe 2. **Grondin A.**, Mauleon R., Vadez V. & Henry A. (2016) Root aquaporins contribute to whole plant water fluxes under drought stress in rice (Oryza sativa L.). *Plant, Cell and Environment* 39, 347–65.
Cette publication est la première dans laquelle j'ai commencé à m'intéresser aux processus hydraulique à l'échelle de la plante entière. Ce travail réalisé à l'IRRI montre la contribution des aquaporines racinaires pour le maintien de la transpiration en condition de stress hydrique chez le riz.

Annexe 3. Campbell M.T., **Grondin A.**, Walia H. & Morota G. (2020) Leveraging genome-enabled growth models to study shoot growth responses to water deficit in rice. *Journal of Experimental Botany* 71, 5669–5679.
Ce travail réalisé à l'Université du Nebraska-Lincoln sur le riz m'a permis de me familiariser avec le phénotypage haut-débit en plateforme, la génétique d'association et la modélisation. Il montre une grande diversité dans la réduction de la croissance aérienne en réponse au stress hydrique chez le riz.

Annexe 4. Affortit P., Effa-Effa B., Ndoye M.S., Moukouanga D., Luchaire N., Cabrera-Bosquet L., … **Grondin A.*** (2022) Physiological and genetic control of transpiration efficiency in African rice, *Oryza glaberrima* Steud. *Journal of Experimental Botany* 73, 5279–5293.
Cette publication résulte d'un premier travail que j'ai porté en tant que chercheur IRD avec l'encadrement de deux étudiants en thèse et Master, et où je suis auteur pour correspondance. Elle suggère des mécanismes de régulation de la vigueur et de l'efficience de la transpiration originaux chez *O. glaberrima*.

Annexe5. Fuente C. de la, **Grondin A.**, Sine B., Debieu M., Belin C., Hajjarpoor A., … Laplaze L. (2023) Glutaredoxin regulation of primary root growth confers early drought stress tolerance in pearl millet. *eLife* 12:RP86169.
Cette publication résulte d'un travail effectué lors de mon expatriation au Sénégal en collaboration avec des collègues de l'ISRA-CERAAS et des sélectionneurs de l'ICRISAT, entre autres. Elle propose le rôle d'un gène pour de la tolérance au stress hydrique de début de cycle chez le mil.

This article is a *Plant Cell* Advance Online Publication. The date of its first appearance online is the official date of publication. The article has been edited and the authors have corrected proofs, but minor changes could be made before the final version is published. Posting this version online reduces the time to publication by several weeks.

Aquaporins Contribute to ABA-Triggered Stomatal Closure through OST1-Mediated Phosphorylation

Alexandre Grondin,[a,1] Olivier Rodrigues,[a] Lionel Verdoucq,[a] Sylvain Merlot,[b] Nathalie Leonhardt,[c] and Christophe Maurel[a,2]

[a] Biochimie et Physiologie Moléculaire des Plantes, Unité Mixte de Recherche 5004, CNRS/INRA/Montpellier SupAgro/Université Montpellier, F-34060 Montpellier, Cedex 2, France
[b] Institute for Integrative Biology of the Cell (I2BC), CEA, CNRS, Université Paris-Sud, Sciences Plant Saclay, F-91198 Gif sur Yvette Cedex, France
[c] Laboratoire de Biologie du Développement des Plantes, CEA Cadarache, Unité Mixte de Recherche 7265, CNRS/CEA/Aix-Marseille Université, F-13108 Saint-Paul-lez-Durance, France

ORCID IDs: 0000-0001-6726-6274 (A.G.); 0000-0002-5392-9732 (N.L.); 0000-0002-4255-6440 (C.M.)

Stomatal movements in response to environmental stimuli critically control the plant water status. Although these movements are governed by osmotically driven changes in guard cell volume, the role of membrane water channels (aquaporins) has remained hypothetical. Assays in epidermal peels showed that knockout *Arabidopsis thaliana* plants lacking the Plasma membrane Intrinsic Protein 2;1 (PIP2;1) aquaporin have a defect in stomatal closure, specifically in response to abscisic acid (ABA). ABA induced a 2-fold increase in osmotic water permeability (P_f) of guard cell protoplasts and an accumulation of reactive oxygen species in guard cells, which were both abrogated in *pip2;1* plants. Open stomata 1 (OST1)/Snf1-related protein kinase 2.6 (SnRK2.6), a protein kinase involved in guard cell ABA signaling, was able to phosphorylate a cytosolic PIP2;1 peptide at Ser-121. OST1 enhanced PIP2;1 water transport activity when coexpressed in *Xenopus laevis* oocytes. Upon expression in *pip2;1* plants, a phosphomimetic form (Ser121Asp) but not a phosphodeficient form (Ser121Ala) of PIP2;1 constitutively enhanced the P_f of guard cell protoplasts while suppressing its ABA-dependent activation and was able to restore ABA-dependent stomatal closure in *pip2;1*. This work supports a model whereby ABA-triggered stomatal closure requires an increase in guard cell permeability to water and possibly hydrogen peroxide, through OST1-dependent phosphorylation of PIP2;1 at Ser-121.

INTRODUCTION

The stomata, microscopic pores delineated by two guard cells in the shoot epidermis of plants, play a central role in plant water homeostasis. Their opening and closing determine the rate of transpiration and plant water loss. These movements result themselves from osmotically induced water flow and reversible turgor fluctuations in guard cells due to variations in intracellular solute concentration. Stomatal movements can be triggered by numerous environmental or hormonal factors. Among these, air humidity or the drought-induced hormone abscisic acid (ABA) are directly connected to the plant water status. The molecular and cellular mechanisms involved in stomatal movements have been particularly well characterized in the context of ABA-induced stomatal closure. ABA was shown to bind to RCAR/PYR/PYL receptors to capture protein phosphatases 2C such as ABA INSENSITIVE1, thereby releasing the inhibition of the Snf1-related protein kinase 2.6 (SnRK2.6), also named Open stomata 1 (OST1) (Joshi-Saha et al., 2011). This in turn activates various membrane targets, including the NADPH oxidases RbohF and RbohD (Kwak et al., 2003; Sirichandra et al., 2009), vacuolar anion exchanger CLCa (Wege et al., 2014), plasma membrane anion efflux channels Slow anion channel 1 (SLAC1) and SLAC1-homolog proteins 1 and 3 (SLAH1 and SLAH3) (Geiger et al., 2009; Lee et al., 2009; Brandt et al., 2012), and, as a consequence, outward rectifying potassium (K^+) channels such as Gated outwardly rectifying K^+ channel (GORK; Hosy et al., 2003). ABA concomitantly inhibits inward rectifying K^+ channels (Sato et al., 2009). ABA signaling is mediated through several secondary messengers, including cytosolic calcium and reactive oxygen species (ROS) (Wang and Song, 2008; Kim et al., 2010). It involves in particular H_2O_2 produced through the combined effects of RbohF and RbohD and apoplastic superoxide dismutase (Kwak et al., 2003). In contrast to stomatal closure, stomatal opening as induced by light is largely due to activation of plasma membrane H^+-ATPase, leading to membrane hyperpolarization and electrophoretic loading of K^+ through activation of inward rectifying K^+ channels. Surprisingly, the mechanisms of membrane water transport during stomatal movement have remained hypothetical.

During stimulus-induced stomatal movements, guard cells can adjust their volume by up to 40% in a few tens of minutes (Franks et al., 2001), with concomitant reshuffling of their vacuolar apparatus. However, it has remained unclear whether the accompanying water flow across the guard cell plasma membrane and tonoplast can simply be mediated by the lipid phase of membranes or whether aquaporins, channel proteins that facilitate transmembrane water transport, are involved. In fact, information on aquaporin expression in guard cells has remained scarce

[1] Current address: University of Nebraska-Lincoln, Department of Agronomy and Horticulture, Lincoln, NE 68583.
[2] Address correspondence to maurel@supagro.inra.fr.
The author responsible for distribution of materials integral to the findings presented in this article in accordance with the policy described in the Instructions for Authors (www.plantcell.org) is: Christophe Maurel (maurel@supagro.inra.fr).
www.plantcell.org/cgi/doi/10.1105/tpc.15.00421

(Sarda et al., 1997; Sun et al., 2001; Fraysse et al., 2005; Shope and Mott, 2006; Yang et al., 2006; Heinen et al., 2014). Plasma membrane intrinsic proteins (PIPs) represent the most abundant aquaporins in the plant plasma membrane (Santoni et al., 2003), and transcriptome analysis indicated expression of 8 and 12 PIP isoforms in stomata of *Arabidopsis thaliana* and stomatal complexes of maize (*Zea mays*), respectively (Leonhardt et al., 2004; Heinen et al., 2014). In the latter material, expression of most *PIP* genes was higher during the day than at night (Heinen et al., 2014). In sunflower (*Helianthus annuus*) guard cells, expression of vacuolar aquaporin SunTIP7 also showed diurnal variations, with an expression peak in phase with stomatal closure (Sarda et al., 1997).

A direct link between aquaporin function and guard cell movement is still lacking. Effects of membrane trafficking inhibitors on guard cell hydraulic conductivity suggested a role for proteins (aquaporins) in membrane water transport (Shope and Mott, 2006). The aquaporin blocker mercury ($HgCl_2$) was shown to alter stomatal aperture in *Vicia faba* (Yang et al., 2006), but this effect has not been reproduced (Shope and Mott, 2006) and can be questioned because of mercury cellular toxicity. Finally, steady state changes in stomatal conductance have been reported in plants with genetically altered aquaporin functions (Hanba et al., 2004; Flexas et al., 2006; Cui et al., 2008; Sade et al., 2010). Yet, these changes could reflect a genuine function of aquaporins in stomata or altered water or CO_2 transport (Flexas et al., 2006) in other leaf tissues. In this case, altered leaf hydraulics or carbon fixation can indeed lead to physiological deregulation of stomata (Pantin et al., 2013). For instance, altered stomatal conductance in transgenic Arabidopsis leaves was observed after expression of a tobacco (*Nicotiana tabacum*) aquaporin in photosynthetic tissues, but not when specifically expressed in guard cells (Sade et al., 2014).

In this work, we searched for direct genetic and physiological evidence for aquaporin function in guard cells. Transgenic Arabidopsis plants with genetically altered PIP aquaporin function and regulation were investigated with respect to stomatal movements in isolated epidermis and water transport in guard cell protoplasts. These and complementary in vitro studies revealed a specific role of the PIP2;1 isoform in ABA-induced stomatal closure, with a tight coupling of aquaporin phosphorylation to hormone signaling.

RESULTS

pip2;1 Mutants Show ABA-Specific Defects in Stomatal Movement

We performed an exploratory screening assay of *pip* T-DNA insertion mutants using peeled epidermal strips exposed to light and ABA treatments and identified stomatal response defects in two allelic *pip2;1* plants. PIP2;1, one of the predominant PIPs in Arabidopsis, is the second most highly expressed member of the PIP2 subclass in guard cells (Leonhardt et al., 2004). PIP2s usually exhibit a more robust water transport activity than members of the PIP1 subclass, when individually expressed in *Xenopus laevis* oocytes. Figure 1A shows that Col-0, *pip2;1-1*, or *pip2;1-2* had similar average stomatal apertures when maintained in the dark. Transfer from darkness to white light (300 $\mu E\ m^{-2}\ s^{-1}$) resulted in stomatal opening with similar kinetics in all genotypes and a 1.5-μm increment in stomatal aperture after 180 min (Figure 1A). The subsequent addition of 10 μM ABA induced a typical sharp closure response in Col-0, by >1 μm in 120 min. By contrast, stomata of *pip2;1-1* and *pip2;1-2* showed a very slow initial closing response and remained open after 180 min. A similar defect in stomatal closure was also observed in the two mutant lines at saturating (50 μM) ABA concentration (Supplemental Figure 1). In contrast to *pip2;1* mutants, *pip2;1-1* plants transformed with the *PIP2;1* genomic sequence (*pip2;1-1 PIP2;1*) had stomatal responses similar to those of Col-0 (Figure 1A; Supplemental Figure 1), indicating complementation. To determine the specificity of the ABA phenotype of *pip2;1* plants, we investigated additional treatments acting on stomatal movement. Under dark conditions, exposure of epidermal peels to the fungal toxin fusicoccin (5 μM) (Supplemental Figure 2) or to CO_2 deprivation (Supplemental Figure 3) resulted in stomatal opening responses, in both Col-0 and *pip2;1* plants. Thus, the latter plants show fully functional stomata for stimulus-induced opening. Col-0 and *pip2;1* epidermal strips also exhibited a similar stomatal closing response following a transition from

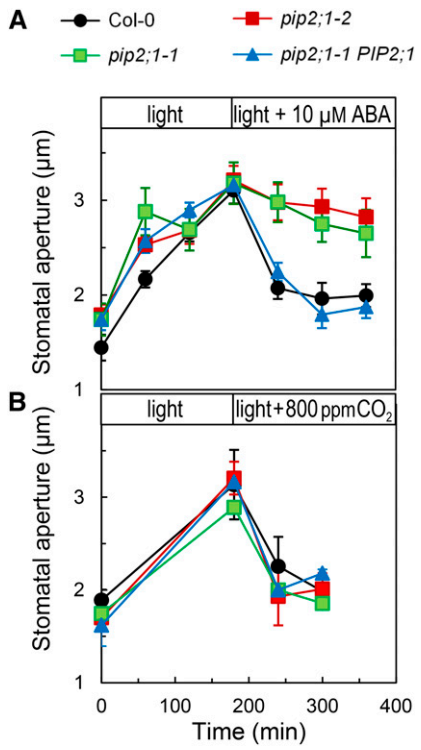

Figure 1. Stomatal Response of Col-0, *pip2;1*, and *PIP2;1*-Complemented *pip2;1* Plants to Light, ABA, and High CO_2.

Peeled epidermal strips from Col-0 (black circles), *pip2;1-1* (green squares), *pip2;1-2* (red squares), or *pip2;1-1 PIP2;1* (blue triangles) were maintained in a bathing solution at ambient air and transferred at t = 0 from darkness to light (300 $\mu E\ m^{-2}\ s^{-1}$). After 180 min, the bathing solution was equilibrated with 10 μM ABA at ambient air **(A)** or with air containing 800 ppm CO_2 **(B)**. Mean stomatal aperture was measured at the indicated time points. Averaged data (±SE; $n > 60$) from $n = 1$ to 3 **(A)** and $n = 2$ **(B)** independent experiments, each with ~60 aperture measurements per time point.

ambient to high (800 ppm) CO_2 under constant light (Figure 1B), a transition under constant darkness from air deprived of CO_2 to air with ambient CO_2 (Supplemental Figure 3), or a light-to-dark transition at ambient CO_2 (Supplemental Figure 4). The similar ABA-dependent stomatal defects of two allelic *pip2;1* mutants and the phenotypic complementation of one of these after expression of a *PIP2;1* genomic sequence indicate that PIP2;1 plays a specific role in ABA-induced stomatal closure.

ABA-Dependent Water Permeability of Guard Cell Protoplasts Is Mediated by PIP2;1

The involvement of aquaporins in ABA-dependent stomatal movement prompted us to investigate the water transport properties of guard cells and their dependency on ABA. Because small plant cell types can hardly be accessed in situ for direct water transport measurements (Postaire et al., 2010; Shatil-Cohen et al., 2011; Prado et al., 2013), protoplasts were isolated from guard cells. These protoplasts have lower mean diameter than mesophyll protoplasts (Supplemental Figure 5) and can easily be distinguished from the former due to their low plastid content (Supplemental Figure 6). The osmotic water permeability (P_f) of guard cell protoplasts was determined from the kinetics of cell volume increase in response to a sudden hypo-osmotic treatment (Figure 2A). Guard cell protoplasts isolated from Col-0 leaf tissues exposed to light, in conditions similar to those used for inducing stomatal opening, showed an average P_f of 59.5 $\pm$ 3.9 μm s^{-1} ($\pm$SE; n = 16) (Figure 2B). When prepared in the same conditions but further exposed to 10 μM ABA for 45 to 150 min in the presence of light, Col-0 protoplasts showed a 2.4-fold increase in P_f (145.3 $\pm$ 7.9 μm s^{-1}; n = 18). By comparison, mesophyll protoplasts that were isolated in parallel from Col-0 plants and were selected for a size comparable to that of guard cell protoplasts showed an ABA-insensitive P_f (Supplemental Figure 6). Guard cell protoplasts isolated from the two *pip2;1* alleles in the presence of light and absence of ABA showed moderate P_f values similar to those of their Col-0 counterparts (*pip2;1-1*, P_f = 58.7 $\pm$ 3.7 μm s^{-1}, n = 19; *pip2;1-2*, P_f = 63.6 $\pm$ 3.3 μm s^{-1}, n = 14). However, no change in P_f was observed after *pip2;1* protoplast treatment with ABA.

Our results indicate that PIP2;1 does not significantly contribute to guard cell water permeability in the absence of ABA but is necessary for its marked increase in response to the hormone.

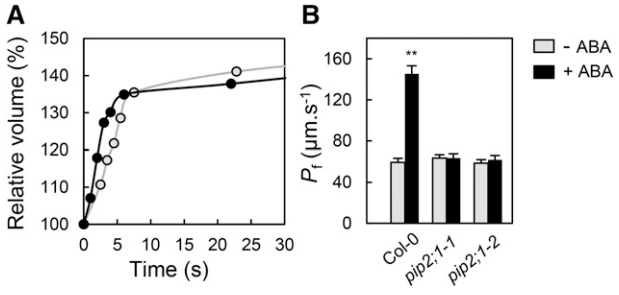

Figure 2. Effects of ABA on Water Permeability of Guard Cell Protoplasts from Col-0 and *pip2;1* Mutant Plants.

(A) Representative swelling kinetics of individual Col-0 guard cell protoplasts. The initial rate of swelling together with protoplast size allows determination of P_f. The protoplasts were prepared in the presence of light (open circles: P_f = 60 μm s^{-1}) or light plus 10 μM ABA (closed circles: P_f = 143 μm s^{-1}).

(B) Averaged P_f ($\pm$SE) of protoplasts prepared in the presence of light (gray bars) or light plus 10 μM ABA (black bars) from the indicated genotype. Data from n = 14 to 19 protoplasts and at least three independent plant cultures (t test; P < 0.01).

ABA-Dependent Accumulation of ROS in Stomata Is Dependent on PIP2;1

ABA signaling is mediated in part by ROS including H_2O_2 (Kwak et al., 2003; Wang and Song, 2008). The capacity of PIP2;1 to transport H_2O_2 after yeast expression (Dynowski et al., 2008) prompted us to investigate whether ABA-dependent ROS accumulation in guard cells was altered in *pip2;1* plants. The nonpolar diacetate ester 2′,7′-dichlorofluorescin diacetate (H_2DCFDA) penetrates the cells by diffusion and is hydrolyzed into 2′7′-dichlorodihydrofluorescin (H_2DCF), which yields the highly fluorescent 2′7′-dichlorofluorescein (DCF) due to intracellular oxidation (Supplemental Figure 7). In agreement with previous studies (Pei et al., 2000; Zhang et al., 2001; Suhita et al., 2004), exogenous ABA (50 μM) induced a time-dependent increase in DCF fluorescence in Col-0 guard cells that reflected an intracellular accumulation of ROS (Figure 3). Guard cells of *pip2;1* plants displayed a similar endogenous DCF oxidizing activity (Supplemental Figure 7) but did not show any ABA-dependent ROS accumulation (Figure 3). The data indicate that PIP2;1 contributes to ABA-dependent signaling. These defects may, together with the lack of ABA-dependent increase in P_f, account for the failure of *pip2;1* stomata to close in response to ABA.

Phosphorylation and Activation of PIP2;1 by OST1 Protein Kinase

Short-term (4 h) ABA treatments do not significantly alter PIP2;1 transcript abundance in guard cells (Leonhardt et al., 2004). While searching for posttranscriptional mechanisms that would mediate ABA-dependent activation of PIP2;1, we noticed that a putative phosphorylation site located at Ser-121, on the first cytosolic loop (*B*), perfectly conforms to the consensus recognition site of OST1, a protein kinase that plays a crucial role in ABA-dependent guard cell signaling (Sirichandra et al., 2010). The ability of OST1 to modify PIP2;1 was investigated in an in vitro phosphorylation assay with ^{32}P-labeled ATP, incubating purified protein kinase with a loop *B* peptide flanking the putative phosphorylation site (LARKV**S^{121}**LPRA). In this assay, OST1 labeled the PIP2;1 peptide with an intensity and affinity (K_m = 18.6 $\pm$ 8.1 μM; n = 4) comparable to that for a previously described AtrbohF NADPH oxidase peptide (Sirichandra et al., 2009) (K_m = 15.0 $\pm$ 1.0 μM; n = 4) (Figure 4A). No radiolabeling was observed when Ser-121 in loop *B* was substituted by an Ala residue (S121A) (Figure 4B). We next used longer PIP2;1 peptides, with 29 residues covering the entire loop *B*, and including three Thr or Ser residues in addition to Ser-121. A peptide containing the wild-type PIP2;1 sequence was labeled by OST1 in vitro, with an activity that was 4-fold lower than in the LARKV**S^{121}**LPRA peptide, but with a 10-fold higher affinity (K_m = 2.6 $\pm$ 0.7 μM; n = 2) (Supplemental Figure 8). In addition,

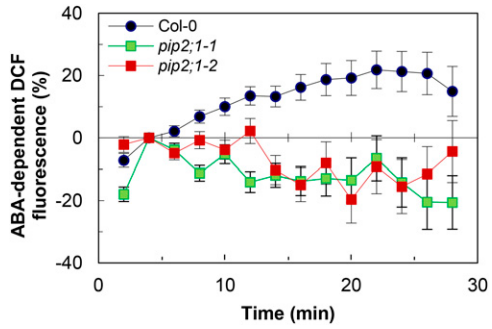

Figure 3. ABA-Dependent Accumulation of ROS in Stomata of Col-0 and *pip2;1* Mutant Plants.

Peeled epidermal strips from Col-0 (blue circles), *pip2;1-1* (green squares), or *pip2;1-2* (red squares) were maintained in a bathing solution under light for 120 min to induce stomatal aperture. They were then incubated in the presence of 50 μM H_2DCFDA for 20 min, and extracellular H_2DCFDA was removed by four successive washings, prior to addition (t = 0) of 50 μM ABA or an equivalent volume of ethanol (mock). Mean stomatal DCF fluorescence intensity was measured at the indicated time and normalized to the initial fluorescence (t = 4 min) (see data in Supplemental Figure 7). The graph shows the relative difference in fluorescence (%) between ABA- and mock-treated stomata. Averaged data (±SE) from *n* = 7 independent experiments and two independent plant cultures, each experiment with 10 to 20 stomata per time point.

phosphorylation of the long peptide was 4.5-fold higher than in its counterpart carrying a S121A mutation (Supplemental Figure 8). To further investigate the specificity of Ser-121 recognition by OST1, we tested the phosphorylation of a peptide covering the native C-terminal sequence of PIP2;1 containing two well-described phosphorylation sites at Ser-280 and Ser-283 (SKSLG**S**^{280}FR**S**^{283}AANV). We observed a very weak in vitro labeling by OST1 (Figure 4B), with a low apparent affinity for the kinase (K_m = 71.2 μM) (data not shown). Although proteomic studies have suggested that phosphorylation at Ser-283 may depend on prior phosphorylation of the adjacent site (Prak et al., 2008; Prado et al., 2013), a peptide carrying a phosphorylated Ser-280 was not significantly labeled by OST1 either (Figure 4B). Together, these data indicate that OST1 can phosphorylate PIP2;1, preferentially at Ser-121. To investigate the functional role of OST1-mediated PIP2;1 phosphorylation, we performed coexpression experiments in *X. laevis* oocytes. Oocyte injection with 1 or 2 ng PIP2;1 cRNA conferred, with respect to uninjected controls, a 4- to 6-fold increase in cell P_f (Figure 5). Coinjection with OST1 cRNA resulted in a further increase in P_f by 34 and 22%, respectively. By comparison, injection with cRNAs encoding a S121A form of PIP2;1 resulted in a smaller increase in P_f (2-fold), which was not enhanced upon coinjection with OST1 cRNA. Thus, OST1 enhances the water transport activity of PIP2;1 in *X. laevis* oocytes through a mechanism that involves Ser-121.

Role of Ser-121 Phosphorylation in ABA-Dependent Guard Cell Water Permeability

Because OST1 is activated in response to ABA, we speculated that in guard cells phosphorylation of PIP2;1 at Ser-121 and, therefore, its water transport activity must be enhanced after exposure to ABA. By introducing mutations of Ser-121 to Ala (S121A) and Asp (S121D) we created phosphorylation-deficient and phosphomimetic forms of PIP2;1, respectively, which were expressed in *pip2;1-2* under the control of a double 35S (d35S) promoter. For each construct, we selected two independently transformed clones (*-1* and *-2*), falling into two distinct classes of protein expression level. The highest expression level, in *S121A-2* and *S121D-2*, was comparable to that in *d35S:PIP2;1ko*, a transgenic line that overexpresses *PIP2;1* in *pip2;1-2* (Prado et al., 2013) (Supplemental Figure 9). Thus, a panel of transformed clones with various expression levels was available for further physiological characterization. We then tested the ability of the PIP2;1 mutant forms to complement the guard cell phenotypes of the *pip2;1-2* mutant. When prepared in the presence or absence of ABA, guard cell protoplasts from the two *S121A* lines showed low P_f values similar to those of *pip2;1-2* protoplasts or Col-0 protoplasts prepared in the absence of ABA (Figure 6). Thus, S121A PIP2;1 was unable to confer increased P_f, even in the presence of ABA. By contrast, the P_f of protoplasts prepared from the two *S121D* lines in the absence of ABA was 2- to 3-fold higher than that of the

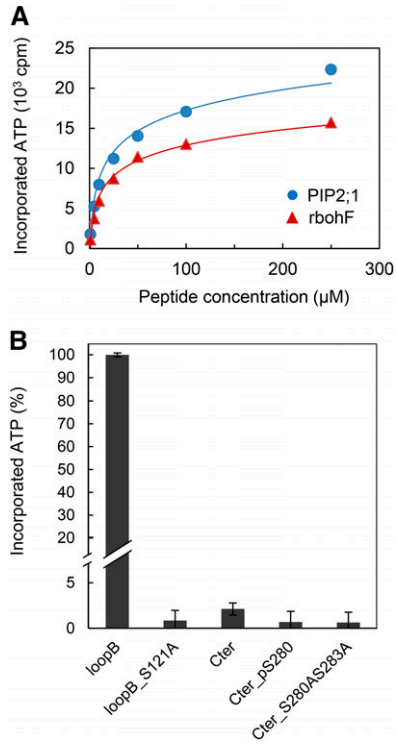

Figure 4. In Vitro Phosphorylation of PIP2;1 Peptides by OST1.

(A) Peptides from PIP2;1 (blue circles) or rbohF (red triangles) and carrying a putative phosphorylation site at Ser-121 or Ser-174, respectively, were incubated at the indicated concentration, in the presence of labeled ATP and purified OST1. Incorporated ATP from *n* = 4 independent experiments. Error bars (±SE) fall into symbols.

(B) Phosphorylation by purified OST1 of native or mutated peptides from the loop *B* and C-terminal region of PIP2;1. Incorporated ATP (±SE) from *n* = 2 to 8 independent experiments was normalized to the signal observed in a native loop *B* peptide.

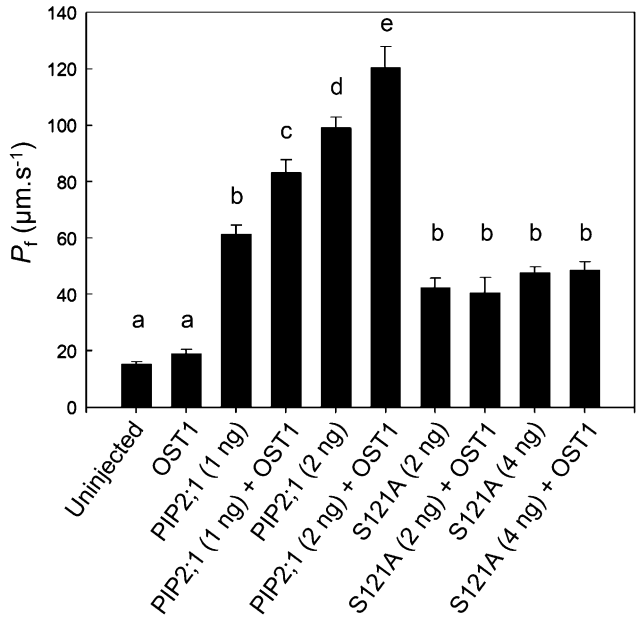

Figure 5. Functional Coexpression in *Xenopus* Oocytes of Wild-Type or Mutated Forms PIP2;1 with OST1.

Oocytes were injected with the indicated amount (nanograms; in parentheses) of cRNAs encoding wild-type (PIP2;1) or mutated (S121A) PIP2;1. When indicated, oocytes were also injected with 5 ng of OST1 cRNA. Uninjected oocytes were used as controls. Osmotic water permeability values (P_f ±SE) from n = 10 to 96 oocytes. Different letters indicate statistically different values (one-way ANOVA; Newman-Keuls, $P < 0.05$).

corresponding Col-0 or *pip2;1-2* protoplasts (Figure 6). Yet, ABA did not further increase the P_f of *S121D* protoplasts. Thus, S121D PIP2;1 confers an ABA-independent increase in P_f in guard cell protoplasts. The overall data indicate that phosphorylation of PIP2;1 at Ser-121 was necessary and sufficient for increasing guard cell water permeability. Pairwise comparisons of the Col-0/*d35S:PIP2;1ko* lines on the one hand, and the two *S121D* lines on the other hand, indicated that maximal P_f was correlated to PIP2;1 expression level, suggesting that PIP2;1 may be limiting for ABA-induced increase in P_f.

Role of Ser-121 Phosphorylation in ABA-Dependent Stomatal Closure

To further investigate the role of Ser-121 phosphorylation, we characterized the opening and closing stomatal responses of *S121A* and *S121D* lines. To facilitate stomatal opening in all lines, epidermal peels were incubated at a low CO_2 concentration in the presence of light, which induced similar apertures in the Col-0, *pip2;1-2*, *S121A*, and *S121D* genotypes (Figure 7). Further addition of ABA (10 μM) resulted in stomatal closure in Col-0 and *S121D*, whereas *S121A* stomata, similar to *pip2;1-2* ones, failed to respond and remained open. The ability of S121D but not S121A to complement the *pip2;1-2* stomatal movement phenotype indicates that phosphorylation of Ser-121 is necessary during ABA-induced stomatal closure.

DISCUSSION

Genetics of Guard Cell Aquaporins

Although stomatal movements critically control plant transpiration and, therefore, the whole plant water status, the mechanisms and genetic bases of water transport in the guard cells themselves have remained elusive. Here, we used a stomatal assay in peeled epidermal strips of Arabidopsis leaves and established that a single aquaporin isoform, PIP2;1, is necessary for ABA-dependent closure and dispensable for CO_2- or light-induced stomatal movements. Consistent with this finding, ABA induced a marked increase in the P_f of guard cell protoplasts, which was abrogated in *pip2;1* plants. These data suggest a model whereby the stomatal closing response to ABA involves an increase in guard cell water permeability mediated by PIP2;1. This function adds to previously described roles of PIP2;1 in root and leaf vein water transport (Da Ines et al., 2010; Péret et al., 2012; Prado et al., 2013) and lateral root emergence (Péret et al., 2012).

Although PIP2;1 is one of the highly expressed PIPs in guard cells, its absolute requirement for ABA-dependent stomatal regulation does not exclude that other PIPs are involved. Preliminary evidence suggests that a *pip1;2* mutant has stomatal alterations in peeled epidermis that resemble those of *pip2;1* plants. A recent reverse genetic study showed that, although three PIP isoforms (PIP1;2, PIP2;1, and PIP2;6) individually contribute to ~20% of Arabidopsis rosette hydraulic conductivity, a corresponding triple mutant showed a leaf hydraulic phenotype similar to those of individual mutants (Prado et al., 2013). Thus, an apparent functional cooperativity of PIPs coexpressed in plants is emerging. The assembly of distinct aquaporin isoforms in heterotetramers may in part contribute to this phenomenon (Zelazny et al., 2007; Yaneff et al., 2014).

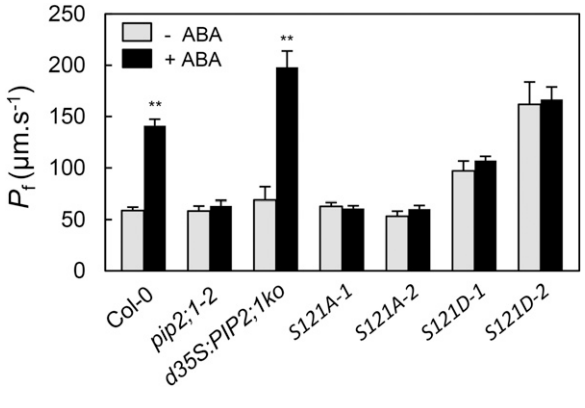

Figure 6. Effects of ABA on P_f of Guard Cell Protoplasts from Plants Expressing PIP2;1 Phosphorylation Mutants.

P_f was measured as exemplified in Figure 2 in guard cell protoplasts of the indicated genotypes prepared in the absence (gray bars) or presence (black bars) of 10 μM ABA. Data (±SE) from n = 7 to 25 protoplasts and at least three independent plant cultures. Asterisks indicate significant effects of ABA on P_f (t test; $P < 0.01$).

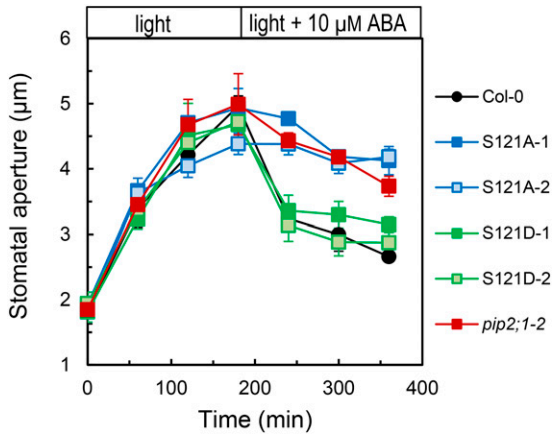

Figure 7. Stomatal Opening and Closing Responses of Plants Expressing PIP2;1 Phosphorylation Mutants.

Stomatal aperture was monitored in Col-0 (black circles), *pip2;1-2* (red squares), or *pip2;1-2* plants expressing S121A (*S121A-1*, dark-blue squares; *S121A-2*, light-blue squares) or S121D (*S121D-1*, dark-green squares; *S121D-2*, light-green squares) as described in Figure 1A, except that stomatal opening (t = 0 to 180 min) was induced in the light and in a solution depleted in CO_2. From t = 180 min, epidermal peels were incubated in the same solution but containing 10 μM ABA. Averaged data (±SE; $n > 150$) from $n = 3$ independent experiments, each with ~60 aperture measurements per time point.

The Role of Aquaporins during Stomatal Closure

Another important finding was that, by contrast to light or dark treatments, ABA enhanced the P_f of guard cell protoplasts. Based on pharmacological inhibition of hydraulic conductivity in *V. faba* guard cells, Shope and Mott (2006) previously suggested that aquaporin function in stomata was specifically associated with water stress (hyperosmotic treatment). However, the role of ABA was not explored in their study. The regulation of guard cell P_f uncovered in this work suggests that among other stomatal responses, ABA-induced closure may be specifically hydraulically limited. Although it represents one of fastest stomatal movements, this response still occurs over several tens of minutes. Cell pressure probe measurements revealed that most individual plant cells show turgor relaxation kinetics that are several orders of magnitude faster than stomatal movements (Steudle, 1989). Thus, it may well be that cell hydraulic conductivity is not limiting during the latter processes and residual water transport across the lipid membrane is sufficient to compensate for defects in aquaporin-mediated water transport. At variance with these ideas, our data rather suggest that a high P_f is required, likely to permit guard cell volume adjustment in the presence of minute osmotic gradients. From this perspective, a defect in membrane water transport would be associated with higher osmotic gradients, which may disturb local ion distributions, thereby impeding the function of ion channels and transporters.

Other, nonhydraulic mechanisms may also contribute to PIP2;1 function during stomatal closure. In particular, aquaporins including PIP2;1 can transport H_2O_2, one important intermediate of ABA signaling (Dynowski et al., 2008). Our finding that ABA-triggered ROS accumulation is altered in guard cells of *pip2;1* mutants first provides a relevant explanation, complementary to altered water transport, for the blockade of ABA-induced stomatal closure in *pip2;1* plants. Furthermore, we speculate that the ABA-induced PIP2;1 activity, as revealed by the enhanced P_f of protoplasts, could provide a path for influx of apoplasmic H_2O_2. For now, H_2O_2 transport by plant aquaporins was only assessed in yeast cells. Thus, the significance of this path and its kinetic variations in conjunction with ABA signaling remain to be determined in guard cells.

The functions of PIP2;1 revealed in epidermal strips and isolated guard cell protoplasts also call for more information on its role in integrated stomatal functioning. When grown under standard conditions, Col-0 and *pip2;1* plants showed similar leaf temperatures as monitored by infrared thermography (Supplemental Figure 10). In addition, water loss from excised rosettes was not significantly modified in *pip2;1* plants (Supplemental Figure 11). This lack of transpiration phenotype should be interpreted with care as it may reflect the cumulative effects of PIP2;1 in guard cells and other cell types/organs. In particular, leaf vein cells are crucial for transferring water from the xylem into the lamina (Ache et al., 2010; Prado et al., 2013). Thus, a lack of function of PIP2;1 at this site may result in a hydraulic limitation in veins, a drop in leaf water potential, and induction of stomatal closure. Conversely, a lack of function of PIP2;1 in guard cells may antagonize stomatal closure. Because of these confounding physiological effects, further studies will require tissue-specific complementation of aquaporin mutants together with assays on isolated stomata, to distinguish between guard cell-specific functions and integrated effects on whole plant water relations. Interestingly, ABA appears to have inhibitory and stimulating effects on cell hydraulic conductivity in leaf veins (Shatil-Cohen et al., 2011) and stomata (this work), respectively. These apparently antagonistic effects are highly relevant, as they both would contribute to stomatal closure under water stress conditions.

Aquaporin Phosphorylation and ABA-Dependent Signaling

Whereas auxin dramatically regulates *PIP2;1* transcription in roots (Péret et al., 2012), ABA-dependent regulation of PIP2;1 in guard cells appears to be essentially posttranslational. We knew that ABA has no effects on *PIP2;1* transcript abundance in guard cells (Leonhardt et al., 2004). Here, we observed that the P_f of *d35S:PIP2;1ko* protoplasts, which constitutively overexpress PIP2;1, was similar in the absence of ABA to the P_f of Col-0 or *pip2;1* protoplasts. By contrast, the P_f of *d35S:PIP2;1ko* protoplasts was higher than in the latter two genotypes in the presence of ABA (Figure 6). Thus, PIP2;1 was only limiting for water transport in ABA-treated cells.

More specifically, our work indicates a crucial role of PIP2;1 phosphorylation in the response of guard cell P_f and stomatal aperture to ABA. First, OST1, a SnRK2 protein kinase closely linked to ABA receptors, was able to phosphorylate PIP2;1 peptides in vitro. In good agreement with its predicted site specificity (Vlad et al., 2008; Sirichandra et al., 2010), OST1 showed a large preference for loop *B* Ser-121, whereas two major C-terminal phosphorylation sites (Ser-280 and Ser-283) were not recognized. Second, coexpression of PIP2;1 with OST1 in oocytes enhanced PIP2;1 water transport activity and mutant analysis showed that

these effects are mediated by Ser-121. The moderate activating effects of OST1 expression on PIP2;1 activity in oocytes (+34% or +22%; Figure 5) may be due to the presence of an endogenous protein kinase that phosphorylates a large part of the PIP2;1 cellular pool at Ser-121. Third, a phosphomimetic form (S121D) but not a phosphodeficient form (S121A) of PIP2;1 was able to restore ABA-dependent stomatal closure in *pip2;1* mutants. In addition, the former but not the latter was sufficient to enhance the P_f of guard cell protoplasts, which thereby lacked the ABA-dependent activation seen in Col-0 protoplasts. This set of data provides univocal evidence that phosphorylation of PIP2;1 at Ser-121 is necessary and sufficient for its ABA-dependent function. Molecular dynamic studies of spinach (*Spinacia oleracea*) PIP2 homolog SoPIP2;1 indicated the crucial role of this phosphorylation event in aquaporin gating (Törnroth-Horsefield et al., 2006). Phospho-specific antibodies have also indicated a role for this modification during the response of maize leaves to cold (Aroca et al., 2005). Unfortunately, the use of these antibodies was not conclusive in Arabidopsis extracts. C-terminal phosphorylation of PIP2;1, which regulates both aquaporin gating and trafficking, is itself responsive to many stimuli, including salt and oxidative stresses, light, and ABA (Prak et al., 2008; Kline et al., 2010; Prado et al., 2013). The ABA-induced dephosphorylation of PIP2;1 Ser-280 seen in Arabidopsis plantlets (Kline et al., 2010) likely corresponds to PIP2;1 from veins, the predominant sites of expression of this aquaporin in leaves. This dephosphorylation may mediate the inhibition of leaf hydraulic conductivity by the hormone (Shatil-Cohen et al., 2011; Pantin et al., 2013). Thus, our work indicates that a single PIP isoform can exhibit opposite cell-specific responses to the same stimulus, through cell-specific regulations at distinct phosphorylation sites.

Deciphering the signaling components that act upstream of aquaporin regulation and mediate the stimulus and cell-specific responses currently represents a major challenge. A sugar-induced receptor kinase was recently shown to phosphorylate the C terminus of several PIP2s (Wu et al., 2013). Here, we identified OST1 as a novel, potent regulator of PIPs through action at a distinct phosphorylation site. However, this does not exclude that PIP2;1 is targeted by other guard cell-expressed protein kinases, including other SnRKs or calcium-dependent protein kinases (CPK6, CPK21, and CPK23) (Geiger et al., 2010; Brandt et al., 2012) involved in ABA-dependent signaling. Because of their general role in ABA and water stress signaling in plants (Boudsocq and Laurière, 2005), SnRK2s may also contribute to hydraulic regulation in cells other than guard cells. In particular, ABA induced a transient increase in cortical cell hydraulic conductivity in maize and sunflower roots (Quintero et al., 1999; Hose et al., 2000).

In conclusion, this work allowed for the identification and molecular dissection of a novel role of aquaporins, involving a class of protein kinases central in hormone and water stress signaling (Boudsocq and Laurière, 2005) and phosphorylation of a specific PIP isoform at a unique site. By revealing the modes of membrane water transport in guard cells, and a possible connection with ROS-dependent signaling, this work also fills a gap in our understanding of stomatal regulation, a fundamental process in plant water relations.

METHODS

Plant Materials and Growth Conditions

All experiments were performed in *Arabidopsis thaliana* Col-0 or derived transgenic lines. The *pip2;1-1* and *pip2;1-2* knockout mutants and the two complemented lines, *pip2;1-1 PIP2;1* and *d35S:PIP2;1ko*, were described elsewhere (Da Ines et al., 2010; Péret et al., 2012; Prado et al., 2013). The former is a *pip2;1-1* mutant allele transformed with the *PIP2;1* genomic sequence (Péret et al., 2012); the latter is a *pip2;1-2* mutant overexpressing a PIP2;1 cDNA under the control of a double enhanced cauliflower mosaic virus 35S promoter (Prado et al., 2013). For subsequent protoplast isolation, plants were grown in soil (Neuhaus Humin Substrat N2; Klasman-Deilmann) in controlled growth chambers with a relative humidity of 70% under an 8-h-light (250 $\mu E\ m^{-2}\ s^{-1}$) at 22°C/16 h dark at 21°C cycle. For stomatal assays, plants were grown in individual pots with a relative humidity of 70% under an 8-h-light (250 $\mu E\ m^{-2}\ s^{-1}$) at 23°C/16 h dark at 19°C cycle.

Site-Directed Mutagenesis and Plant Transformation

Site-directed mutants of Arabidopsis PIP2;1 were prepared as described (Verdoucq et al., 2008) by PCR-mediated primer extension using a QuikChange mutagenesis kit (Stratagene). Mutations of Ser-121 to alanine (S121A) and to aspartate (S121D) were introduced by amplifying *PIP2;1* cDNA inserted into a pBSK-derived vector using pairs of complementary mutagenic primers (Supplemental Table 1). The presence of the mutations was verified by sequencing (GATC Biotech). Mutated forms of PIP2;1 cDNA were excised using *Eco*RI and *Cla*I and subcloned into the T-DNA portion of a pGreenII 00179 vector, upstream of a double enhanced cauliflower mosaic virus 35S promoter and downstream of a nopaline synthase terminator (Hellens et al., 2000). The resulting plasmid was introduced into *Agrobacterium tumefaciens* strain GV3101 and used to transfer the mutated form of PIP2;1 into Arabidopsis *pip2;1-2* plants by the floral dip method (Clough and Bent, 1998). Monoinsertional locus homozygous plants were selected from segregation analysis of hygromycin resistance. Transformed plants were further screened for expression of the mutated form of PIP2;1 by ELISAs, using an anti-PIP2 antibody (Santoni et al., 2003) on total leaf protein extracts from 3-week-old plants.

Measurements of Stomatal Aperture

Stomatal aperture was measured on epidermal peels excised from the abaxial side of leaves of 3- to 4-week-old plants, essentially as described by Montillet et al. (2013). In all cases, two epidermal peels from two independent plants of the indicated genotype were first incubated for 30 min in darkness at ambient air in a bathing solution containing 30 mM KCl, 1 mM $CaCl_2$, and 10 mM MES/Tris pH6.0, prior to exposure to the indicated treatment. Average stomatal aperture was then measured every hour in >60 stomata. This experiment was repeated two to four times for each of two to five independent plant cultures. Unless otherwise indicated, the ABA response was tested as follows. Dark-adapted epidermal peels were first exposed to white light (300 $\mu E\ m^{-2}\ s^{-1}$) to induce maximal stomatal opening, 10 μM ABA was added to the bathing solution after 180 min, and stomatal aperture was monitored during the next 120 min. Similar to ABA, the effects of darkness on stomatal closure were monitored in epidermal peels that had first been exposed to white light (300 $\mu E\ m^{-2}\ s^{-1}$) for 180 min. By contrast, the effects of fusicoccin (5 μM) were investigated under darkness. To create low CO_2 conditions and promote stomatal aperture, the epidermal peels were maintained under darkness in a closed Petri dish and the bathing solution was bubbled with CO_2-free air. After 180 min, stomatal closure was induced by removing the cap of the Petri dish, thereby placing the epidermal peels in contact with atmospheric air. Alternatively, stomatal closure was induced in the light (300 $\mu E\ m^{-2}\ s^{-1}$) by bubbling the bathing solution with high CO_2 (800 ppm) air.

Osmotic Water Permeability of Guard Cell Protoplasts

Guard cell protoplasts were prepared as described (Leonhardt et al., 2004). Around 50 rosette leaves were homogenized in water during 3×10 s in a Waring blender at room temperature. Blended tissues were collected over a 100-μm nylon mesh and then placed into 20 mL of solution A (0.5 mM ascorbic acid, 0.5 mM $MgCl_2$, 0.5 mM $CaCl_2$, 0.57 M sorbitol, and 5 mM MES, pH 5.5) complemented with 0.25% BSA, 1.5% cellulase RS, and 0.03% Pectolyase Y23 (Kalys), and incubated for 2 h in darkness at 27°C with linear shaking. The homogenate containing leaf protoplasts was filtered through a 37-μm nylon mesh and centrifuged at 700*g* for 5 min. Isolated protoplasts were resuspended in 4 mL of solution A and kept under darkness before exposure to light (300 μE m^{-2} s^{-1}) and treatment with 10 μM ABA for 45 to 150 min. Guard cell protoplasts were identified, within the leaf protoplast suspension, according to their size (7 to 15 μm) and low chloroplast content, and similar morphologies were considered in all genotypes and conditions investigated. For subsequent water transport assay, guard cell protoplasts were individually selected from the leaf protoplast suspension using a micropipette (Supplemental Figure 6). Briefly, swelling measurements were performed at 20°C by transfer of individual protoplasts into a hypotonic solution B (solution A but with 0.42 M sorbitol) under a microscope, using a previously described micromanipulation procedure (Ramahaleo et al., 1999). The concentration ratio between solutions A and B allows a theoretical protoplast swelling of 35%. Protoplasts showing nonlinear initial swelling kinetics or a volume increase of <16% or >56% were discarded from the analyses. The osmotic water permeability (P_f) of guard cell protoplasts was determined from the initial rate of volume increase. It was checked that similar P_f values were obtained when measurements were performed under hyperosmotic conditions (transfer from solution A to solution B with 0.95 M sorbitol).

Measurements of ROS Content

Epidermal peels isolated using similar plants and procedures as for aperture measurements were incubated for 120 min under light (250 μE m^{-2} s^{-1}) in a bathing solution as above (30 mM KCl, 1 mM $CaCl_2$, and 10 mM MES/Tris, pH6.0). After 120 min, stomata were fully opened and 50 μM H_2DCFDA (Sigma-Aldrich) was added to the bathing solution. This nonpolar, unreactive molecule diffuses intracellularly where it is deacetylated by endogenous esterase, to release H_2DCF (Coelho et al., 2002; Foreman et al., 2003). H_2DCF is then oxidized by H_2O_2, OH· and possibly other ROS to highly fluorescent DCF (Schopfer et al., 2001, and references therein). After 20 min in the presence of H_2DCFDA, epidermal peels were thoroughly washed four consecutive times with fresh bathing solution to eliminate all remaining extracellular H_2DCFDA. To monitor ROS content of guard cells, a randomly chosen epidermal peal area containing 10 to 20 stained stomata was observed under constant light (250 μE m^{-2} s^{-1}) using an epifluorescence microscope (Olympus IX70) equipped with a CCD camera (Andor Ixon +) connected to a computer operating Metafluor (Universal Imaging Corporation) image acquisition software. At t = 0, the bathing solution was equilibrated with 50 μM ABA or an equivalent concentration (0.5%) of ethanol (mock) and the fluorescence intensity was captured, in complete darkness, every 2 min for 30 min. Between each imaging process, the selected leaf area was reilluminated using the light source of the microscope. Average inner stomatal fluorescence was measured using ImageJ (http://rsb.info.nih.gov/ij/).

In Vitro Phosphorylation

OST1 kinase activity was assayed essentially as described (Vlad et al., 2008) using the following synthetic peptides (Proteogenix) purified to >80% by HPLC and with the indicated sequences: rbohF, MALDRTRSSAQRKKK; loopB, MALARKVSLPRAKKK; loopB_S121A, MALARKVALPRAKKK; Cter, MASKSLGSFRSAANVKKK; Cter_pS280, MASKSLGpSFRSAANVKKK; and C-ter_S280AS283A, MASKSLGAFRAAANVKKK. In another series of experiments, longer peptides, containing 29 PIP2;1 residues and covering the entire loop *B* were used. These peptides carry the PIP2;1 sequence, either native (loopB-L, MACTAGISGGHINPAVTFGLFLARKVSLPRAKKK) or with a S121A mutation (loopB_S121A-L: MACTAGISGGHINPAVTFGLFLARKV*A*LPRAKKK). In all experiments, peptides (1 to 250 μM) were incubated at 25°C in 250 μL of a reaction mixture containing 100 ng purified OST1, 100 μM [γ-^{32}P]ATP (0.1 μCi $nmol^{-1}$), 25 mM β-glycerophosphate, 20 mM $MgCl_2$, 1 mM DTT, and 50 mM HEPES, pH 7.4. At the selected time points, 40 μL aliquots of the reaction mixture were spotted on a P81 phosphocellulose paper and rapidly dried. P81 paper was washed for 3×10 min in 0.85% phosphoric acid, once in acetone and dried. Radioactivity was measured on a Packard TRI-CARB phosphor imager.

Oocyte Expression

The cDNA of wild-type and S121A forms of PIP2;1 were cloned in a pSP64T-derived oocyte expression vector (Maurel et al., 1993). The Arabidopsis OST1 cDNA was PCR amplified from leaf cDNA using *BamHI-OST1* and *OST1-EcoRI* primers (Supplemental Table 1) and inserted at the *Bam*HI and *Eco*RI restriction sites of a pGEM-Xho oocyte expression vector (Liman et al., 1992). All constructs were checked by full sequencing. cRNA production, expression in *Xenopus laevis* oocytes, and P_f measurements were performed as previously described (Maurel et al., 1993).

Accession Numbers

Sequence data from this article can be found in the Arabidopsis Genome Initiative or GenBank/EMBL databases under the following accession numbers: *PIP2;1* (At3g53420) and *OST1* (At4g33950).

Supplemental Data

Supplemental Figure 1. Stomatal response of Col-0, *pip2;1*, and *PIP2;1*-complemented *pip2;1* plants to 50 μM ABA.

Supplemental Figure 2. Stomatal response of Col-0 and *pip2;1* plants to fusicoccin.

Supplemental Figure 3. Stomatal response of Col-0, *pip2;1*, and *PIP2;1*-complemented *pip2;1* plants to various CO_2 concentrations.

Supplemental Figure 4. Stomatal response of Col-0 and *pip2;1* plants to changing light.

Supplemental Figure 5. Diameter repartition of mesophyll and guard cell protoplasts isolated from Col-0 plants.

Supplemental Figure 6. Comparative effects of ABA on P_f of guard cell and mesophyll cell protoplasts.

Supplemental Figure 7. Accumulation of ROS in ABA- and mock-treated stomata of Col-0 and *pip2;1* mutant plants.

Supplemental Figure 8. In vitro phosphorylation of loop *B* PIP2;1 peptides by OST1.

Supplemental Figure 9. PIP2 abundance in leaves of the indicated genotypes.

Supplemental Figure 10. Leaf temperature of Col-0, *pip2;1*, and *PIP2;1*-complemented *pip2;1.*

Supplemental Figure 11. Kinetics of water loss from excised rosettes of Col-0, *pip2;1*, and *PIP2;1*-complemented *pip2;1.*

Supplemental Table 1. Nucleotide sequences of primers used for OST1 cDNA amplification and site-directed mutagenesis of PIP2;1

ACKNOWLEDGMENTS

A.G. and O.R. were both supported by doctoral fellowships from the French Ministry of Higher Education.

AUTHOR CONTRIBUTIONS

A.G., O.R., L.V., N.L., and C.M. designed the research. A.G., O.R., L.V., and N.L. performed the research. S.M. purified the protein kinase. A.G., O.R., L.V., N.L., and C.M. analyzed the data. C.M. wrote the article, which was read by all of the authors.

Received May 14, 2015; revised June 17, 2015; accepted June 17, 2015; published July 10, 2015.

REFERENCES

Ache, P., Bauer, H., Kollist, H., Al-Rasheid, K.A., Lautner, S., Hartung, W., and Hedrich, R. (2010). Stomatal action directly feeds back on leaf turgor: new insights into the regulation of the plant water status from non-invasive pressure probe measurements. Plant J. **62:** 1072–1082.

Aroca, R., Amodeo, G., Fernández-Illescas, S., Herman, E.M., Chaumont, F., and Chrispeels, M.J. (2005). The role of aquaporins and membrane damage in chilling and hydrogen peroxide induced changes in the hydraulic conductance of maize roots. Plant Physiol. **137:** 341–353.

Boudsocq, M., and Laurière, C. (2005). Osmotic signaling in plants: multiple pathways mediated by emerging kinase families. Plant Physiol. **138:** 1185–1194.

Brandt, B., Brodsky, D.E., Xue, S., Negi, J., Iba, K., Kangasjärvi, J., Ghassemian, M., Stephan, A.B., Hu, H., and Schroeder, J.I. (2012). Reconstitution of abscisic acid activation of SLAC1 anion channel by CPK6 and OST1 kinases and branched ABI1 PP2C phosphatase action. Proc. Natl. Acad. Sci. USA **109:** 10593–10598.

Clough, S.J., and Bent, A.F. (1998). Floral dip: a simplified method for *Agrobacterium*-mediated transformation of *Arabidopsis thaliana.* Plant J. **16:** 735–743.

Coelho, S.M., Taylor, A.R., Ryan, K.P., Sousa-Pinto, I., Brown, M.T., and Brownlee, C. (2002). Spatiotemporal patterning of reactive oxygen production and Ca(2+) wave propagation in fucus rhizoid cells. Plant Cell **14:** 2369–2381.

Cui, X.H., Hao, F.S., Chen, H., Chen, J., and Wang, X.C. (2008). Expression of the *Vicia faba VfPIP1* gene in *Arabidopsis thaliana* plants improves their drought resistance. J. Plant Res. **121:** 207–214.

Da Ines, O., Graf, W., Franck, K.I., Albert, A., Winkler, J.B., Scherb, H., Stichler, W., and Schäffner, A.R. (2010). Kinetic analyses of plant water relocation using deuterium as tracer - reduced water flux of *Arabidopsis* pip2 aquaporin knockout mutants. Plant Biol. (Stuttg.) **12** (suppl 1.): 129–139.

Dynowski, M., Schaaf, G., Loque, D., Moran, O., and Ludewig, U. (2008). Plant plasma membrane water channels conduct the signalling molecule H_2O_2. Biochem. J. **414:** 53–61.

Flexas, J., Ribas-Carbó, M., Hanson, D.T., Bota, J., Otto, B., Cifre, J., McDowell, N., Medrano, H., and Kaldenhoff, R. (2006). Tobacco aquaporin *Nt*AQP1 is involved in mesophyll conductance to CO_2 *in vivo.* Plant J. **48:** 427–439.

Foreman, J., Demidchik, V., Bothwell, J.H., Mylona, P., Miedema, H., Torres, M.A., Linstead, P., Costa, S., Brownlee, C., Jones, J.D., Davies, J.M., and Dolan, L. (2003). Reactive oxygen species produced by NADPH oxidase regulate plant cell growth. Nature **422:** 442–446.

Franks, P.J., Buckley, T.N., Shope, J.C., and Mott, K.A. (2001). Guard cell volume and pressure measured concurrently by confocal microscopy and the cell pressure probe. Plant Physiol. **125:** 1577–1584.

Fraysse, L.C., Wells, B., McCann, M.C., and Kjellbom, P. (2005). Specific plasma membrane aquaporins of the PIP1 subfamily are expressed in sieve elements and guard cells. Biol. Cell **97:** 519–534.

Geiger, D., Scherzer, S., Mumm, P., Marten, I., Ache, P., Matschi, S., Liese, A., Wellmann, C., Al-Rasheid, K.A., Grill, E., Romeis, T., and Hedrich, R. (2010). Guard cell anion channel SLAC1 is regulated by CDPK protein kinases with distinct Ca^{2+} affinities. Proc. Natl. Acad. Sci. USA **107:** 8023–8028.

Geiger, D., Scherzer, S., Mumm, P., Stange, A., Marten, I., Bauer, H., Ache, P., Matschi, S., Liese, A., Al-Rasheid, K.A., Romeis, T., and Hedrich, R. (2009). Activity of guard cell anion channel SLAC1 is controlled by drought-stress signaling kinase-phosphatase pair. Proc. Natl. Acad. Sci. USA **106:** 21425–21430.

Hanba, Y.T., Shibasaka, M., Hayashi, Y., Hayakawa, T., Kasamo, K., Terashima, I., and Katsuhara, M. (2004). Overexpression of the barley aquaporin HvPIP2;1 increases internal CO_2 conductance and CO_2 assimilation in the leaves of transgenic rice plants. Plant Cell Physiol. **45:** 521–529.

Heinen, R.B., Bienert, G.P., Cohen, D., Chevalier, A.S., Uehlein, N., Hachez, C., Kaldenhoff, R., Le Thiec, D., and Chaumont, F. (2014). Expression and characterization of plasma membrane aquaporins in stomatal complexes of *Zea mays*. Plant Mol. Biol. **86:** 335–350.

Hellens, R.P., Edwards, E.A., Leyland, N.R., Bean, S., and Mullineaux, P.M. (2000). pGreen: a versatile and flexible binary Ti vector for *Agrobacterium*-mediated plant transformation. Plant Mol. Biol. **42:** 819–832.

Hose, E., Steudle, E., and Hartung, W. (2000). Abscisic acid and hydraulic conductivity of maize roots: a study using cell- and root-pressure probes. Planta **211:** 874–882.

Hosy, E., et al. (2003). The Arabidopsis outward K^+ channel GORK is involved in regulation of stomatal movements and plant transpiration. Proc. Natl. Acad. Sci. USA **100:** 5549–5554.

Joshi-Saha, A., Valon, C., and Leung, J. (2011). A brand new START: abscisic acid perception and transduction in the guard cell. Sci. Signal. **4:** re4.

Kim, T.H., Böhmer, M., Hu, H., Nishimura, N., and Schroeder, J.I. (2010). Guard cell signal transduction network: advances in understanding abscisic acid, CO_2, and Ca^{2+} signaling. Annu. Rev. Plant Biol. **61:** 561–591.

Kline, K.G., Barrett-Wilt, G.A., and Sussman, M.R. (2010). *In planta* changes in protein phosphorylation induced by the plant hormone abscisic acid. Proc. Natl. Acad. Sci. USA **107:** 15986–15991.

Kwak, J.M., Mori, I.C., Pei, Z.M., Leonhardt, N., Torres, M.A., Dangl, J.L., Bloom, R.E., Bodde, S., Jones, J.D., and Schroeder, J.I. (2003). NADPH oxidase AtrbohD and AtrbohF genes function in ROS-dependent ABA signaling in Arabidopsis. EMBO J. **22:** 2623–2633.

Lee, S.C., Lan, W., Buchanan, B.B., and Luan, S. (2009). A protein kinase-phosphatase pair interacts with an ion channel to regulate ABA signaling in plant guard cells. Proc. Natl. Acad. Sci. USA **106:** 21419–21424.

Leonhardt, N., Kwak, J.M., Robert, N., Waner, D., Leonhardt, G., and Schroeder, J.I. (2004). Microarray expression analyses of *Arabidopsis* guard cells and isolation of a recessive abscisic acid hypersensitive protein phosphatase 2C mutant. Plant Cell **16:** 596–615.

Liman, E.R., Tytgat, J., and Hess, P. (1992). Subunit stoichiometry of a mammalian K^+ channel determined by construction of multimeric cDNAs. Neuron **9:** 861–871.

Maurel, C., Reizer, J., Schroeder, J.I., and Chrispeels, M.J. (1993). The vacuolar membrane protein γ-TIP creates water specific channels in *Xenopus* oocytes. EMBO J. **12:** 2241–2247.

Montillet, J.L., et al. (2013). An abscisic acid-independent oxylipin pathway controls stomatal closure and immune defense in *Arabidopsis.* PLoS Biol. **11:** e1001513.

Pantin, F., Monnet, F., Jannaud, D., Costa, J.M., Renaud, J., Muller, B., Simonneau, T., and Genty, B. (2013). The dual effect of abscisic acid on stomata. New Phytol. **197:** 65–72.

Pei, Z.M., Murata, Y., Benning, G., Thomine, S., Klüsener, B., Allen, G.J., Grill, E., and Schroeder, J.I. (2000). Calcium channels activated by hydrogen peroxide mediate abscisic acid signalling in guard cells. Nature **406:** 731–734.

Péret, B., et al. (2012). Auxin regulates aquaporin function to facilitate lateral root emergence. Nat. Cell Biol. **14:** 991–998.

Postaire, O., Tournaire-Roux, C., Grondin, A., Boursiac, Y., Morillon, R., Schäffner, A.R., and Maurel, C. (2010). A PIP1 aquaporin contributes to hydrostatic pressure-induced water transport in both the root and rosette of Arabidopsis. Plant Physiol. **152:** 1418–1430.

Prado, K., Boursiac, Y., Tournaire-Roux, C., Monneuse, J.-M., Postaire, O., Da Ines, O., Schäffner, A.R., Hem, S., Santoni, V., and Maurel, C. (2013). Regulation of *Arabidopsis* leaf hydraulics involves light-dependent phosphorylation of aquaporins in veins. Plant Cell **25:** 1029–1039.

Prak, S., Hem, S., Boudet, J., Viennois, G., Sommerer, N., Rossignol, M., Maurel, C., and Santoni, V. (2008). Multiple phosphorylations in the C-terminal tail of plant plasma membrane aquaporins: role in subcellular trafficking of AtPIP2;1 in response to salt stress. Mol. Cell. Proteomics **7:** 1019–1030.

Quintero, J.M., Fournier, J.M., and Benlloch, M. (1999). Water transport in sunflower root systems: effects of ABA, Ca^{2+} status and $HgCl_2$. J. Exp. Bot. **50:** 1607–1612.

Ramahaleo, T., Morillon, R., Alexandre, J., and Lassalles, J.-P. (1999). Osmotic water permeability of isolated protoplasts. Modifications during development. Plant Physiol. **119:** 885–896.

Sade, N., Gallé, A., Flexas, J., Lerner, S., Peleg, G., Yaaran, A., and Moshelion, M. (2014). Differential tissue-specific expression of NtAQP1 in *Arabidopsis thaliana* reveals a role for this protein in stomatal and mesophyll conductance of CO_2 under standard and salt-stress conditions. Planta **239:** 357–366.

Sade, N., Gebretsadik, M., Seligmann, R., Schwartz, A., Wallach, R., and Moshelion, M. (2010). The role of tobacco Aquaporin1 in improving water use efficiency, hydraulic conductivity, and yield production under salt stress. Plant Physiol. **152:** 245–254.

Santoni, V., Vinh, J., Pflieger, D., Sommerer, N., and Maurel, C. (2003). A proteomic study reveals novel insights into the diversity of aquaporin forms expressed in the plasma membrane of plant roots. Biochem. J. **373:** 289–296.

Sarda, X., Tousch, D., Ferrare, K., Legrand, E., Dupuis, J.M., Casse-Delbart, F., and Lamaze, T. (1997). Two TIP-like genes encoding aquaporins are expressed in sunflower guard cells. Plant J. **12:** 1103–1111.

Sato, A., Sato, Y., Fukao, Y., Fujiwara, M., Umezawa, T., Shinozaki, K., Hibi, T., Taniguchi, M., Miyake, H., Goto, D.B., and Uozumi, N. (2009). Threonine at position 306 of the KAT1 potassium channel is essential for channel activity and is a target site for ABA-activated SnRK2/OST1/SnRK2.6 protein kinase. Biochem. J. **424:** 439–448.

Schopfer, P., Plachy, C., and Frahry, G. (2001). Release of reactive oxygen intermediates (superoxide radicals, hydrogen peroxide, and hydroxyl radicals) and peroxidase in germinating radish seeds controlled by light, gibberellin, and abscisic acid. Plant Physiol. **125:** 1591–1602.

Shatil-Cohen, A., Attia, Z., and Moshelion, M. (2011). Bundle-sheath cell regulation of xylem-mesophyll water transport via aquaporins under drought stress: a target of xylem-borne ABA? Plant J. **67:** 72–80.

Shope, J.C., and Mott, K.A. (2006). Membrane trafficking and osmotically induced volume changes in guard cells. J. Exp. Bot. **57:** 4123–4131.

Sirichandra, C., Davanture, M., Turk, B.E., Zivy, M., Valot, B., Leung, J., and Merlot, S. (2010). The Arabidopsis ABA-activated kinase OST1 phosphorylates the bZIP transcription factor ABF3 and creates a 14-3-3 binding site involved in its turnover. PLoS One **5:** e13935.

Sirichandra, C., Gu, D., Hu, H.C., Davanture, M., Lee, S., Djaoui, M., Valot, B., Zivy, M., Leung, J., Merlot, S., and Kwak, J.M. (2009). Phosphorylation of the Arabidopsis AtrbohF NADPH oxidase by OST1 protein kinase. FEBS Lett. **583:** 2982–2986.

Steudle, E. (1989). Water flow in plants and its coupling to other processes: an overview. Methods Enzymol. **174:** 183–225.

Suhita, D., Raghavendra, A.S., Kwak, J.M., and Vavasseur, A. (2004). Cytoplasmic alkalization precedes reactive oxygen species production during methyl jasmonate- and abscisic acid-induced stomatal closure. Plant Physiol. **134:** 1536–1545.

Sun, M.-H., Xu, W., Zhu, Y.-F., Su, W.-A., and Tang, Z.-C. (2001). A simple method for in situ hybridization to RNA in guard cells of *Vicia faba* L.: The expression of aquaporins in guard cells. Plant Mol. Biol. Rep. **19:** 129–135.

Törnroth-Horsefield, S., Wang, Y., Hedfalk, K., Johanson, U., Karlsson, M., Tajkhorshid, E., Neutze, R., and Kjellbom, P. (2006). Structural mechanism of plant aquaporin gating. Nature **439:** 688–694.

Verdoucq, L., Grondin, A., and Maurel, C. (2008). Structure-function analysis of plant aquaporin *At*PIP2;1 gating by divalent cations and protons. Biochem. J. **415:** 409–416.

Vlad, F., Turk, B.E., Peynot, P., Leung, J., and Merlot, S. (2008). A versatile strategy to define the phosphorylation preferences of plant protein kinases and screen for putative substrates. Plant J. **55:** 104–117.

Wang, P., and Song, C.P. (2008). Guard-cell signalling for hydrogen peroxide and abscisic acid. New Phytol. **178:** 703–718.

Wege, S., De Angeli, A., Droillard, M.J., Kroniewicz, L., Merlot, S., Cornu, D., Gambale, F., Martinoia, E., Barbier-Brygoo, H., Thomine, S., Leonhardt, N., and Filleur, S. (2014). Phosphorylation of the vacuolar anion exchanger AtCLCa is required for the stomatal response to abscisic acid. Sci. Signal. **7:** ra65.

Wu, X.N., Sanchez Rodriguez, C., Pertl-Obermeyer, H., Obermeyer, G., and Schulze, W.X. (2013). Sucrose-induced receptor kinase SIRK1 regulates a plasma membrane aquaporin in *Arabidopsis.* Mol. Cell. Proteomics **12:** 2856–2873.

Yaneff, A., Sigaut, L., Marquez, M., Alleva, K., Pietrasanta, L.I., and Amodeo, G. (2014). Heteromerization of PIP aquaporins affects their intrinsic permeability. Proc. Natl. Acad. Sci. USA **111:** 231–236.

Yang, H.M., Zhang, X.Y., Tang, Q.L., and Wang, G.X. (2006). Extracellular calcium is involved in stomatal movement through the regulation of water channels in broad bean. Plant Growth Regul. **50:** 79–83.

Zelazny, E., Borst, J.W., Muylaert, M., Batoko, H., Hemminga, M.A., and Chaumont, F. (2007). FRET imaging in living maize cells reveals that plasma membrane aquaporins interact to regulate their subcellular localization. Proc. Natl. Acad. Sci. USA **104:** 12359–12364.

Zhang, X., Zhang, L., Dong, F., Gao, J., Galbraith, D.W., and Song, C.P. (2001). Hydrogen peroxide is involved in abscisic acid-induced stomatal closure in *Vicia faba*. Plant Physiol. **126:** 1438–1448.

Plant, Cell and Environment (2015) doi: 10.1111/pce.12616

Original Article

Root aquaporins contribute to whole plant water fluxes under drought stress in rice (*Oryza sativa* L.)

Alexandre Grondin[1,3], Ramil Mauleon[1], Vincent Vadez[2] & Amelia Henry[1]

[1]*International Rice Research Institute, Crop Environmental Sciences Division, DAPO Box 7777, Metro Manila, Philippines,* [2]*International Crops Research Institute for the Semi-Arid Tropics, Patancheru, 502 324, Andhra Pradesh, India and* [3]*University of Nebraska-Lincoln, Department of Agronomy and Horticulture, Lincoln, NE 68583, USA*

ABSTRACT

Aquaporin activity and root anatomy may affect root hydraulic properties under drought stress. To better understand the function of aquaporins in rice root water fluxes under drought, we studied the root hydraulic conductivity (*Lp*r) and root sap exudation rate (*S*r) in the presence or absence of an aquaporin inhibitor (azide) under well-watered conditions and following drought stress in six diverse rice varieties. Varieties varied in *Lp*r and *S*r under both conditions. The contribution of aquaporins to *Lp*r was generally high (up to 79% under well-watered conditions and 85% under drought stress) and differentially regulated under drought. Aquaporin contribution to *S*r increased in most varieties after drought, suggesting a crucial role for aquaporins in osmotic water fluxes during drought and recovery. Furthermore, root plasma membrane aquaporin (PIP) expression and root anatomical properties were correlated with hydraulic traits. Three chromosome regions highly correlated with hydraulic traits of the OryzaSNP panel were identified, but did not co-locate with known aquaporins. These results therefore highlight the importance of aquaporins in the rice root radial water pathway, but emphasize the complex range of additional mechanisms related to root water fluxes and drought response.

Key-words: aquaporins; plasma membrane intrinsic proteins; azide; root hydraulic conductivity; sap exudation; leaf water potential; transpiration rate.

INTRODUCTION

The root system is responsible for capturing water and nutrients and thus has been intensively studied in order to improve rice adaptation to drought stress (Gowda *et al.* 2011; Rogers & Benfey 2015). Limitations to rice root water uptake under drought have mostly been studied in terms of root architecture; more research is needed on the functionality of the root system under drought (Vadez 2014). Because of its ability to grow in flooded paddies as well as in dry soil, in large and diverse cultivation areas worldwide, rice varieties offer a potentially unique panel of variability in root water uptake functionality and regulation that can be use for quantitative analyses (Henry *et al.* 2011; Gowda *et al.* 2012).

Rice roots tend to have lower hydraulic conductivity than other herbaceous species such as maize (*Zea mays*) or common bean (*Phaseolus vulgaris*; Fiscus 1986; Zimmermann *et al.* 2000; Miyamoto *et al.* 2001), and are not able to extract as much water from drying soil (Kamoshita *et al.* 2000; Kondo *et al.* 2000). The apoplastic barriers are exceptionally developed in rice roots and are reportedly responsible for the overall low root hydraulic conductivity (Miyamoto *et al.* 2001; Ranathunge *et al.* 2003, 2004). Apart from the apoplastic path in which water flow can be modulated by such barriers, the composite model of radial water transport in roots also predicts cell-to-cell water movement, i.e. symplastic routes through cytoplasmic continuity and transcellular paths crossing cell membranes (Steudle 2000). The transcellular path can play a major role as it is facilitated by water channel proteins, aquaporins (Javot & Maurel 2002). In rice, the contributions of the apoplastic and transcellular paths have been explored using ink as a partial apoplastic blocker or mercuric chloride as an aquaporin inhibitor, and the results suggested a relatively larger apoplastic flow in the outer part of the root cross section (Ranathunge *et al.* 2004).

Depending on the environmental conditions, plants can alter the relative contributions of the apoplastic and cell-to-cell pathways and therefore their overall root hydraulic conductivity (Javot & Maurel 2002). Suberization has been observed to be reduced at the exodermis but increased at the endodermis in rice plants grown in dry soil, suggesting reduced dependence on the apoplastic pathway at the inner part of the roots under such conditions (Henry *et al.* 2012). Furthermore, modulation of root hydraulic conductivity (*Lp*r) through aquaporin function can contribute to maintaining or adjusting transpiration and shoot growth according to water availability (Maurel *et al.* 2010). In rice seedlings, root-to-leaf conductance and shoot growth were significantly affected by mercuric chloride application under water-limited conditions, but not in well-watered conditions, suggesting predominantly apoplastic water transport under well-watered conditions and an upregulation of the transcellular path under water deficit (Lu & Neumann 1999). Additionally, a strong positive correlation between root hydraulic conductance and shoot dry weight was observed in three rice varieties under reduced soil

Correspondence: A. Henry. e-mail: a.henry@irri.org

water availability, but not under well-irrigated conditions (Matsuo *et al.* 2009). Studies of comparative responses of aquaporin expression, root water fluxes and plant water use measured at different times of day suggested that coordinated up-regulation of root aquaporin expression could prevent reduction in transpiration by increasing root water flow (Sakurai-Ishikawa *et al.* 2011; Nada & Abogadallah 2014). Altogether, these observations suggest that aquaporins are good target proteins for understanding limitations to rice water uptake and drought response.

In rice, 33 aquaporin isoforms have been identified, including about 11 plasma membrane intrinsic proteins (PIPs) which are the most abundant aquaporins at the plasma membrane, 10 tonoplast intrinsic proteins (TIPs), 10 nodulin 26-like intrinsic proteins (NIPs) and two small intrinsic proteins (SIPs; Sakurai *et al.* 2005; Guo *et al.* 2006; Nguyen *et al.* 2013). Aquaporins are present throughout the rice plant, some isoforms showing distinct cell-specific and tissue-specific localizations (Guo *et al.* 2006; Sakurai *et al.* 2008). For instance, PIP2;3 and PIP2;5, showed predominant accumulation in the endodermis (Sakurai *et al.* 2008). In rice and other species, the expression of PIPs fluctuates with the time of day, and also in response to various stresses such as salt, drought, cold and submergence (Malz & Sauter 1999; Lian *et al.* 2004; Ahamed *et al.* 2012; Henry *et al.* 2012; Liu *et al.* 2013). Expression analysis of PIPs under simulated drought conditions using PEG or after abscisic acid application showed different time- and stress severity-dependant responses among isoforms, where the mRNA level of some PIPs was significantly upregulated while others remained unchanged or were down-regulated (Guo *et al.* 2006; Lian *et al.* 2006). Interestingly, comparison of PIP expression between lowland (more susceptible to drought) and upland (typically more resistant to drought) varieties suggested different regulation mechanisms of PIP expression, with upland varieties showing specific up-regulation of PIP isoform genes (Lian *et al.* 2006).

Given the converging evidence linking aquaporin function to drought stress in rice, we hypothesized that aquaporin function would explain differences in root water uptake between varieties, and consequently resistance to drought stress. To our knowledge, the function of aquaporins in rice drought resistance has only been assessed using transgenic strategies (Katsuhara *et al.* 2003; Lian *et al.* 2004, 2006; Guo *et al.* 2006; Li *et al.* 2008), in which the beneficial effect of the aquaporin transgene expression in terms of growth or water content was described after growing the plants in hydroponic conditions with simulated drought stress. In this study, we assessed the variability of root hydraulic response to drought in soil-grown rice using a subset of six varieties from the OryzaSNP panel (Azucena, Moroberekan, FR13 A, Dular, IR64 and Swarna) showing a wide range of response to drought (Henry *et al.* 2011; Gowda *et al.* 2012), and we used the full OryzaSNP panel for genetic mapping. Our approach was to focus on aquaporin inhibition while taking into account the variation in PIP expression, root anatomy and plant water status in order to better understand rice root water fluxes and drought response.

MATERIALS AND METHODS

Plant material and growth conditions

Two groups of rice varieties were used in this study: (1) a subset of six rice varieties from the OryzaSNP panel comprising Azucena (japonica group), Dular (aus group) and Moroberekan (japonica group) that are typically considered as upland varieties with moderate drought tolerance, and FR13 A (aus group), IR64 (indica group) and Swarna (indica group) that are considered as lowland varieties with low drought tolerance; and (2) the 20 varieties of the OryzaSNP panel, which has been mapped for 160 000 SNP markers and shows a wide range of response to drought (McNally *et al.* 2009; Henry *et al.* 2011; Gowda *et al.* 2012). The subset of six rice varieties was used for detailed characterization of hydraulic properties under well-watered and drought stress conditions in Experiments 1–4 (Table 1). All 20 varieties were used to correlate hydraulic and plants water use traits with genomic regions in Experiments 5–7 (Table 1).

Six independent pot/cylinder studies were conducted to evaluate the contribution of aquaporins to rice root water fluxes, and the relationship between root aquaporin function and leaf water status (Table 1). The size of the pots/cylinders used was determined according to the objectives of the experiment: 0.785 L mylar tubes that fit inside the pressure chamber were used for root hydraulic conductivity and aquaporin expression studies; 1.5 L pots that facilitate frequent weighing were used for sap exudation and transpiration studies.

Experiments 1–5 were performed in a greenhouse at the International Rice Research Institute (IRRI), Los Baños, Philippines (14° 11′N, 121° 15′E) in pots or cylinders arranged on tables in a randomized complete block design. Experiment 6 was performed at the International Crops Research Institute for the Semi-Arid Tropics (ICRISAT), Patancheru, India (17° 30′N, 78° 16′E) in pots arranged randomly on tables in a greenhouse. Seeds were germinated in Petri-dishes for four days at 30 °C before sowing in soil. Experiments 1 and 3 were performed using 50 cm long and 5 cm diameter mylar tubes closed at the bottom with cheesecloth-like fabric to allow absorption of solution at the lower part of the soil column. Mylar tubes were filled with 0.95 kg of dried and sieved upland soil to a height of 40 cm for a bulk density of 1.2 g cm^{-3} and placed into 40 cm long, 5.5 cm diameter PVC cylinders to keep the root zone in the dark. In Experiments 2, 4 and 5, plants were grown in 1.5 L pots filled with 1 kg of soil from the IRRI upland farm (Table S1), or with black soil mixed with vermicompost in Experiment 6. Fertilizer was not added to the soil in Experiments 1–4 as no nutrient deficiencies were observed. In Experiment 5, fertilizer (14N–14P–14K) at a rate of 0.3 g kg^{-1} was added at 20 days after sowing (das). The well-watered condition consisted of keeping the soil saturated with water, while the drought stress treatment was applied seven days after sowing through gradual dry-down by withholding water. Pots/cylinders in the drought stress treatment were weighed three times per week to monitor the dry down rate, and, if needed, water was added to maintain the soil at 30–40% of field capacity until the end of the study.

Table 1. List of experiments. das: days after sowing; *Lp*r: root hydraulic conductivity; *Lp*r_Inh: relative *Lp*r inhibition; LWP: leaf water potential; *S*r: sap exudation rate; *S*r_Inh: relative *S*r inhibition; *T*r: transpiration rate; *T*r_Inh: relative *T*r inhibition; CT: canopy temperature; SDW: shoot dry weight; DRI: drought response index; WW: well-watered; DS: drought stress

Experiment	Number of varieties	Number of replications	Environment	Measurements; soil moisture treatments	Plant age at measurement (das)	Average temperature (°C)
1	6	15	Greenhouse (IRRI)	*Lp*r, *Lp*r_Inh, LWP, Root anatomy; WW, DS	29	29.5
2	6	6	Greenhouse (IRRI)	*S*r, *S*r_Inh; WW, DS	35	32.8
3	6	3	Greenhouse (IRRI)	Sampling for root PIP expression; WW, DS	29	29.8
4	6	8	Greenhouse (IRRI)	*T*r, *T*r_Inh; WW, DS	28	28.3
5	20	6	Greenhouse (IRRI)	*S*r, *S*r_Inh; WW	35	32.8
6	20	6	Greenhouse (ICRISAT)	*T*r, *T*r_Inh; WW	31	30
7	20	4	Lowland field (IRRI)	*S*r, CT, SDW, DRI; WW, DS	65 to 95	26.7

A field experiment (Experiment 7) was also conducted under transplanted lowland field conditions at IRRI during the 2014 dry season (January to April) in order to investigate relationships between root and leaf hydraulics and plant water use related traits. Four replications of 3.5 m^2 plots (6 rows of 15 hills) were arranged in a randomized complete block design. Well-watered plots were maintained flooded during the entire experiment while drought was applied and managed in stress plots by withholding irrigation at 60 das as described by Henry *et al.* (2011). Tensiometers (Soilmoisture Equipment Corp., CA, USA) were installed at a depth of 30 cm in the drought stress treatment to monitor the soil water potential (Figure S1). Ambient conditions were monitored throughout the experiment (Figure S2). Basal fertilizer was applied before transplanting using complete fertilizer (14N–14P–14K) at the rate of 40 kg N ha^{-1}, and a topdressing of 50 kg N ha^{-1} ammonium sulfate was applied before panicle initiation. Manual weeding was done when needed.

Root hydraulic conductivity

Root hydraulic conductivity (*Lp*r) was measured according to a protocol adapted from Henry *et al.* (2012). Seeds were sown at staggered intervals (12 cylinders per day) according to the number of plants that could be measured per day for *Lp*r using two pressure chambers. In a preliminary experiment, different *Lp*r inhibition protocols were explored on plants grown in soil in a growth chamber (temperature: 29 °C day, 21 °C night; relative humidity: 70%; photoperiod: 12 h) using two aquaporin inhibitors, salt (500 mM $NaCl_2$) and azide (4 mM NaN_3). The efficiency of the two inhibitors was tested in solution after washing the roots or by direct application into the soil, and after two treatment times (30 or 60 min; Figure S3). Azide application into the soil for 30 min was chosen to conduct further inhibition assays. In Experiment 1, *Lp*r was measured at 29 das from 7:30 AM to 1:00 PM in a greenhouse in which a total of 150 mL of water (control) or 4 mM azide solution was added directly to the soil surface and at the bottom of the mylar tube (within the outer PVC cylinder) 30 min before excising the shoots to start the *Lp*r measurements. The mylar tube was placed in a 1.6 L pressure chamber (300HGBL Plant Water Status Console, Soilmoisture Equipment Corp., CA, USA). The main tiller was cut at a height of about 5 cm above the soil surface and passed throughout a silicone grommet in the lid of the pressure chamber while the intact root system was sealed inside. Roots were pressurized with compressed air first at 0.2 MPa for 10 min to equilibrate, and then xylem sap was collected at pressures of 0.2, 0.35 and 0.5 MPa for 10 min using pre-weighed 2 mL Eppendorf tubes filled with cotton. The mass of xylem sap exuded at each pressure was determined by weighing the cotton-filled tubes. After the sap collections, maximum root depth of each plant was measured and roots were washed and stored in 75% ethanol until scanning at 600 dpi (Epson Perfection V700, Epo America, CA, USA). The scanned roots were analysed for total root length, surface area, and length within diameter classes using WhinRhizo Pro v. 2013e (Regent Instruments, Quebec, Canada). The proportion of lateral roots for each plant was calculated by dividing the length of roots <0.2 mm in diameter by the total root length. *Lp*r was calculated as the slope of xylem sap flux at each pressure, and normalized for root surface area. Relative *Lp*r inhibition (*Lp*r_Inh) for each azide treated plant was calculated as: $(Lpr_{water}$ (variety mean) $- Lpr_{azide}$ (individual replicate)) / Lpr_{water} (variety mean) × 100 (Eqn 1).

Sap exudation rate

Sap exudation rate (*S*r) measurements were carried out at 35 das in Experiments 2 and 5, and at 82 das in Experiment 7, according to the protocol described by Morita & Abe (2002) and Henry *et al.* (2012). Shoots were cut at a height of around 15 cm from the soil surface, and the sap coming from the root zone was collected by covering the cut stems with a cotton towel inside a polyethylene bag sealed at the base with a rubber band. After 4 h, the previously weighed towel, plastic bag and rubber band were collected and immediately weighed again to quantify the exuded sap from the intact root system. In Experiments 2 and 5 but not in Experiment 7, 150 mL of water or azide solution at 4 mM was added to the soil just before excising the shoots to collect the sap. Shoots and roots were washed after sap collection, oven-dried and weighed to determine root biomass. *S*r was

calculated as grams of sap exuded per hour, and values were normalized by root mass of the plant from which sap was collected in Experiments 2 and 5. In field Experiment 7, because root mass was not measured, *S*r (*S*r_DS) was normalized by the shoot dry weight of the hill from which sap was collected in order to account for variation in plant size. Relative *S*r inhibition (*S*r_Inh) for each azide treated plant was calculated as: (Sr_{water} (variety mean) – Sr_{azide} (individual replicate)) / Sr_{water} (variety mean) × 100 (Eqn 2).

Leaf water potential

Leaf water potential (LWP) was measured in Experiment 1 by inserting one leaf into a pressure chamber (300HGBL Plant Water Status Console, Soilmoisture Equipment Corp., CA, USA) and pressurizing the leaf using compressed N_2 until the first drop of sap was visible at the base of the stem, at which time the pressure was recorded. LWP was measured on one leaf before adding 150 mL of water or 4 mM azide solution to the soil, and on another leaf just before cutting the shoots to measure the *Lp*r 30 min after the addition of solution.

Transpiration rate under rising vapour pressure deficit

Transpiration rate (*T*r) was measured in a growth chamber at 28 and 31 das in Experiments 4 and 6, respectively, according to the protocol of Kholová *et al.* (2010). Twelve hours before the measurement, plants were transferred from the greenhouse to the growth chamber for night-time acclimation (23 °C and 80% relative humidity), and the soil surface around each plant was covered with a plastic bag to reduce water evaporation from the soil. On the day of measurement, each pot was weighed hourly from 8:00 AM to 4:00 PM, while the vapour pressure deficit (VPD) in the growth chamber was increased by 0.4 kPa every hour (starting from 0.6 kPa at 8:00 AM to 4.1 kPa at 4:00 PM; Table S2). After the 11:00 AM weighing, 150 mL of water or 4 mM azide solution was added directly to the soil. After the last weighing (4:00 PM), shoots were harvested and stored in a plastic bag inside an ice box, and leaf area was measured with a roller-belt-type leaf area meter (LI-3100C, Li-Cor, Nebraska, USA). Plant *T*r was calculated as the cumulative water loss between 11:00 AM and 1:00 PM in grams per hour, and values were normalized by the total leaf area. Relative *T*r inhibition (*T*r_Inh) for each azide-treated plant was calculated as: ($Water\_loss_{water}$ (variety mean) – $Water\_loss_{azide}$ (individual replicate)) / $Water\_loss_{water}$ (variety mean) × 100 (Eqn 3).

Real-time reverse transcription-polymerase chain reaction

Roots from plants grown in Experiment 3 were sampled for PIP expression analysis from 10:00 AM to 11:00 AM at 29 das, and rinsed carefully and quickly. A 15 cm length of root was collected from the apex of the longest nodal root and immediately placed into liquid nitrogen for grinding with a frozen mortar and pestle. Powdered root tissue (150 mg) was used for RNA extraction using an RNeasy Plant mini kit (Qiagen, Germany). Three microlitres of the extracted RNA was treated with RQ1 RNase-Free DNase (Promega, Wisconsin, USA), and first strand cDNA was synthesized using a Transcriptor First Strand cDNA Synthesis kit (Roche, Switzerland) according to the manufacturers' instructions. Real-time reverse transcription-polymerase chain reaction (RT-PCR) was performed using 1 μL of diluted RNA (1:9) with a LightCycler® 480 SYBR Green I Master in a LightCycler® 480 system (Roche, Switzerland). The reaction was repeated for 30–35 cycles at annealing temperatures of 58 °C for *PIP1*;*3*/*PIP2*;*2*/*PIP2*;*4*/*PIP2*;*6* primers, 60 °C for *PIP2*;*1*/*PIP2*;*5* primers and 64 °C *PIP1*;*1*/*PIP1*;*2*/*PIP2*;*8* primers. Primers used to amplify the different aquaporin isoforms (Table S3) were derived from primers designed by Sakurai *et al.* (2005). Primer efficiency was tested by DNA amplification in each variety. *PIP2*;*5* was not included in the analysis because of the uncertainty in the sequence. Furthermore, non-specific amplification was observed for *PIP2*;*3* and *PIP2*;*7* at increased annealing temperatures in all varieties making those results not suitable for analysis.

Root anatomy

Roots from Experiment 1 were sampled after the *Lp*r measurement (29 das) and used to investigate root anatomical properties of the six different varieties. Three intact nodal roots from single plants were randomly selected and hand-sectioned under a dissecting microscope at 1.5 and 5 cm from the root apex. Images of four sections per location along the nodal root were acquired with a Zeiss Axioplan 2 compound microscope at 50× and 100× magnification. For each section, the 50× images were used for measuring root diameter (RD), stele diameter (SD) and cortical cell file number (CCN; Lynch 2013), while the 100× images were used for measuring metaxylem diameter (MD), in both cases using Image J. v 1.46r (Abramoff *et al.* 2004). Cortical width (CW) was calculated as RD minus SD, and cortex cell diameter (CCD) was estimated as CW divided by CCN. In each image, root cortical aerenchyma (Ae) was measured on 50× images using the magic wand tool of Gimp v. 2.8.10 (GNU Image manipulation programme) and calculated as a percentage of the root cortex area.

Plant water use related measurements in the field

Canopy temperature (CT) was measured in Experiment 7 with a hand-held data-logging infrared sensor (Apogee Instruments, Logan UT, USA) at three locations per plot throughout the drought stress treatment. Data recorded at 81 das are presented (Table S13). Time to flowering was recorded when 50% of the plants in the plot reached flowering and was expressed as das. At physiological maturity, plants from an area

of 1.5 m^2 per plot were harvested for shoot dry weight (SDW) and grain weight (GY) measurements expressed as g m^{-2}. Reduction in SDW under drought stress (DS) compared to the well-watered treatment (WW) was calculated as: (SDW_{WW} (variety mean) − SDW_{DS} (individual replicate)) / SDW_{WW} (variety mean) × 100 (Eqn 4). Drought response index (DRI) was calculated according to Bidinger *et al.* (1987) as: (GYS_{act} − GYS_{pred}) / SE of GYS_{pred} (Eqn 5), where GYS_{act} is the actual GY measured in the drought stress treatment, GYS_{pred} the predicted GY for stress based on the GY and DTF under well-watered treatment as determined by multiple regression ($GY_{DS} = a + (b \times GY_{WW}) + (c \times DTF_{WW})$) (Eqn 6). Regression curves were determined using SigmaPlot v. 11.0 (Systat Software, Inc.). DRI was calculated based on the following equation: $GY_{DS} = 211.5 + (0.149 \times GY_{WW}) - (2.5 \times DTF_{ww})$ with SE = 35.6 (Eqn 7).

Identification of chromosomal regions correlated with hydraulic component traits

To identify genome blocks from the OryzaSNP panel that correlate with hydraulic and drought response traits, an introgression block regression analysis was performed according to Jahn *et al.* (2011) and Wade *et al.* (2015). Traits related to plant water transport (*S*r, *S*r_Inh, *T*r, *T*r_Inh and *S*r_DS) or plant water use (CT, SDW reduction and DRI) measured in Experiments 5, 6 and 7, together with traits related to water uptake previously measured on this panel including volumetric soil moisture (VSM) in the field (Henry *et al.* 2011) and total water uptake (TWU) and total water uptake per total root length (TWU/TRL) in lysimeters (Gowda *et al.* 2012), were included in the analysis (Table S13). Briefly, introgression patterns (indica-type blocks into aus or japonica genomes, aus-type blocks within indica or japonica genomes, or japonica-type blocks within indica or aus genomes) were defined based on SNP patterns in 100 kb windows across the genome (McNally *et al.* 2009). The 11 traits were correlated with these introgression blocks by linear regression and significant correlations identified by one-way ANOVA. A subset of 177 introgressed regions correlated with these traits was selected using the significance cutoff of $p < 0.005$. These introgressions were plotted to the rice chromosome map (MSU release 6.1; (Ouyang *et al.* 2007)) using Mapchart v. 2.2 (Voorrips 2002). Gene content in those three regions based on the Nipponbare genome annotation (genome regions translated to Michigan State University rice genome annotation project release 7; Kawahara *et al.* 2013) was identified using the IRRI GSL-Galaxy tool (http://175.41.147.71:8080).

Statistical analyses

Statistical analyses were performed in R v. 2.15.1 (R Development Core Team, 2008) using ANOVA (*aov* script) to detect significant differences and Least Significant Difference (LSD) test to group varieties into letter classes. PCA and correlation analyses were performed using STAR v 2.0.1 (IRRI, Philippines).

RESULTS

Selection of an aquaporin inhibitor treatment

Salt and azide are among the aquaporin inhibitors frequently used in the literature to evaluate the contribution of these proteins to *Lp*r. We tested the effects of these two inhibitors on *Lp*r either (1) after washing and transferring the roots from soil to solution or (2) by direct application into the soil. In solution, root treatment by salt and azide for 30 min did not alter *Lp*r compared to treatment with water (Figure S3). After 60 min in solution, *Lp*r was reduced after salt treatment and remained unchanged after azide treatment. In soil, *Lp*r was not affected by 30 min of salt treatment but was significantly decreased after the same duration of azide treatment. For both salt and azide, roots treated in soil for 60 min showed no significant differences in *Lp*r compared to water-treated roots. Therefore, in order to keep the soil-grown root system undisturbed and minimize the duration of the inhibitor treatment, application of azide directly into the soil for 30 min was used in this study to inhibit aquaporin function.

Contribution of aquaporins to Lpr

To investigate the variability of aquaporin contribution to root hydrostatic water fluxes, we measured the *Lp*r under well-watered conditions and drought stress after adding 150 mL of water (control) or 4 mM azide solution directly to the soil in Experiment 1 (Table 2). Under well-watered conditions, Azucena, Moroberekan, and FR13 A showed the highest *Lp*r values (from 5 to 6×10^{-8} m^3 m^{-2} s^{-1} MPa^{-1}) while Dular, IR64 and Swarna showed the lowest *Lp*r values (around 3×10^{-8} m^3 m^{-2} s^{-1} MPa^{-1}) after water treatment. *Lp*r was significantly reduced by drought stress, except in Swarna where it remained similar to the value observed under well-watered conditions. After drought stress, Azucena, Moroberekan, FR13 A and Swarna showed the highest *Lp*r values (from 2 to 3×10^{-8} m^3 m^{-2} s^{-1} MPa^{-1}) while Dular and IR64 showed the lowest values (around 1×10^{-8} m^3 m^{-2} s^{-1} MPa^{-1}). Azide treatment consistently reduced the *Lp*r, with significant differences among varieties and soil moisture treatments. The percentage of relative *Lp*r inhibition by azide (*Lp*r_Inh), which was interpreted as the contribution of aquaporins to the *Lp*r, varied from 40% in Dular to 80% in Azucena under well-watered conditions, and from 35% in IR64 to 85% in FR13 A under drought stress. Aquaporin contribution to *Lp*r (i.e. *Lp*r_Inh) was significantly reduced by drought stress in Azucena and IR64, significantly increased by drought stress in FR13 A and Dular and not changed in Moroberekan and Swarna. Because *Lp*r is subject to diurnal variation (Sakurai-Ishikawa *et al.* 2011; Henry *et al.* 2012), we further investigated potential changes in *Lp*r over two time periods in Experiment 1. The *Lp*r measured in the early morning (7 AM to 10 AM) was generally similar to the *Lp*r measured at mid-day (10 AM to 1 PM), except in Dular and FR13 A where *Lp*r significantly increased at mid-day under drought stress conditions only (Figure S4A and B).

Table 2. Root hydraulic conductivity (*Lp*r) and inhibition by azide of selected rice varieties. Exuded xylem sap was measured after pressurizing roots from plants grown in Experiment 1 under well-watered conditions (WW) or drought stress (DS). Prior to each measurement, soil was rewatered with 150 mL of water or azide solution (4 mM) for 30 min. *Lp*r_Inh: Relative *Lp*r inhibition. Mean ± se of $n = 12$–15 plants are presented. Letters indicate different significance groups in the water or azide treatments

Variety	Soil moisture	Water treatment 10^{-8} $m^3\,m^{-2}\,s^{-1}\,MPa^{-1}$	Azide treatment 10^{-8} $m^3\,m^{-2}\,s^{-1}\,MPa^{-1}$	*Lp*r_Inh %
Azucena	WW	5.95 ± 0.9a	1.49 ± 0.4bc	79 ± 5ab
	DS	2.90 ± 0.5cd	1.14 ± 0.2cde	61 ± 6cd
Moroberekan	WW	5.23 ± 0.6ab	2.57 ± 0.4a	51 ± 7def
	DS	2.40 ± 0.3cde	0.90 ± 0.2cdef	63 ± 5bcd
FR13 A	WW	6.03 ± 0.8a	2.69 ± 0.3a	55 ± 4cde
	DS	3.01 ± 0.4cd	0.44 ± 0.1f	85 ± 2a
Dular	WW	3.16 ± 0.3c	1.84 ± 0.3b	42 ± 11ef
	DS	1.56 ± 0.2de	0.47 ± 0.1ef	70 ± 3abc
IR64	WW	3.78 ± 0.4bc	1.05 ± 0.2cdef	72 ± 4abc
	DS	1.12 ± 0.2e	0.67 ± 0.1def	35 ± 2f
Swarna	WW	3.28 ± 0.6c	1.40 ± 0.6bcd	57 ± 9cde
	DS	3.04 ± 0.3cd	0.94 ± 0.1cdef	69 ± 4abc

Similarly, the contribution of aquaporins to *Lp*r (i.e. *Lp*r_Inh) was generally maintained between early and mid-day (Figure S4C and D), except in FR13 A, where *Lp*r_Inh was significantly reduced at mid-day (Figure S4C).

Contribution of aquaporins to Sr

To estimate the variability of aquaporin contribution to osmotic water fluxes, we measured *S*r under well-watered conditions and drought stress after treating the plants with 150 mL of water (control) or 4 mM azide in Experiment 2 (Table 3). Under well-watered conditions, Azucena, Moroberekan and Dular showed the highest *S*r values (0.3 $g_{sap}\,h^{-1}\,g_{root}^{-1}$), and FR13 A, Dular, IR64 and Swarna showed the lowest *S*r values (0.14 to 0.19 $g_{sap}\,h^{-1}\,g_{root}^{-1}$) after water treatment. Under drought stress, the absolute amount of exuded sap and the root dry weight was markedly lower compared to the well-watered conditions (data not shown), but after normalization for root dry weight, *S*r was higher under drought in all varieties, with Azucena, Moroberekan, FR13 A, Dular and Swarna showing the highest values (0.4 to 0.5 $g_{sap}\,h^{-1}\,g_{root}^{-1}$) and IR64 showing the lowest value (0.3 $g_{sap}\,h^{-1}\,g_{root}^{-1}$). After azide treatment, *S*r was systematically reduced until being almost completely eliminated in Azucena under drought stress. Furthermore, significant differences in relative *S*r inhibition (*S*r_Inh, i.e. the contribution of aquaporins to *S*r) were observed between soil moisture treatments, with Azucena and Dular displaying contrasting behaviour; Azucena showed the lowest *S*r_Inh under well-watered conditions but the highest under drought stress, and Dular showed the highest *S*r_Inh under well-watered conditions but the lowest under drought stress. The contribution of aquaporins to *S*r was significantly increased by drought stress in Azucena,

Table 3. Sap exudation rate (*S*r) and inhibition by azide of selected rice varieties. Xylem sap was collected for 4 h from roots of plants grown in Experiment 2 under well-watered conditions (WW) or drought stress (DS). Prior to the measurement, soil was rewatered with 150 mL of water or azide solution (4 mM) for 30 min. *S*r_Inh: Relative *S*r inhibition. Mean ± se of $n = 3$–6 are presented. Letters indicate different significance groups in the water or azide treatments

Variety	Soil moisture	Water treatment $g_{sap}\,h^{-1}\,g_{root}^{-1}$	Azide treatment $g_{sap}\,h^{-1}\,g_{root}^{-1}$	*S*r_Inh %
Azucena	WW	0.30 ± 0.01bc	0.22 ± 0.01a	27 ± 2g
	DS	0.44 ± 0.04a	0.01 ± 0.01e	97 ± 1a
Moroberekan	WW	0.30 ± 0.05bc	0.21 ± 0.03ab	39 ± 4efg
	DS	0.50 ± 0.00a	0.15 ± 0.06abcd	69 ± 13bcd
FR13 A	WW	0.18 ± 0.01de	0.12 ± 0.01cd	35 ± 6fg
	DS	0.40 ± 0.02ab	0.19 ± 0.01abc	53 ± 3def
Dular	WW	0.23 ± 0.04cd	0.06 ± 0.00de	73 ± 1bc
	DS	0.43 ± 0.08a	0.25 ± 0.07a	40 ± 12efg
IR64	WW	0.14 ± 0.02e	0.06 ± 0.00de	56 ± 1cde
	DS	0.30 ± 0.04bc	0.07 ± 0.04de	86 ± 11ab
Swarna	WW	0.19 ± 0.02de	0.13 ± 0.01bcd	29 ± 7g
	DS	0.45 ± 0.04a	0.23 ± 0.01a	48 ± 3ef

Moroberekan, FR13 A, IR64 and Swarna, and significantly decreased by drought stress in Dular.

Aquaporin expression profiles under well-watered and drought stress conditions

To investigate the variability of PIP expression in the roots of the six selected varieties, we measured the transcript abundance of 10 rice PIP genes (*PIP1*;*1*, *PIP1*;*2*, *PIP1*;*3*, *PIP2*;*1*, *PIP2*;*2*, *PIP2*;*3*, *PIP2*;*4*, *PIP2*;*6*, *PIP2*;*7* and *PIP2*;*8*) under well-watered and drought stress conditions using RT-PCR in Experiment 3. *PIP2*;*4* was not detected in Azucena or Moroberekan at the DNA and RNA level by the designed primers. Except for *PIP2*;*3* and *PIP2*;*7*, unique melting curves combined with single amplification fragments of the expected size were observed in all varieties after RT-PCR indicating PIP isoform specific amplification (Figure S5). Under well-watered conditions, significant variation in PIP relative transcript abundance was observed among varieties ($p < 0.001$ for *PIP1*;*1*, *PIP1*;*2* and *PIP2*;*1*; $p < 0.01$ for *PIP1*;*3*, *PIP2*;*2* and *PIP2*;*6*; $p < 0.05$ for *PIP2*;*4* and $p < 0.01$ for *PIP2.8*; Fig. 1a). Overall, IR64 showed relatively low PIP transcript abundance compared to the other varieties while Moroberekan showed the highest relative transcript abundance of *PIP1*;*1*, *PIP1*;*2*, *PIP2*;*2*, *PIP2*;*6* and *PIP2*;*8* among the selected varieties and no transcript for *PIP2*;*1*. Under drought stress, the variation in PIP relative transcript abundance among varieties was less, although it was significant for *PIP2*;*1* ($p < 0.001$), *PIP1*;*3* and *PIP2*;*2* ($p < 0.01$), and *PIP1*;*1*, *PIP1*;*2* and *PIP2*;*8* ($p < 0.05$; Fig. 1b). In general, Swarna showed the highest level of transcript abundance for most of the PIP isoforms under drought stress, especially for *PIP1*;*3*.

The effect of drought stress on PIP expression was also investigated by calculating the relative expression of each PIP under drought as the fold-level increase compared to its expression under well-watered conditions for each variety

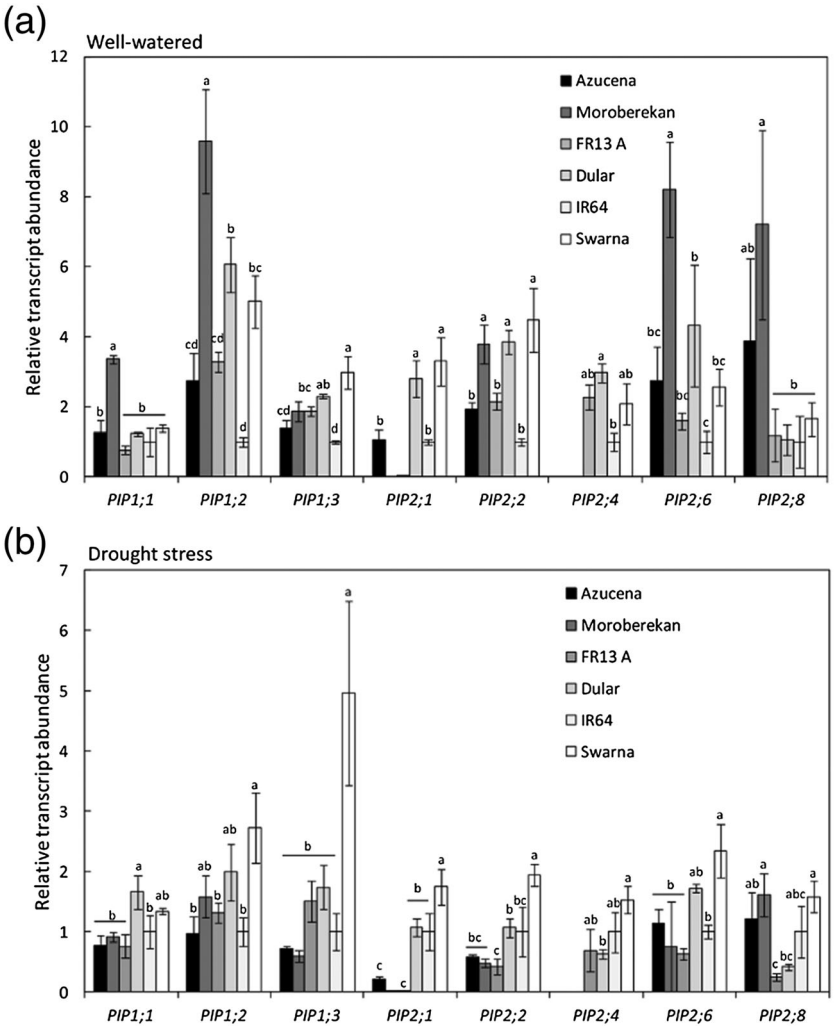

Figure 1. Relative transcript abundance of eight PIP genes in six selected rice varieties. RNA was extracted from roots grown under well-watered conditions (a) or drought stress (b) during Experiment 3. Transcript abundance of the indicated PIP gene was measured in each variety and soil moisture by RT-PCR and normalized to the expression of the same gene in IR64. Bars show mean values ± se of $n = 3$ biological replicates, each with triplicate RT-PCR. Letters indicate different significance groups for transcript abundance of one particular PIP gene.

(Fig.2). In general, PIP transcript accumulation was reduced (*PIP2*;*8*) or slightly induced (*PIP1*;*1*) by drought stress, although some exceptions were observed. For instance, *PIP1*;*2* and *PIP2*;*2* were particularly induced in IR64, as well as *PIP2*;*6* and *PIP2*;*8* in IR64 and Swarna.

Covariation of hydraulic properties and PIP expression

In order to better understand the relationships between PIP expression and root hydraulic traits, we performed principal component analysis (PCA) of the PIP transcript abundance, *Lp*r, *Lp*r inhibition (*Lp*r_Inh), *S*r and *S*r inhibition (*S*r_Inh) measured in the six selected varieties. Under well-watered conditions, the first principal component (PC1), which accounted for 61.91% of the variability, was positive for the *Lp*r components but negative for *S*r components and aquaporin transcript abundance (Fig. 3a). The second principal component explained 21.65% of the variability and was positive for *PIP1*;*1*, *PIP1*;*3*, *PIP2*;*1*, *PIP2*;*2* and *PIP2*;*8*, but negative for *PIP1*;*2*, *PIP2*;*4* and *PIP2*;*6* as well as *Lp*r and *S*r components. Overall, the PCA analysis suggested negative correlations of *Lp*r and *Lp*r_inh with several PIP isoforms, and covariation of *S*r with *PIP2*;*6* and *PIP2*;*4*. Pearson's correlation test confirmed a weak negative correlation between the transcript abundance of a number of PIPs and the *Lp*r and *Lp*r_Inh under well-watered conditions (Table S4). Positive correlations were also observed between *S*r and *PIP2*;*4* ($p < 0.05$), *PIP2*;*6* ($p = 0.0992$) and *PIP2*;*8* ($p < 0.05$). Under drought stress, PCA analysis indicated little variation among varieties for PIP transcript abundance, all showing positive PC1 values, and negative or low positive PC2 values (Fig. 3b). No clear correlation profile was observed between *Lp*r, *Lp*r_Inh, *S*r, *S*r_Inh and PIP transcript abundance by Pearson's correlation analysis (Table S5). However, significant positive correlations among the transcript abundance of several PIP isoforms were observed under drought stress as well as under well-watered conditions (Tables S4 and S5).

PCA analysis of the effect of drought on PIP expression with *Lp*r and *S*r components revealed a principal component explaining 62.59% of the variability that was positive for most PIP isoforms, *Lp*r *Lp*r_Inh and *S*r, and negative for *PIP1*;*1* and *S*r_Inh (Fig. 4). Covariation of all PIP relative expression levels with *Lp*r and *S*r was also revealed (Table S6). Indeed, except for *PIP1*;*1*, positive correlations were observed between PIP relative expression, *Lp*r and *S*r, with significance between *PIP2*;*6* and *S*r ($p < 0.05$).

Root architecture and anatomy

Because root architecture and anatomy can strongly affect root water fluxes, we investigated the variations of these two parameters in the selected varieties in Experiments 1 and 2. Significant differences in maximum root depth were observed among varieties ($p < 0.001$), with Moroberekan showing the highest value and Swarna the lowest value under both well-watered conditions and drought stress (Table S7). Significant differences among varieties were also observed in total root length ($p < 0.001$), root surface area ($p < 0.001$) under both conditions and percentage of fine roots ($p < 0.001$) under drought stress. No significant differences were observed in root mass and root:shoot ratio. Except for the maximum root depth and the percentage of fine roots, root architecture parameters and the root:shoot ratio were reduced by drought stress.

Root anatomy was investigated in cross sections of nodal roots taken at 1.5 and 5 cm from the root apex (Table 4, Figs. 5 and S6). Azucena, Moroberekan, FR13 A and Dular had larger root diameter (RD) than FR13 A, IR64 and Swarna under well-watered conditions at both locations of the apex. Root diameter was significantly reduced by drought in all varieties, but the reduction was less marked in Moroberekan. In general, varieties with larger RD under well-watered conditions and drought stress also showed larger cortical width (CW; data not shown), stele diameter (SD), and metaxylem diameter (MD). This trend was confirmed by significant positive correlation between RD and

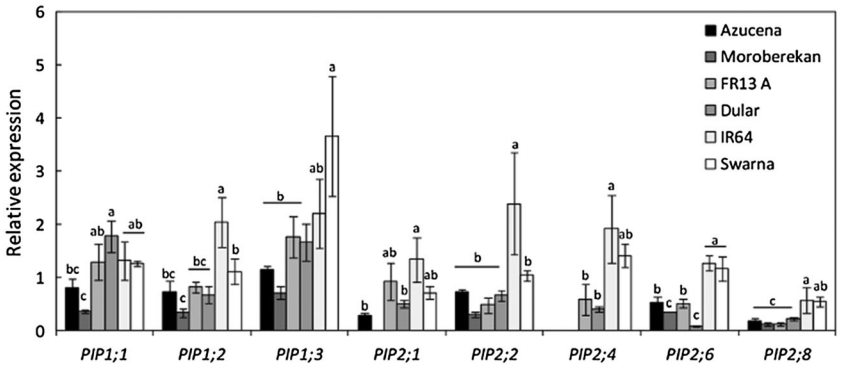

Figure 2. Variation of PIP relative expression in response to drought in six selected rice varieties. The relative transcript abundance of a particular PIP under drought was calculated in one variety as the fold increase relative to the transcript abundance in the same variety under well-watered conditions. Bars show mean values ± se of $n = 3$ biological replicates, each with triplicate RT-PCR. Letters indicate different significance groups for transcript abundance variation of one particular PIP gene.

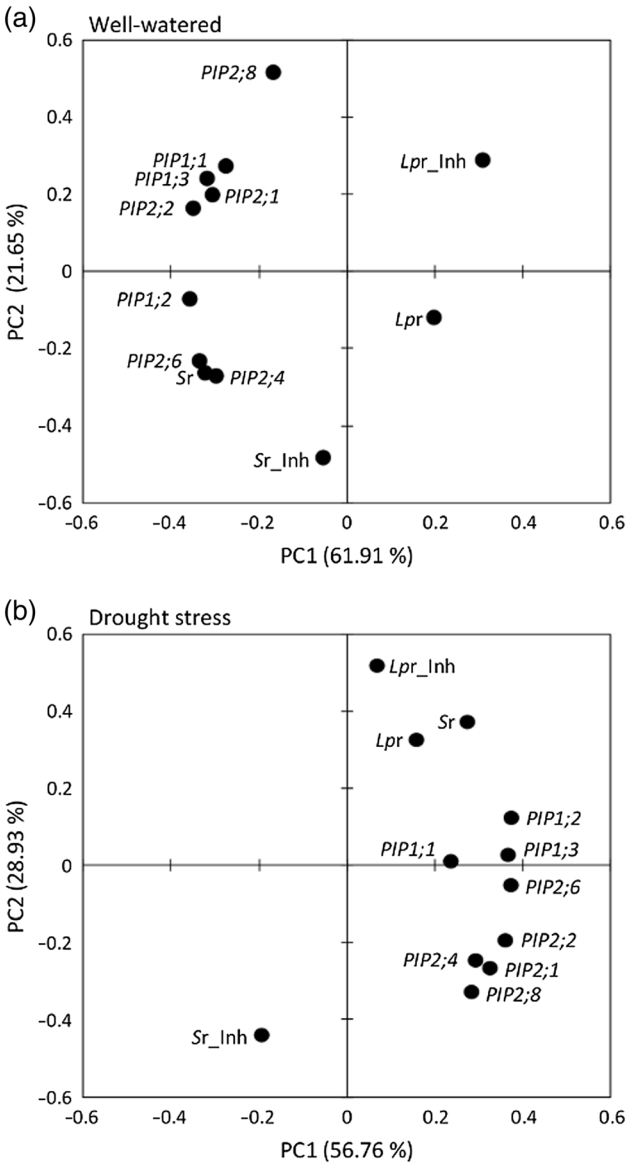

Figure 3. Covariation of root hydraulics and PIP expression in six selected rice varieties. Mean values of PIP transcript abundance, and *Lp*r, *Lp*r_Inh, *Sr* and *Sr*_Inh obtained after water treatment of well-watered (a) and drought-stressed (b) plants were used for Principal Component Analysis (PCA). The contribution of each PCA axis (PC1 and PC2) is indicated on the graph.

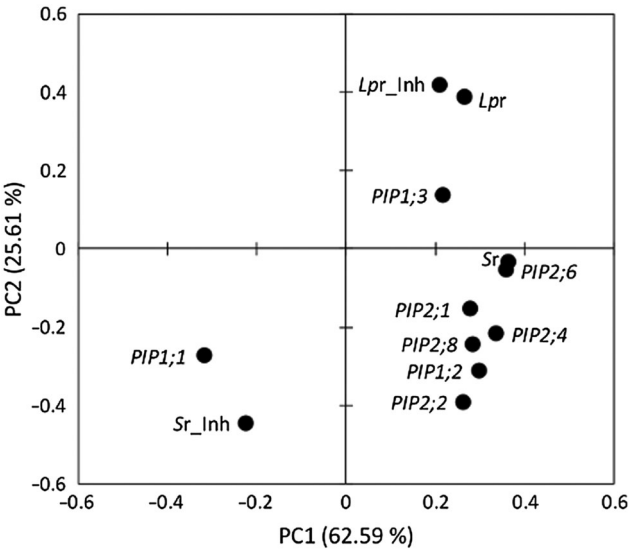

Figure 4. Covariation of root hydraulics and PIP variation in response to drought in the selected varieties. Mean values of variation of PIPs transcript abundance, *Lp*r, *Lp*r_Inh, *Sr* and *Sr*_Inh obtained after water treatment of drought-stressed plants were used for Principal Component Analysis (PCA). The contribution of each PCA axis (PC1 and PC2) is indicated on the graph.

SD ($p < 0.05$), and RD and MD ($p < 0.05$) under well-watered conditions and drought stress at both sectioning locations (Tables S8–S11). The variability in cortical cell diameter (CCD) among varieties and soil moisture treatments was low at both sectioning locations ($p = 0.12$ at 1.5 cm and $p = 0.137$ at 5 cm; Table 4), and no correlations among CCD, RD, SD and MD were observed (Tables S8–S11). At 1.5 cm, the aerenchyma formation (Ae) varied among varieties ($p < 0.01$) and was higher in roots grown under drought stress compared to roots grown under well-watered conditions at 1.5 cm (Table 4). At 5 cm, no significant differences in Ae were observed among varieties and between soil moisture treatments ($p = 0.567$).

Correlation analyses were also performed among *Lp*r, *Lp*r_Inh, *Sr*, *Sr*_Inh and all measured root anatomical parameters in order to better understand the relationship between root anatomy and root hydraulics. The analysis revealed that *Sr* was significantly positively correlated with SD ($p < 0.05$) and MD ($p < 0.05$) under well-watered conditions at both distances from the root apex (Tables S8 and S10). Under drought stress, the correlation between the stele characteristics and *Sr* remained positive but became less evident, with significant correlations only between *Sr* and MD at 1.5 cm ($p < 0.05$; Tables S9 and S11). This analysis also revealed significant positive correlations between *Lp*r and the percentage of cortical aerenchyma ($p < 0.05$) under well-watered conditions at 1.5 cm only (Table S8). No clear correlations were observed between hydraulic properties and visual observations of suberization profiles under both well-watered and drought stress.

Effect of root aquaporin inhibition on LWP and Tr

To investigate if root aquaporin function can impact leaf hydraulics in rice, we measured the LWP of well-watered and drought stressed plants before and after treatments with 150 mL of water or 4 mM azide for 30 min in Experiment 1. Under well-watered conditions, the LWP measured after water or azide treatment was similar to the LWP measured before treatment in Azucena, Moroberekan and Swarna (Fig. 6a). In FR13 A, Dular and IR64, treatment with water or azide induced an increase (less negative) of LWP in the well-watered plants, which was less marked after azide treatment in FR13 A and IR64 compared to that induced by water. Under drought stress, LWP was significantly increased (less negative) in all varieties after water treatment, whereas the recovery in LWP after azide

Table 4. Root anatomical traits of selected rice varieties. Nodal roots from Experiment 1 were sampled, washed and hand-sectioned at 1.5 cm and 5 cm from the root apex for imaging. Images were used for measuring root diameter (RD), cortical cell diameter (CCD), percentage of cortical aerenchyma (Ae), stele diameter (SD) and metaxylem diameter (MD) per nodal root segment and per variety. Letters indicate different significance groups at each distance from the root apex

Variety	Soil moisture	RD		CCD		Ae		SD		MD	
		μm		μm		%		μm		μm	
		1.5 cm	5 cm	1.5 cm	5 cm	1.5 cm	5 cm	1.5 cm	5 cm	1.5 cm	5 cm
Azucena	WW	1090 ± 35a	1059 ± 27a	80 ± 2abc	116 ± 16abc	7 ± 3efg	40 ± 7ab	271 ± 14a	268 ± 5ab	53 ± 1a	57 ± 1a
	DS	608 ± 109def	733 ± 107c	98 ± 41abc	68 ± 1c	33 ± 6a	38 ± 4ab	196 ± 30bcd	236 ± 22bcd	38 ± 3cd	43 ± 0.2bcde
Moroberekan	WW	986 ± 122a	953 ± 108ab	64 ± 3c	87 ± 8bc	4 ± 0.4fg	33 ± 2ab	249 ± 35ab	250 ± 32bc	51 ± 7ab	51 ± 5ab
	DS	760 ± 90bcd	848 ± 18bc	77 ± 12bc	93 ± 10bc	28 ± 8ab	35 ± 2ab	269 ± 43a	315 ± 40a	41 ± 5bc	50 ± 5abc
FR13 A	WW	922 ± 44ab	993 ± 46ab	83 ± 7abc	97 ± 6bc	12 ± 2def	37 ± 5ab	194 ± 8bcd	212 ± 14bcde	38 ± 1cd	42 ± 1cde
	DS	677 ± 81cde	691 ± 59c	79 ± 11bc	165 ± 41a	14 ± 2cde	32 ± 4ab	179 ± 19cd	196 ± 5cde	34 ± 3cd	35 ± 1ef
Dular	WW	1020 ± 47a	1012 ± 43ab	76 ± 5bc	107 ± 14abc	2 ± 1g	37 ± 7ab	229 ± 5abc	224 ± 8bcd	41 ± 1c	44 ± 2bcd
	DS	646 ± 49def	648 ± 71cd	118 ± 2a	92 ± 14bc	26 ± 1ab	45 ± 1a	191 ± 13bcd	198 ± 24cde	38 ± 3cd	42 ± 6cde
IR64	WW	901 ± 78abc	853 ± 23bc	71 ± 4bc	78 ± 1bc	1 ± 0g	30 ± 1ab	177 ± 13cd	176 ± 8def	39 ± 3cd	40 ± 1cdef
	DS	455 ± 57f	511 ± 65d	98 ± 17ab	152 ± 33ab	19 ± 3bcd	30 ± 3ab	143 ± 12d	157 ± 9ef	30 ± 1d	35 ± 2ef
Swarna	WW	776 ± 14bcd	777 ± 7c	74 ± 4bc	90 ± 16bc	3 ± 2fg	29 ± 4b	163 ± 4d	164 ± 3ef	34 ± 1cd	38 ± 1def
	DS	508 ± 72ef	472 ± 82d	113 ± 15a	147 ± 37ab	24 ± 2abc	32 ± 5ab	140 ± 21d	132 ± 21f	33 ± 5cd	32 ± 3f

treatment under drought was partly or completely eliminated in FR13 A, Dular, IR64, Swarna and Azucena (Fig. 6b). By contrast, azide treatment did not affect the recovery of LWP after drought stress in Moroberekan.

Using a similar approach, we investigated the effects of root aquaporin inhibition on transpiration 2 h after treating well-watered and drought-stressed plants with 150 mL of water or 4 mM azide solution in Experiment 4 (Table 5). Under well-watered conditions, around 2-fold variation in *T*r was observed among varieties with 2.99 ± 0.40 g_{water} h^{-1} cm_{leaf}^{-2} in IR64 and 6.19 ± 0.51 g_{water} h^{-1} cm_{leaf}^{-2} in Azucena after water treatment. Compared to the well-watered conditions, *T*r under drought stress was significantly reduced by 1.3 to 1.9-fold in Moroberekan, IR64, Dular and Azucena, and remained similar in FR13 A and Swarna. Azide treatment to well-watered plants induced no or low *T*r inhibition (*T*r_Inh) in FR13 A and Moroberekan, and moderate *T*r_Inh (24 to 39%) in Azucena, Dular, IR64 and Swarna with little significant differences among varieties because of the variability in the measurement. Drought stress did not induce significant changes in *T*r_inh compared to the well-watered conditions, except in Moroberekan and FR13 A where it was significantly increased.

Pearson's correlation test was performed using values of *Lp*r, *Lp*r_Inh, *S*r, *S*r_Inh, LWP, *T*r and *T*r_Inh obtained after water treatment under well-watered and drought stress conditions (Table S12). Under well-watered conditions, *Lp*r was negatively but non-significantly correlated with *T*r_Inh ($p = 0.0885$; Fig. 7a), whereas under drought stress the correlation between these two parameters was positive and significant (Fig. 7b; $p < 0.05$). Non-significant positive correlations were also observed between *S*r and *T*r_inh ($p = 0.0951$), and *S*r and LWP ($p = 0.0937$) under drought stress (Table S12).

Chromosomal regions correlated with hydraulics and plant water use related traits

To correlate hydraulic traits with genomic regions, Experiments 5 and 6 were conducted using the 20 varieties of the OryzaSNP panel in which *S*r and *T*r were measured under well-watered conditions in the presence of water or azide (Table S13). Significant differences in *S*r and *T*r values were observed after water or azide treatments ($p < 0.001$ in both cases). *S*r_Inh showed significant variation among varieties ($p < 0.05$), while *T*r_Inh values showed that *T*r was either increased (negative values) or inhibited (positive values) by azide application, although non significantly ($p = 0.058$). After water treatment, positive correlations were observed between *S*r and *S*r_Inh ($p < 0.05$; Figure S7A), and between *T*r and *T*r_Inh, respectively ($p < 0.01$; Figure S7B). Furthermore, to determine if genetic regions correlated with hydraulic traits would align with plant water use related traits, Experiment 7 was conducted in field conditions, where significant differences among varieties were measured for *S*r_DS ($p < 0.01$), canopy temperature (CT; $p < 0.001$) and shoot dry weight reduction (SDW reduction; $p < 0.001$). Large variation in drought response index

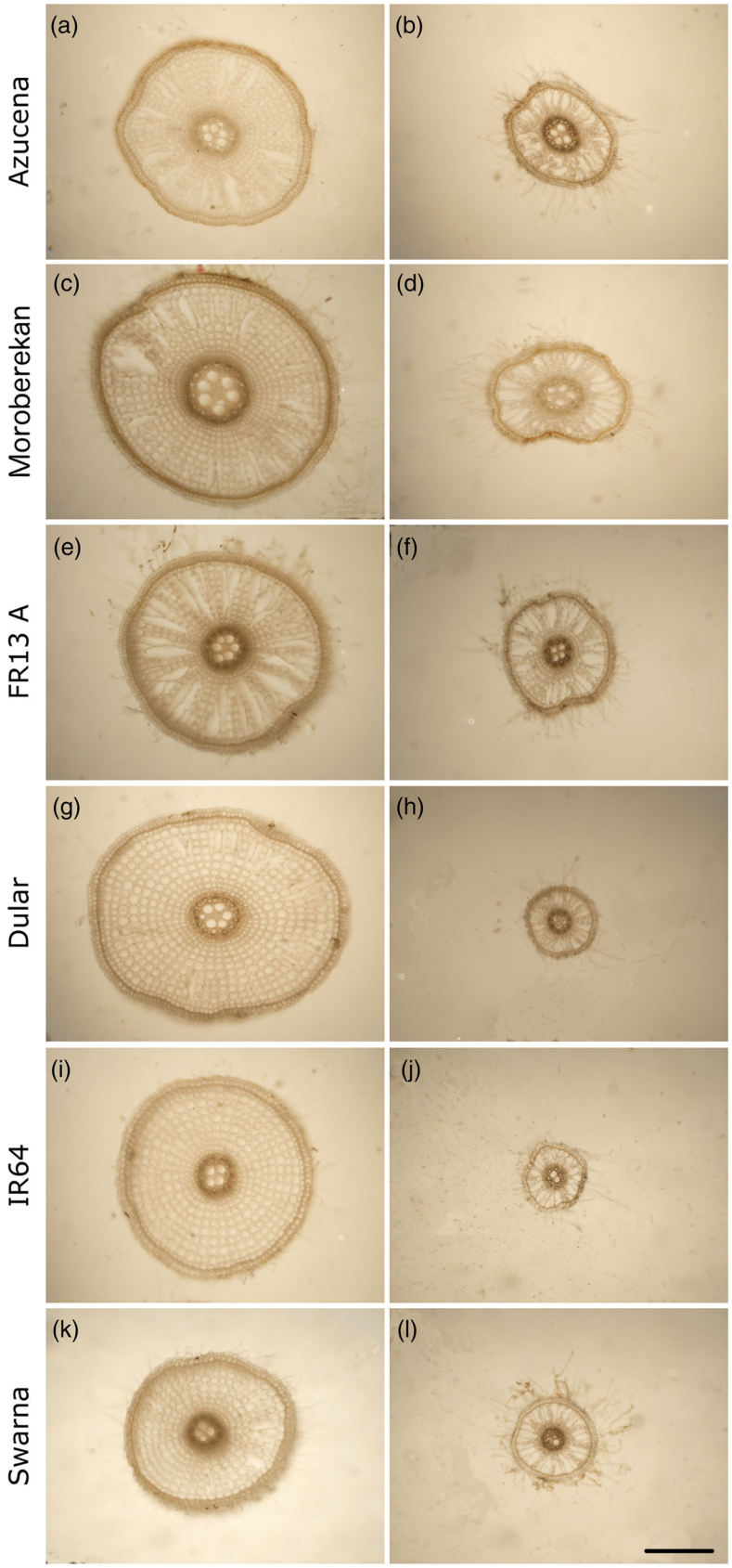

Figure 5. Root anatomy of Azucena, Moroberekan, FR13 A, Dular, IR64 and Swarna. Representative images from cross sections of nodal roots at 1.5 cm from the root apex of plants grown under well-watered conditions (a, c, e, g, i and k and drought stress (b, d, f, h, j and l) in Experiment 1 are shown. The bar represents 400 μm.

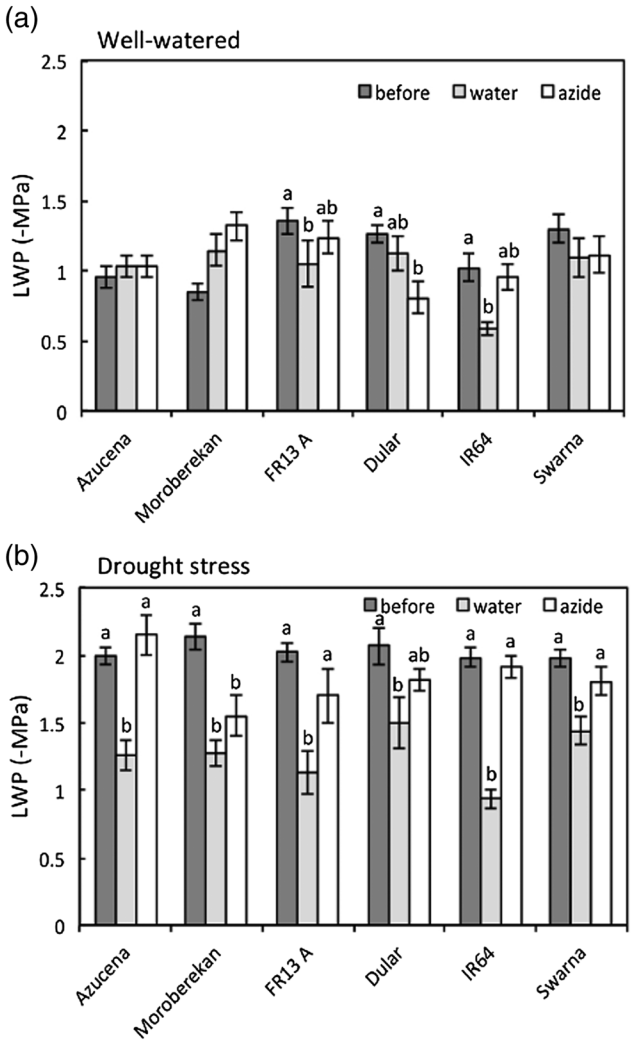

Figure 6. Effect of *Lp*r inhibition on leaf water potential (LWP) in six selected rice varieties. LWP was measured in Experiment 1 on leaves grown under well-watered conditions (a) or drought stress (b). Measurements were performed before and after treatment with water or azide solution (4 mM) for 30 min. Bars represent mean values ± se of $n = 30$ (before) or $n = 15$ (water, azide) replicates. Letters indicate different significance groups between treatments for a particular variety.

(DRI) with values from −0.94 in Swarna to 1.81 in Dular were also observed.

Introgression block regression analysis of data from Experiments 5, 6 and 7, along with published data of water uptake on the 20 OryzaSNP varieties reported by Gowda *et al.* (2012) and Henry *et al.* (2011), resulted in identification of 177 significantly correlated genome regions. To further increase the confidence level of the introgressions, three regions where introgression for at least three different traits overlapped were selected (Fig. 8a); (1) region 1 on chromosome 1 (Chr01) from 8.6 to 9.3 Mb with introgressed segments correlated with *S*r_Inh (indica-type), *T*r (indica-type) and CT (aus-type); (2) region 2 on chromosome 6 (Chr06) from 5.8 to 7.9 Mb with introgressed segments correlated with *S*r_Inh (aus-type), TWU (aus-type) and CT (aus-type); (3) region 3 on chromosome 12 (Chr12) from 12.4 to 14.5 Mb with introgressed segments correlated with VSM (japonica-type), *T*r (aus-type), TWU/TRL (aus-type) and *S*r_Inh (aus-type). Gene annotation in these regions (based on the Nipponbare reference genome) showed that region 1 and 2 are relatively rich in expressed proteins (76% and 78% of the total number of genes, respectively), while region 3 is mostly composed of retrotransposons and transposons (58% of the total; Fig. 8b). No aquaporin genes were annotated in these regions, except in region 2 where a silicon influx transporter belonging to the Nodulin-26 like aquaporin subfamily (Lsi6/NIP2-2; Os06g0228200) was identified.

DISCUSSION

Based on the high degree of aquaporin inhibition observed, this study suggests that aquaporins can largely contribute to rice root hydrostatic and osmotic water fluxes under well-watered conditions, under drought stress and during the recovery of whole-plant water fluxes following drought stress. The analysis of PIP expression in rice roots highlights the possible role of specific PIPs in these processes, such as PIP2;4, PIP2;6 or PIP2;8. Structural parameters of rice roots such as cortical aerenchyma and stele diameter were also observed to affect root water fluxes.

Contribution of aquaporins to rice root hydraulics

We observed substantial variation in *Lp*r (1.9-fold under well-watered conditions and 2.7-fold drought stress) and *S*r (2.1-fold under well-watered conditions and 1.6-fold under drought stress) among rice varieties, which could be respectively inhibited up to 85% in FR13 A and 97% in Azucena under drought stress. Because the percentage of inhibition of *Lp*r or *S*r by azide can be interpreted as a reflection of the contribution of aquaporins to these processes, these results indicate that aquaporins are functional and can contribute to root water fluxes under well-watered conditions and drought stress in some rice varieties. The larger contribution of apoplastic water flow compared to aquaporin-dependent water flow that was previously reported (Ranathunge *et al.* 2004) may be a consequence of different aquaporin functional roles predominating at different parts of the root radial cross-section. This assumption is supported by the higher level of accumulation of some PIPs in the endodermis compared to other root cells (Sakurai *et al.* 2008). However, although aquaporins showed an important role in rice root function, *T*r was not or only slightly affected by azide application under well-watered conditions and upon re-watering after a period of drought. This suggests that the aquaporin-dependent path can contribute but is not limiting to root hydrostatic water fluxes, and confirms that the apoplastic path is dominant under these conditions (Steudle 2000).

Because osmotic gradients within the roots can determine their exudation capacity (Javot & Maurel 2002), the sap exudation rate (*S*r; also termed 'bleeding rate') can be considered as a result of osmotically driven water fluxes that involve the transcellular water pathway. The systematic

Table 5. Transpiration rate (*Tr*) and inhibition by azide of selected rice varieties. Transpiration rate was calculated in Experiment 4 as the cumulative water loss 2 h after rewatering plants grown under well-watered conditions (WW) or drought stress (DS) with water or azide solution (4 mM). *Tr*_Inh: Relative *Tr* inhibition. Mean ± se of $n = 5$–8 plants are presented. Letters indicate different significance groups in the water or azide treatments

		Water treatment	Azide treatment	
		10^{-2}	10^{-2}	*Tr*_Inh
Variety	Soil moisture	$g_{water}\ h^{-1}\ cm^{-2}{}_{leaf}$	$g_{water}\ h^{-1}\ cm^{-2}{}_{leaf}$	%
Azucena	WW	6.19 ± 0.51a	4.69 ± 0.58a	24 ± 9abc
	DS	3.24 ± 0.25ef	2.26 ± 0.24d	30 ± 7a
Moroberekan	WW	4.54 ± 0.39bcd	4.41 ± 0.49ab	3 ± 11bc
	DS	3.34 ± 0.47ef	2.17 ± 0.13d	35 ± 4a
FR13 A	WW	4.11 ± 0.52cdef	4.20 ± 0.65ab	−2 ± 16c
	DS	4.26 ± 0.30cde	2.69 ± 0.24cd	37 ± 6a
Dular	WW	5.65 ± 0.65ab	3.46 ± 0.63bcd	39 ± 11a
	DS	3.51 ± 0.38def	2.35 ± 0.22cd	28 ± 5ab
IR64	WW	4.65 ± 0.31bcd	3.52 ± 0.30abcd	24 ± 7abc
	DS	2.99 ± 0.40f	2.38 ± 0.12cd	20 ± 4abc
Swarna	WW	4.89 ± 0.46abc	3.58 ± 0.17abc	27 ± 4ab
	DS	4.38 ± 0.55cde	2.74 ± 0.30cd	37 ± 7a

reduction in *S*r after azide application in all varieties (Table 3) corroborates this hypothesis and demonstrates the contribution of aquaporins to root osmotic conductivity in rice. Furthermore, after a drought period, the contribution of aquaporins to *S*r was significantly increased in all varieties except in Dular. However, *S*r could also be affected by substantial variation in the osmotic pressure of the xylem sap, or by other unknown mechanisms contributing to root pressure (Wegner 2014). Thus, the relative *S*r inhibition by azide measured in this study may not strictly reflect the function of aquaporins in osmotic water fluxes and may be considered as an "apparent" aquaporin contribution only, which may explain the lack of correlation between *S*r and *Lp*r. Regardless of these considerations, by showing an increase in the aquaporin-dependent osmotic water path under drought stress, our data support a role for root aquaporins in responding to drought stress and restoring root water fluxes upon rewatering. These observations are in line with previous observations showing a role for aquaporins under water limited conditions in tobacco (*Nicotiana tabacum*) and Arabidopsis (*Arabidopsis thaliana*; Martre *et al.* 2002; Siefritz *et al.* 2002). Altogether, our data suggest an increased role for aquaporins in the modulation of rice root osmotic water fluxes under drought stress compared with well-watered conditions.

Our pharmacological approach to aquaporin inhibition using soil-grown roots involved rewatering before the measurement and treatment with an inhibitor that would effectively access the root without being absorbed by soil particles or compounds. Azide, which induces intracellular acidosis by blocking respiration via the cytochrome pathway leading to the H^+-dependent closure of PIPs (Tournaire-Roux *et al.* 2003; Törnroth-Horsefield *et al.* 2006; Verdoucq *et al.* 2008; Sutka *et al.* 2011), is a commonly-used aquaporin inhibitor (Zhang & Tyerman 1991; Kamaluddin & Zwiazek 2001; Tournaire-Roux *et al.* 2003; Postaire *et al.* 2010; Sutka *et al.* 2011). Because complete time-dependent reversible inhibitory effects of azide have been observed in Arabidopsis upon stopping the treatment by washing (Tournaire-Roux *et al.* 2003; Postaire *et al.* 2010), azide is generally considered to be less toxic than mercuric chloride, another common aquaporin inhibitor. In this study, azide successfully induced significant reduction of rice *Lp*r after 30 min of application with reversible effects after 60 min (Figure S3, Table 2). However, as a respiratory inhibitor, azide also induces rapid reduction in cell metabolism and membrane depolarization (Reid *et al.* 1985). Therefore, changes in osmotic pressure gradients, especially during the *S*r measurements in this study, might have caused non-specific side effects on sap exudation that could have introduced an overestimation of the contribution of PIP aquaporins.

Functional determinants of root hydraulics

For further insight into the determinants of rice root hydraulics, we looked for correlation between hydraulic traits and PIP relative transcript abundance in six selected varieties. Under well-watered conditions, *S*r was generally positively correlated with the overall PIP transcript abundance, especially with *PIP2;4* and *PIP2;8* (Table S4). These results suggest a specificity of these two isoforms as major contributors to osmotic water fluxes in rice, which could be particularly limiting under drought stress or during drought recovery. The correlation analyses also revealed that the induction of *PIP2;6* was particularly important in maintaining osmotic water fluxes (Table S6). *Lp*r and its relative inhibition by azide were generally negatively correlated with PIP transcript abundance under well-watered conditions and to a lesser extent under drought stress (Fig. 3a,b and Tables S4 and S5). This surprising relationship was also observed in Arabidopsis in which *Lp*r and *Lp*r_Inh were negatively correlated with transcript abundance of *AtPIP2;6* and *AtPIP2;8* (Sutka *et al.* 2011). An increase in *Lp*r and aquaporin transcript abundance was previously observed in rice within 1 to 2 h after the beginning of the light

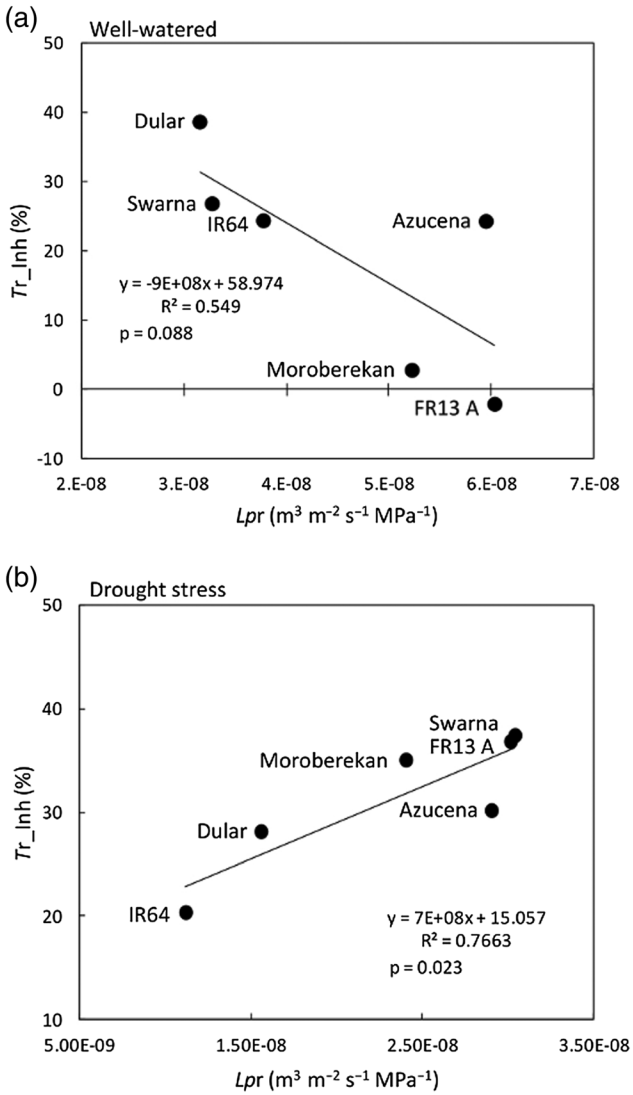

Figure 7. Correlation between *Lp*r and *T*r_Inh in the selected varieties. Mean values of *Lp*r from water-treated plants and *T*r_Inh by azide for each variety measured in Experiments 1 and 4, respectively, under well-watered conditions (a) or drought stress (b) are presented (see Tables 2, 5 and S12).

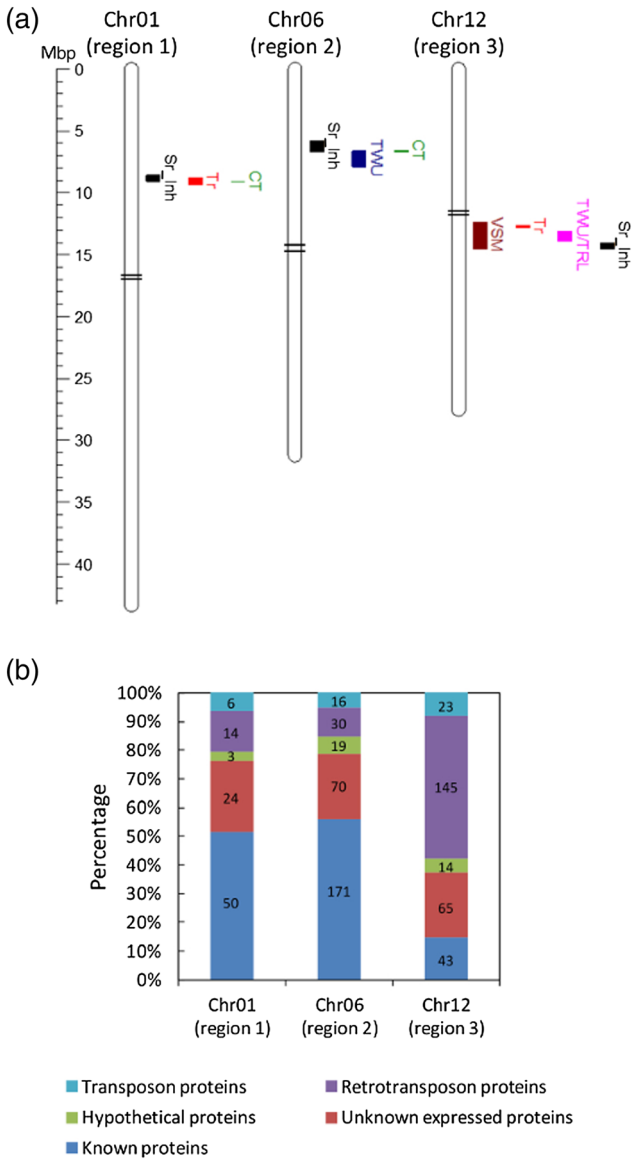

Figure 8. Chromosomal segments correlated with hydraulic and plant water use related traits. (a) Chromosome map representing genomic regions identified by introgression block regression analysis aligning for at least three different traits on chromosome 1 (Chr01), chromosome 6 (Chr06) and chromosome 12 (Chr12). Region 1 on Chr01 is located from 8.6 to 9.3 Mb and shows introgressed segments correlated with *Sr*_Inh (indica-type, p = 0.00227), *Tr* (indica-type, p = 0.00237) and CT (aus-type, p = 0.0048). Region 2 on Chr06 is located from 5.8 to 7.9 Mb and show introgressed segments correlated with *Sr*_Inh (aus-type, p = 0.00128), TWU (aus-type, p = 0.00338) and CT (aus-type, p = 0.004); Region 3 Chr12 is located from 12.4 to 14.5 Mb and show introgressed segments correlated with VSM (japonica-type, p = 0.00431), *Tr* (aus-type, p = 0.0009), TWU/TRL (aus-type, p = 0.00032) and *Sr*_Inh (aus-type, p = 0.0039). *Sr*_Inh: relative sap exudation inhibition; *Tr*: transpiration rate; CT: canopy temperature; TWU: total water uptake; VSM: volumetric soil moisture; TWU/TRL: total water uptake per total root length. (b) Gene content within the three regions based on percentage of genes belonging to different gene classes (based on the Nipponbare reference genome). Regions 1, 2 and 3 contain 97, 306 and 290 annotated elements respectively. The numbers of genes belonging to each class are presented on the graph.

period, followed by a gradual decrease during the day (Sakurai-Ishikawa *et al.* 2011). Furthermore, a stronger reduction of PIP transcript abundance at mid-day was observed under drought stress compared to well-watered conditions (Henry *et al.* 2012). To limit this time of day effect, *Lp*r and PIP transcript abundance were measured at a specific time in this study. However, gradual PIP downregulation may explain negative correlations observed between *Lp*r and PIP transcript abundance, and further investigation of PIP expression over the course of the day in the 6 selected varieties under well-watered and drought stress conditions is needed. Although the physiological relevance of such relationships is still unclear, these results might also be explained by multiple post-translational modifications that can affect plant aquaporins (Li *et al.* 2014), implying that expression level and translation

might not be strictly related to aquaporin function. The importance of drought-induced post-translational modification of rice root aquaporins is also supported by the fact that the contribution of aquaporins to *Lp*r was differentially affected by drought in different varieties, and that no clear correlations were observed between the modulation of PIP transcript abundance and the relative aquaporin contribution to *Lp*r (i.e. *Lp*r_Inh) under drought. The concept of post-translational modification regulating aquaporin activity or localization is further supported by the identification of rice aquaporin phosphorylation sites (Whiteman *et al.* 2008; Li *et al.* 2014).

Our results showing unchanged or decreased PIP transcript abundance by drought depending on the variety is somewhat different to what was reported previously in hydroponics using PEG (Guo *et al.* 2006; Lian *et al.* 2006), and might be explained by the time of sampling, the growth conditions and the severity of the stress applied. Interestingly, we observed that the transcript abundance of certain PIPs was strongly correlated with the transcript abundance of others (Tables S4 and S5), and that some PIPs showed significant co-variation in response to drought (Table S6). This behaviour might reflect co-functionalities among aquaporins for heterotetramer formation, for instance (Fetter *et al.* 2004; Zelazny *et al.* 2007).

Structural determinants of root hydraulics

Aerenchyma formation in rice is not limited to hypoxic conditions and is also observed under aerated conditions (Jackson & Armstrong 1999). Our data obtained in soil conditions, in which a higher level of aerenchyma formation was observed in dry soil compared to well-watered conditions at 1.5 cm but not at 5 cm from the root apex, likely reflects differences in root growth rate between the well-watered and drought stress treatments. Therefore, better growth in the well-watered treatment may not yet have resulted in aerenchyma formation at the same distance from the apex as in the drought stress treatment. A positive correlation between *Lp*r and the percentage of root cortical aerenchyma was observed under well-watered conditions at 1.5 cm from the root apex but not at 5 cm or under drought stress (Tables 4, and S8–S11). Hypoxia is known to induce an acidification of root cell cytoplasm which induces the blockage of PIPs that can account for a reduction in *Lp*r (Tournaire-Roux *et al.* 2003). Although aerenchyma are typically assumed to reduce radial water flow, aerenchyma formation in the region close to the root apex, by maintaining root oxygenation, might indirectly contribute to maintaining *Lp*r by reducing cytoplasm acidification and PIP inhibition, particularly under flooded conditions. Aerenchyma could therefore have dual roles in root water fluxes, to which further investigation is needed. These results may also suggest variable water fluxes along the root axis, highlighting the importance of regions close to the root apex for water uptake. In addition to this, the observation that *S*r was significantly positively correlated with SD and MD, particularly under well-watered conditions (Tables S8–S10), supports the idea that root anatomical properties affect rice root hydraulics.

Root–shoot hydraulic interactions for drought tolerance

The role of aquaporins in hydraulic interactions between roots and shoots has been emphasized in several species (Maurel *et al.* 2010). For instance, modulation of maize *Lp*r using aquaporin inhibitors induced a decrease in cell turgor in the leaf elongation zone followed by a decrease in the leaf elongation rate (Ehlert *et al.* 2009). We observed that in drought-stressed plants, unlike those treated with azide, plants treated with water showed partial to complete LWP recovery (Fig. 6), suggesting that root water fluxes mediated by aquaporins play an important role in root–shoot water fluxes for LWP recovery after drought stress. This hypothesis is supported by a positive, although not significant, correlation between LWP recovery and *S*r under drought stress ($p = 0.0937$; Table S12). A similar role of root aquaporins has been suggested in transgenic lowland rice overexpressing *RWC3* (*PIP1*;*3*), which exhibited higher root osmotic hydraulic conductivity, LWP and cumulative transpiration after a period of 10 h of PEG treatment (Lian *et al.* 2004). Here, we observed that *T*r recovery was more dependent on aquaporin function after drought stress than under well-watered conditions (Table 5). We also observed that *T*r was significantly positively correlated with *T*r_Inh (Table S12), and plants showing an activation of *T*r by azide generally showed low *T*r. These results suggest an isohydric-type behaviour in rice varieties with activated *T*r that was eliminated after azide application, indicating linkages between rice plant water-balance strategies and aquaporin function in roots. Therefore the down-regulation of aquaporins may even contribute to drought tolerance in some varieties by allowing the plant to adopt a conservative strategy to maintain water fluxes and transpiration during drought stress.

Manipulating plant aquaporins in order to increase crop yield under irrigated and drought stress conditions has been addressed in several studies but with no major progress, and a better molecular understanding of the role of specific PIPs and how the plants regulate their water balance and water use efficiency, especially under drought stress conditions, is still needed (Moshelion *et al.* 2014). In this study for instance, it does not appear clearly that drought tolerance in rice is associated with high *Lp*r and *S*r. Indeed, Azucena and Moroberekan (mildly drought tolerant), but also FR13 A and Swarna (drought susceptible) showed highest *Lp*r and *S*r under drought stress, suggesting that other functional properties could be more related to grain yield under drought. Only in tomato (*Solanum lycopersicum*), the overexpression of a tonoplast aquaporin (*Si*TIP2;2) induced higher transpiration and significant increase in plant yield, harvest index and plant mass relative to the non-transgenic plants under well-watered and drought conditions (Sade *et al.* 2009). Because the OryzaSNP panel is a small set of genotypes that provides possibilities for testing genetic correlations with

phenotypic components, it is a very useful tool to relate functional traits that are relatively complex to measure with genomic regions by introgression block regression analysis (Jahn *et al.* 2011; Wade *et al.* 2015). Here, three genomic segments showing correlation with both root water uptake (*S*r_Inh, TWU, TWU/TRL and VSM) and shoot performance (*T*r and CT) were identified (Fig. 8a), which support our observations of the hydraulic interactions between roots and shoots. These segments are mostly from aus-type introgressions, which is a subgroup with characteristically more drought tolerance compared to indica- and japonica-type varieties (Glaszmann 1987). Although our study provides evidence that aquaporins are key determinants of root water fluxes in rice, no aquaporins with known water transport activity were identified in these regions (based on the Nipponbare reference genome). The absence of co-location of aquaporin genes likely reflects the complexity of root water fluxes. Modulation of water uptake to sustain shoot function under drought requires coordination of processes that are likely under the control of aquaporin-regulatory genes. Regions 1 and 2 in particular contain a number of stress-related genes such as zinc-finger proteins that could be involved (Sugano *et al.* 2003; Mukhopadhyay *et al.* 2004; Maruyama *et al.* 2012; Jan *et al.* 2013). In addition to being influenced by aquaporin expression, localization, or activity, root hydraulics also appear to depend on environmental and plant characteristics, including soil moisture, root anatomy, osmotic gradients and leaf water status.

CONCLUSIONS

Root water fluxes in rice, as in many species, were not observed to be strictly determined by the function of aquaporins, but we observed that the physiological role of these proteins became more important under drought stress. Our results suggest that rice root aquaporins can contribute but are not limiting to hydrostatic water fluxes when transpiration is high, and that they play a major role in osmotic water fluxes occurring when transpiration is low. Differences in root water fluxes were related to differences in aquaporin function, particularly for some PIP isoforms. The large genetic diversity observed among rice varieties for aquaporin expression, hydraulic properties and root anatomy, as well as the three genetic regions correlated with multiple hydraulic traits that have been identified, indicate the potential for improvement of rice water fluxes under drought. More research is necessary to pinpoint specifically how modulation of root water fluxes should be improved in order to increase the drought tolerance of rice.

ACKNOWLEDGEMENTS

This work was funded by the Generation Challenge Programme project G3008.06 'Targeting Drought-Avoidance Root Traits to Enhance Rice Productivity under Water-Limited Environments'. We thank D. Morales, L. Satioquia, A. Reyes, E. Mateo, P. Zambrano, A. Oxina, A. Los Años, E. Mico, M. Natividad, N. Sadiasa, M. Quintana, N. Turingan, C. L. Cabral and R. Torres from the IRRI Drought physiology group for technical support. At IRRI, we are also grateful to Dr. I. H. Slamet-Loedin, Dr. N. Tsakirpaloglou and Dr. K. R. Trijatmiko for their support and advice on the RT-PCR experiment, to J. Detras for support with the Map Chart software, to V. Juanillas for support on IRRI-GSL-Galaxy analysis, to V. Bartolome for statistical support and to Dr. A. Ismail for helpful comments on the manuscript. At ICRISAT, we thank Dr. J. Kholova, S. Mallayee and M. Anjaiah for useful discussions and help in transpiration measurements, and A. C. Pandey for assistance in plant culture.

REFERENCES

Abramoff M.D., Magalhaes P.J. & Ram S.J. (2004) Image processing with ImageJ. *Biophotonics International* **11**, 36–42.

Ahamed A., Murai-Hatano M., Ishikawa-Sakurai J., Hayashi H., Kawamura Y. & Uemura M. (2012) Cold stress-induced acclimation in rice is mediated by root-specific aquaporins. *Plant & Cell Physiology* **53**, 1445–1456.

Bidinger F., Mahalakshmi V. & Rao G. (1987) Assessment of drought resistance in pearl millet (*Pennisetum americanum* (*L.*) *Leeke*). II. Estimation of genotype response to stress. *Australian Journal of Agricultural Research* **38**, 49–59.

Ehlert C., Maurel C., Tardieu F. & Simonneau T. (2009) Aquaporin-mediated reduction in maize root hydraulic conductivity impacts cell turgor and leaf elongation even without changing transpiration. *Plant Physiology* **150**, 1093–1104.

Fetter K., Van Wilder V., Moshelion M. & Chaumont F. (2004) Interactions between plasma membrane aquaporins modulate their water channel activity. *The Plant Cell* **16**, 215–228.

Fiscus E.L. (1986) Diurnal changes in volume and solute transport coefficients of phaseolus roots. *Plant Physiology* **80**, 752–759.

Glaszmann J.C. (1987) Isozymes and classification of Asian rice varieties. *Theoretical and Applied Genetics* **74**, 21–30.

Gowda V.R.P., Henry A., Vadez V., Shashidhar H.E. & Serraj R. (2012) Water uptake dynamics under progressive drought stress in diverse accessions of the OryzaSNP panel of rice (*Oryza sativa*). *Functional Plant Biology* **39**, 402–411.

Gowda V.R.P., Henry A., Yamauchi A., Shashidhar H.E. & Serraj R. (2011) Root biology and genetic improvement for drought avoidance in rice. *Field Crops Research* **122**, 1–13.

Guo L., Wang Z.Y., Lin H., Cui W.E., Chen J., Liu M., … Gu H. (2006) Expression and functional analysis of the rice plasma-membrane intrinsic protein gene family. *Cell Research* **16**, 277–286.

Henry A., Cal A.J., Batoto T.C., Torres R.O. & Serraj R. (2012) Root attributes affecting water uptake of rice (*Oryza sativa*) under drought. *Journal of Experimental Botany* **63**, 4751–4763.

Henry A., Gowda V.R.P., Torres R.O., McNally K.L. & Serraj R. (2011) Variation in root system architecture and drought response in rice (*Oryza sativa*): phenotyping of the OryzaSNP panel in rainfed lowland fields. *Field Crops Research* **120**, 205–214.

Jackson M.B. & Armstrong W. (1999) Formation of aerenchyma and the processes of plant ventilation in relation to soil flooding and submergence. *Plant Biology* **1**, 274–287.

Jahn C.E., Mckay J.K., Mauleon R., Stephens J., McNally K.L., Bush D.R., … Leach J.E. (2011) Genetic variation in biomass traits among 20 diverse rice varieties. *Plant Physiology* **155**, 157–168.

Jan A., Maruyama K., Todaka D., Kidokoro S., Abo M., Yoshimura E., … Yamaguchi-Shinozaki K. (2013) OsTZF1, a CCCH-tandem zinc finger protein, confers delayed senescence and stress tolerance in rice by regulating stress-related genes. *Plant Physiology* **161**, 1202–1216.

Javot H. & Maurel C. (2002) The role of aquaporins in root water uptake. *Annals of Botany* **90**, 301–313.

Kamaluddin M. & Zwiazek J.J. (2001) Metabolic inhibition of root water flow in red-osier dogwood (*Cornus stolonifera*) seedlings. *Journal of Experimental Botany* **52**, 739–745.

Kamoshita A., Wade L.J. & Yamauchi A. (2000) Genotypic variation in response of rainfed lowland rice to drought and rewatering. III. Water extraction during the drought period. *Plant Production Science* **3**, 189–196.

Katsuhara M., Koshio K., Shibasaka M., Hayashi Y., Hayakawa T. & Kasamo K. (2003) Over-expression of a barley aquaporin increased the shoot/root ratio and raised salt sensitivity in transgenic rice plants. *Plant & Cell Physiology* **44**, 1378–1383.

Kawahara Y., Bastide M.D. Hamilton J.P., Kanamori H., Mccombie W.R., Ouyang S., … Matsumoto T. (2013) Improvement of the *Oryza sativa* Nipponbare reference genome using next generation sequence and optical map data. *Rice* **6**, 1–10.

Kholová J., Hash C.T., Kumar P.L., Yadav R.S., Kocová M. & Vadez V. (2010) Terminal drought-tolerant pearl millet [*Pennisetum glaucum* (*L.*) *R. Br.*] have high leaf ABA and limit transpiration at high vapour pressure deficit. *Journal of Experimental Botany* **61**, 1431–1440.

Kondo M., Murty M.V.R. & Aragones D.V. (2000) Characteristics of root growth and water uptake from soil in upland rice and maize under water stress. *Soil Science and Plant Nutrition* **46**, 721–732.

Li G.-W., Peng Y.H., Yu X., Zhang M.H., Cai W.M., Sun W.N., … Su W.A. (2008) Transport functions and expression analysis of vacuolar membrane aquaporins in response to various stresses in rice. *Journal of Plant Physiology* **165**, 1879–1888.

Li G., Santoni V. & Maurel C. (2014) Plant aquaporins: roles in plant physiology. *Biochimica et Biophysica Acta* **1840**, 1574–1582.

Lian H.L., Yu X., Lane D., Sun W.N., Tang Z.C. & Su W.A. (2006) Upland rice and lowland rice exhibited different PIP expression under water deficit and ABA treatment. *Cell Research* **16**, 651–660.

Lian H.L., Yu X., Ye Q., Ding X., Kitagawa Y., Kwak S.O., … Ding X.S. (2004) The role of aquaporin RWC3 in drought avoidance in rice. *Plant & Cell Physiology* **45**, 481–489.

Liu C., Fukumoto T., Matsumoto T., Gena P., Frascaria D., Kanedo T., … Kitagawa Y. (2013) Aquaporin *Os*PIP1;1 promotes rice salt resistance and seed germination. *Plant Physiology and Biochemistry* **63**, 151–158.

Lu Z. & Neumann P.M. (1999) Water stress inhibits hydraulic conductance and leaf growth in rice seedlings but not the transport of water via mercury-sensitive water channels in the root. *Plant Physiology* **120**, 143–151.

Lynch J.P. (2013) Steep, cheap and deep: an ideotype to optimize water and N acquisition by maize root systems. *Annals of Botany* **112**, 347–357.

Malz S. & Sauter M. (1999) Expression of two PIP genes in rapidly growing internodes of rice is not primarily controlled by meristem activity or cell expansion. *Plant Molecular Biology* **40**, 985–995.

Martre P., Morillon R., Barrieu F., North G.B., Nobel P.S. & Chrispeels M.J. (2002) Plasma membrane aquaporins play a significant role during recovery from water deficit. *Plant Physiology* **130**, 2101–2110.

Maruyama K., Todaka D., Mizoi J., Yoshida T., Kidokoro S., Matsukura S., … Yamaguchi-Shinozaki K. (2012) Identification of cis-acting promoter elements in cold-and dehydration-induced transcriptional pathways in arabidopsis, rice, and soybean. *DNA Research* **19**, 37–49.

Matsuo N., Ozawa K. & Mochizuki T. (2009) Genotypic differences in root hydraulic conductance of rice (*Oryza sativa L.*) in response to water regimes. *Plant and Soil* **316**, 25–34.

Maurel C., Simonneau T. & Sutka M. (2010) The significance of roots as hydraulic rheostats. *Journal of Experimental Botany* **61**, 3191–3198.

McNally K.L., Childs K.L., Bohnert R., Davidson R.M., Zhao K., Ulat V.J., … Leach J.E. (2009) Genomewide SNP variation reveals relationships among landraces and modern varieties of rice. *Proceedings of the National Academy of Sciences of the United States of America* **106**, 12273–12278.

Miyamoto N., Steudle E., Hirasawa T. & Lafitte R. (2001) Hydraulic conductivity of rice roots. *Journal of Experimental Botany* **52**, 1835–1846.

Morita S. & Abe J. (2002) Diurnal and phenological changes of bleeding rate in lowland rice plants. *Japanese Journal of Crop Science* **71**, 383–388.

Moshelion M., Halperin O., Wallach R., Oren R. & Way D. (2014) Role of aquaporins in determining transpiration and photosynthesis in water-stressed plants: crop water-use efficiency, growth and yield. *Plant, Cell & Environment* doi: 10.1111/pce.12410.

Mukhopadhyay A., Vij S. & Tyagi A.K. (2004) Overexpression of a zinc-finger protein gene from rice confers tolerance to cold, dehydration, and salt stress in transgenic tobacco. *Proceedings of the National Academy of Sciences of the United States of America* **101**, 6309–6314.

Nada R.M. & Abogadallah G.M. (2014) Aquaporins are major determinants of water use efficiency of rice plants in the field. *Plant Science: an International Journal of Experimental Plant Biology* **227**, 165–180.

Nguyen M.X., Moon S. & Jung K.-H. (2013) Genome-wide expression analysis of rice aquaporin genes and development of a functional gene network mediated by aquaporin expression in roots. *Planta* **238**, 669–681.

Ouyang S., Zhu W., Hamilton J., Lin H., Campbell M., Childs K., … Buell C.R. (2007) The TIGR rice genome annotation resource: improvements and new features. *Nucleic Acids Research* **35**, D883–D887.

Postaire O., Tournaire-Roux C., Grondin A., Boursiac Y., Morillon R., Shäffner A.R., … Maurel C. (2010) A PIP1 aquaporin contributes to hydrostatic pressure-induced water transport in both the root and rosette of Arabidopsis. *Plant Physiology* **152**, 1418–1430.

Ranathunge K., Kotula L., Steudle E. & Lafitte R. (2004) Water permeability and reflection coefficient of the outer part of young rice roots are differently affected by closure of water channels (aquaporins) or blockage of apoplastic pores. *Journal of Experimental Botany* **55**, 433–447.

Ranathunge K., Steudle E. & Lafitte R. (2003) Control of water uptake by rice (*Oryza sativa L.*): role of the outer part of the root. *Planta* **217**, 193–205.

Reid R.J., Dejaegere R. & Pitman M.G. (1985) Regulation of electrogenic pumping in barley by pH and ATP. *Journal of Experimental Botany* **36**, 535–549.

Rogers E.D. & Benfey P.N. (2015) Regulation of plant root system architecture: implications for crop advancement. *Current Opinion in Biotechnology* **32**, 93–98.

Sade N., Vinocur B.J., Diber A., Shatil A., Ronen G., Nissan H., … Moshelion M. (2009) Improving plant stress tolerance and yield production: is the tonoplast aquaporin *Si*TIP2;2 a key to isohydric to anisohydric conversion? *New Phytologist* **181**, 651–661.

Sakurai-Ishikawa J., Murai-Hatano M., Hayashi H., Ahamed A., Fukushi K., Matsumoto T. & Kitagawa Y. (2011) Transpiration from shoots triggers diurnal changes in root aquaporin expression. *Plant, Cell & Environment* **34**, 1150–1163.

Sakurai J., Ahamed A., Murai M., Maeshima M. & Uemura M. (2008) Tissue and cell-specific localization of rice aquaporins and their water transport activities. *Plant & Cell Physiology* **49**, 30–39.

Sakurai J., Ishikawa F., Yamaguchi T., Uemura M. & Maeshima M. (2005) Identification of 33 rice aquaporin genes and analysis of their expression and function. *Plant & Cell Physiology* **46**, 1568–1577.

Siefritz F., Tyree M.T., Lovisolo C., Schubert A. & Kaldenhoff R. (2002) PIP1 plasma membrane aquaporins in tobacco: from cellular effects to function in plants. *The Plant Cell* **14**, 869–876.

Steudle E. (2000) Water uptake by roots : effects of water deficit. *Journal of Experimental Botany* **51**, 1531–1542.

Sugano S., Kaminaka H., Rybka Z., Catala R., Salinas J., Matsui K., … Takatsuji H. (2003) Stress-responsive zinc finger gene *ZPT2-3* plays a role in drought tolerance in petunia. *The Plant Journal* **36**, 830–841.

Sutka M., Li G., Boudet J., Boursiac Y., Doumas P. & Maurel C. (2011) Natural variation of root hydraulics in Arabidopsis grown in normal and salt-stressed conditions. *Plant Physiology* **155**, 1264–1276.

Törnroth-Horsefield S., Wang Y., Hedfalk K., Johanson U., Karlsson M., Tajkhorshid E., … Kjellbom P. (2006) Structural mechanism of plant aquaporin gating. *Nature* **439**, 688–694.

Tournaire-Roux C., Sutka M., Javot H., Gout E., Gerbeau P., Luu D.T., … Maurel C. (2003) Cytosolic pH regulates root water transport during anoxic stress through gating of aquaporins. *Nature* **425**, 393–397.

Vadez V. (2014) Root hydraulics: the forgotten side of roots in drought adaptation. *Field Crops Research* **165**, 15–24.

Verdoucq L., Grondin A. & Maurel C. (2008) Structure–function analysis of plant aquaporin *At*PIP2;1 gating by divalent cations and protons. *The Biochemical Journal* **415**, 409–416.

Voorrips R.E. (2002) MapChart : software for the graphical presentation of linkage maps and QTLs. *The Journal of Heredity* **93**, 77–78.

Wade L., Bartolome V., Mauleon R., Vasant V., Prabakar S., Chelliah M., … Henry A. (2015) Environmental response and genomic regions correlated with rice root growth and yield under drought in the OryzaSNP panel across multiple study systems. *PLoS One* doi: 10.1371/journal.pone.0124127.

Wegner L.H. (2014) Root pressure and beyond: energetically uphill water transport into xylem vessels? *Journal of Experimental Botany* **65**, 381–393.

Whiteman S.A., Nühse T.S., Ashford D., Sanders D. & Maathuis F.J.M. (2008) A proteomic and phosphoproteomic analysis of *Oryza sativa* plasma membrane and vacuolar membrane. *The Plant Journal* **56**, 146–156.

Zelazny E., Borst J.W., Muylaert M., Batoko H., Hemminga M.A. & Chaumont F. (2007) FRET imaging in living maize cells reveals that plasma membrane aquaporins interact to regulate their subcellular localization. *Proceedings of the National Academy of Sciences of the United States of America* **104**, 12359–12364.

Zhang W.H. & Tyerman S.D. (1991) Effect of low O_2 concentration and azide on hydraulic conductivity and osmotic volume of the cortical cells of wheat roots. *Functional Plant Biology* **18**, 603–613.

Zimmermann H.M., Hartmann K., Schreiber L. & Steudle E. (2000) Chemical composition of apoplastic transport barriers in relation to radial hydraulic conductivity of corn roots (*Zea mays L.*). *Planta* **210**, 302–311.

Received 23 April 2015; accepted for publication 26 July 2015

SUPPORTING INFORMATION

Additional Supporting Information may be found in the online version of this article at the publisher's web-site:

Table S1. Characteristics of the soil used for the experiments in this study, as analyzed by the Analytical Service Laboratory (ASL) at IRRI. Soil characteristics were not available for Experiment 6.

Table S2. Conditions in the growth chamber at the time of transpiration rate measurements. The pots were weighed every hour from 8 AM to 4 PM while the VPD conditions were increasing inside the growth chamber.

Table S3. Table of primers used for RT-PCR. Primer sequences were derived from Sakurai et al. (2005).

Table S4. Correlation between root PIP transcript abundance, root hydraulic properties (Lpr, Sr) and root hydraulic inhibition by azide (Lpr_Inh and Sr_Inh) under well-watered conditions (WW) in six selected rice varieties. Values indicate the Pearson's coefficient of correlation. *: p-values < 0.05; **: p-values < 0.01.

Table S5. Correlation between root PIP transcript abundance, root hydraulic properties (Lpr, Sr) and root hydraulic inhibition by azide (Lpr_Inh and Sr_Inh) under drought stress conditions (DS) in six selected rice varieties. Values indicate the Pearson's coefficient of correlation. *: p-values < 0.05; **: p-values < 0.01.

Table S6. Correlation between root PIP transcript variation under drought, root hydraulic properties (Lpr, Sr) and root hydraulic inhibition by azide (Lpr_Inh and Sr_Inh) under drought stress conditions in six selected rice varieties. Values indicate the Pearson's coefficient of correlation. *: p-values < 0.05; **: p-values < 0.01. ***: p-values < 0.05.

Table S7. Root morphology of six selected rice varieties. Roots of plants grown under well-watered conditions (WW) or drought stress (DS) in Experiment 1 ($) and Experiment 2 (*) were sampled and washed to remove soil residues at 29 and 35 das, respectively. Mean values ± se of n=29-30$ and n=8-12* biological replications are presented. Letters indicate different significant groups in WW or DS soil moisture treatment. No significant differences were observed among varieties for root mass or root:shoot ratio.

Table S8. Correlation between root anatomical traits at 1.5 cm from the root apex, root hydraulic properties (Lpr, Sr) and root hydraulic inhibition by azide (Lpr_Inh and Sr_Inh) under well-watered conditions (WW) in six selected rice varieties. RD: root diameter; CCD: cortex cell diameter; Ae: percent cortical aerenchyma; SD: stele diameter; MD: metaxylem diameter. Values indicate the Pearson's coefficient of correlation.

Table S9. Correlation between root anatomical traits at 1.5 cm from the root apex, root hydraulic properties (Lpr, Sr) and root hydraulic inhibition by azide (Lpr_Inh and Sr_Inh) under well-watered conditions (WW) in six selected rice varieties. RD: root diameter; CCD: cortex cell diameter; Ae: percent cortical aerenchyma; SD: stele diameter; MD: metaxylem diameter. Values indicate the Pearson's coefficient of correlation.

Table S10. Correlation between root anatomical traits at 1.5 cm from the root apex, root hydraulic properties (Lpr, Sr) and root hydraulic inhibition by azide (Lpr_Inh and Sr_Inh) under well-watered conditions (WW) in six selected rice varieties. RD: root diameter; CCD: cortex cell diameter; Ae: percent cortical aerenchyma; SD: stele diameter; MD: metaxylem diameter. Values indicate the Pearson's coefficient of correlation.

Table S11. Correlation between root anatomical traits at 5 cm from the root apex, root hydraulic properties (Lpr, Sr) and root hydraulic inhibition by azide (Lpr_Inh and Sr_Inh) under drought-stress conditions (DS) in six selected rice varieties. RD: root diameter; CCD: cortex cell diameter; Ae: percent cortical aerenchyma; SD: stele diameter; MD: metaxylem diameter. Values indicate the Pearson's coefficient of correlation. *: p-values < 0.05; **: p-values < 0.01.

Table S12. Correlations among root hydraulic properties (Lpr, Sr), root hydraulic inhibition by azide (Lpr_Inh and Sr_Inh), leaf transpiration (Tr), inhibition of transpiration by azide (Tr_Inh) and leaf water potential (LWP) under well-watered conditions and drought stress in six selected rice varieties. LprW, LprW_Inh, SrW, SrW_Inh, TrW, TrW_Inh and LWPW were measured from water-treated plants grown under well-watered conditions. LprD, LprD_Inh, SrD, SrD_Inh, TrD, TrD_Inh and LWPD were measured from water-treated plants grown under drought stress. Values indicate the Pearson's coefficient of correlation. *: p-values < 0.05; **: p-values < 0.01.

Table S13. Data set used for the identification of introgressed chromosome segments correlated with hydraulic and drought tolerance related traits presented in Figure 8. Sr, Sr_inh: Sr and relative Sr inhibition by azide were measured on plants grown under well-watered conditions in Experiment 5. Tr, Tr_inh: cumulative water loss by transpiration 2 hours after rewatering the plants with water normalized by the leaf area, and relative Tr inhibition by azide were measured in Experiment 6; TWU, TWU/TRL: total water uptake and total water uptake per total root length data are from Gowda et al. (2012). VSM: volumetric soil moisture data are from Henry et al. (2011); Sr_DS: Sr normalized by the shoot dry weight measured under drought stress is from Experiment 7 at 82 das. CT: canopy temperature measured under drought stress is from Experiment 7 at 81 das. SDW reduction: reduction in shoot dry weight measured under drought stress compared to shoot dry weight measured under well-watered conditions at maturity (117 das) is from Experiment 7. DRI: drought response index was measured in Experiment 7.

Figure S1. Soil water potential readings during the field experiment. Tensiometers were installed at a depth of 30 cm in Experiment 7. Soil was rewatered at 95 das. Mean values ± se of n=3 tensiometer readings are presented.

Figure S2. Environmental characteristics during Experiment 7. The field experiment was performed during the dry season 2014 at the IRRI farm, Los Baños, Philippines (14° 11'N, 121° 15'E). Weather data are from the IRRI Climate Unit.

Figure S3. Optimization of the *Lpr* inhibition measurement protocol using aquaporin inhibitors. Plants were grown in soil-filled mylar tubes for 29 days under well-watered conditions. (A) Roots were washed to remove soil compounds and placed into water, salt (500 mM; left panel) or azide solution

(4 mM; right panel). (B) Soil was directly rewatered with 150 ml of water, salt (500 mM; left panel) or azide solution (4 mM; right panel). *Lp*r was measured by collecting exuded xylem sap flux after pressurizing the roots after 30 or 60 minutes of water or inhibitor treatments. Bars show mean values ± se of n=2-5 plants. *: p-values < 0.05.

Figure S4. Effect of time of day on *Lp*r and relative *Lp*r inhinibition (*Lp*r_Inh) by azide under well-watered and drought stress conditions. *Lp*r from water-treated plants (A, B) and *Lp*r_Inh (C, D) were measured in Experiment 1 from 7:30 AM to 10:00 AM (early) and from 10:00 AM to 1:00 PM (mid) under well-watered (A, C) and drought stress conditions (B, D). Bars show mean ± se of *n*=3-10 plants. *: p-values < 0.05; **: p-values < 0.01.

Figure S5. Visualization of plasma membrane aquaporin (PIP) amplicons after RT-PCR. cDNA was prepared from roots grown in Experiment 3 under well-watered and drought stress conditions. 20μL of RT-PCR products of PIP1;1 (A), PIP1;2 (B), PIP1;3 (C), PIP2;1 (D), PIP2;2 (E), PIP2;4 (F), PIP2;6 (G) and PIP2;8 (H) together with products of ubiquitin from the three biological replicates per variety amplified in the same RT-PCR run were stained using SYBR® safe DNA (Invitrogen, California, USA) and subjected to agarose gel electrophoresis. The signal intensity of the bands was observed by an Infinity ST5 v16.08a imaging system (Vilber Lourmat, France).

Figure S6. Root anatomy of Azucena, Moroberekan, FR13 A, Dular, IR64 and Swarna. Representative images from cross sections of nodal roots at 5 cm from the root apex of plants grown under well-watered conditions (A, C, E, G, I and K) and drought stress (B, D, F, H, J and L) in Experiment 1 are shown. The bar represents 400 μm.

Figure S7. Correlation of Sr and Tr with their respective level of inhibition by azide under well-watered conditions in the OryzaSNP panel. Positive correlation between *S*r and *S*r_Inh (A) and between *T*r and *T*r_Inh (B) were observed under well-watered conditions in Experiments 5 and 6, respectively (see Table S12).

Journal of Experimental Botany
doi:10.1093/jxb/eraa280 Advance Access Publication 12 June, 2020
This paper is available online free of all access charges (see https://academic.oup.com/jxb/pages/openaccess for further details)

RESEARCH PAPER

Leveraging genome-enabled growth models to study shoot growth responses to water deficit in rice

Malachy T. Campbell[1,2,*], Alexandre Grondin[2,3], Harkamal Walia[2] and Gota Morota[1]

[1] Department of Animal and Poultry Sciences Virginia Polytechnic Institute and State University Blacksburg, VA, USA
[2] Department of Agronomy and Horticulture University of Nebraska-Lincoln, Lincoln, NE, USA
[3] UMR DIADE, Université de Montpellier Institut de Recherche pour le Développement (IRD) Montpellier, France

*Correspondence: campbell.malachy@gmail.com

Received 4 July 2019; Editorial decision 27 May 2020; Accepted 9 June 2020

Editor: Greg Rebetzke, CSIRO Agriculture and Food, Australia

Abstract

Elucidating genotype-by-environment interactions and partitioning its contribution to phenotypic variation remains a challenge for plant scientists. We propose a framework that utilizes genome-wide markers to model genotype-specific shoot growth trajectories as a function of time and soil water availability. A rice diversity panel was phenotyped daily for 21 d using an automated, high-throughput image-based, phenotyping platform that enabled estimation of daily shoot biomass and soil water content. Using these data, we modeled shoot growth as a function of time and soil water content, and were able to determine the time point where an inflection in the growth trajectory occurred. We found that larger, more vigorous plants exhibited an earlier repression in growth compared with smaller, slow-growing plants, indicating a trade-off between early vigor and tolerance to prolonged water deficits. Genomic inference for model parameters and time of inflection (TOI) identified several candidate genes. This study is the first to utilize a genome-enabled growth model to study drought responses in rice, and presents a new approach to jointly model dynamic morpho-physiological responses and environmental covariates.

Keywords: Aquaporin, drought, genome-wide association study, genomics, growth model, phenomics, rice.

Introduction

Rice is one of the most important food crops and is a major source of food security for >3.5 billion people worldwide. Adequate water availability is essential for proper vegetative growth and grain development. Approximately 40 Mha of rainfed rice is grown worldwide, with the majority of production being concentrated in developing nations (Singh and Singh, 2000). Erratic precipitation events, as well as the increased competition for fresh water for non-agricultural uses, has become a major constraint for rice production (Korres *et al.*, 2017).

Given the socioeconomic impacts of water limitations, improving drought tolerance is a major target for breeding programs. However, the multiple and often unpredictable drought stress scenarios in drought-prone environments makes improvement of drought tolerance in rice challenging. Further, traits that are important for adaptation to limited

Abbreviations: DAT, days after transplantation;FC, field capacity;Gomp, Gompertz; GWAS, genome-wide association study;LASSO, least absolute shrinkage and selection operator; PSA, projected shoot area;QTL, quantitative trait locus;RGB, red–green–blue; SNP, single nucleotide polymorphism;TOI, time of inflection; WSI, water stress index; WU, water use.

water availability, particularly morpho-physiological traits, are complex and often have low heritability (Kamoshita *et al.*, 2008). These characteristics impede the discovery of loci that confer large effects on the phenotype, and limit the utility of marker-assisted selection for improving drought tolerance.

Recent advances in phenomics and genomics have offered new tools for discovering and quantifying traits associated with drought adaptation and their genetic basis (Berger *et al.*, 2010; Furbank and Tester, 2011; Araus and Cairns, 2014). Access to high-throughput, image-based phenomic systems in the public sector has allowed researchers to non-destructively measure traits of interest for large populations in highly controlled greenhouse or field environments. These platforms provide an effective means to study temporal developmental and/or physiological processes and assess how these processes are influenced by environmental factors such as drought (Berger *et al.*, 2010). Several studies have leveraged functional approaches to describe these temporal phenotypes using simple mathematical models, and leveraged genetic mapping approaches to identify loci that may affect trait trajectories (Ma *et al.*, 2002, Malosetti *et al.*, 2006; Das *et al.*, 2011; Bac-Molenaar *et al.*, 2015, 2016; Campbell *et al.*, 2015).

In addition to the temporal phenotypes generated with these platforms, many field- and greenhouse-based platforms also collect high-resolution environmental data (Tardieu *et al.*, 2017). These data provide additional insight into how temporal physiological and/or morphological responses are influenced by environmental conditions. Several studies have used these traits as covariates in the conventional genomic prediction frameworks to increase prediction accuracies for agronomic traits such as yield (Aguate *et al.*, 2017; Montesinos-López *et al.*, 2017; Sun *et al.*, 2017; Krause *et al.*, 2019). However, with these approaches, secondary phenotypes are utilized as linear predictors without directly considering how they give rise to the observed phenotype.

Process-based eco-physiological models seek to predict outcomes by explicitly modeling the interaction of biological processes with environmental covariates (Batchelor *et al.*, 2002; Ittersum *et al.*, 2003; Parent and Tardieu 2014). However, a major disadvantage of these models is that genotypic variation is often unaccounted for or not optimally utilized in the predictions (Onogi *et al.*, 2016). Thus, their application in genomic prediction or inference studies is limited. Several studies have sought to integrate crop growth models with established quantitative genetic frameworks (Technow *et al.*, 2015; Onogi *et al.*, 2016; Wang *et al.*, 2019). For instance, Technow *et al.* (2015) used an approximate Bayesian computation framework to integrate crop growth modeling and whole-genome prediction to predict yield in maize. They showed a clear advantage of the genome-enabled crop growth model over the conventional genomic prediction approach using simulated data. More recently, Onogi *et al.* (2016) leveraged a crop growth model to predict heading date in rice that integrated the phenological model proposed by Yin *et al.* (1997) and implemented by Nakagawa *et al.* (2005) with a whole-genome prediction using a hierarchical Bayesian approach. The hierarchical Bayesian approach outperformed conventional genomic prediction models as well as approaches that fit the crop growth model and genomic prediction model in separate steps. The advantage of the integrated approaches proposed by Technow *et al.* (2015) and Onogi *et al.* (2016) is that model parameter estimates are informed by the genomic relationships among the accessions, which can improve the accuracy of the parameter estimates. Moreover, since these approaches are based on a Bayesian whole-genome regression framework, marker effects are predicted, facilitating marker-level associations with model parameters. However, to date no studies have leveraged these genome-enabled crop growth models for biological inference, or to elucidate the genetic loci that influence model parameters.

In the current study, we sought to leverage the frameworks developed by Onogi *et al.* (2016) to study the effects of water deficit on shoot growth trajectories for a diverse set of rice accessions. To this end, accessions were subjected to drought stress [20% field capacity (FC)], and shoot growth was quantified over 21 d using an image-based phenomics platform. A corresponding set of accessions was maintained under optimal water conditions (90% FC). The automated phenotyping system allowed daily water use (WU) for each accession and soil water content to be estimated. Together, these data were used to develop a novel growth model that models shoot growth trajectories as a function of soil water content and time. This growth model was integrated into the hierarchical Bayesian framework of Onogi *et al.* (2016) to elucidate the genes underlying model parameters. This approach provides a biologically meaningful framework that simultaneously (i) models the inter-relationship between growth rate and soil water availability; (ii) estimates quantitative trait loci (QTLs) effects for model parameters; and (iii) provides genetic values for model parameters that can be used for genetic evaluation.

Materials and methods

Plant materials and greenhouse conditions

A subset of the Rice Diversity Panel 1 was used in this study (Zhao *et al.*, 2011). Seed preparation was performed following Campbell *et al.* (2015). Briefly, seeds were surface sterilized with Thiram fungicide and were germinated on moist paper towels in plastic boxes for 3 d. Three uniform seedlings were selected and transplanted to pots (150 mm diameter×200 mm height) filled with ~2.5 kg of UC Mix. Square containers were placed below each pot to allow water to collect. Temperatures in the greenhouses were maintained at 28/26.0 °C (day/night), and relative humidity was maintained at ~60% throughout the day and night.

Experimental design

A total of 378 accessions were phenotyped at the Plant Accelerator, Australian Plant Phenomics Facility, at the University of Adelaide, SA, Australia in three independent experiments performed from February to April 2016. A subset of 54 accessions were replicated twice in each experiment. The 54 accessions were selected based on seed availability and uniform germination. Each experiment consisted of 432 pairs of pots (378 and the 54 replicated accessions). Accessions were randomly assigned to each pair of pots, and water regimes were randomly assigned within pairs. Pairs were randomly partitioned in two smarthouses, each of which consisted of 24 lanes.

Seven days after transplantation (DAT) to soil, plants were thinned to one seedling per pot, and two layers of blue mesh were placed on top

of the soil to reduce soil water evaporation. At 11 DAT, the plants were loaded on the imaging system and were watered to 90% FC. Water was withheld from one of the two pots for each accession beginning at 13 DAT. Water was withheld until the end of the experiment or until the FC reached 20%, after which the plants were maintained at 20% FC.

Image analysis

The plants were imaged each day from 13 to 33 DAT using a visible [red–green–blue (RGB) camera; Basler Pilot piA2400-12 gc, Ahrensburg, Germany] from two side view angles separated by 90° and a single top view. The LemnaGrid software was used to extract 'plant pixels' from RGB images. The image analysis pipeline is identical to that described in Campbell *et al.* (2018). 'Plant pixels' from each of the RGB images for each plant and time point were summed and were used as a proxy for shoot biomass, which is referred to as projected shoot area (PSA). Several studies have shown that this metric is an accurate representation of shoot biomass (Golzarian *et al.*, 2011 Campbell *et al.*, 2015; Knecht *et al.*, 2016). Outlier plants at each time point were detected for each trait using the 1.5× interquartile range rule. Potential outliers were plotted and inspected visually, and those that exhibited abnormal growth patterns were removed prior to downstream analyses. In total, 34 plants were removed, leaving 2558 plants for downstream analyses. Since the genome-enabled crop growth model does not accommodate missing data, accessions with missing values were excluded from further analyses, resulting in a total of 349 accessions being used for downstream analyses.

Modeling shoot growth as a function of time and soil water content

The Gompertz growth model has been used extensively to model asymptotic processes that exhibit a sigmoid trend (Winsor, 1932). The classical Gompertz model is given by $PSA(t) = PSA_{max}e^{-e^{-r(t-T_o)}}$, where t is a vector of time values, r is the absolute growth rate, PSA_{max} is the maximum biomass (e.g. asymptote), and T_0 is the inflection point in the growth curve where the relative growth rate begins to slow. For the drought conditions imposed in the current study, we expect shoot growth to follow an exponential trajectory during the initial time points when soil water is not limiting. However, as the soil dries out, the growth rate should slow and, eventually, when soil water content falls below some threshold, growth should cease completely. Thus, the basic framework provided by the Gomertz model should capture these expected patterns.

To model the effects of water deficit on shoot growth trajectories, we devised a growth model that is an extension of the classical Gompertz growth model. The Gompertz growth model was modified so that shoot growth trajectories were modeled as a function of time and soil water content. This model is referred to as the WSI-Gomp model in the remainder of this manuscript. The WSI-Gomp model is given by

$$PSA(t) = PSA_{max}e^{-e^{-r(t-WSI^{\alpha})}}$$

where PSA_{max} is a parameter that describes the maximum biomass achieved by the plant; r describes the absolute growth rate; t is a vector of standardized time values [0,1]; and α is a genotype-specific tuning parameter that modifies the effect of WSI on PSA. WSI is the water stress index, a unitless index that describes the severity of water stress, and is given by

$$WSI = \frac{FC_t - FC_{Crit}}{FC_{Opt} - FC_{Crit}}$$

FC_t is the portion of FC at time t; FC_{Crit} (critical FC) is the proportion of FC in which growth ceases; and FC_{Opt} is the proportion of FC that is optimal for growth. FC was calculated at each time point from pot weights given by the automated watering system. Since FC_{Crit} and FC_{Opt} are unknown and likely to be genotype dependent, we assumed that the optimal conditions for growth in rice occur when the soil is completely saturated (i.e. FC_{Opt}=1), and FC_{Crit} is equal to 0.1. Although these assumptions require empirical evidence to validate, they provide a standardized metric that describes soil water content in a decreasing non-linear trend that is on the same scale as the standardized time values.

These characteristics allow PSA to be modeled as a function of time and soil water content using the Gompertz growth model. Figure 1 provides a graphical summary of the classical Gompertz and WSI-Gomp growth models for simulated soil water content values that would be typical for water-stressed plants in the current study, and Supplementary Fig. S1 at *JXB* online shows the effects of varying model parameters on shoot growth trajectories.

Leveraging whole-genome regression to estimate model parameters

The 'integrated approach' developed by Onogi *et al.* (2016) uses a hierarchical Bayesian framework to simultaneously infer growth model parameters and marker effects. The models were fit using the R package GenomeBasedModel (Onogi, 2020; https://github.com/Onogi/GenomeBasedModel). Briefly, solutions for the growth model parameters are regressed on genome-wide markers, and extended Bayesian LASSO (least absolute shrinkage and selection operator; EBL) is used to predict marker effects for each of the model parameters. The regression model is given by

$$\mathbf{y} = \mu + \mathbf{W}\beta + \mathbf{e}$$

$\mathbf{W}$ is an $n \times m$ matrix of marker genotypes coded as −1, 0, 1, n is the number of accessions (349), and m is the number of markers (33 697); μ is the intercept for each parameter; and β is an $m \times 1$

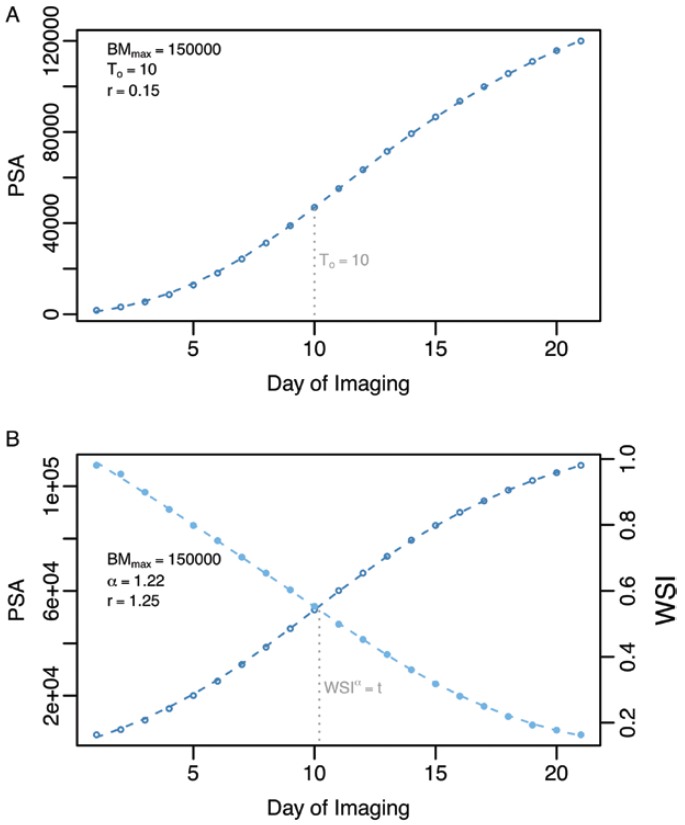

Fig. 1. Graphical representation of the classical Gompertz model and the WSI-Gomp model. (A) The classical Gompertz growth model was used to generate PSA values over a 21 d period. The parameter values used are provided in the top left corner of the plot. The gray, vertical broken line indicates the inflection point (T_0). (B) The WSI-Gomp growth model was used to generate PSA values over a 21 d period. PSA values are shown using dark blue points and a broken line. The light blue points and line indicate the WSI values over the 21 d period. WSI was calculated from simulated soil water content values that are typically of those experienced by water-stressed plants in the current study. The gray, vertical broken line indicates the inflection point (T_0).

vector of predicted marker effect for each model parameter. Markers were obtained from RiceDiversity.org and have been described by Zhao *et al.* (2011). The prior distribution of marker effects for marker i is

$$\begin{aligned}\beta_i &\sim \mathcal{N}(0, \tfrac{1}{\tau_0^2 \tau_i^2})\\ \tau_i^2 &\sim inverse-gamma(1, \tfrac{\delta^2 \eta_i^2}{2})\\ \delta^2 &\sim gamma(\phi, \omega)\\ \eta_i^2 &\sim gamma(\psi, \theta)\end{aligned}$$

τ_i^2 is the precision for the effect of marker i; η_i^2 is the marker-specific shrinkage parameter for marker i; δ^2 is the global shrinkage parameter; and ω, ϕ, θ, and ψ are hyperparameters. Default values were used for hyperparameters. We assume the following for WSI-Gomp model parameters

$$\begin{aligned}PSA_{max} &\sim \mathcal{N}(\mu_{PSA_{max}} + \mathbf{W}\beta_{PSA_{max}}, \tfrac{1}{\tau^2_{0,PSA_{max}}})\\ r &\sim \mathcal{N}(\mu_r + \mathbf{W}\beta_r, \tfrac{1}{\tau^2_{0,r}})\\ \alpha &\sim \mathcal{N}(\mu_\alpha + \mathbf{W}\beta_\alpha, \tfrac{1}{\tau^2_{0,\alpha}})\end{aligned}$$

$\tau^2_{0,p}$ is the residual precisions for model parameter p. Moreover, for the residuals, we assume N $(0, 1/\tau^2_0)$]. With the 'integrated approach' proposed by Onogi *et al.* (2016), model parameters are inferred using a variational Bayes approach in which means and variances of the growth model parameters are obtained using Markov chain Monte Carlo sampling and are used to update EBL parameters.

Genome-wide association for time of inflection

We sought to utilize the WSI-Gomp model to identify genomic loci that influenced the timing of the transition to a declining growth rate. To this end, we used model parameters obtained from the hierarchical Bayesian approach described above and observed WSI values to solve for the time of inflection (TOI). In the classical Gompertz growth model, $PSA(t) = PSA_{max}e^{-e^{-r(t-T_0)}}$, the growth rate begins to decline when the $(t-T_0)$ term becomes positive (i.e. when t exceeds T_0). Thus, T_0 can be defined as the time of inflection. In the WSI-Gomp model, this component is given by $(t-\text{WSI}^{\alpha})$. Thus, the TOI occurs when $t \geq \text{WSI}^{\alpha}$. Using the hierarchical Bayesian approach, we obtained estimates for α for each accession in drought and control conditions, and used these values to solve for TOI using WSI values for each accession in each experiment. TOI was defined as the first day in which $(t-\text{WSI}^{\alpha})$ was positive. This yielded a single TOI value for each accession in each experiment.

These TOI values were used as a derived phenotype for further genome-wide association study (GWAS) analysis. The following Bayesian LASSO regression model was fit using the BGLR package (Pérez and Los Campos, 2014)

$$\mathbf{y} = \mathbf{X}\beta + \mathbf{Za} + \mathbf{e}$$

where $\mathbf{y} = \mathbf{X}$ is an incidence matrix relating the vector β of fixed effects for experiment to observations, $\mathbf{Z}$ is an incidence matrix relating the vector of random marker effects $\mathbf{a}$ to $\mathbf{y}$, and $\mathbf{e}$ is the residual. Since the vector $\mathbf{y}$ is a vector of discrete TOI values, $\mathbf{y}$ was treated as an ordinal response, and a probit link function was used. In Bayesian LASSO, the marginal prior distribution for each marker effect is a double exponential function that includes an unknown parameter λ^2 with a prior distribution $\lambda^2 \sim$gamma (r, s) (Pérez and Los Campos, 2014). BGLR sets s=1.1 by default and solves for r based on the prior R^2 of the model. Details on the BL approach implemented in BGLR is provided in the package vignette. A Gaussian prior with mean zero and variance equal to 1×10^{10} was used for fixed effects.

Results

Image-based phenotyping captures the sensitivity of rice to drought stress

To examine drought responses in rice (*Oryza sativa*), a diversity panel was phenotyped over a period of 21 d during the early vegetative stage using an automated high-throughput phenotyping platform (Supplementary Dataset S1). Control plants were maintained at 90% FC, while water was withheld from drought-treated plants until a final FC of 20% was reached. A *t*-test was carried out at each time point to determine when a significant reduction in soil water availability was experienced. A significant difference in pot water content (FC) was observed from the second day of imaging (Fig. 2A; P<0.0024, Bonferroni's correction with α =0.05) when the drought plants on average were at 90.9% FC.

The impact of drought stress on shoot growth (biomass) was estimated from RGB images and expressed as a digital metric called PSA. An ANOVA was carried out at each time point using the a linear model that included main effects for treatment and accession and the interaction between treatment and accession. Significant effects for the interaction between accession and treatment were observed from day 16 onward. Drought treatment had a significant effect on PSA beginning on the fourth day of imaging (Fig. 2B; P<0.0024, Bonferroni's correction with α =0.05). Interestingly, at this time point drought-treated plants, on average, were at 81.9% FC, which is only ~12.5% below control plants. These data suggest that even a small limitation of water can have a

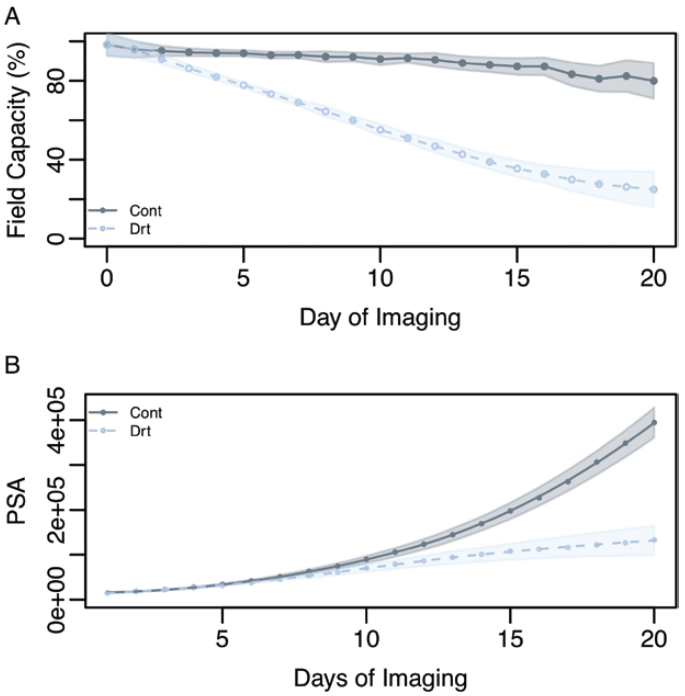

Fig. 2. Effect of water deficit on shoot growth. (A) Mean percentage field capacity in drought and control conditions over the 21 d of imaging. (B) Mean shoot growth trajectories (PSA) in drought and control conditions over 21 d of imaging. Water was withheld starting at day 1 of imaging. The shaded regions indicate the SD for each treatment. (This figure is available in color at *JXB* online.)

significant impact on shoot growth in rice, thus confirming the high level of drought sensitivity reported for rice (Lafitte *et al.*, 2004).

Defining the growth model

The Gompertz growth model has been used extensively to model asymptotic processes that exhibit a sigmoid trend (Winsor, 1932). This sigmoid/asymptotic trend is to some degree visible in the mean growth trajectory in Fig. 2B. While the classical Gompertz model provides an intuitive framework to model asymptotic growth trajectories as a function of time, it does not accommodate environmental data, and therefore cannot be used to address how shoot growth varies in response to soil water content.

To address this limitation, we sought to modify the Gompertz growth model so that shoot growth trajectories could be modeled as a function of time and soil water content. We defined an index (water stress index, WSI) from daily records of soil water content for each plant that reflects the severity of water stress. WSI is given by $WSI = \frac{FC_t - FC_{Crit}}{FC_{Opt} - FC_{Crit}}$, where FC_t indicates the percentage FC at time t, FC_{Opt} is the optimal percentage FC for growth, and FC_{Crit} is the percentage FC at which growth ceases. Since these values are expected to vary depending on the genotype, we assumed that growth will cease at 10% FC (FC_{Crit}=1) and the growth will proceed optimally when the soil is saturated (FC_{Opt}=100). This equation provides a unitless metric that will vary between 0 and 1, with higher values indicating lower water stress and lower values indicating a greater stress. For this metric to be introduced into the Gompertz growth model, we standardized the time values so that they ranged from 0 to 1. Finally, we introduced a third parameter (α) into the model that acts as a genotype-dependent tuning parameter and modifies the effect of WSI on growth rate. This new WSI-integrated model (WSI-Gomp) is given by $PSA(t) = PSA_{max} e^{-e^{-r(t-WSI^{\alpha})}}$. The WSI-Gomp model is shown in Fig. 2B.

To capture the effects of soil water deficit on growth trajectories, the WSI-Gomp model was fit to growth trajectories in drought and control conditions for each of the 349 accessions using a hierarchical Bayesian approach that leverages the genetic relationships among lines to obtain solutions for the model parameters (Onogi *et al.*, 2016). Model parameter estimates for each accession were used to predict growth trajectories employing observed WSI values. The ability of the WSI-Gomp model to capture these dynamic responses was assessed by comparing predicted PSA values and observed values at each time point using two metrics: root mean squared error (RMSE) and Pearson's correlation. Overall, the WSI-Gomp model provided a good fit to the observed shoot growth trajectories (Fig. 3). The correlation between observed and predicted PSA values ranged from 0.41 to 0.87 in the control, while the correlation was slightly lower in drought conditions and ranged from 0.52 to 0.75. Correlation values were lowest for early time points in both control and drought conditions, suggesting that predictions for these time points may be inaccurate. However, at later time points, there was a high agreement between predicted and observed values for PSA. Collectively, these

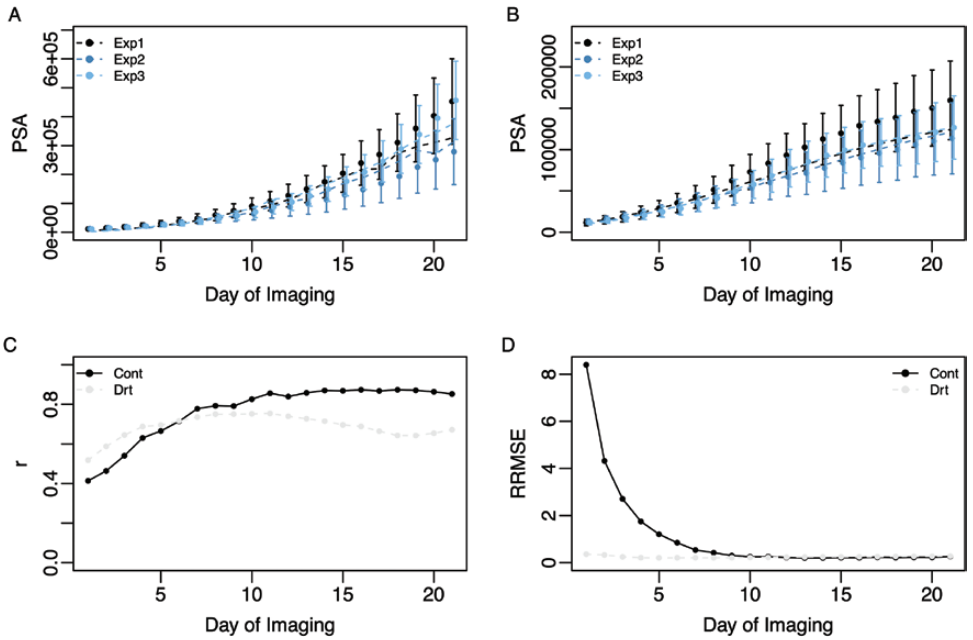

Fig. 3. Capturing shoot growth trajectories using the WSI-Gomp model. Observed (points) and predicted (broken line) mean shoot growth trajectories for each experiment under control (A) and drought (B) conditions. For both (A) and (B), Nelder–Mead optimization was used to fit the WSI-Gomp model to the mean shoot growth trajectories for each experiment. (C) Average correlation between predicted trajectories and observed PSA values. (D) Relative root mean squared error (RRMSE) between predicted trajectories and observed PSA values. RRMSE was calculated as RMSE at time *t* divided by the mean predicted values at time *t*. For both (C) and (D), the WSI-Gomp model was fit using the hierarchical Bayesian model, and predicted PSA values were compared at each time point with observed values for each accession. (This figure is available in color at *JXB* online.)

results suggest that the WSI-Gomp captures shoot growth trajectories in contrasting water regimes; however, other factors not accounted for in the growth model also influence observed PSA values.

Leveraging the growth model for biological inference

The WSI-Gomp model provides a means to model PSA trajectories as a function of declining soil water content and allows the inflection point in growth curves to be estimated using observed WSI values. With this in mind, we next sought to determine what observable characteristics influence the timing of this inflection point in drought conditions. To this end, we calculated the TOI for each plant in drought by determining the earliest time in which the (t–WSI α) component of the model became positive (Supplementary Dataset S2). As expected, the predicted TOIs were lower in drought conditions compared with control, indicating that the inflection of the growth curve occurs early under drought conditions compared with well-watered conditions (Fig. 4A). TOI in drought-treated plants ranged from 8 d to 16 d of imaging, while in control plants TOI values ranged from 14 d to 20 d.

To determine how observable phenotypes influenced TOI, the predicted TOI values were compared with WU, PSA, and the ratio of these values in drought and control (indicated by the subscript 'dr' meaning drought response) over the course of the experiment. Relationships were assessed using Spearman's correlation with a 3 d sliding window (Fig. 4B, C). In drought conditions, we observed a negative relationship between TOI in drought (TOI_D) and PSA in both control and drought conditions (PSA_C and PSA_D, respectively), indicating that larger plants tend to have earlier retardation of shoot growth rate (Fig. 4B). The relationship between TOI_D and PSA_D became weaker as the soil water declined and drought became more severe. This trend is probably because at these time points shoot growth in large plants was likely to have already been repressed by drought. Similar, albeit slightly stronger, negative correlations were observed between WU in control (WU_C) and TOI in drought (TOI_D). An interesting trend was observed for WU_D and TOI_D. At early time points (e.g. days 0–14) a negative correlation was observed between TOI_D and WU_D. However, around days 15–18, this trend is reversed completely, with a positive correlation observed between WU_D and TOI_D. As expected, TOI_D showed a positive relationship with PSA_{dr} (i.e. the ratio of PSA in drought to control), indicating that accessions with early inflection points tend to show a larger reduction in PSA under drought relative to control.

Similar trends were observed in control conditions; however, the values of the correlation coefficients were different compared with drought (Fig. 4C). A negative relationship was observed between TOI in control (TOI_C) and PSA in control (PSA_C), which is consistent with the relationship observed for TOI_D and PSA. However, TOI_C and PSA_C showed a very weak relationship, with a slight negative correlation during initial time points and a very weak positive relationship observed at later time points. Consistent with drought conditions, the relationship between WU_C and TOI_C showed a strong negative correlation. Moreover, the correlation between TOI_C and WU_D was negative at early time points and positive at later time points, which is similar to the trend observed between TOI_D and WU_D. Although the interpretation of α and TOI in control conditions is not very straightforward because plants were grown in the absence of water stress, the observed correlation suggests that these parameters may have a similar interpretation to that in drought conditions.

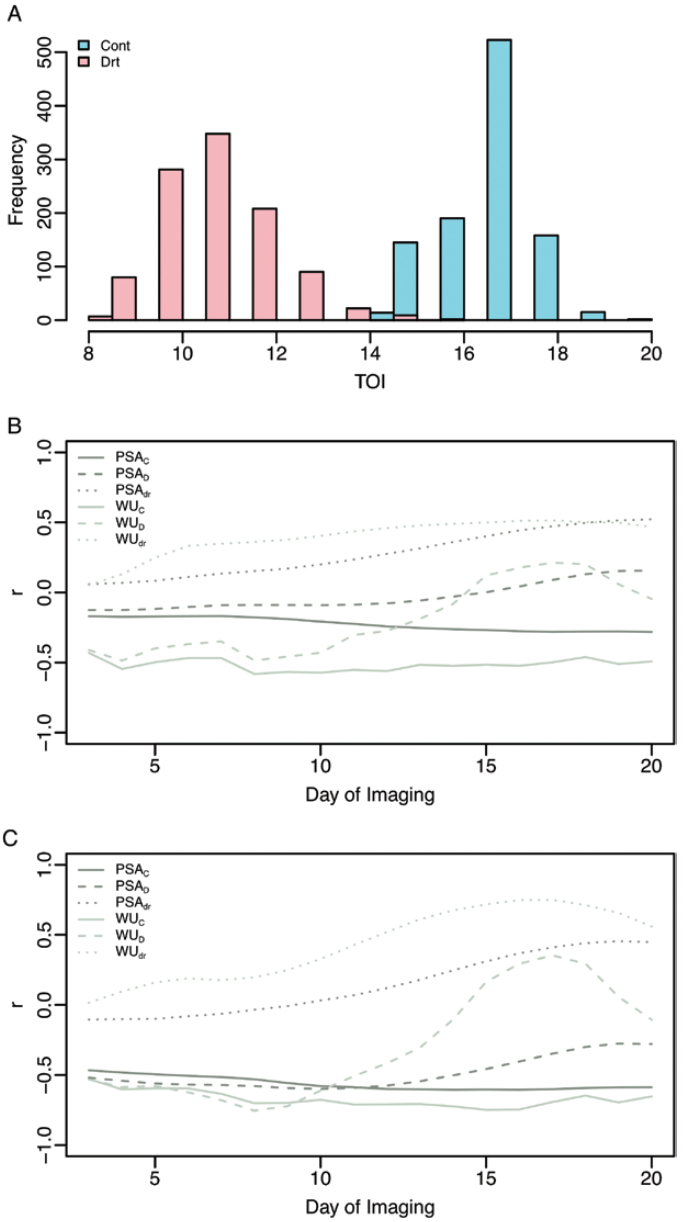

Fig. 4. Distribution and interpretation of predicted time of infection. (A) The distribution of time of inflection (TOI) values in control and drought conditions. Correlation between time of inflection in control (B) and drought (C), and empirical observations for projected shoot area (PSA) and water use (WU). WU for a given day is calculated as the difference in soil water content from the previous day and soil water content on the current day. In cases where the plant received water (e.g. control plants), pot weights after watering were used to calculate soil water content values for the previous day, and pot weights prior to watering were used for soil water content values for the current day. Spearman's correlation was performed using a 3 d sliding window. (This figure is available in color at *JXB* online.)

Genome-wide association provides insight into loci influencing shoot growth trajectories

Model parameter estimates for the WSI-Gomp model were obtained using a hierarchical Bayesian framework, wherein the growth model is fit in the first level, and in the second level an EBL approach is used to predict marker effects from model parameters. Thus, this information can be leveraged to identify QTLs and potential candidate genes that may influence shoot growth trajectories in response to water deficit. To this end, we sought to utilize the inferred marker effects to identify genomic regions that regulate model parameters and influence dynamic shoot growth trajectories in response to water availability. The absolute values of inferred marker effects are provided in the Manhattan plots in Fig. 5 and Supplementary Dataset S3. Since obtaining *P*-values from Bayesian approaches is non-trivial, we report loci and candidate genes for the top-20 single nucleotide polymorphisms (SNPs) ranked based on the absolute value of marker effects ($|\beta|$).

The model parameters *r* and α in both control and drought conditions exhibit a polygenic genetic architecture. We identified several markers with small contributions to the parameter values. Although the model parameters α and *r* showed a polygenic architecture, several notable genes were identified within the regions defined by SNPs with relatively larger effects (Supplementary Dataset S4). For instance, at ~6.7 Mb on chromosome 1, a gene encoding an osmotin protein (*OSM34*) was found ~75 kb upstream of the top SNP associated with α in drought within this region. Osmotin proteins play a role in plant biotic and abiotic stress responses, particularly drought stress (Narasimhan *et al.*, 2009; Sharma *et al.*, 2013). Additionally, a membrane-bound protein involved in chilling tolerance, *COLD1*, was found ~27 kb downstream of the SNP with the largest effect on chromosome 4 for α in drought (Ma *et al.*, 2015). The presence of these two genes known to be involved in abiotic stress responses warrants further investigation.

The parameter PSA_{max} showed a simpler genetic architecture in control and drought conditions. In control conditions, one large QTL was identified on chromosome 4 with the SNP, with the largest effect located at ~31.4 Mb on chromosome 4. Within this region, a gene involved with the regulation of polar auxin transport, *Narrow Leaf1* (*NAL1*),

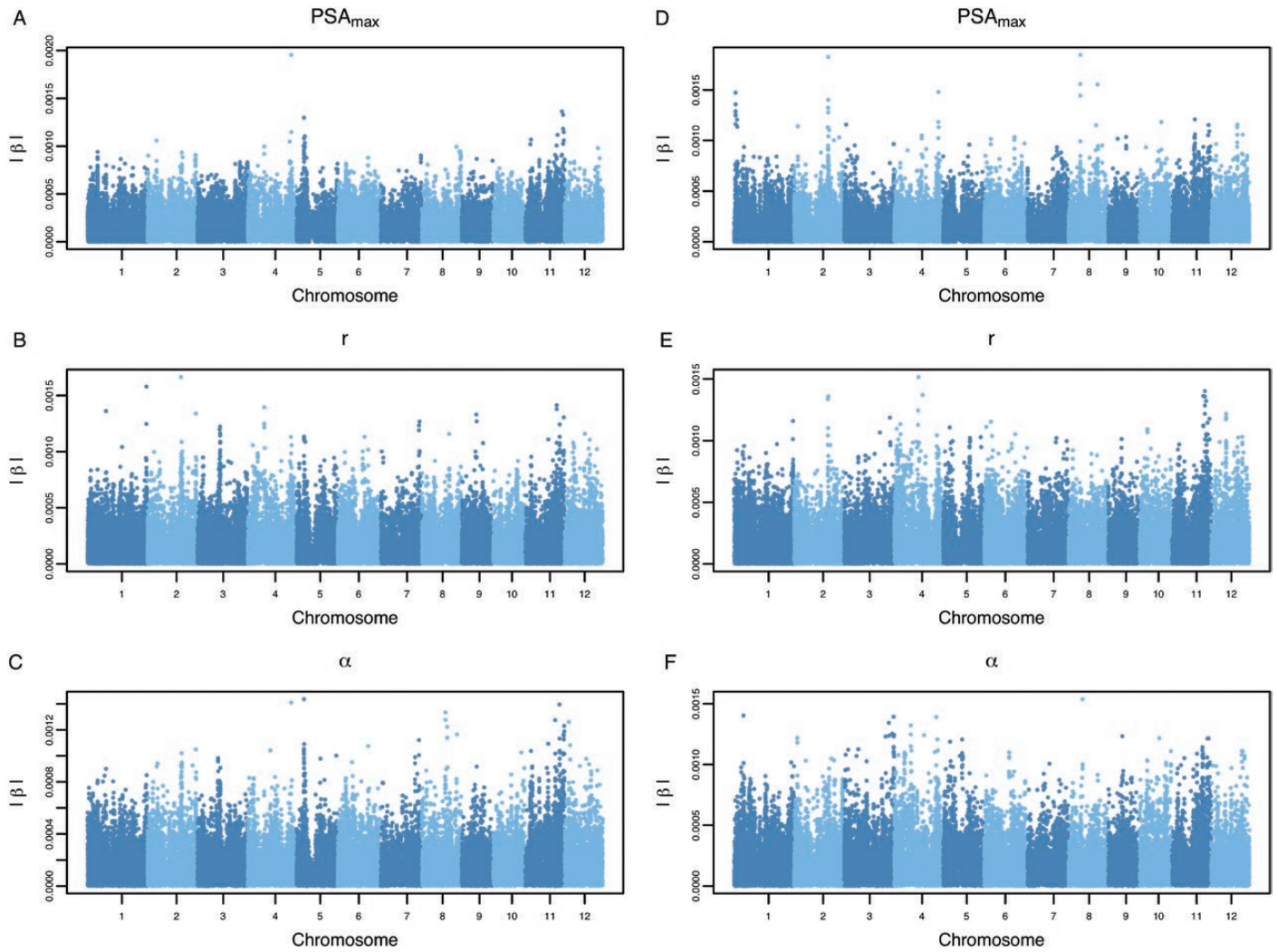

Fig. 5. Genomic regions influencing model parameters. Predicted marker effects are shown for each of the WSI-Gomp model parameters. (A–C) Marker effects for model parameters fit to growth trajectories in control conditions; (D–F) marker effects for drought conditions. The absolute value of predicted marker effects ($|\beta|$) is shown on the *y*-axis. (This figure is available in color at *JXB* online.)

was identified. Several studies have reported that variants in the *NAL* gene have pleiotropic effects and alter plant vascular patterning, spikelet number, leaf size, root system architecture, and shoot biomass (Qi *et al.*, 2008; Fujita *et al.*, 2013). In drought conditions, several QTLs were identified for PSA_{max}, with notable peaks located on chromosomes 1, 2, 4, and 8. The SNP with the largest effect was located at ~21 Mb on chromosome 8. Within this region, a gene known to regulate flowering time under short-day conditions was identified, *GF14c* (Purwestri *et al.*, 2009). Moreover, a second gene known to influence biomass and seed size, *OsMPS*, was identified on chromosome 2 at ~24.5 Mb (Schmidt *et al.*, 2013). Since PSA_{max} is a parameter that describes the maximum biomass for each accession, the presence of genes known to regulate flowering time and biomass is promising and suggests that this parameter is biologically meaningful.

Elucidating the genetic loci influencing time of inflection in contrasting water regimes

In addition to the parameters explicitly defined by the model, TOI can also be considered an additional phenotype that can be analyzed using conventional GWAS frameworks. With this in mind, we sought to identify QTLs that were associated with TOI using a Bayesian whole-genome regression approach (Supplementary Dataset S3). Estimates for model parameters were combined with observed environmental covariates to solve for the TOI for each accession in drought and control conditions. Marker associations with TOI were assessed using a GWAS approach that accounted for the ordinal response variable, and results are discussed in the context of the top-20 ranked SNPs based on $|\beta|$ (Fig. 6).

GWAS for TOI in control conditions showed that many SNPs have a small effect on the phenotype, indicating a complex genetic architecture for TOI in control conditions (Fig. 6A). However, for drought conditions, GWAS revealed two notable regions characterized by SNPs with relatively larger effects (Fig. 6B). The first peak was identified at ~27 Mb on chromosome 2, while the second peak was located at 22.9 Mb on chromosome 11.

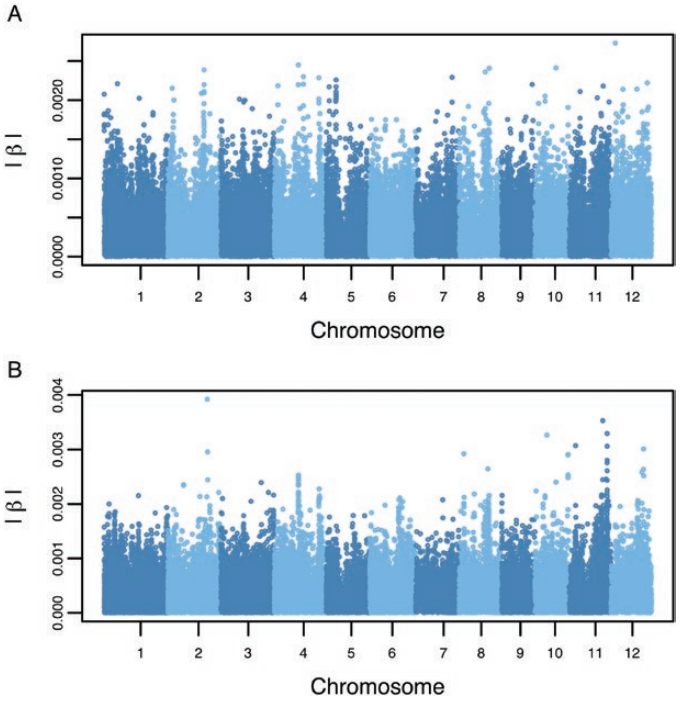

Fig. 6. Manhattan plots for time of inflection (TOI). GWAS was conducted using TOI values in control (A) and drought conditions (B). Each point indicates an SNP marker, and the *y*-axis shows the absolute value of predicted marker effects (|β|).(This figure is available in color at *JXB* online.)

Discussion

Drought tolerance during the vegetative growth stage is most simply defined as the ability to maintain growth under water deficit. It is determined by the amount of water available to the plant and how efficiently the water is used to gain biomass. In terminal drought environments, where a fixed amount of water is available during the early season, the ability to maintain growth will be dependent on how well the plant can manage these resources throughout the season. Thus, when studying drought tolerance, especially in terminal drought environments, it is important to jointly consider these factors. In the current study, we imposed a severe drought stress by completely withholding water for a period of 20 d (or until pots reached 20% FC). The effects of this severe stress were apparent soon after withholding water, as drought-stressed plants showed a significant reduction in shoot biomass after 4 d compared with control plants (Fig. 2).

Given the importance of accounting for water availability when modeling temporal shoot growth trajectories, we developed a growth model that jointly models shoot biomass and soil water content. While the model parameters themselves can be used to describe characteristics of the growth curve and provide insight into the processes that influence shoot growth, the model can also be leveraged for additional biological inferences. For instance, we used genotype-specific parameter estimates to determine the point in which the growth rate begins to decline (i.e. TOI). While this information can also be obtained with the classical Gompertz growth model, the WSI-Gomp model leverages both time and temporal soil water availability while the former only utilizes time. Since the time values are standardized to be on the same scale as the WSI with the WSI-Gomp model, this metric can be interpreted in two ways: (i) the time in which the growth rate begins to decline; or (ii) the soil water content value that begins to repress growth. Regardless of the interpretation, this approach provides a means to assess drought sensitivity while accounting for variation in soil water content between plants.

Joint modeling suggests a trade-off between vigor and drought tolerance

The TOI provided biological insight into the relationship between plant size or vigor and morphological responses to a severe water deficit. Temporal correlation analyses between

TOI and morphological and physiological responses revealed that large, vigorous plants tend to have an earlier decline in growth rate under severe drought conditions (Fig. 4). Moreover, these plants tend to have high water demands in control conditions, and quickly exhaust soil water resources in drought conditions. The link between early vigor and drought responses has been studied extensively. Although some studies suggest that early vigor is advantageous in drought-prone environments, these benefits are highly dependent on the type of drought stress that is prevalent in these regions (Tardieu, 2011). A study by Kamoshita *et al.* (2004) evaluated six rice accessions under short and prolonged drought and examined the relationship between root system architecture, osmotic adjustment, and biomass production. They found that highly vigorous accessions rapidly developed a dense root system and extracted water quickly, but were also more sensitive to prolonged drought stress compared with low vigor genotypes. However, these plants tended to recover more quickly after rewatering compared with low vigor accessions. A more recent study by Rebolledo *et al.* (2012) found similar results and suggested that vigorous accessions also quickly exhaust starch reserves under prolonged drought, resulting in a greater decline in biomass production compared with less vigorous accessions. Collectively, these studies support the observed negative correlation between plant size and drought sensitivity (as assessed with TOI), and suggest a trade-off between vigorous growth and the maintenance of growth in prolonged drought stress. Further studies are necessary to determine whether these relationships can be decoupled, or to identify the optimal balance between these two attributes.

Leveraging the genome-enabled growth model for candidate gene discovery

The hierarchical Bayesian framework developed by Onogi *et al.* (2016) provides a powerful approach to improve the estimation of model parameters and to estimate the genomic contributions to the model parameters. Since the model parameters are regressed on genome-wide SNP markers, this framework provides a means to identify important loci that influence trait trajectories (i.e. GWAS). While the initial study by Onogi *et al.* (2016) showed both applications of the approach, their primary objective was genomic prediction. Here, we leveraged the genome-enabled growth modeling approach to identify genomic regions that influence dynamic drought responses.

Many of the model parameters show a complex genetic architecture characterized by many loci with small effects (Fig. 5). However, several notable regions exhibiting relatively large effects were identified that harbored potential candidate genes. For instance, two notable peaks were identified on chromosomes 1 and 4 for the parameter α in drought conditions (Fig. 5F). Both regions harbored candidate genes that have been reported to regulate drought and/or osmotic stress responses in plants. The region on chromosome 4 harbored a gene that is known to regulate chilling tolerance in rice, *COLD1* (Ma *et al.*, 2015). *COLD1* was shown to be involved with the Ca^{2+} signaling response to cold stress. In Arabidopsis, the *COLD1* orthologs, *GTG1* and *GTG2*, are membrane-bound abscisic acid receptors (Pandey *et al.*, 2006, 2009). However, *COLD1* exhibits GTPase activity that is absent in *GTG1/2* (Ma *et al.*, 2015). Thus, further studies are necessary to determine whether *COLD1* participates in drought responses.

In addition to the candidate genes associated by model parameters, whole-genome regression performed with TOI in drought conditions revealed a potential role for additional genes in the genetic regulation of the timing of growth responses to drought (Fig. 6). An aquaporin gene, *OsPIP1;1*, was identified within a prominent peak on chromosome 2 associated with TOI in drought conditions. Aquaporins are a large family of proteins that were initially reported to act as water transporters, but have since been shown to also transport CO_2 and H_2O_2 (Dynowski *et al.*, 2008; Uehlein *et al.*, 2003; Bienert and Chaumont, 2014; Maurel *et al.*, 2015; Wang *et al.*, 2016; Rodrigues *et al.*, 2017). Aquaporins have received considerable attention as a potential target to modify whole-plant water transport and improve water status during drought stress (Sadok and Sinclair, 2009; Devi *et al.*, 2012; Choudhary and Sinclair, 2014; Schoppach *et al.*, 2014; Grondin *et al.*, 2016). Work by Grondin *et al.* (2016) showed that aquaporins account for ~85% of root hydraulic conductivity in rice under drought stress, and demonstrated that the expression of *PIP1;1* is induced by drought stress.

Concluding remarks

Improving drought tolerance in rice is a challenging objective. Efforts to improve drought tolerance are hindered by the heterogenity in drought-prone environments, the breadth and complexity of traits underlying drought adaptation, and the difficulty in characterizing large populations for these traits. Recent advances in phenotyping technologies have provided an effective means to measure morpho-physiological traits frequently throughout the growing season, and provide plant breeders and geneticists with dense phenotypic data describing complex responses. However, these technological advances must be coupled with frameworks that accommodate these multidimensional data sets, while providing a means to leverage high density genotypic data to predict phenotypes and novel biological inference. In this context, the genome-enabled growth model proposed is a significant advancement towards addressing this need. The WSI-Gomp model provides a simple, biologically meaningful framework that can describe complex temporal responses using few parameters. Moreover, since genome-wide markers are used to estimate model parameters, the inferred marker effects can be used to identify genes that may contribute to these responses, estimate genetic values for model parameters for known individuals, as well as predict the phenotypes for new, uncharacterized individuals. Thus, these data can both be leveraged for genetic inference of complex drought responses, and make selections based on model parameters. This study is the first to leverage a genome-enabled growth model for genomic inference in rice, and provides novel insights into the basis of dynamic growth responses to drought stress.

Supplementary data

Supplementary data are available at *JXB* online.

Fig. S1. Predicted shoot growth trajectories from the WSI-Gomp model with varying model parameters.

Dataset S1. Raw phenotypic data for all 349 accessions used to fit the WSI-Gomp model.

Dataset S2. Model parameter and time of inflection estimates for all 349 accessions obtained from the WSI-Gomp model.

Dataset S3, Marker effects for GWAS for model parameters and time of inflection.

Dataset S4. Candidate genes for model parameters and time of inflection.

Data availability

All data and codes used in this study can be accessed at https://github.com/malachycampbell/RiceCGM/tree/master.

Acknowledgements

Funding for this research was provided by the National Science Foundation (United States) through award no. 1238125 to HW, and award no. 1736192 to HW and GM.

References

Aguate FM, Trachsel S, González Pérez L, Burgueño J, Crossa J, Balzarini M, Gouache D, Bogard M, de los Campos G. 2017. Use of hyperspectral image data outperforms vegetation indices in prediction of maize yield. Crop Science **57**, 2517–2524.

Araus JL, Cairns JE. 2014. Field high-throughput phenotyping: the new crop breeding frontier. Trends in Plant Science **19**, 52–61.

Bac-Molenaar JA, Granier C, Keurentjes JJB, Vreugdenhil D. 2016. Genome-wide association mapping of time-dependent growth responses to moderate drought stress in Arabidopsis. Plant, Cell & Environment **39**, 88–102.

Bac-Molenaar JA, Vreugdenhil D, Granier C, Keurentjes JJB. 2015. Genome-wide association mapping of growth dynamics detects time-specific and general quantitative trait loci. Journal of Experimental Botany **66**, 5567–5580.

Batchelor WD, Basso B, Paz JO. 2002. Examples of strategies to analyze spatial and temporal yield variability using crop models. European Journal of Agronomy **18**, 141–158.

Berger B, Parent B, Tester M. 2010. High-throughput shoot imaging to study drought responses. Journal of Experimental Botany **61**, 3519–3528.

Bienert GP, Chaumont F. 2014. Aquaporin-facilitated transmembrane diffusion of hydrogen peroxide. Biochimica et Biophysica Acta **1840**, 1596–1604.

Campbell MT, Knecht AC, Berger B, Brien CJ, Wang D, Walia H. 2015. Integrating image-based phenomics and association analysis to dissect the genetic architecture of temporal salinity responses in rice. Plant Physiology **168**, 1476–1489.

Campbell M, Walia H, Morota G. 2018. Utilizing random regression models for genomic prediction of a longitudinal trait derived from high-throughput phenotyping. Plant Direct **2**, e00080.

Choudhary S, Sinclair TR. 2014. Hydraulic conductance differences among sorghum genotypes to explain variation in restricted transpiration rates. Functional Plant Biology **41**, 270–75.

Das K, Li J, Wang Z, *et al*. 2011. A dynamic model for genome-wide association studies. Human Genetics **129**, 629–639.

Devi MJ, Sadok W, Sinclair TR. 2012. Transpiration response of de-rooted peanut plants to aquaporin inhibitors. Environmental and Experimental Botany **78**, 167–172.

Dynowski M, Schaaf G, Loque D, Moran O, Ludewig U. 2008. Plant plasma membrane water channels conduct the signalling molecule H_2O_2. The Biochemical Journal **414**, 53–61.

Fujita D, Trijatmiko KR, Tagle AG, *et al*. 2013. *NAL1* allele from a rice landrace greatly increases yield in modern *Indica* cultivars. Proceedings of the National Academy of Sciences, USA **110**, 20431–20436.

Furbank RT, Tester M. 2011. Phenomics—technologies to relieve the phenotyping bottleneck. Trends in Plant Science **16**, 635–644.

Golzarian MR, Frick RA, Rajendran K, Berger B, Roy S, Tester M, Lun DS. 2011. Accurate inference of shoot biomass from high-throughput images of cereal plants. Plant Methods **7**, 2.

Grondin A, Mauleon R, Vadez V, Henry A. 2016. Root aquaporins contribute to whole plant water fluxes under drought stress in rice (*Oryza sativa* L.). Plant, Cell & Environment **39**, 347–365.

Ittersum MK, Leffelaar PA, Van Keulen H, Kropff MJ, Bastiaans L, Goudriaan J. 2003. On approaches and applications of the Wageningen crop models. European Journal of Agronomy **18**, 201–234.

Kamoshita A, Babu RC, Boopathi NM, Fukai S. 2008. Phenotypic and genotypic analysis of drought-resistance traits for development of rice cultivars adapted to rainfed environments. Field Crops Research **109**, 1–23.

Kamoshita A, Rodriguez R, Yamauchi A, Wade L. 2004. Genotypic variation in response of rainfed lowland rice to prolonged drought and rewatering. Plant Production Science **7**, 406–20.

Knecht AC, Campbell MT, Caprez A, Swanson DR, Walia H. 2016. Image harvest: an open-source platform for high-throughput plant image processing and analysis. Journal of Experimental Botany **67**, 3587–3599.

Korres NE, Norsworthy JK, Burgos NR, Oosterhuis DM. 2017. Temperature and drought impacts on rice production: an agronomic perspective regarding short- and long-term adaptation measures. Water Resources and Rural Development **9**, 12–27.

Krause MR, González-Pérez L, Crossa J, *et al*. 2019. Hyperspectral reflectance-derived relationship matrices for genomic prediction of grain yield in wheat. G3: Genes, Genomes, Genetics **9**, 1231–1247.

Lafitte HR, Ismail A, Bennett J. 2004. Abiotic stress tolerance in rice for Asia: progress and the future. In: Proceeding of 4th International Crop Science Congress, Brisbane, Australia.

Liu C, Fukumoto T, Matsumoto T, Gena P, *et al*. 2013. Aquaporin Ospip1;1 promotes rice salt resistance and seed germination. Plant Physiology and Biochemistry **63**, 151–158.

Ma C-X, Casella G, Wu R. 2002. Functional mapping of quantitative trait loci underlying the character process: a theoretical framework. Genetics **161**, 1751–1762.

Ma Y, Dai X, Xu Y, *et al*. 2015. *COLD1* confers chilling tolerance in rice. Cell **160**, 1209–1221.

Malosetti M, Visser RG, Celis-Gamboa C, van Eeuwijk FA. 2006. QTL methodology for response curves on the basis of non-linear mixed models, with an illustration to senescence in potato. Theoretical and Applied Genetics **113**, 288–300.

Maurel C, Boursiac Y, Luu D-T, Santoni V, Shahzad Z, Verdoucq L. 2015. Aquaporins in plants. Physiological Reviews **95**, 1321–1358.

Montesinos-López OA, Montesinos-López A, Crossa J, de los Campos G, Alvarado G, Suchismita M, Rutkoski J, González-Pérez L, Burgueño J. 2017. Predicting grain yield using canopy hyperspectral reflectance in wheat breeding data. Plant Methods **13**, 4.

Nakagawa H, Yamagishi J, Miyamoto N, Motoyama M, Yano M, Nemoto K. 2005. Flowering response of rice to photoperiod and temperature: a QTL analysis using a phenological model. Theoretical and Applied Genetics **110**, 778–786.

Narasimhan ML, Bressan RA, D'Urzo MP, Jenks MA, Mengiste T. 2009. Unexpected turns and twists in structure/function of pr-proteins that connect energy metabolism and immunity. Advances in Botanical Research **51**, 439–489.

Onogi A. 2020. Connecting mathematical models to genomes: joint estimation of model parameters and genome-wide marker effects on these parameters. Bioinformatics **36**, 3169–3176.

Onogi A, Watanabe M, Mochizuki T, Hayashi T, Nakagawa H, Hasegawa T, Iwata H. 2016. Toward integration of genomic selection with crop modelling: the development of an integrated approach to predicting rice heading dates. Theoretical and Applied Genetics **129**, 805–817.

Pandey S, Chen J-G, Jones AM, Assmann SM. 2006. G-protein complex mutants are hypersensitive to abscisic acid regulation of germination and postgermination development. Plant Physiology **141**, 243–256.

Pandey S, Nelson DC, Assmann SM. 2009. Two novel Gpcr-Type G proteins are abscisic acid receptors in Arabidopsis. Cell **136**, 136–148.

Parent B, Tardieu F. 2014. Can current crop models be used in the phenotyping era for predicting the genetic variability of yield of plants subjected to drought or high temperature? Journal of Experimental Botany **65**, 6179–6189.

Pérez P, de Los Campos G. 2014. Genome-wide regression and prediction with the BGLR statistical package. Genetics **198**, 483–495.

Purwestri YA, Ogaki Y, Tamaki S, Tsuji H, Shimamoto K. 2009. The 14-3-3 protein Gf14c acts as a negative regulator of flowering in rice by interacting with the Florigen Hd3a. Plant & Cell Physiology **50**, 429–438.

Qi J, Qian Q, Bu Q, *et al*. 2008. Mutation of the rice narrow leaf1 gene, which encodes a novel protein, affects vein patterning and polar auxin transport. Plant Physiology **147**, 1947–1959.

Rebolledo M-C, Dingkuhn M, Clément-Vidal A, Rouan L, Luquet D. 2012. Phenomics of rice early vigour and drought response: are sugar related and morphogenetic traits relevant? Rice **5**, 22.

Rodrigues O, Reshetnyak G, Grondin A, Saijo Y, Leonhardt N, Maurel C, Verdoucq L. 2017. Aquaporins facilitate hydrogen peroxide entry into guard cells to mediate ABA- and pathogen-triggered stomatal closure. Proceedings of the National Academy of Sciences **114**, 9200–9205.

Sadok W, Sinclair TR. 2009. Transpiration response of 'Slow-Wilting' and commercial soybean [*Glycine max* (L.) Merr.] genotypes to three aquaporin inhibitors. Journal of Experimental Botany **61**, 821–829.

Schmidt R, Schippers JHM, Mieulet D, Obata T, Fernie AR, Guiderdoni E, Mueller-Roeber B. 2013. MULTIPASS, a rice R2r3-type Myb transcription factor, regulates adaptive growth by integrating multiple hormonal pathways. The Plant Journal **76**, 258–273.

Schoppach R, Wauthelet D, Jeanguenin L, Sadok W. 2014. Conservative water use under high evaporative demand associated with smaller root metaxylem and limited trans-membrane water transport in wheat. Functional Plant Biology **41**, 257–269.

Sharma S, Lin W, Villamor JG, Verslues PE. 2013. Divergent low water potential response in *Arabidopsis thaliana* accessions Landsberg erecta and Shahdara. Plant, Cell & Environment **36**, 994–1008.

Singh VP, Singh RK. 2000. A sourcebook of best practices and strategies in Eastern India. Los Banos, Philippines: International Rice Research Institute.

Sun J, Rutkoski JE, Poland JA, Crossa J, Jannink J-L, Sorrells ME. 2017. Multitrait, random regression, or simple repeatability model in high-throughput phenotyping data improve genomic prediction for wheat grain yield. The Plant Genome **10**, doi: 10.3835/plantgenome2016.11.0111.

Tardieu F. 2011. Any trait or trait-related allele can confer drought tolerance: just design the right drought scenario. Journal of Experimental Botany **63**, 25–31.

Tardieu F, Cabrera-Bosquet L, Pridmore T, Bennett M. 2017. Plant phenomics, from sensors to knowledge. Current Biology **27**, R770–R783.

Technow F, Messina CD, Totir LR, Cooper M. 2015. Integrating crop growth models with whole genome prediction through approximate bayesian computation. PLoS One **10**, e0130855.

Uehlein N, Lovisolo C, Siefritz F, Kaldenhoff R. 2003. The tobacco aquaporin Ntaqp1 is a membrane CO_2 pore with physiological functions. Nature **425**, 734.

Wang C, Hu H, Qin X, Zeise B, Xu D, Rappel W-J, Boron WF, Schroeder JI. 2016. Reconstitution of CO_2 regulation of Slac1 anion channel and function of CO_2-permeable Pip2;1 aquaporin as carbonic anhydrase4 interactor. The Plant Cell **28**, 568–582.

Wang DR, Guadagno CR, Mao X, Mackay DS, Pleban JR, Baker RL, Weinig C, Jannink J-L, Ewers BE. 2019. A framework for genomics-informed ecophysiological modeling in plants. Journal of Experimental Botany **70**, 2561–2574.

Winsor CP. 1932. The Gompertz curve as a growth curve. Proceedings of the National Academy of Sciences, USA **18**, 1–8.

Yin X, Kropff MJ, Horie T, Nakagawa H, Centeno HGS, Zhu D, Goudriaan J. 1997. A model for photothermal responses of flowering in rice I. Model description and parameterization. Field Crops Research **51**, 189–200.

Zhao K, Tung C-W, Eizenga GC, *et al*. 2011. Genome-wide association mapping reveals a rich genetic architecture of complex traits in *Oryza sativa*. Nature Communications **2**, 467.

Journal of Experimental Botany, Vol. 73, No. 15 pp. 5279–5293, 2022
https://doi.org/10.1093/jxb/erac156 Advance Access Publication 16 April 2022

RESEARCH PAPER

Physiological and genetic control of transpiration efficiency in African rice, *Oryza glaberrima* Steud

Pablo Affortit[1,†], Branly Effa-Effa[1,2,†], Mame Sokhatil Ndoye[1,3], Daniel Moukouanga[1], Nathalie Luchaire[4], Llorenç Cabrera-Bosquet[4], Maricarmen Perálvarez[5], Raphaël Pilloni[1], Claude Welcker[4], Antony Champion[1], Pascal Gantet[1], Abdala Gamby Diedhiou[6], Baboucarr Manneh[7], Ricardo Aroca[5], Vincent Vadez[1,3,8,9], Laurent Laplaze[1,8], Philippe Cubry[1] and Alexandre Grondin[1,3,8,*]

[1] DIADE, Université de Montpellier, IRD, CIRAD, Montpellier, France
[2] CENAREST, Libreville, Gabon
[3] CERAAS, Thiès, Senegal
[4] LEPSE, Université de Montpellier, INRAE, Institut Agro, Montpellier, France
[5] CSIC, Granada, Spain
[6] Université Cheikh Anta Diop, Dakar, Senegal
[7] AfricaRice center, Saint-Louis, Senegal
[8] LMI LAPSE, Dakar, Senegal
[9] ICRISAT, Patancheru, India

† These authors contributed equally to this work.
* Correspondence: alexandre.grondin@ird.fr

Received 28 November 2021; Editorial decision 6 April 2022; Accepted 13 April 2022

Editor: Michela Janni, National Research Council, Italy

Abstract

Improving crop water use efficiency, the amount of carbon assimilated as biomass per unit of water used by a plant, is of major importance as water for agriculture becomes scarcer. In rice, the genetic bases of transpiration efficiency, the derivation of water use efficiency at the whole-plant scale, and its putative component trait transpiration restriction under high evaporative demand remain unknown. These traits were measured in 2019 in a panel of 147 African rice (*Oryza glaberrima*) genotypes known to be potential sources of tolerance genes to biotic and abiotic stresses. Our results reveal that higher transpiration efficiency is associated with transpiration restriction in African rice. Detailed measurements in a subset of highly contrasted genotypes in terms of biomass accumulation and transpiration confirmed these associations and suggested that root to shoot ratio played an important role in transpiration restriction. Genome wide association studies identified marker-trait associations for transpiration response to evaporative demand, transpiration efficiency, and its residuals, with links to genes involved in water transport and cell wall patterning. Our data suggest that root–shoot partitioning is an important component of transpiration restriction that has a positive effect on transpiration efficiency in African rice. Both traits are heritable and define targets for breeding rice with improved water use strategies.

Keywords: Genome-wide association study, high-throughput phenotyping, rice, roots, transpiration

Introduction

Rice is the staple food for more than half the world's population and its consumption is continuously growing. In Africa, rice is mainly cultivated in the western part of the continent, where its production increased by 104.3% from 2009 to 2019 (FAO, 2021). A further increase of 79.4% will be needed by 2025 to meet the projected local demand (FAO, 2021). In West Africa, improving rice productivity is challenged by poor water management (Katic *et al.*, 2013), a phenomenon that is amplified by the dryer and hotter climates brought about by climate change (van Oort and Zwart, 2018). In this context, developing agronomic approaches for more efficient water management (e.g. aerobic rice or alternate wet and dry cultivation) and rice varieties with better water use efficiency (WUE) are of major interest.

WUE corresponds to the ratio of plant carbon gain to water use (Leakey *et al.*, 2019). Beneath this simple definition lie a number of component traits (root water uptake or photosynthesis for instance) and numerous surrogate traits (e.g. carbon isotope discrimination or specific leaf area) making WUE a broad idea that can be conceptualized at multiple scales (Hatfield and Dold, 2019). At the plant scale, WUE is described as transpiration efficiency (TE), i.e. the ratio between biomass (usually shoot biomass) and total water transpired to produce this biomass (Vadez *et al.*, 2014). Heritable variations in TE have been observed in a number of species including Arabidopsis (Vasseur *et al.*, 2014), sorghum (Vadez *et al.*, 2011), groundnut (Vadez and Ratnakumar, 2016), and foxtail millet (Krishnamurthy *et al.*, 2016; Feldman *et al.*, 2018). In rice, genetic determinants of intrinsic WUE measured through carbon isotope discrimination have been observed (This *et al.*, 2010), but although genetic variation in TE exists (Ouyang *et al.*, 2017), genetic dissection of TE has not been reported. Enhanced expression of several genes involved in diverse physiological mechanisms, such as gibberellin-plant mediated architecture modifications (*OsGA2*; Lo *et al.*, 2017), promotion of lateral root initiation (*OsHVA1*; Chen *et al.*, 2015), reduced stomatal density (*AtERECTA*; Shen *et al.*, 2015), and promotion of photosynthesis assimilation in mesophyll cells (*AtHARDY*; Karaba *et al.*, 2007), specifically improved TE under irrigated conditions in rice, highlighting the complexity of this trait.

Transpiration restriction is another physiological mechanism that can improve TE (Sinclair *et al.*, 2017). For the plant, this strategy translates into opening its stomata and maximizing C assimilation when the vapor pressure deficit (VPD) in the air is below a certain threshold (usually between 1.5 and 2.5 kPa), and closing its stomata when VPD exceeds this threshold resulting in lower stomatal conductance and consequently reduced water use (Condon, 2020). Transpiration restriction can be measured by the slope of the transpiration response to increasing VPD or by the inflection point in transpiration response (usually inversely correlated with the slope). Large genetic variations in transpiration response to increasing VPD have been observed in maize (Gholipoor *et al.*, 2013), wheat (Medina *et al.*, 2019), sorghum (Choudhary and Sinclair, 2014; Choudhary *et al.*, 2020), and pearl millet (Kholová *et al.*, 2010), suggesting that this response is determined by genetic factors (Vadez *et al.*, 2014; Sinclair *et al.*, 2017). In pearl millet, transpiration restriction was associated with terminal drought tolerance, and quantitative trait loci (QTLs) controlling both traits were found to co-localize (Kholová et al., 2010, 2012). Although transpiration restriction can lead to reduction in biomass as observed in wheat plants grown in irrigated environments (Medina *et al.*, 2019), it can also lead to soil water conservation at vegetative stage and improve yield in pearl millet plants grown under drought stress (Vadez *et al.*, 2013). Transpiration restriction could therefore be an interesting trait to deploy for improving TE and drought tolerance of upland rice grown under dry, hot, and drought-prone environments of West Africa.

African rice (*Oryza glaberrima* Steud.) was domesticated in the inner Niger delta from a wild Sahelian ancestor, *Oryza barthii* A. Chev. (Cubry *et al.*, 2018). It is adapted to dry environments and has raised the interest of the scientific community because of its potential reservoir of tolerance genes to biotic and abiotic stresses (Wang *et al.*, 2014). Recently, high-depth re-sequencing data of 163 *O. glaberrima* genotypes originating from diverse environments in West Africa was used to infer the origin of domestication of African rice (Cubry *et al.*, 2018). This panel was further used to identify QTLs associated with flowering time, panicle architecture and resistance to *Rice yellow mottle virus*, providing insights into the adaptive variation of African rice as compared with Asian rice (Cubry *et al.*, 2020). Due to its adaptation to contrasted environments, we hypothesized that *O. glaberrima* could also be a source of interesting alleles for improving TE. To identify genomic regions controlling TE in African rice and heterotic genotypes useful for further physiological characterization and breeding, we phenotyped 147 *O. glaberrima* genotypes (amongst which 144 were fully sequenced) for shoot growth and water use dynamics to derive transpiration restriction, TE, and its residuals at 29 d after sowing. A subset of contrasted genotypes for TE were further studied to better understand the physiological determinants of these complex traits, and genome wide association studies (GWAS) allowed the dissection of their genetic bases.

Material and methods

Plant material

A panel of 147 traditional cultivated genotypes of African rice (*O. glaberrima*) that were sampled from 1974 to 2005 mainly in West Africa, with a few genotypes from East Africa, were used in this study (Cubry *et al.*, 2018). Passport data of the different genotypes with information about

country of origin, and when available, geographic position and adaptation to agroecosystem are provided in Supplementary Dataset S1.

Plant growth conditions and measurements

Large-scale phenotyping

Large-scale phenotyping of shoot growth and water use in the *O. glaberrima* panel was performed using the PhenoArch platform hosted at M3P, Montpellier Plant Phenotyping Platforms (https://www6.montpellier.inrae.fr/lepse/Plateformes-de-phenotypage/Montpellier-Plant-Phenotyping-Platforms-M3P), located at INRAE Montpellier (43°37′03.6″N; 3°51′27.9″E). Dehusked seeds were sown in biodegradable tray pots (55% white peat and 45% woodpulp, pH 5.0; Jiffy) containing a mix of fine clay (20%) and fine, blond and black (30, 10 and 40%, respectively) peats at pH 6, amended with 1.5 kg of 14–16–18 N–P–K per 25 liters (Substrat SP 15%, Klasmann). From sowing to 15 d after sowing (DAS), plants were grown under irrigated conditions in a greenhouse at the Institut de Recherche pour le Développement (IRD) in Montpellier (43°38′41.31″N; 3°51′57.3″E) under a 12h photoperiod, day temperature of 28 °C, night temperature of 25 °C and with 60–70% humidity. Fifteen days after sowing, plants were transferred to the PhenoArch greenhouse, and individual seedlings in their biodegradable pot were transplanted into 9-liter pots filled with the same soil. Plants were exposed to the same environmental conditions as in IRD facilities and grown for two more weeks under irrigated conditions (soil water potential maintained at −0.05 MPa). The experiment was arranged in a randomized complete block design with seven replications.

The PhenoArch platform was structured as a conveyor belt feeding the plants to imaging or watering units as described in Cabrera-Bosquet *et al.* (2016). The shoot imaging unit was composed of three cabins equipped with top and side RGB cameras and LED illumination. The watering units were composed of five weighing terminals and high-precision pumps that allow monitoring of the soil water content. Imaging and watering routines were sequentially performed every day from 17 to 29 DAS. Plants were further moved back to the same position and orientation in order to keep their position throughout the experiment.

Shoot biomass and leaf area were estimated daily from plant images. Briefly, RGB images were taken for each plant from 13 views (12 side views from 30° rotational difference and one top view) and pixels from each image were extracted from those of the background as described in Brichet *et al.* (2017). Plant pixels from side view images were segmented from those in the background using a combination of two threshold algorithms, a 'mean shift' method and a thresholding method. For the top view images, plant pixels were segmented from the background using a random forest algorithm. Image analysis methods were implemented in Python/OpenCV libraries, available at (https://github.com/openalea/phenomenal). Whole plant leaf area and shoot fresh weight were then estimated using calibration curves built with multiple linear regression models based on processed images against ground truth measurements of leaf area and fresh biomass (Supplementary Fig. S1).

Leaf area and daily water lost by the pot was used to measure transpiration rate. Plant daily water uptake from 17 to 29 DAS was added to calculate total water uptake. TE was measured as the ratio between shoot fresh weight and total water uptake at 29 DAS. At this date, all plants were at the vegetative stage and were producing tillers, and none had started flowering. Because shoot mass is intrinsically related to plant water use, the residuals of TE (TEr) were calculated as the genotype-specific deviation from the least squares linear regression between total water uptake and shoot fresh weight measured at 29 DAS. Reference evapotranspiration was calculated according to the Penman–Monteith formula (Zotarelli *et al.*, 2014), as a proxy for the evaporative demand. Averaged transpiration rate was then plotted against maximum reference evapotranspiration for five windows of time, i.e. at 23, 25, 26, 27, and 28 DAS for each genotype and the slope of the corresponding linear regression was calculated to evaluate transpiration response to evaporative demand (SlopeTR).

Small-scale phenotyping experiment

A subset of 10 genotypes contrasting for shoot biomass (Og_118, Og_12, Og_162, Og_61, Og_62, Og_15, Og_184, Og_185, Og_408, and Og_43) were grown at IRD in 5.5-liter pots containing a potting mixture (M2 substrate, Jiffy), receiving optimal fertilization, and under the same environmental conditions as above with five replications per genotypes. Pots were randomized and soil was well irrigated and covered with 2–3 cm of plastic beads to prevent soil evaporation. At 29 DAS, pots were transferred into an adjacent greenhouse on top of balances monitoring weight every 30 min (Phenospex Ltd). VPD was monitored and reached values around 4–5 kPa around noon. At 36 DAS, leaves were harvested to measure leaf area using a planimeter (LI-3100C, LI-COR), shoot fresh weight, and tiller number. Plant water uptake from 29 to 36 DAS was used to calculate total water uptake. The root system was carefully washed from the soil and placed, along with fresh shoots, in an oven for 3 d at 60 °C to measure root dry weight, shoot dry weight, and root to shoot ratio. TE and TEr were calculated from shoot fresh weight and total water uptake at 36 DAS as in the large-scale experiment. Transpiration profiles and features characterizing these profiles were obtained from an adapted automated pipeline developed by Kar *et al.* (2020). Leaf area measured at 36 DAS was further used to measure transpiration rate at 35 DAS, assuming marginal changes in leaf area between 35 and 36 DAS. Averaged transpiration rate for each genotype was plotted against time between 10.00 and 16.00 h, as a proxy for the evaporative demand, and the segmented R package v1.2.0 (Muggeo, 2008) was used to calculate the slope of the initial linear regression and an inflection point in the transpiration response.

Data analysis

For each plant, a non-parametric smoothing approach was used to detect outliers in the time-course of shoot fresh weight and water uptake from the large-scale phenotyping experiment (Millet *et al.*, 2021). This approach uses a *locfit()* function that fits a local regression at a set of points and a *predict()* function to interpolate this fit to other points. A confidence interval is calculated and points located outside the interval are considered as outliers.

Shoot fresh weight and total water uptake datasets were further analysed for detection of plant outliers. For this, a multi-criteria analysis with expert rules function was used (Millet *et al.*, 2021). Leaf area, shoot fresh weight, and plant height were modeled considering fixed experimental effects, and random genotypic, replicate, and spatial effects using SpATS (Spatial Analysis of Trials using Splines; Rodríguez-Álvarez *et al.*, 2015). Plants with shoot fresh weight deviations (residuals) lesser or greater than the confidence interval were considered as outliers and removed from the dataset.

Shoot fresh weight and total water uptake values were finally corrected for spatial heterogeneity in the PhenoArch greenhouse using the StatgenHTP R package (Millet *et al.*, 2021). This package is based on SpATS and provides corrected values for the considered variable by separating the genetic effect from the spatial effect at each time point.

Genome wide association studies

The *O. glaberrima* panel used in this study was previously subjected to in-depth re-sequencing to identify single nucleotide polymorphisms (SNPs) based on mapping to the *O. sativa japonica* cv. Nipponbare reference genome MSU7 (Cubry *et al.*, 2018). A total of 892 539 SNPs was identified for this panel with a genome-wide high linkage disequilibrium at short distance (0.2 for at least 150 kb) that slowly decayed (Cubry *et al.*, 2020). Missing data remaining in the SNP matrix (less than 5% of missing data

per SNP) were imputed using the *impute* function of the LEA R package v3.1.0 (Frichot and François, 2015; Gain and François, 2021).

Association between genomic polymorphisms and mean phenotypic variables was performed using a pipeline described in Cubry *et al.* (2020). In this pipeline, SNPs displaying a minimal allele frequency (frequency of the minor allele) lower than 5% are filtered out. A simple non-corrected linear model (analysis of variance, ANOVA) was performed to assess the effect of confounding factors such as relatedness and population structure on false positive rates. Two genome-wide association methods were further used: (i) a latent factor mixed model as implemented in the LFMM v2 R package that jointly estimated associations between genotype and phenotype and confounding factors (Frichot *et al.*, 2013); and (ii) an efficient mixed model analysis (EMMA) as implemented in the EMMA R package (Kang *et al.*, 2008). Population structure was corrected using four latent factors in the LFMM model and a similarity-based kinship matrix in the EMMA model (Cubry *et al.*, 2020). The results of all analyses were graphically represented as Manhattan plots and QQ plots to assess efficiency of confounding factors correction using the qqman R package v0.1.4 (Turner, 2018). A *P*-value threshold of 10^{-5} was used to select significant SNPs. Candidate genes were selected in a 150 kb region upstream and downstream of the significant SNPs by intersecting the region with the MSU7 genome annotation (Kawahara *et al.*, 2013).

Statistical analyses

Statistical analyses were performed with R version 4.0.2 (R Development Core Team, 2018) using ANOVA (aov function) to detect genotypic and environmental effects. To determine to what extent the measured traits were genetically determined, broad-sense heritability (H^2) was calculated according to Oakey *et al.* (2006) using the *inti* R package v0.4.3 (Lozano-Isla, 2021) with the following formula:

$$H^2_{\text{Cullis}} = 1 - \frac{v_{\Delta}^{-\text{BLUP}}}{2\,\sigma^2_{\text{g}}}$$

where σ^2 refers to the variance, g to the genotype, $v_{\Delta}^{-\text{BLUP}}$ to the average standard error of the genotypic best linear unbiased prediction (BLUP).

Results

Water use-related traits are highly variable and heritable in African rice

In order to measure variation in water use-related traits in *O. glaberrima*, 147 genotypes from a diversity panel were grown in the INRAE-PhenoArch high-throughput phenotyping platform where shoot growth and water uptake were monitored daily by imaging and pot weighing from 17 to 29 DAS. These data were used to calculate plant leaf area, water uptake, transpiration rate, and shoot fresh weight during the course of the experiment. Shoot biomass accumulation over time was accompanied by an increase in water uptake and better discrimination between genotypes (Fig. 1A, B). Large genotypic variation in shoot fresh weight and total water uptake was observed at 29 DAS (coefficient of variation of 31.68% and 10.17%, respectively; Table 1). Transpiration efficiency (TE) calculated from shoot fresh weight and total water uptake at 29 DAS ranged from 1.82 to 11.35 and showed a coefficient of variation of 23.89% (Table 1; Fig. 1C). Residuals representing the genotype-specific deviation from the least squares linear regression between total water uptake and shoot fresh weight measured at 29 DAS were calculated and named TEr (Supplementary Fig. S2). TEr represents the genotype-specific component of shoot biomass that is independent of water uptake or, in other words, the difference of shoot biomass produced for the same amount of water consumed. TEr varied from −5.24 to 3.34 in the panel (Table 1). Except for transpiration rate, all traits were subject to a significant genotypic effect resulting in high heritability (>0.9 for shoot fresh weight, total water uptake, and TE, and 0.7 for TEr; Supplementary Tables S1–S5; Supplementary Figs S3–S7).

In order to check the repeatability of the traits measured in the large-scale phenotyping experiment, a subset of 10 genotypes contrasting for shoot fresh weight, total water uptake, and TE were selected and used in a small-scale experiment to measure the same variables at 36 DAS. Genotypes Og_118, Og_12, Og_162, Og_61, and Og_62 had low shoot fresh weight, total water uptake and TE, while genotypes Og_15, Og_184, Og_185, Og_408, and Og_43 had high shoot fresh weight, total water uptake and TE (Supplementary Fig. S8). Shoot fresh weight and total water uptake were significantly positively correlated ($P<0.01$) between the two experiments showing their robustness between environments (Supplementary Fig. S9). Similarly, significant correlations were observed between TE measured in the large-scale and small-scale experiments ($P<0.05$; Fig. 1D).

Since transpiration response to increasing evaporative demand contributes to modulate TE, we calculated the slope of the regression between transpiration rate and maximum reference evapotranspiration at 23, 25, 26, 27, and 28 DAS in the large-scale experiment (Supplementary Fig. S10). The slope of the linear regression (SlopeTR) represents the transpiration response to increasing evaporative demand as follows: the lower the slope, the lower the genotype responds to the evaporative demand, the higher it restricts its transpiration. SlopeTR showed a coefficient of variation of 34.71% in the population and a broad-sense heritability of 0.42 (Table 1; Supplementary Fig. S11).

Overall, our data show that water use-related traits were variable and highly heritable in the *O. glaberrima* panel. These variations appeared to be conserved in a subset of genotypes across environments.

Transpiration restriction under high evaporative demand contributes to increased TE in African rice

To better understand the relationship between the different water use-related traits, we performed correlation analyses between each trait measured in the *O. glaberrima* panel. A significant positive correlation was observed between shoot fresh weight (SFW) and total water uptake (TWU; $P<0.001$; Fig. 2A) indicating that plants that grew a bigger biomass used

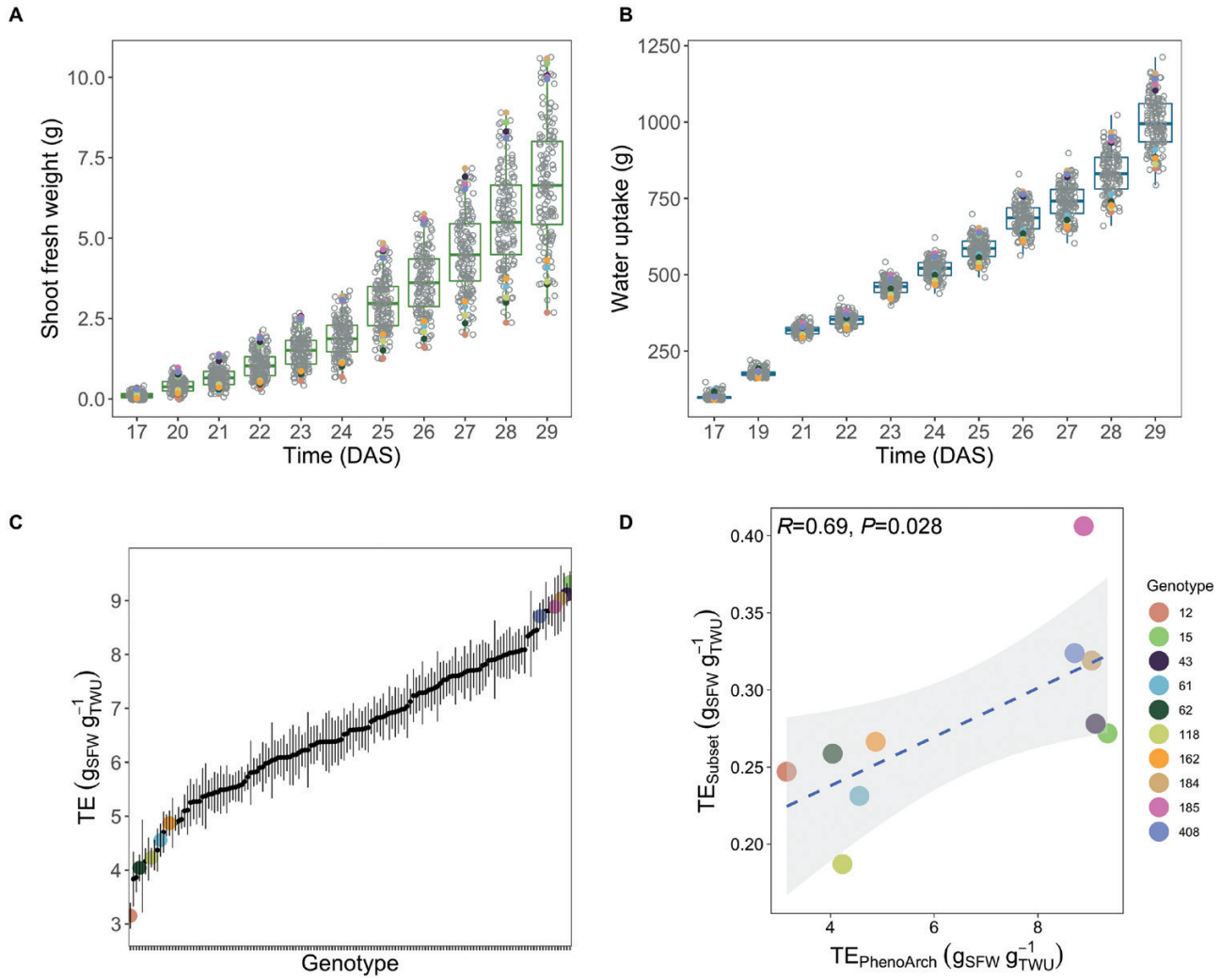

Fig. 1. Variation in shoot fresh weight, water uptake and transpiration efficiency (TE) in *O. glaberrima*. (A, B) Variation in shoot fresh weight (A) and water uptake (B) from 17 to 29 d after sowing (DAS) during the large-scale experiment. (C) Variation in TE measured as the ratio between shoot fresh weight and total water uptake at 29 DAS in the large-scale experiment. (D) Covariation between TE measured in the large-scale experiment (PhenoArch) and in a subset of genotypes in the small-scale experiment. *R*, Pearson's correlation coefficient; *P*, *P*-value of Pearson's correlation test. Genotypes from the subset are highlighted in (A–C) following the same color legend as in (D).

Table 1. Variation of water-use related traits in the *O. glaberrima* panel

Acronym	Trait	Range	Mean	SD	CV	H^2
SFW	Shoot fresh weight (g)	1.28–14.24	6.71	2.12	31.68	0.92
TWU	Total water uptake (g)	704.26–1382.86	999.1	101.6	10.17	0.88
TE	Transpiration efficiency (g SFW g^{-1} TWU)	1.82–11.35	6.60	1.58	23.89	0.91
TEr	Residuals of transpiration efficiency	–5.24 to 3.34	0.0009	1.09	126167	0.73
TR	Transpiration rate (ml water s^{-1} cm^{-2})	0.01–0.05	0.03	0.006	18.71	0.16
SlopeTR	Transpiration response to increasing evaporative demand	0.2–3.26	0.69	0.24	34.71	0.42

Range, mean, standard deviation (SD), coefficient of variation (CV), and broad-sense heritability (H^2) for shoot fresh weight (SFW), total water uptake (TWU), transpiration efficiency (TE), and residuals of transpiration efficiency (TEr) were measured at 29 d after sowing. Transpiration rate (TR) was plotted against maximum reference evapotranspiration at 23, 25, 26, 27, and 28 d after sowing and the slope of the corresponding linear regression was used to estimate transpiration response to evaporative demand (SlopeTR).

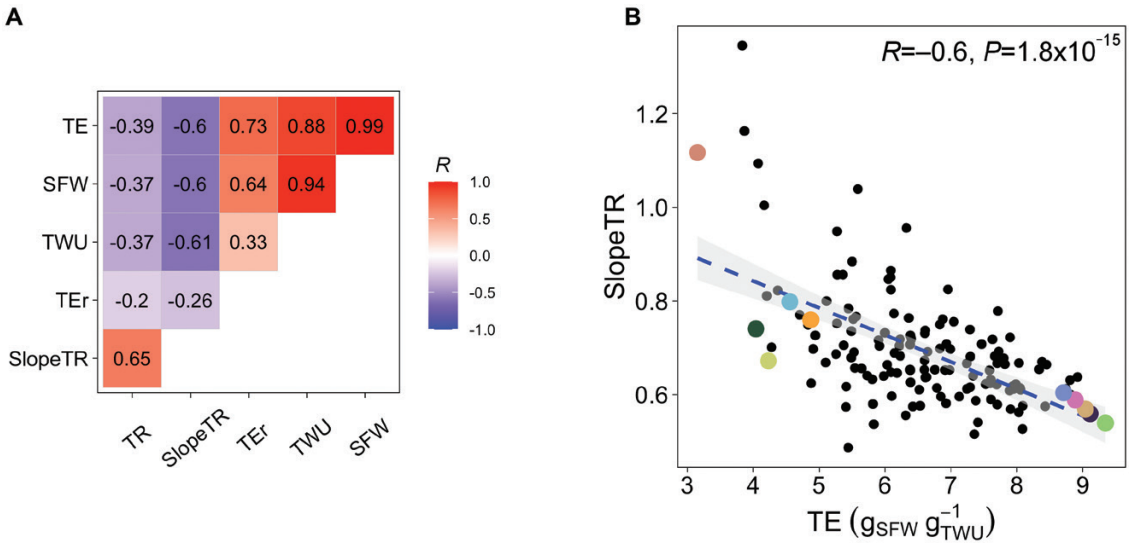

Fig. 2. Correlation between water use-related traits in *O. glaberrima*. (A) Pearson's correlation coefficient (*R*) between averaged values of shoot fresh weight (SFW), total water uptake (TWU), transpiration rate (TR), transpiration efficiency (TE), residuals of transpiration efficiency (TEr) at 29 d after sowing, and transpiration response to evaporative demand (SlopeTR) measured in the large-scale experiment. (B) Covariation between TE and SlopeTR. Circles represent the averaged TE plotted against the average SlopeTR for individual genotypes. Genotypes highlighted in color are from the subset used in the small-scale experiment, following the same color legend as in Fig. 1.

more water. Similarly, a positive significant correlation was observed between TE and both shoot fresh weight and total water uptake ($P<0.001$). On the other hand, TEr was correlated with TE ($R=0.73$) and less so with shoot fresh weight and total water uptake, although all correlations were significant ($P<0.001$; Fig. 2A). Interestingly, a significant negative correlation was observed between TE and transpiration response to evaporative demand (SlopeTR; $P<0.001$; Fig. 2B), suggesting that genotypes with lower transpiration at higher evaporative demand had higher TE. This suggests that transpiration restriction under high evaporative demand might contribute to increased TE in African rice.

To test this hypothesis, we studied the transpiration response to VPD across 1 d in the same subset of contrasted genotypes as above at 35 DAS. During this experiment, VPD gradually increased to reach its maximum around 17.00 h and further decreased (Fig. 3A). Transpiration rate followed the same pattern until 16.00 h where it reached its maximum for most of the genotypes and further decreased (Fig. 3A). Large variation in the transpiration response to VPD was observed among genotypes, with Og_185 and Og_118 having the lowest and highest maximum transpiration rate at 16.00 h (Fig. 3A). To further quantify this response, we measured the slope of transpiration response to increasing VPD and the time of transpiration inflection between 10.00 and 16.00 h (Supplementary Fig. S12). While the inflection time did not significantly vary among genotypes, significant differences were observed in the slope of transpiration response (SlopeTR; $P<0.01$; Supplementary Table S7). Principal component analyses showed that the first principal component that separated the genotypes with low shoot fresh weight from those with high shoot fresh weight accounted for 73.3% of the global variation (Fig. 3B). Genotypes with low shoot fresh weight co-varied with transpiration rate and transpiration response to evaporative demand (SlopeTR) while genotypes with higher shoot fresh weight co-varied with root dry weight, total water uptake, and TE (Fig. 3B). Transpiration response to evaporative demand (SlopeTR) was significantly negatively correlated with shoot fresh weight ($P<0.05$), total water uptake ($P<0.01$), and TE ($P<0.05$; Fig. 3C; Supplementary Fig. S13). Interestingly, the ratio of root to shoot dry weight (root:shoot ratio) was significantly positively correlated with transpiration response to evaporative demand (SlopeTR; $P<0.05$; Fig. 3D) and tended to co-vary with transpiration rate ($R=0.4$), although this co-variation was not significant (Supplementary Fig. S13).

Altogether, precise measurements of transpiration under increasing evaporative demand in the subset of genotypes confirmed that transpiration restriction at high evaporative demand (lower SlopeTR) was associated with higher TE in African rice. Our results further demonstrated that shoot biomass and the balance between root and shoot growth played important roles in the transpiration response to increasing evaporative demand.

Identification of genomic regions associated with water use-related traits by association genetics

As our data showed that water use-related traits were variable and highly heritable in the *O. glaberrima* panel, we performed association genetics to identify polymorphisms associated with their variation. Genomic regions associated with shoot fresh weight, total water uptake, TE, its residuals (TEr), and

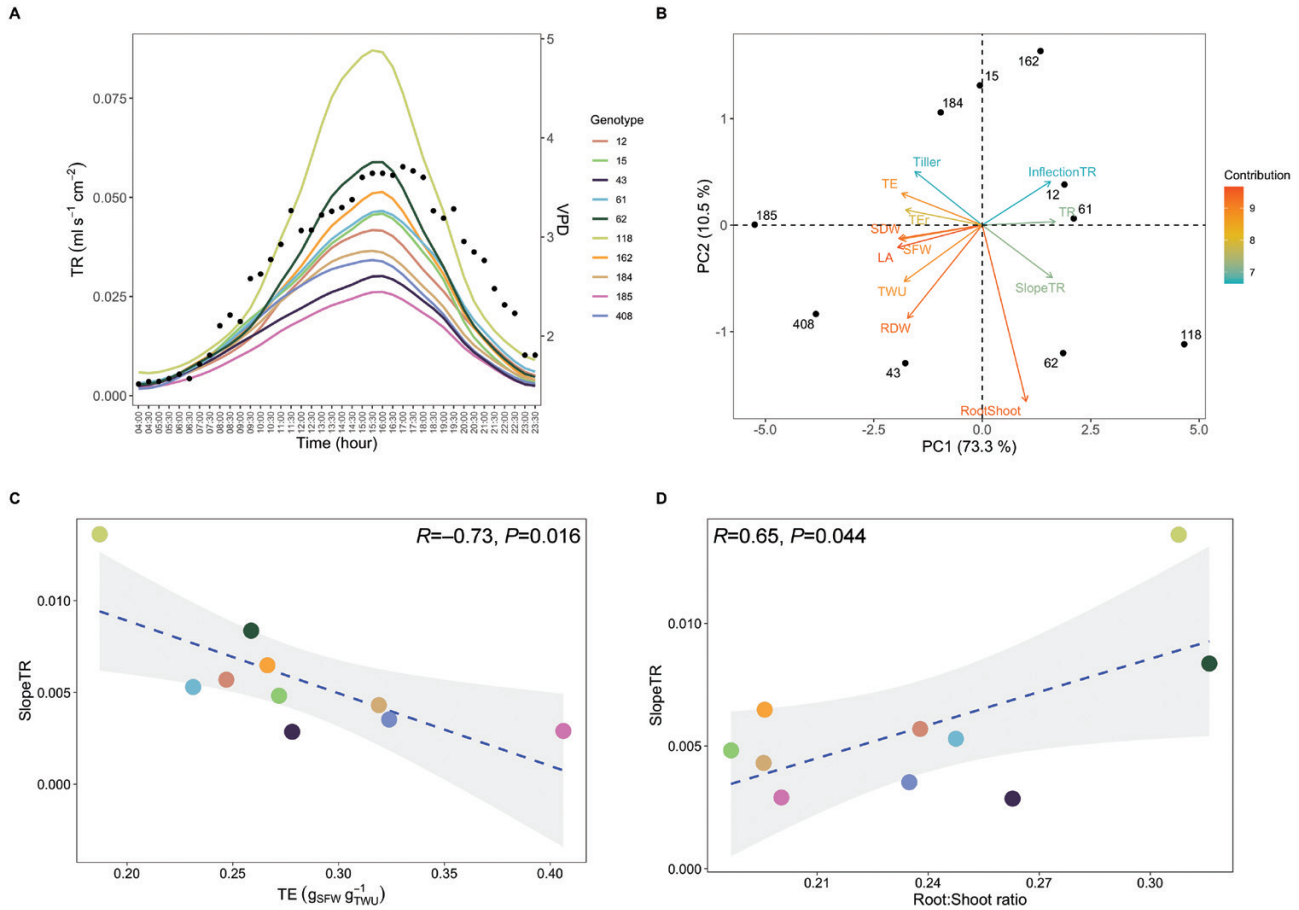

Fig. 3. Relation between water use-related traits and plant morphology in a subset of *O. glaberrima* genotypes. (A) Evolution of transpiration rate (TR; colored lines) upon increasing vapor pressure deficit (VPD; black circles) measured in the small-scale experiment at 35 d after sowing. (B) Relationship between tiller number (Tiller), transpiration efficiency (TE), residuals of transpiration efficiency (TEr), shoot fresh weight (SFW), shoot dry weight (SDW), leaf area (LA), total water uptake (TWU), root dry weight (RDW), root to shoot ratio (RootShoot), transpiration response to increasing evaporative demand (SlopeTR), TR, and TR inflection in response to increasing evaporative demand (InflectionTR) measured at 35 d after sowing in the small-scale experiment, and analysed using principal component (PC) analysis. (C, D) Covariation between TE and SlopeTR (C) and between root to shoot ratio and SlopeTR (D). Circles represent the averaged TE or root to shoot ratio plotted against the average SlopeTR for individual genotypes. *R*, Pearson's correlation coefficient; *P*, *p*-value of Pearson's correlation test. Color legend is the same as in (A).

transpiration response to increasing evaporative demand (SlopeTR) were identified using two GWAS methods (LFMM and EMMA). Applying a 10^{-5} *P*-value threshold, we observed a total of 42, 59, 49, 95, and 29 significant marker-trait associations in both methods for shoot fresh weight, total water uptake, TE, TEr, and SlopeTR, respectively (Figs 4A–D, 5A; Supplementary Figs S14A–D, S15A). The two methods allowed an efficient correction for false positives linked to genetic structure (QQ plots, Figs 4E–F, 5B; Supplementary Figs S14E–F, S15B).

Significant associations were observed for shoot fresh weight and TE on chromosome 5, and for shoot fresh weight and total water uptake on chromosome 6 using both LFMM and EMMA methods (Fig. 4; Supplementary Fig. S14). Further significant associations were observed with LFMM on chromosome 1 for total water uptake ($-\log_{10}(P)$=4.63 in EMMA; Fig. 4B; Supplementary Fig. S14B) and on chromosome 7 for TE ($-\log_{10}(P)$=3.89 in EMMA; Fig. 4C; Supplementary Fig. S14C). Although not significant, similar associations were observed on chromosome 1 for shoot fresh weight and chromosome 7 for shoot fresh weight and TEr in LFMM (Fig. 4A, D). More specific associations were observed for TEr on chromosome 1 in LFMM and EMMA and on chromosome 4 in EMMA ($-\log_{10}(P)$=3.73 in LFMM; Fig. 4D; Supplementary Fig. S14D). For transpiration response to evaporative demand (SlopeTR), the two most significant associations were observed on chromosome 2 and 11 in both LFMM and EMMA (Fig. 5A; Supplementary Fig. S15A).

Interestingly, the GWAS association located on chromosome 5 position 26971730 for shoot fresh weight and TE co-localized with a previously reported QTL for early vigor in Asian rice (*Oryza sativa*; Cui *et al.*, 2002). Two alleles were present for the corresponding SNP with plants carrying either an adenine (A; 45.5% of the panel) or a guanidine (G; 54.5% of the panel),

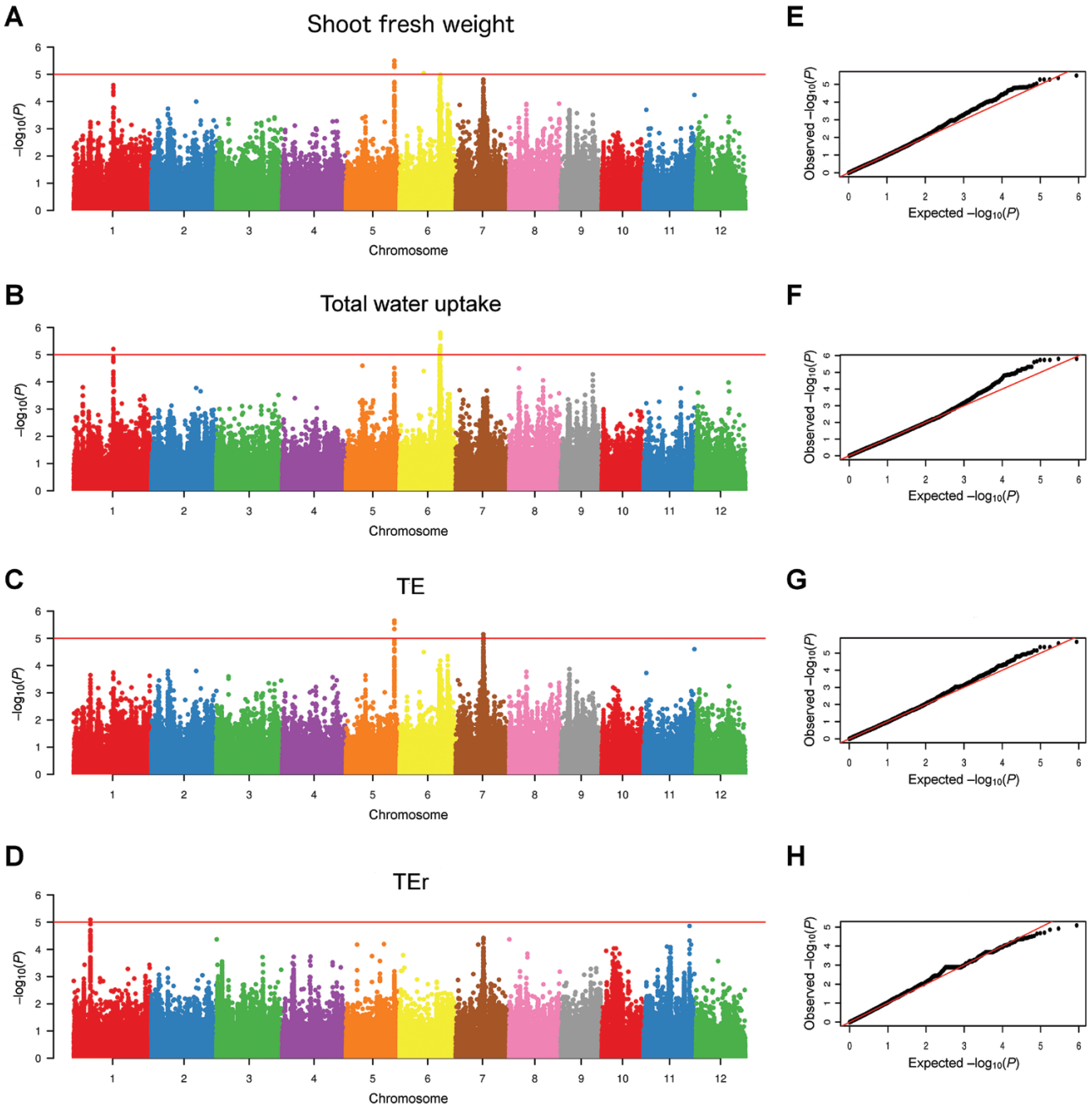

Fig. 4. Genome wide association studies for shoot fresh weight, total water uptake, transpiration efficiency (TE), and residuals of transpiration efficiency (TEr) in *O. glaberrima*. Manhattan plots (A–D) and QQ plots (E–H) obtained with the latent factor mixed model (LFMM) are shown. Manhattan plots show the log10 *P*-value (*y*-axis) at each SNP position on the different chromosomes (*x*-axis). The red lines in (A–D) delimit the threshold for highly significant SNPs ($P<10^{-5}$).

with plants carrying the G allele having a 25.2% shoot biomass gain (Supplementary Fig. S16). Genotypes with low shoot fresh weight (Og_12, Og_61, Og_62, Og_118, and Og_162) grown in the small-scale experiment carried the A allele while genotypes with high shoot fresh weight (Og_15, Og_43, Og_184, Og_185, Og_408) carried the G allele (Supplementary Fig. S8), confirming the allelic distribution observed in the large-scale experiment. Hence, our results confirmed the importance of this genomic region to control early shoot growth and the conservation of this QTL in Asian and African rice.

Altogether, our association genetics approach identified at least 14 potential genetic regions associated with water use-related traits in African rice, some of which are specific to TE, TEr, or transpiration response to evaporative demand.

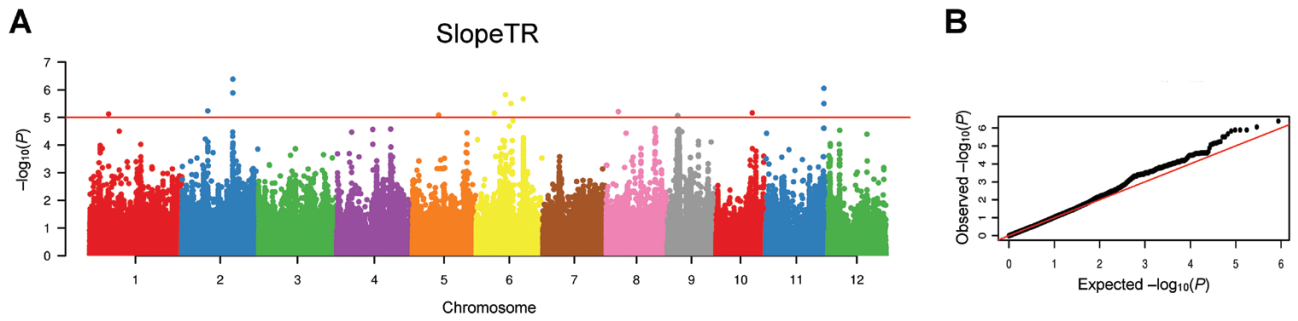

Fig. 5. Genome wide association studies for transpiration response to increasing evaporative demand in *O. glaberrima*. Manhattan plots (A) and QQ plots (B) obtained with the latent factor mixed model (LFMM) are shown. Manhattan plots show the log10 *P*-value (*y*-axis) at each SNP position on the different chromosomes (*x*-axis). The red line in (A) delimits the threshold for highly significant SNPs ($P<10^{-5}$).

Genes potentially involved in photosynthesis, regulation of water transport, and drought responses underlie associations for water use-related traits

We next analysed the genes present in genetic regions associated with shoot fresh weight, total water uptake, TE, TEr, and transpiration response to evaporative demand. Since linkage disequilibrium is high at short distance then slowly decays to values below 0.2 after around 150 kb in this panel (Cubry *et al.*, 2018, 2020), we considered genes in a 300 kb region surrounding the most significant SNP at each association peak (Table 2). The most significant SNP on chromosome 5 (position 26971730) associated with shoot fresh weight and TE mapped in an intergenic region at 1.8 kb of a gene encoding a polyprenyl synthetase and 10.2 kb of a gene encoding a Ras-related nuclear protein (RAN) GTPase-activating protein. Polyprenyl synthetase catalyses the synthesis of isopentenyl diphosphate that is involved in the biosynthesis pathway of plastoquinones, which are essential coenzymes for the photosynthesis machinery carrying electrons in the linear and alternative electron chains (Liu *et al.*, 2019; Havaux, 2020). RAN GTPases are involved in nucleocytoplasmic transport, mitotic progression, membrane trafficking, cytoskeletal organization, and cell polarity, and have important roles in plant growth, development and response to stress conditions (Nielsen, 2020). In particular, Arabidopsis RanBP1c and wheat Ran1 are involved in auxin-induced root growth and development through the control of mitotic progression (Kim *et al.*, 2001; Wang *et al.*, 2006). Heterologous overexpression of a wheat RAN GTPase in rice reduced the number of lateral roots and induced hypersensitivity to auxin (Wang *et al.*, 2006).

The GWAS peak for total water uptake on chromosome 1 (position 21989359) is located in an intergenic region at 3.5 kb of a gene coding the C-type C2H2 zinc finger protein ZOS1-10 (Table 2). C2H2-type zinc finger proteins form a large family of 189 members in rice (Agarwal *et al.*, 2007), having many roles in plant growth, development, and abiotic and biotic resistances (Han *et al.*, 2020). The rice C2H2 zinc finger protein Drought and Salt Tolerance (DST) is, for instance, involved in leaf morphology and water use through stomatal control, its loss of function increasing rice and salt tolerance (Huang *et al.*, 2009).

The most significant SNP on chromosome 7 associated with TE mapped on the 3′ untranslated region of a gene encoding an unknown protein (LOC_Os07g26595). A cluster of four Plasma membrane Intrinsic Proteins (PIPs) primarily expressed in roots are located from 47–98 kb away from this SNP (Sakurai *et al.*, 2005; Guo *et al.*, 2006). Plasma membrane aquaporins are water channels located on the plasma membrane and were described as important contributors of root radial water transport (Grondin *et al.*, 2016) and water use efficiency in rice (Nada and Abogadallah, 2014). Another interesting gene, coding for OsRR7, a type-A response regulator, is located at 130 kb from this SNP. In Arabidopsis, a type-A response regulator protein, ARR5, is phosphorylated by SnRK2s protein and amplifies the ABA-mediated stress response while inhibiting the cytokinin-responsive genes promoting growth and development (Huang *et al.*, 2018). In maize, a recent report demonstrated that natural variation in a type-A response regulator confers chilling tolerance (Zeng *et al.*, 2021).

The GWAS associations for TEr and transpiration response to evaporative demand on chromosome 1 (position 9237408 and 8982662, respectively) mapped to intergenic regions near a gene homologous to the *SUPER APICAL DOMINANT* (*SAD1*) gene encoding an ortholog of the polymerase 1 subunit RPA34.5 that plays important roles in shoot and root growth and branching in rice (Li *et al.*, 2015). Another gene, coding for a heterotrimeric Gβ protein potentially involved in the control of cell expansion via interaction with lipid metabolic pathways, was identified in the region (Choudhury *et al.*, 2019). Two genes encoding a TCP transcription factor and a glycosyltransferase were located at around 48 kb upstream and downstream of the most significant SNP associated with TEr in EMMA on chromosome 4. *THEOSINTE BRANCHED1_CYCLOIDEA_PROLIFERATING CELL FACTOR1* (*TCP*) genes are involved in leaf shape in Arabidopsis (Koyama *et al.*, 2010) and they improved agronomic traits when overexpressed in rice (Li *et al.*, 2020), while glycosyltransferase mediates the biosynthesis of prominent hemicellulose xylan (an important

Table 2. List of candidate genes identified in genetic regions associated with shoot fresh weight (SWF), total water uptake (TWU), transpiration efficiency (TE), residuals of transpiration efficiency (TEr), and transpiration response to evaporative demand (SlopeTR)

Trait	Chr_position	Locus (MSU)	Annotation	Hypothetical function	Reference
SFW, TE	Chr5_26971730	LOC_Os05g46560	RAN GTPase-activating protein 1	Auxin-mediated root development	Kim *et al.* (2001), Wang *et al.* (2006)
		LOC_Os05g46580	Polyprenyl synthetase	Photosynthesis through plastoquinone biosynthesis	Liu *et al.* (2019), Havaux (2020)
TWU	Chr1_21989359	LOC_Os01g39110	ZOS1-10 C2H2 zinc finger family protein	Drought tolerance via stomatal control	Huang *et al.* (2009)
TE	Chr7_15311728	LOC_Os07g26630 LOC_Os07g26660 LOC_Os07g26690	Plasma membrane aquaporins	Water transport and use, response to abiotic stresses	Sakurai *et al.* (2005), Guo *et al.* (2006)
		LOC_Os07g26720	OsRR7, type-A response regulator	Abiotic responses through abscisic acid and cytokinin signaling	Huang *et al.* (2018), Zeng *et al.* (2021)
TEr, SlopeTR	Chr1_9237408	LOC_Os01g16220	Sad1—UNC-like C-terminal domain	Shoot and root growth and branching	Li *et al.* (2015)
		LOC_Os01g15979	Gβ protein	Cell expansion and lipid metabolism	Choudhury *et al.* (2019)
TEr	Chr4_6544212	LOC_Os04g11830	TCP family transcription factor	Leaf development	Koyama *et al.* (2010), Li *et al.* (2020)
		LOC_Os04g12010	Glycosyltransferase	Cell wall formation	Anders *et al.* (2012), Lin *et al.* (2016)
SlopeTR	Chr2_23902475	LOC_Os02g39590	GDSL-like lipase/acylhydrolase	Cell wall formation and patterning	Zhang *et al.* (2017)

component of primary and secondary cell walls) in rice (Anders *et al.*, 2012; Lin *et al.*, 2016).

The most significant SNP on chromosome 2 (position 23902475) for transpiration response to evaporative demand is located at 9.5 kb from a gene encoding a C2H2 zinc finger protein and 8 kb from a gene encoding a GDSL-like lipase/acylhydrolase. The rice GDSL *BRITTLE LEAF SHEATH1* (*BS1*) gene was reported to play an important role in the maintenance of proper acetylation level on the xylan backbone (Zhang *et al.*, 2017). In particular, BS1 affects secondary cell wall pattern in vessels, the *bs1* mutant having larger metaxylem pit size and reduced agronomical performances (Zhang *et al.*, 2017).

Discussion

In this study, 147 *O. glaberrima* genotypes were phenotyped in a high-throughput phenotyping platform for shoot growth and water uptake dynamics at early vegetative stage. Image-based monitoring of shoot traits (fresh weight and leaf area) and gravimetric monitoring of water loss allowed us to measure shoot fresh weight, total water uptake, daily transpiration rate, and TE at 29 DAS (Fig. 1). Strong positive and significant correlations were observed between shoot fresh weight, total water uptake and TE in our study ($P<0.001$; Fig. 2A). Our results for *O. glaberrima* are in line with observations in foxtail millet (Feldman *et al.*, 2018). However, they are not consistent with the absence of correlations observed between TE and shoot biomass or total water use in sorghum or pearl millet (Vadez et al., 2011, 2013) and previous considerations that high water use efficiency is related to reduced biomass productivity and, by extension, yield (Condon *et al.*, 2002; Blum, 2009). In fact, the relationship between TE, water use, and shoot growth depends on the species, the environments or the way water use efficiency is measured (for extensive review see Vadez *et al.*, 2014). In our experimental conditions, it appears that larger and more vigorous *O. glaberrima* plants consume more water from the soil, but are relatively more efficient at producing biomass from that amount of water consumed. Interestingly, a significant negative correlation was observed between TE and transpiration rate ($P<0.001$; Fig. 2A), indicating that, although water loss by transpiration is higher in larger plants, transpiration per unit of leaf surface at the whole plant level is lower. We also measured the residuals of TE (TEr) that correspond in our study to the genotype-specific deviation from the relationship between biomass and water use, with genotypes deviating above the relationship being more efficient at using water than those deviating below the relationship. TEr was also significantly negatively correlated with transpiration rate, although the correlation coefficient was lower ($P<0.05$; Fig. 2A). These intriguing results suggest a stomatal regulation of transpiration rate in *O. glaberrima* genotypes with higher TE. We hypothesized that this regulation was linked to a transpiration restriction strategy in response to increasing evaporative demand.

To study the links between transpiration efficiency and transpiration response to increasing evaporative demand, we took a similar approach to Alvarez Prado *et al.* (2017), plotting daily transpiration rate with maximum reference evapotranspiration. Due to environmental conditions in the high-throughput experiment, the range of maximum evapotranspiration remained relatively low during the experiment (from 1.1 to 1.23). Still, the slope of this relationship was considered as a proxy of transpiration response to increasing evaporative demand. It was highly variable in *O. glaberrima* and under genetic control as illustrated by the relatively high broad-sense heritability. Interestingly, we observed a significant negative correlation between TE (and TEr to a lesser extent) and transpiration response to increasing evaporative demand (Fig. 2). These transpiration responses and correlations were further confirmed in a subset of genotypes in which transpiration responses to much larger variation in evaporative demand (from 1.5 to 3.7) were precisely measured (Fig. 3). Altogether, these results indicate that transpiration restriction in conditions of high evaporative demand was linked to improved TE in African rice. Transpiration response to evaporative demand is regarded as an important component trait of water use efficiency, particularly for crops growing in arid and drought-prone areas (Vadez *et al.*, 2014; Shekoofa and Sinclair, 2018). In pearl millet, reducing transpiration when the evaporative demand exceeds a certain threshold allowed water conservation during vegetative growth that could be used at reproductive stage to improve seed production (Vadez *et al.*, 2013). Early vigor accompanied by increased TE through transpiration restriction may be particularly advantageous for upland rice genotypes growing in rainfed agroecosystems, especially when competing against weeds or during drought stress.

Exhaustive measurements of transpiration profile under changing temperature and relative humidity over the course of the day allowing precise measurement of the transpiration restriction phenotype has often been low throughput (Gholipoor et al., 2010, 2013; Devi *et al.*, 2010; Jauregui *et al.*, 2018). To our knowledge, our study is a pioneer in reporting measurements of transpiration restriction in a crop at a throughput compatible with association genetic analyses. Recent development of an imaging platform combined with lysimetric capacity allowing monitoring of transpiration response to high VPD in natural conditions (Vadez *et al.*, 2015) and generation of transpiration profile features in an automated fashion (Kar *et al.*, 2020) will be instrumental for high-throughput phenotyping of plant water use-related traits and identification of their genetic determinants with breeding perspectives.

Roots are the primary sites of water uptake and play important roles in maintaining whole plant water status, balancing water acquisition and water flow to match shoot water demand (Maurel *et al.*, 2010; Vadez, 2014). Root traits controlling radial root conductance, including aquaporin functions (Reddy *et al.*, 2017; Sivasakthi et al., 2017, 2020; Grondin *et al.*, 2020) and apoplastic barriers (Calvo-Polanco *et al.*, 2021; Reyt *et al.*, 2021), as well as those controlling root axial conductance, including metaxylem diameter (Richards and Passioura, 1989), have been linked to water balance and plant transpiration efficiency in several crops. In this study, we observed a positive significant correlation between root to shoot ratio and transpiration response to increasing evaporative demand ($P<0.05$; Fig. 3D). Assuming that root dry weight is largely related to root surface, these results indicate that the balance between root and shoot surfaces is important for transpiration response to increasing evaporative demand. Plants with larger root surface as compared with shoot surface appeared more sensitive to the increase in evaporative demand, possibly due to the ability of the root system to maintain water acquisition in response to the increased water demands by the shoots. Our results therefore suggest that decreased carbon allocation towards the roots, and possibly decreased root surface, may be beneficial for reduced sensitivity to the increase in evaporative demand, i.e. the transpiration restriction phenotype. Further investigations are needed to determine the contribution of root architectural, anatomical, and physiological traits in the transpiration restriction phenotype. While saving water, such reduction in transpiration at the hottest hours of the day would reduce carbon fixation and cause an increase in leaf temperature that may have detrimental effects on metabolic processes (Zandalinas *et al.*, 2017). Still, in our conditions the genotypes showing transpiration restriction phenotypes were those with higher vigor and shoot biomass production at early vegetative stage. Evaluating the effect of the transpiration restriction phenotype on shoot biomass and yield during the whole crop cycle in *O. glaberrima* and how it relates to drought or heat stress tolerance would be of particular interest.

Interestingly, our GWAS approach confirmed the importance of roots in the control of TE and transpiration response to increasing evaporative demand. Indeed, we identified several genetic regions associated with these traits that contain genes potentially involved in root development or water transport. In particular, a cluster of aquaporin genes was located near the association for TE observed on chromosome 7 (Fig. 4C), amongst which LOC_Os07g26660 appears root-specific. These genes encode type-2 Plasma membrane Intrinsic Proteins that are known to play important roles in root radial water transport. Their expression has also been associated with the control of TE and transpiration restriction as they may quickly regulate root water flow to respond, or not, to changes in transpiration when the evaporative demand is increasing (Shekoofa and Sinclair, 2018). Aquaporin functions also have important roles in root and shoot growth coordination (Ehlert *et al.*, 2009; Maurel *et al.*, 2010). In fact, this GWAS association on chromosome 7 was also found for shoot fresh weight, although just below the significance threshold (Fig. 4A).

A strong marker-trait association for TE and shoot fresh weight at 29 DAS was located on chromosome 5 (Fig. 4C). This association collocated with a known QTL for early vigor identified in *O. sativa* (Cui *et al.*, 2002). This suggests that this

QTL for early vigor is conserved in Asian and African rice. An interesting candidate gene coding for a polyprenyl synthetase protein potentially involved in plastoquinone biosynthesis and more generally in photosynthesis was located close to the most significant SNP, suggesting a link between efficiency of the photosynthetic machinery and early vigor. Further work will be needed to test this exciting hypothesis.

TEr and transpiration response to increasing evaporative demand shared an association on chromosome 1 (Figs 4D, 5A) where a candidate gene potentially involved in cell wall biosynthesis was identified. This result confirms the links between these two traits and supports the hypothesis that transpiration restriction is an important component of TE in *O. glaberrima*. Another candidate gene encoding a GDSL protein possibly involved in cell wall biosynthesis was identified in close vicinity of the most significant association on chromosome 2 for transpiration response to increasing evaporative demand (Zhang *et al.*, 2017). Cell wall properties potentially play important roles in the apoplastic water flow in roots and shoots. This apoplastic path, complementary to the symplasmic path (from cell to cell through aquaporins or plasmodesmata), is supposedly predominant under increasing evaporative demand, i.e. under conditions in which transpiration restriction occurs (Tharanya *et al.*, 2018; Sivasakthi *et al.*, 2020). The effects of cell wall content and mechanical properties on plant water transport properties have been poorly studied. Simulations using a model coupling water fluxes and cell wall mechanics recently suggested that heterogeneities in cell wall mechanical parameters impacted water flow in tissues and growth rate (Cheddadi *et al.*, 2019). Moreover, affecting cell wall composition had significant effects on xylem vessel wall patterning in rice, which may further impact axial water flow (Zhang *et al.*, 2017).

In conclusion, high-throughput phenotyping of water use-related traits in *O. glaberrima* showed that reducing transpiration under increasing evaporative demand contributes to improved TE. The control of the transpiration response to higher evaporative demand may partly depend on the coordination between root and shoot functions, which opens interesting perspectives in the identification of root traits with integrative hydraulic functions. Association genetics analyses pointed to mechanisms linked to the control of root architecture likely through developmental processes, and water fluxes possibly through aquaporin functions or cell wall composition and patterning. Our results further show that, at an early vegetative stage, increased TE was associated with higher plant vigor. Such characteristics may be particularly interesting for breeding, for instance to improve rice adaptation to rainfed agroecosystems and enable rice to better compete with weeds for limited water resources.

Supplementary data

The following supplementary data are available at *JXB* online.

Fig. S1. Regression model used to estimate shoot fresh biomass and leaf area based on ground truth measurements.

Fig. S2. Residuals of transpiration efficiency.

Fig. S3. Histograms, QQ plots, and plots of residuals against fitted or index values for fixed (fix) or random (ran) genotypic effects on shoot fresh weight measured at 29 d after sowing in the large-scale experiment.

Fig. S4. Histograms, QQ plots, and plots of residuals against fitted or index values for fixed (fix) or random (ran) genotypic effects on total water uptake measured at 29 d after sowing in the large-scale experiment.

Fig. S5. Histograms, QQ plots, and plots of residuals against fitted or index values for fixed (fix) or random (ran) genotypic effects on transpiration efficiency measured at 29 d after sowing in the large-scale experiment.

Fig. S6. Histograms, QQ plots, and plots of residuals against fitted or index values for fixed (fix) or random (ran) genotypic effects on residuals of transpiration efficiency measured at 29 d after sowing in the large-scale experiment.

Fig. S7. Histograms, QQ plots, and plots of residuals against fitted or index values for fixed (fix) or random (ran) genotypic effects on transpiration rate measured at 29 d after sowing in the large-scale experiment.

Fig. S8. Water use-related traits in the subset of *O. glaberrima* genotypes.

Fig. S9. Correlation between water use-related traits measured in the large-scale experiment at 29 d after sowing (PhenoArch) and in the small-scale experiment at 35 d after sowing (Subset).

Fig. S10. Transpiration response to increasing evaporative demand.

Fig. S11. Histograms, QQ plots, and plots of residuals against fitted or index values for fixed (fix) or random (ran) genotypic effects on transpiration response to increasing evaporative demand (SlopeTR) measured in the large-scale experiment.

Fig. S12. Transpiration response to increasing evaporative demand in the subset of *O. glaberrima* genotypes.

Fig. S13. Correlation between water use-related traits and plant morphology in a subset of *O. glaberrima* genotypes.

Fig. S14. Genome wide association studies for shoot fresh weight, total water uptake, transpiration efficiency (TE), and residuals of transpiration efficiency (TEr) in *O. glaberrima*.

Fig. S15. Genome wide association studies for transpiration response to increasing evaporative demand in *O. glaberrima*.

Fig. S16. Repartition of shoot fresh weight according to the allelic version at the most significant SNP (Chr5_26971730) for the GWAS association on chromosome 5.

Table S1. Analysis of variance for shoot fresh weight (SFW) measured at 29 d after sowing in *O. glaberrima* in the large-scale experiment.

Table S2. Analysis of variance for total water uptake (TWU) measured at 29 d after sowing in *O. glaberrima* in the large-scale experiment.

Table S3. Analysis of variance for transpiration efficiency (TE) measured at 29 d after sowing in *O. glaberrima* in the large-scale experiment.

Table S4. Analysis of variance for residuals of transpiration efficiency (TEr) measured at 29 d after sowing in *O. glaberrima* in the large-scale experiment.

Table S5. Analysis of variance for transpiration rate (TR) measured at 29 d after sowing in *O. glaberrima* in the large-scale experiment.

Table S6. Analysis of variance for transpiration response to increasing evaporative demand (SlopeTR) measured in *O. glaberrima* in the large-scale experiment.

Table S7. Transpiration response (SlopeTR) and inflection in transpiration rate (InflectionTR) under increasing evaporative demand measured in the subset of *O. glaberrima* genotypes in the small-scale experiment.

Dataset S1: Passport data of the different *O. glaberrima* genotypes. List of genotypes used in this study with accession numbers from different databases, country of origin and, when available, geographic position of the sampling with adaptation to agroecosystem.

Acknowledgements

We are grateful to Harold Chrestin and Laurence Albar (IRD) for providing seeds of the *O. glaberrima* genotypes, to Gabriel Quiroga García (CISC, Spain), Romane Le Roy (INRAE, France), and all the PhenoArch staff for the technical support, to Emilie Millet (Wageningen University, Netherlands) for her kind support in the PhenoArch data analyses, to all the *Cereal Root Systems* team of UMR DIADE and to Soumyashree Kar (Indian Institute of Technology, India) for her kind support on the data analysis of the Phenospex experiment.

Author contributions

LCB, CW, AC, PG, AGD, BM, RA, VV, LL, PC, and AG designed the study. PA, BEE, DM, MSN, MP, NL, and LCB performed the experiments with help from all co-authors. PA, BEE, MSN, NL, RP, LCB, VV, LL, PC, and AG analysed the data. AG, PC, LCB, LL, and VV wrote the first draft of the manuscript, which was edited and approved by all co-authors.

Conflict of interest

The authors have no conflicts to declare.

Funding

This work was supported by the Institut de Recherche pour le Développement, the CGIAR Research Program (CRP) on rice-agrifood systems (RICE, 2017-2022) and the Agence Nationale de la Recherche (grant ANR-17-MPGA-0011 to VV). Financial support by the Access to Research Infrastructures activity in the Horizon 2020 Programme of the EU (EPPN^{2020} Grant Agreement 731013) is gratefully acknowledged. PA was supported by a doctoral fellowship from the French Ministry of Higher Education. BEE was supported by the Centre National de la Recherche Scientifique et Technologique of Gabon. The authors acknowledge the IRD iTrop HPC (South Green Platform) at IRD Montpellier for providing HPC resources (https://bioinfo.ird.fr, http://www.southgreen.fr).

Data availability

The data supporting the findings of this study are available from the corresponding author upon request.

References

Agarwal P, Arora R, Ray S, Singh AK, Singh VP, Takatsuji H, Kapoor S, Tyagi AK. 2007. Genome-wide identification of C2H2 zinc-finger gene family in rice and their phylogeny and expression analysis. Plant Molecular Biology **65**, 467–485.

Alvarez Prado S, Cabrera-Bosquet L, Grau A, Coupel-Ledru A, Millet EJ, Welcker C, Tardieu F. 2017. Phenomics allows identification of genomic regions affecting maize stomatal conductance with conditional effects of water deficit and evaporative demand. Plant, Cell and Environment **41**, 314–326.

Anders N, Wilkinson MD, Lovegrove A, *et al*. 2012. Glycosyl transferases in family 61 mediate arabinofuranosyl transfer onto xylan in grasses. Proceedings of the National Academy of Sciences, USA **109**, 989–993.

Blum A. 2009. Effective use of water (EUW) and not water-use efficiency (WUE) is the target of crop yield improvement under drought stress. Field Crops Research **112**, 119–123.

Brichet N, Fournier C, Turc O, Strauss O, Artzet S, Pradal C, Welcker C, Tardieu F, Cabrera-Bosquet L. 2017. A robot-assisted imaging pipeline for tracking the growths of maize ear and silks in a high-throughput phenotyping platform. Plant Methods **13**, 96.

Cabrera-Bosquet L, Fournier C, Brichet N, Welcker C, Suard B, Tardieu F. 2016. High-throughput estimation of incident light, light interception and radiation-use efficiency of thousands of plants in a phenotyping platform. New Phytologist **212**, 269–281.

Calvo-Polanco M, Ribeyre Z, Dauzat M, *et al*. 2021. Physiological roles of Casparian strips and suberin in the transport of water and solutes. New Phytologist **232**, 2295–2307.

Cheddadi I, Génard M, Bertin N, Godin C. 2019. Coupling water fluxes with cell wall mechanics in a multicellular model of plant development. PLoS Computational Biology **15**, e1007121.

Chen YS, Lo SF, Sun PK, Lu CA, Ho THD, Yu SM. 2015. A late embryogenesis abundant protein HVA1 regulated by an inducible promoter enhances root growth and abiotic stress tolerance in rice without yield penalty. Plant Biotechnology Journal **13**, 105–116.

Choudhary S, Guha A, Kholova J, Pandravada A, Messina CD, Cooper M, Vadez V. 2020. Maize, sorghum, and pearl millet have highly contrasting species strategies to adapt to water stress and climate change-like conditions. Plant Science **295**, 110297.

Choudhary S, Sinclair TR. 2014. Hydraulic conductance differences among sorghum genotypes to explain variation in restricted transpiration rates. Functional Plant Biology **41**, 270–275.

Choudhury SR, Marlin MA, Pandey S. 2019. The role of Gβ protein in controlling cell expansion via potential interaction with lipid metabolic pathways. Plant Physiology **179**, 1159–1175.

Condon AG. 2020. Drying times: Plant traits to improve crop water use efficiency and yield. Journal of Experimental Botany **71**, 2239–2252.

Condon AG, Richards RA, Rebetzke GJ, Farquhar GD. 2002. Improving intrinsic water-use efficiency and crop yield. Crop Science **42**, 122–131.

Cubry P, Pidon H, Ta KN, *et al.* 2020. Genome wide association study pinpoints key agronomic QTLs in African rice *Oryza glaberrima*. Rice **13**, 66.

Cubry P, Tranchant-Dubreuil C, Thuillet AC, *et al*. 2018. The rise and fall of African rice cultivation revealed by analysis of 246 new genomes. Current Biology **28**, 2274–2282.e6.

Cui KH, Peng SB, Xing YZ, Xu CG, Yu SB, Zhang Q. 2002. Molecular dissection of seedling-vigor and associated physiological traits in rice. Theoretical and Applied Genetics **105**, 745–753.

Devi MJ, Sinclair TR, Vadez V. 2010. Genotypic variation in peanut for transpiration response to vapor pressure deficit. Crop Science **50**, 191–196.

Ehlert C, Maurel C, Tardieu F, Simonneau T. 2009. Aquaporin-mediated reduction in maize root hydraulic conductivity impacts cell turgor and leaf elongation even without changing transpiration. Plant Physiology **150**, 1093–1104.

FAO. 2021. FAOSTAT. Rome: Food and Agriculture Organization of the United Nations. http://www.fao.org/faostat/en/#data.

Feldman MJ, Ellsworth PZ, Fahlgren N, Gehan MA, Cousins AB, Baxter I. 2018. Components of water use efficiency have unique genetic signatures in the model C_4 grass *Setaria*. Plant Physiology **178**, 699–715.

Frichot E, François O. 2015. LEA: An R package for landscape and ecological association studies. Methods in Ecology and Evolution **6**, 925–929.

Frichot E, Schoville SD, Bouchard G, François O. 2013. Testing for associations between loci and environmental gradients using latent factor mixed models. Molecular Biology and Evolution **30**, 1687–1699.

Gain C, François O. 2021. LEA 3: Factor models in population genetics and ecological genomics with R. Molecular Ecology Resources **21**, 2738–2748.

Gholipoor M, Choudhary S, Sinclair TR, Messina CD, Cooper M. 2013. Transpiration response of maize hybrids to atmospheric vapour pressure deficit. Journal of Agronomy and Crop Science **199**, 155–160.

Gholipoor M, Prasad PVV, Mutava RN, Sinclair TR. 2010. Genetic variability of transpiration response to vapor pressure deficit among sorghum genotypes. Field Crops Research **119**, 85–90.

Grondin A, Affortit P, Tranchant-Dubreuil C, de la Fuente-Cantó C, Mariac C, Gantet P, Vadez V, Vigouroux Y, Laplaze L. 2020. Aquaporins are main contributors to root hydraulic conductivity in pearl millet [*Pennisetum glaucum* (L) R. Br.]. PLoS One **15**, e0233481.

Grondin A, Mauleon R, Vadez V, Henry A. 2016. Root aquaporins contribute to whole plant water fluxes under drought stress in rice (*Oryza sativa* L.). Plant, Cell and Environment **39**, 347–365.

Guo L, Wang ZY, Lin H, *et al*. 2006. Expression and functional analysis of the rice plasma-membrane intrinsic protein gene family. Cell Research **16**, 277–286.

Han G, Lu C, Guo J, Qiao Z, Sui N, Q, iu N, Wang B. 2020. C2H2 zinc finger proteins: Master regulators of abiotic stress responses in plants. Frontiers in Plant Science **11**, 115.

Hatfield JL, Dold C. 2019. Water-use efficiency: Advances and challenges in a changing climate. Frontiers in Plant Science **10**, 103.

Havaux M. 2020. Plastoquinone in and beyond photosynthesis. Trends in Plant Science **25**, 1252–1265.

Huang XY, Chao DY, Gao JP, Zhu MZ, Shi M, Lin HX. 2009. A previously unknown zinc finger protein, DST, regulates drought and salt tolerance in rice via stomatal aperture control. Genes and Development **23**, 1805–1817.

Huang X, Hou L, Meng J, You H, Li Z, Gong Z, Yang S, Shi Y. 2018. The antagonistic action of abscisic acid and cytokinin signaling mediates drought stress response in *Arabidopsis*. Molecular Plant **11**, 970–982.

Jauregui I, Rothwell SA, Taylor SH, Parry MAJ, Carmo-Silva E, Dodd IC. 2018. Whole plant chamber to examine sensitivity of cereal gas exchange to changes in evaporative demand. Plant Methods **14**, 97.

Kang HM, Zaitlen NA, Wade CM, Kirby A, Heckerman D, Daly MJ, Eskin E. 2008. Efficient control of population structure in model organism association mapping. Genetics **178**, 1709–1723.

Kar S, Tanaka R, Korbu LB, Kholová J, Iwata H, Durbha SS, Adinarayana J, Vadez V. 2020. Automated discretization of 'transpiration restriction to increasing VPD' features from outdoors high-throughput phenotyping data. Plant Methods **16**, 140.

Karaba A, Dixit S, Greco R, Aharoni A, Trijatmiko KR, Marsch-Martinez N, Krishnan A, Nataraja KN, Udayakumar M, Pereira A. 2007. Improvement of water use efficiency in rice by expression of *HARDY*, an *Arabidopsis* drought and salt tolerance gene. Proceedings of the National Academy of Sciences, USA **104**, 15270–15275.

Katic PG, Namara RE, Hope L, Owusu E, Fujii H. 2013. Rice and irrigation in West Africa: achieving food security with agricultural water management strategies. Water Resources and Economics **1**, 75–92.

Kawahara Y, Bastide M, De Hamilton JP, *et al*. 2013. Improvement of the *Oryza sativa* Nipponbare reference genome using next generation sequence and optical map data. Rice **6**, 4.

Kholová J, Hash CT, Kumar PL, Yadav RS, Kocová M, Vadez V. 2010. Terminal drought-tolerant pearl millet [*Pennisetum glaucum* (L.) R. Br.] have high leaf ABA and limit transpiration at high vapour pressure deficit. Journal of Experimental Botany **61**, 1431–1440.

Kholová J, Nepolean T, Tom Hash C, *et al*. 2012. Water saving traits co-map with a major terminal drought tolerance quantitative trait locus in pearl millet [*Pennisetum glaucum* (L.) R. Br.]. Molecular Breeding **30**, 1337–1353.

Kim SH, Arnold D, Lloyd A, Roux SJ. 2001. Antisense expression of an Arabidopsis Ran binding protein renders transgenic roots hypersensitive to auxin and alters auxin-induced root growth and development by arresting mitotic progress. The Plant Cell **13**, 2619–2630.

Koyama T, Mitsuda N, Seki M, Shinozaki K, Ohme-Takagi M. 2010. TCP transcription factors regulate the activities of ASYMMETRIC LEAVES1 and miR164, as well as the auxin response, during differentiation of leaves in *Arabidopsis*. The Plant Cell **22**, 3574–3588.

Krishnamurthy L, Upadhyaya HD, Kashiwagi J, Purushothaman R, Dwivedi SL, Vadez V. 2016. Variation in drought-tolerance components and their interrelationships in the minicore collection of finger millet germplasm. Crop Science **56**, 1914–1926.

Leakey ADB, Ferguson JN, Pignon CP, Wu A, Jin Z, Hammer GL, Lobell DB. 2019. Water use efficiency as a constraint and target for improving the resilience and productivity of C_3 and C_4 crops. Annual Review of Plant Biology **70**, 781–808.

Li W, Chen G, Xiao G, *et al*. 2020. Overexpression of TCP transcription factor OsPCF7 improves agronomic trait in rice. Molecular Breeding **40**, 48.

Li W, Yoshida A, Takahashi M, Maekawa M, Kojima M, Sakakibara H, Kyozuka J. 2015. SAD1, an RNA polymerase I subunit A34.5 of rice, interacts with Mediator and controls various aspects of plant development. The Plant Journal **81**, 282–291.

Liu M, Ma Y, Du Q, Hou X, Wang M, Lu S. 2019. Functional analysis of polyprenyl diphosphate synthase genes involved in plastoquinone and ubiquinone biosynthesis in *Salvia miltiorrhiza*. Frontiers in Plant Science **10**, 893.

Lin F, Manisseri C, Fagerström A, *et al*. 2016. Cell wall composition and candidate biosynthesis gene expression during rice development. Plant and Cell Physiology **57**, 2058–2075.

Lo SF, Ho THD, Liu YL, *et al*. 2017. Ectopic expression of specific GA2 oxidase mutants promotes yield and stress tolerance in rice. Plant Biotechnology Journal **15**, 850–864.

Lozano-Isla F. 2021. inti: tools and statistical procedures in plant science. R package version 0.4.3. https://CRAN.R-project.org/package=inti.

Maurel C, Simonneau T, Sutka M. 2010. The significance of roots as hydraulic rheostats. Journal of Experimental Botany **61**, 3191–3198.

Medina S, Vicente R, Nieto-Taladriz MT, Aparicio N, Chairi F, Vergara-Diaz O, Araus JL. 2019. The plant-transpiration response to vapor pressure deficit (VPD) in durum wheat is associated with differential yield performance and specific expression of genes involved in primary metabolism and water transport. Frontiers in Plant Science **9**, 1994.

Millet EJ, Rodriguez Alvarez MX, Perez Valencia DM, Sanchez I, Hilgert N, van Rossum B-J. 2021. StatgenHTP: High throughout phenotyping (HTP) data analysis. R package version 1.0.5. https://CRAN.R-project.org/package=statgenHTP.

Muggeo VMR. 2008. segmented: an R package to fit regression models with broken-line relationships. R package version 1.2.0. https://cran.r-project.org/doc/Rnews/.

Nada RM, Abogadallah GM. 2014. Aquaporins are major determinants of water use efficiency of rice plants in the field. Plant Science **227**, 165–180.

Nielsen E. 2020. The small GTPase superfamily in plants: a conserved regulatory module with novel functions. Annual Review of Plant Biology **71**, 247–272.

Oakey H, Verbyla A, Pitchford W, Cullis B, Kuchel H. 2006. Joint modeling of additive and non-additive genetic line effects in single field trials. Theoretical and Applied Genetics **113**, 809–819.

Ouyang W, Struik PC, Yin X, Yang J. 2017. Stomatal conductance, mesophyll conductance, and transpiration efficiency in relation to leaf anatomy in rice and wheat genotypes under drought. Journal of Experimental Botany **68**, 5191–5205.

Reddy PS, Tharanya M, Sivasakthi K, Srikanth M, Hash CT, Kholova J, Sharma KK, Vadez V. 2017. Molecular cloning and expression analysis of Aquaporin genes in pearl millet [*Pennisetum glaucum* (L) R. Br.] genotypes contrasting in their transpiration response to high vapour pressure deficits. Plant Science **265**, 167–176.

Reyt G, Ramakrishna P, Salas-González I, *et al*. 2021. Two chemically distinct root lignin barriers control solute and water balance. Nature Communications **12**, 2320.

Richards RA, Passioura JB. 1989. A breeding program to reduce the diameter of the major xylem vessel in the seminal roots of wheat and its effect on grain yield in rain-fed environments. Australian Journal of Agricultural Research **40**, 943–950.

Rodríguez-Álvarez MX, Lee DJ, Kneib T, Durbán M, Eilers P. 2015. Fast smoothing parameter separation in multidimensional generalized P-splines: the SAP algorithm. Statistics and Computing **25**, 941–957.

Sakurai J, Ishikawa F, Yamaguchi T, Uemura M, Maeshima M. 2005. Identification of 33 rice aquaporin genes and analysis of their expression and function. Plant and Cell Physiology **46**, 1568–1577.

Shekoofa A, Sinclair T. 2018. Aquaporin activity to improve crop drought tolerance. Cells **7**, 123.

Shen H, Zhong X, Zhao F, *et al*. 2015. Overexpression of receptor-like kinase ERECTA improves thermotolerance in rice and tomato. Nature Biotechnology **33**, 996–1003.

Sinclair TR, Devi J, Shekoofa A, Choudhary S, Sadok W, Vadez V, Riar M, Rufty T. 2017. Limited-transpiration response to high vapor pressure deficit in crop species. Plant Science **260**, 109–118.

Sivasakthi K, Tharanya M, Kholová J, Wangari Muriuki R, Thirunalasundari T, Vadez V. 2017. Chickpea genotypes contrasting for vigor and canopy conductance also differ in their dependence on different water transport pathways. Frontiers in Plant Science **8**, 1663.

Sivasakthi K, Tharanya M, Zaman-Allah M, Kholová J, Thirunalasundari T, Vadez V. 2020. Transpiration difference under high evaporative demand in chickpea (*Cicer arietinum* L.) may be explained by differences in the water transport pathway in the root cylinder. Plant Biology **22**, 769–780.

Tharanya M, Sivasakthi K, Barzana G, Kholová J, Thirunalasundari T, Vadez V. 2018. Pearl millet (*Pennisetum glaucum*) contrasting for the transpiration response to vapour pressure deficit also differ in their dependence on the symplastic and apoplastic water transport pathways. Functional Plant Biology **45**, 719–736.

This D, Comstock J, Courtois B, Xu Y, Ahmadi N, Vonhof WM, Fleet C, Setter T, McCouch S. 2010. Genetic analysis of water use efficiency in rice (*Oryza sativa* L.) at the leaf level. Rice **3**, 72–86.

Turner SD. 2018. qqman: an R package for visualizing GWAS results using QQ and manhattan plots. Journal of Open Source Software **3**, 731.

Vadez V. 2014. Root hydraulics: The forgotten side of roots in drought adaptation. Field Crops Research **165**, 15–24.

Vadez V, Kholová J, Hummel G, Zhokhavets U, Gupta SK, Hash CT. 2015. LeasyScan: A novel concept combining 3D imaging and lysimetry for high-throughput phenotyping of traits controlling plant water budget. Journal of Experimental Botany **66**, 5581–5593.

Vadez V, Kholova J, Medina S, Kakkera A, Anderberg H. 2014. Transpiration efficiency: New insights into an old story. Journal of Experimental Botany **65**, 6141–6153.

Vadez V, Kholová J, Yadav RS, Hash CT. 2013. Small temporal differences in water uptake among varieties of pearl millet (*Pennisetum glaucum* (L.) R. Br.) are critical for grain yield under terminal drought. Plant and Soil **371**, 447–462.

Vadez V, Krishnamurthy L, Hash CT, Upadhyaya HD, Borrell AK. 2011. Yield, transpiration efficiency, and water-use variations and their interrelationships in the sorghum reference collection. Crop and Pasture Science **62**, 645–655.

Vadez V, Ratnakumar P. 2016. High transpiration efficiency increases pod yield under intermittent drought in dry and hot atmospheric conditions but less so under wetter and cooler conditions in groundnut (*Arachis hypogaea* (L.)). Field Crops Research **193**, 16–23.

van Oort PAJ, Zwart SJ. 2018. Impacts of climate change on rice production in Africa and causes of simulated yield changes. Global Change Biology **24**, 1029–1045.

Vasseur F, Bontpart T, Dauzat M, Granier C, Vile D. 2014. Multivariate genetic analysis of plant responses to water deficit and high temperature revealed contrasting adaptive strategies. Journal of Experimental Botany **65**, 6457–6469.

Wang M, Yu Y, Haberer G, *et al*. 2014. The genome sequence of African rice (*Oryza glaberrima*) and evidence for independent domestication. Nature Genetics **46**, 982–988.

Wang X, Xu Y, Han Y, Bao S, Du J, Yuan M, Xu Z, Chong K. 2006. Overexpression of *RAN1* in rice and Arabidopsis alters primordial meristem, mitotic progress, sensitivity to auxin. Plant Physiology **140**, 91–101.

Zandalinas SI, Mittler R, Balfagón D, Arbona V, Gómez-Cadenas A. 2017. Plant adaptations to the combination of drought and high temperatures. Physiologia Plantarum **162**, 2–12.

Zeng R, Li Z, Shi Y, Fu D, Yin P, Cheng J, Jiang C, Yang S. 2021. Natural variation in a type-A response regulator confers maize chilling tolerance. Nature Communications **12**, 4713.

Zhang B, Zhang L, Li F, Zhang D, Liu X, Wang H, Xu Z, Chu C, Zhou Y. 2017. Control of secondary cell wall patterning involves xylan deacetylation by a GDSL esterase. Nature Plants **3**, 17017.

Zotarelli L, Dukes MD, Romero CC, Migliaccio KW, Morgan KT. 2014. Step by step calculation of the Penman–Monteith evapotranspiration (FAO-56 Method). Gainesville: University of Florida Institute of Food and Agricultural Sciences. https://edis.ifas.ufl.edu/pdf/AE/AE45900.pdf

Plant Biology

Glutaredoxin regulation of primary root growth confers early drought stress tolerance in pearl millet

Reviewed Preprint

Published from the original preprint after peer review and assessment by eLife.

About eLife's process

Reviewed preprint posted
31 May 2023 (this version)

Posted to bioRxiv
3 February 2023

Sent for peer review
1 February 2023

Carla de la Fuente, Alexandre Grondin, Bassirou Sine, Marilyne Debieu, Christophe Belin, Amir Hajjarpoor, Jonathan A. Atkinson, Sixtine Passot, Marine Salson, Julie Orjuela, Christine Tranchant-Dubreuil, Jean-Rémy Brossier, Maxime Steffen, Charlotte Morgado, Hang Ngan Dinh, Bipin K. Pandey, Julie Darmau, Antony Champion, Anne- Sophie Petitot, Celia Barrachina, Marine Pratlong, Thibault Mounier, Pascal Gantet, Prakash Gangashetty, Yann Guédon, Vincent Vadez, Jean-Philippe Reichheld, Malcolm J. Bennett, Ndjido Kane, Soazig Guyomarc'h, Darren M. Wells, Yves Vigouroux, Laurent Laplaze

DIADE, Université de Montpellier, IRD, CIRAD, Montpellier, France • LMI LAPSE, Dakar, Senegal • CERAAS, ISRA, Thies, Senegal • LGDP, Université de Perpignan, Perpignan, France • School of Biosciences, University of Nottingham, Sutton Bonington, UK • Montpellier GenomiX, Montpellier, France • Be More Specific, Montpellier, France • ICRISAT, Hyderabad, India • AGAPi, Université de Montpellier, CIRAD, INRAE, SupAgroM, Montpellier, France • LGDP, CNRS, Perpignan, France

Abstract

Seedling root traits impact plant establishment under challenging environments. Pearl millet is one of the most heat and drought tolerant cereal crops that provides a vital food source across the sub-Saharan Sahel region. Pearl millet's early root system features a single fast-growing primary root which we hypothesize is an adaptation to the Sahelian climate. Using crop modelling, we demonstrate that early drought stress is an important constraint in agrosystems in the Sahel where pearl millet was domesticated. Furthermore, we show that increased pearl millet primary root growth is correlated with increased early water stress tolerance in field conditions. Genetics including GWAS and QTL approaches identify genomic regions controlling this key root trait. Combining gene expression data, re-sequencing and re- annotation of one of these genomic regions identified a glutaredoxin-encoding gene *PgGRXC9* as the candidate stress resilience root growth regulator. Functional characterization of its closest Arabidopsis homolog *AtROXY19* revealed a novel role for this glutaredoxin (GRX) gene clade in regulating cell elongation. In summary, our study suggests a conserved function for GRX genes in conferring root cell elongation and enhancing resilience of pearl millet to its Sahelian environment.

eLife assessment

This is an **important** paper that combines methods ranging from agronomy and plant breeding to Arabidopsis functional genetics, to construct a plausible argument that polymorphism in a single gene affects crop yield by affecting root cell elongation and drought stress resilience in a poorly studied crop. The overall argument is plausible but rests on a diverse set of claims that are supported by **solid**, but also partly **incomplete** evidence.

Introduction

Pearl millet was domesticated about 4,500 years ago in the Sahelian part of West Africa (Burgarella et al., 2018) and is one of the most heat and drought tolerant cereal crops (Debieu et al., 2017; Varshney et al., 2017). Today, it is the sixth cereal in terms of world production, and it is mostly cultivated in arid regions of sub-Saharan Africa and India where it plays an important role for food security. However, in Africa, pearl millet yield remains low compared to its genetic potential because it is mostly cultivated in marginal lands in low-input and rainfed agricultural systems and the development and adoption of improved varieties is still limited (Olodo et al., 2020).

The plant root system is responsible for water and nutrient acquisition from the soil. Breeding for root traits that could improve the crop root system efficiency has been proposed as one of the pillars of a second green revolution (Den Herder et al., 2010; (Lynch, 2019), (2007)). Improved crops with optimized soil resources acquisition might be particularly relevant in low input and rainfed agrosystems found in the Sahelian region of Africa (Ndoye et al., 2022). This strategy relies on the selection of root traits suitable for the specific characteristics of the target environment such as soil and climate but also agricultural practices (Lynch, 2019; Ndoye et al., 2022; van der Bom et al., 2020). It requires a better understanding of stress patterns and the performance of individual root traits in real conditions and in response to different constraints. However, only a few studies have addressed the importance of individual root traits in field conditions.

Primary root development is an important contributor to seedling vigor and greatly influences plant establishment (Peter et al., 2009). Pearl millet embryonic root system development is characterized by the formation of a fast-growing primary root that is the only architectural component of the root system for the first 6 days after germination (DAG) (Passot et al., 2016). No seminal roots are present in pearl millet and crown and lateral roots were only observed 6 DAG (Passot et al., 2016). We hypothesized that the fast-growing primary root might be an adaptation to the Sahelian environment (Passot et al., 2016). Here, we show that early drought stress after germination is a major constraint in Sahelian environments and that primary root growth is correlated with increased tolerance to this stress under field conditions in pearl millet. Differences in root growth seem to be mainly regulated by changes in cell elongation. A combination of GWAS and bulk segregant analysis on a bi-parental population identified one genomic region controlling this trait. Combining RNAseq, re-sequencing and re- annotation of this region, we identified a glutaredoxin-encoding gene, *PgGRXC9* as a potential candidate regulator. Functional characterization of the closest homolog in Arabidopsis reveals a new role for GRX in the regulation of root growth through cell elongation in the root apical meristem.

Results

Early drought stress episodes are an important constraint in Sahelian agrosystems

We previously hypothesized that the fast-growing primary root might be an adaptation to the Sahelian environment and, in particular, to early cycle drought stress episodes (Passot et al., 2016). To analyze the frequency and impact of such early drought stress, we first studied meteorological data collected for the past 21 years (2000-2020) at the CNRA Bambey station, located at the center of the pearl millet growing region of Senegal and highly representative of the climate found in Sahelian West Africa. Crops such as pearl millet are traditionally sown before or shortly after the first rain event of the rainy season. Moisture from the first rain event is used by seed to germinate and initiate their growth. We observed frequent intervals between the first and the second significant rainfall event (> 10 mm) that could last up to 40 days (Figure S1). These periods were unrelated to the timing of the first rain event.

A crop model was parameterized using soil and meteorological data (2000 to 2020) from the Bambey experimental station to determine when pearl millet faced drought stress and predict its impact on crop yield. Using a widely cultivated variety of pearl millet (Souna3) for modelling, we simulated the daily fraction of transpirable soil water (FTSW) profiles in different years to identify periods of the growth cycle when access to water was limiting. FTSW below 0.3 was considered a stressful condition. Clustering the trend of FTSW in the 21 years studied (based on the methodology of (Pašiaková et al., 2013)) revealed three stress patterns: early-stress, late-stress, and no-stress (blue, red and green line on Figure 1A). The crop faced early stress at a frequency of 24% over the 21 years, which resulted in an average 43% grain yield penalty compared to years without stress. Biomass production (an important source of fodder for livestock) was also reduced by 44% on average. Late-stress occurred in 19% of the years and resulted in 25% and 12% of yield and biomass penalty, respectively. No-stress was observed in 57% of the years. Hence, our analysis confirms that early drought episodes are a major constraint in Sahelian agrosystems of West Africa affecting crops during the vegetative stage.

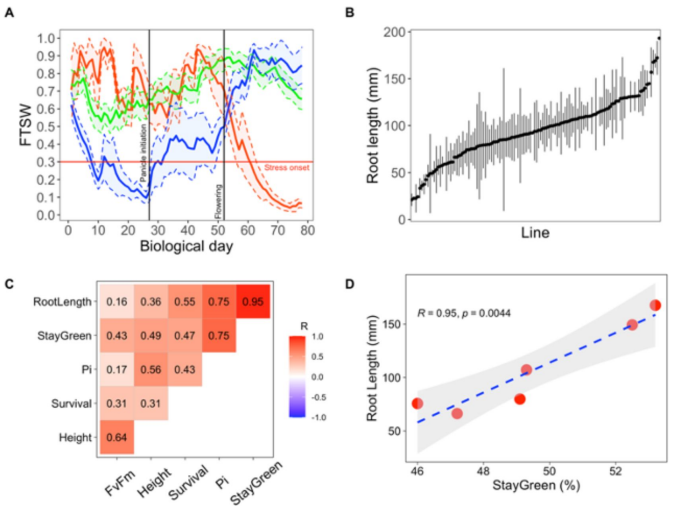

Figure 1.

Early primary root growth and its relation with drought-tolerance related traits measured in field conditions.

(A) Stress patterns identified by clustering of simulated fraction of transpirable soil water (FTSW) trend during the crop growth of 2000-2021 years in Bambey station. FTSW = 0.3 (horizontal red line) was considered as the onset of water stress. Each point is the average of a few daily FTSW based on the biological day which was used instead of daily FTSW to highlight the critical stages (panicle initiation and flowering, black lines). Thick lines and shaded area show the mean and two times standard error, respectively. Blue red and green line correspond to early-stress, late-stress, and no-stress respectively. (B) Root length in 122 pearl millet inbred lines derived from West and Central African landraces. Root length was measured at 6 days after germination in a paper-based hydroponic system installed in a growth chamber. Points represent mean +/- se. (C) Correlation between root length and the field measured

traits using adjusted lsmeans across both years. The Pearson correlation coefficients are indicated for each pair of traits. (D) Linear regression between root length and stay-green. Red points represent the lsmean for the 6 inbred lines that were common between the two field trials.

Primary root growth is correlated with increased tolerance to early drought stress

In order to test if a fast-growing primary root after germination might be an adaptive trait to early drought stress, we first phenotyped a diversity panel of pearl millet inbred lines representative of the genetic diversity of the crop (Debieu et al., 2018). As primary root growth is linear in the first days of growth (Passot et al., 2016), root length was measured as a proxy of growth on a paper-based hydroponic system 6 days after germination in 122 pearl millet inbred lines (5 plants/line in average for a total of 853 plants). Primary root length ranged from 21.1 to 193.2 mm with an average of 94.4 mm and a standard deviation of 32.5 mm, thus showing that a large diversity was available for this trait (Figure 1B).

The importance of early root growth for plant tolerance to early drought stress was then evaluated in field trials in 2 independent years using 9 inbred lines with contrasted root growth (slow, intermediate, and fast primary root growth). Field trials were set up during the hot dry season (March-June) in 2018 and 2020. Seeds were sown and irrigation equivalent to a 30 mm rainfall was applied. Irrigation was then stopped to mimic an early drought stress episode and plant growth and ecophysiological parameters were analyzed for the following 6 weeks (Table S1). We then analyzed the correlations between primary root length, measured in the lab, and plant performance measured in field conditions. Principal component analyses revealed a covariation of early primary root growth and stay-green (the % of leaves that remained green) as well as the performance index of photosynthesis (PI) measured both in 2018 and 2020 (Figure S2). Correlations between variables adjusted means across the two field trials showed a strong and significant relationship between early primary root growth and stay-green at the vegetative stage, an indicator of plant tolerance to drought stress ($R = 0.95$, $p < 0.01$; Figures 1C and 1D). Hence, our field experiments support the hypothesis that rapid growth of the primary root is beneficial for pearl millet plants to cope with early drought stress episodes after germination.

Identification of genomic regions in pearl millet controlling early primary root growth

We next studied the genetic determinants of primary root growth in pearl millet. First, the heritability of early primary root growth was analyzed using our paper-based phenotyping data on the panel of inbred lines. Heritability of 0.53 was computed indicating that early primary root growth is under strong genetic control in pearl millet. We therefore conducted a genome wide association study (GWAS). Genotyping by sequencing of the panel of pearl millet inbred lines provided 392,493 SNPs for association, after filtering on quality, with an average density of 2.5 SNPs per 10 kb [9]. For the current study, a set of 392,216 SNPs polymorphic for the 122 inbred lines with a phenotype was selected to conduct genome wide association analysis (GWAS) (de la Fuente Cantó et al., 2022). GWAS was performed using the ridge LFMM algorithm (Caye et al., 2019). In addition, we considered other GWAS methods to contrast the results (ANOVA, EMMA, or MLM; Figure S3). Our analysis revealed a total of 447 significant SNPs across the pearl millet genome associated with primary root growth from which, 109 SNPs were found highly significant with at least two other methods for association analysis at p-value < 10^{-4} (Table S2). Only two of these markers located on

chromosome 1 and 3, were above the 0.05 false discovery rate (FDR) significance threshold (Figure 2A).

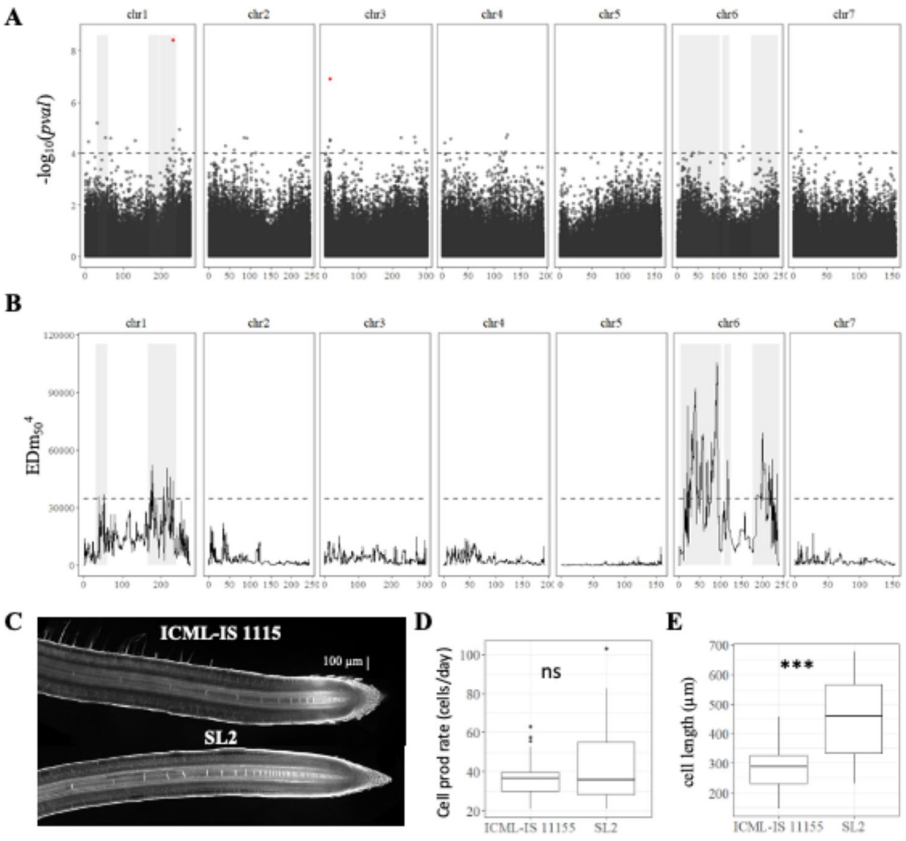

Figure 2.

Genetic dissection of primary root length in pearl millet and cellular analysis of root apical meristem and primary root growth of contrasted pearl millet lines in two experimental systems. (A) Manhattan plot of the GWAS by lfmm ridge method (Caye *et al.,* 2019). The horizontal axes correspond to the map position of each of the 392,216 SNPs identified by GBS in a group of 122 inbred lines. The vertical axes indicates the $-\log_{10}$*p value* of the statistic. The dash line delimits the threshold for highly significant SNPs (*p value* < 10^{-4}). Highlighted in red, significant SNP markers above the 0.05 FDR significance threshold. (B) BSA identification of significant regions associated with primary root length using bulks of contrasted F2 lines from a bi-parental cross. The plot shows the Euclidean Distance statistic profile (y axes) across the seven pearl millet chromosomes (x axes). The dash line indicates the 95% confidence interval threshold for the localisation of significant regions. In both plots, the shaded area delimits the extent of the six significant regions identified by BSA and therefore the overlap with significant SNPs identified by GWAS (A) and the correspondence with the BSA peaks found (B). (C) Confocal image of the root tip of the contrasted inbred lines for primary root growth (ICML- IS-1115 and SL2 with slow and fast growth respectively). (D) Estimation of cell production rate for each genotype according to (Beemster *et al* (2002)). (E) Maximum cell length reached in the root elongation zone for each genotype. *** p-value < 0.0001, ** p-value < 0.001, * p-value < 0.01, *ns* not significant.

To validate our GWAS analysis, we generated a bi-parental population from two inbred lines with contrasting early primary root growth. The two lines, ICML-IS 11155 (low primary root growth) and SL 2 (high primary root growth), were selected based on our initial paper-based root phenotyping experiment. The significant difference in primary root growth between these two lines was confirmed 7 days after germination in a paper roll phenotyping system (Figure S4A), as well as in soil using X-ray microCT 10 days after germination (Figure S4B), thus demonstrating their contrasting primary root phenotypes were robust and independent of the experimental system.

Lines SL2 and ICML-IS 11155 were crossed and 737 F2 plants were phenotyped for early root growth together with their parents (33 ICML-IS 11155 and 30 SL2 plants). The phenotypes of F2 plants showed a normal distribution encompassing the range of phenotypes from the 2 parents (Figure S5). 75 F2 plants were selected for each extreme phenotype (75 highest and 75 lowest growth) and were used for bulk DNA extraction. The corresponding DNA was then

used for genotyping by sequencing. Mean average sequencing depth in the bulks corresponded to 1028X (High growth) and 814X (Low growth). After filtering, a group of 33 582 SNP variants (2.1 SNP per 100 kb in average) identified between the bulks was used to assess the differences in allele frequency linked to the root length phenotype. Bulk Segregant Analysis (BSA) revealed differences in allele frequency for 1,285 SNPs (Figure 2B, Table S3). Six regions consisting of clusters of neighboring markers with overlapping region of significance defined by simulations (de la Fuente Cantó and Vigouroux, 2022) and equivalent to ±8 Mbp around each significant marker were identified on chromosome 1 (RL1.1, RL1.2, RL1.3) and chromosome 6 (RL6.1, RL6.2, RL6.3; Figure 2B). Eighteen marker-trait associations (MTAs) identified by GWAS co-localized with these BSA regions of significance (Table S4) including the most significant GWAS SNP on chromosome 1 at position 231264526 (Figure 2A).

Root growth is dependent on cell division and cell elongation activities occurring at the root tip. To identify the cellular process responsible for changes in root growth between the two parental lines, ICML-IS 11155 and SL2, we used confocal microscopy to image and measure cell elongation in the root tip starting from the quiescent center (Figure 2C, Figure S6). While cell production rates were similar in both lines (Figure 2D), SL2 (fast growth line) exhibited a significantly higher cell elongation rate than ICML-IS 11155 (Figure 2E). Hence, the significant difference in root growth between inbred lines SL2 (fast growth) and ICML-IS 11155 (slow growth) was mainly driven by changes in root cell elongation.

As differences in root growth between the two parent lines was mainly driven by cell elongation, we hypothesized that it might be linked to genes that are expressed in the root tip. We therefore profiled gene expression using RNAseq in the primary root tip (2 cm apex) of inbred lines ICML-IS 11155 (slow growth) and SL 2 (fast growth). Reads were mapped to the CDSs predicted in the reference genome [13] for expression analyses. 1778 genes showed significant differences in gene expression between the two contrasted lines using three combined statistical tests (EdgeR, DESeq et DESeq2, p-value < 0.01). Unexpectedly, a large proportion of the reads (31,48% in average in the 6 RNAseq experiments) did not map to predicted genes on the reference genome. Hence, our transcriptomics analysis identified genes that are differentially expressed in the root tip of inbred lines ICML-IS 11155 and SL 2 but revealed that some genes expressed in root tips are not annotated in the current version of the pearl millet genome.

Re-sequencing of the root length QTL region reveals a new GRX-encoding gene

We re-analyzed a 1 Mbp genomic region on chromosome 1 around the most significant GWAS marker-trait association, corresponding to SNP chr1_231264526, that co-localizes with a BSA QTL. This region contained a large proportion of unknown nucleotides (16.39% N) thus making gene annotation difficult. To obtain better quality sequence information, long reads (Nanopore technology, (Yuan et al., 2017)) corresponding to the target QTL regions were recovered and re-annotated using structural and gene expression (RNAseq) data. Re-annotation revealed one novel 465 bp CDS, 1103 bp downstream of the significantly associated SNP (chr1_231264526, Figure 3A & B). This new CDS encodes a protein with strong homology to glutaredoxin (GRX) C9-like proteins from various cereals and was named *PgGRXC9*.

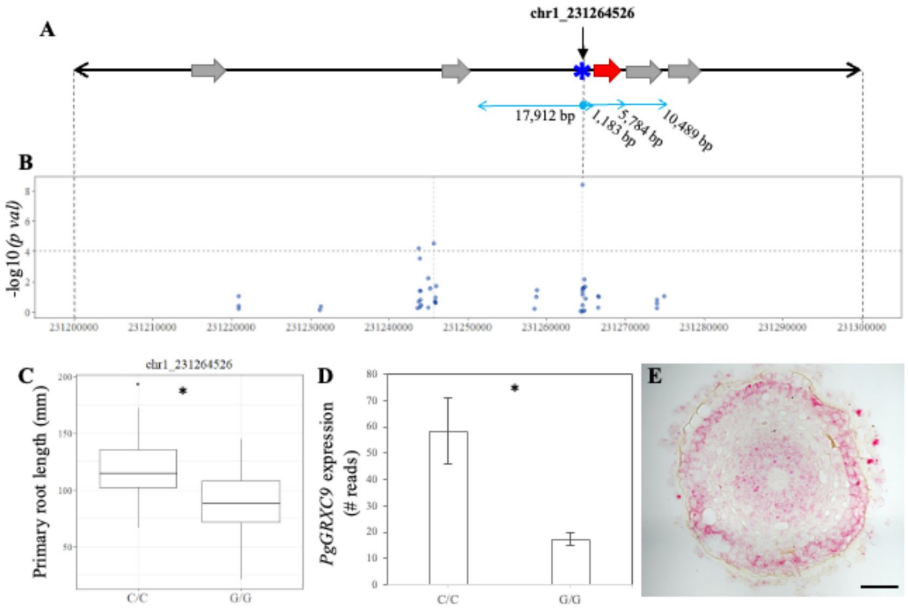

Figure 3.

Identification of candidate genes for primary root length in pearl millet. (A) Annotated genes in 100 kb region of chromosome 1 harbouring significant SNPs identified by GWAS and coincident with a BSA significant region. Blue asterisk shows the position of the SNP with the most significant association. Grey arrows represent the predicted genes according to the reference genome (Varshney *et al,* 2017). The red arrow represents the new predicted gene, *PgGRXC9,* identified as a result of reannotation of the genomic interval using *de novo* pearl millet assembly based on contig sequences. (B) GWAS Manhattan plot zoomed in the 100 kb interval on chromosome 1. Dots represent the -log 10 *(pval)* of the lfmm ridge statistic (y axis) for the SNPs identified in the region. The dashed horizontal line shows the threshold for highly significant SNPs. Positions and physical distance between genes and markers are displayed in bp. (C) Primary root length phenotype associated to the allelic variants of the two significant SNPs in the region: chrl _231264526 ($N_{c/c}$=26, N_{GG}= 74)). (D) Expression of *PgGRXC9* for the two alleles from the RNAseq data. * *p*-value < 0.01. (E) Transversal section in the elongation zone of a primary root showing the expression profile of *PgGRXC9* as indicated by RNAscope. Scalebar = 50 µm.

Two alleles at this locus exist in our population (C or G) with plants carrying a homozygous C/C allele (21.3% of the lines in our population) having a significantly higher root growth than plants carrying the G/G homozygous allele (60.7% of the lines; Figure 3C). We found that *PgGRXC9* expression was significantly higher in the root tip of the line carrying the allele associated with higher root growth (C/C) compared to the line carrying the lower growth allele (G/G; Figure 3D). *In situ* hybridization using the RNAscope technology revealed expression in the stele and epidermis in the root tip and elongation zone (Figure 3E, Figure S7). Expression was also observed in the columella cells of the root cap and in the stele of the differentiated part of the root (Figure S7). We then used the RNAseq data to search for polymorphisms between the two contrasted parent lines used for BSA. No sequence polymorphisms were found in the predicted coding sequence of the gene between the two parent lines. However, 2 polymorphisms were detected in the 5'UTR region. Altogether, our results suggest that *PgGRXC9* is a positive regulator of root growth and that a polymorphism in the promoter region of *PgGRXC9* associated with changes in its expression level appeared responsible for a quantitative difference in root growth between the two lines.

PgGRXC9 Arabidopsis ortholog *ROXY19* also regulates root cell elongation

To test the hypothesis that changes in *PgGRXC9* expression level are responsible for a change in root growth, we studied its ortholog in the model plant *Arabidopsis thaliana* (as functional genomic studies are not possible in pearl millet). The closest homolog in Arabidopsis was *ROXY19* (*AT1G28480*) with 56% identity at the protein level (Figure 4A; Figure S8). The ROXY

family is a land plant-specific family of GRX, with 21 members in Arabidopsis (Meyer et al., 2009). They all harbor a Cys-Cys (CC) putative active site and bind to TGA type transcription factors via the C-terminal domain (Meyer et al., 2012). Several of them contain a final ALWL C-terminal motif responsible for binding to TOPLESS and TPR transcriptional co-repressors (Uhrig et al., 2017). All these important amino acids were conserved in PgGRXC9 (Figure S8). ROXY19 belongs to a subgroup of 4 ROXYs (ROXY18-21) that contain a specific N-terminal domain of unknown function, that was also present in PgGRXC9 (Figure S8).

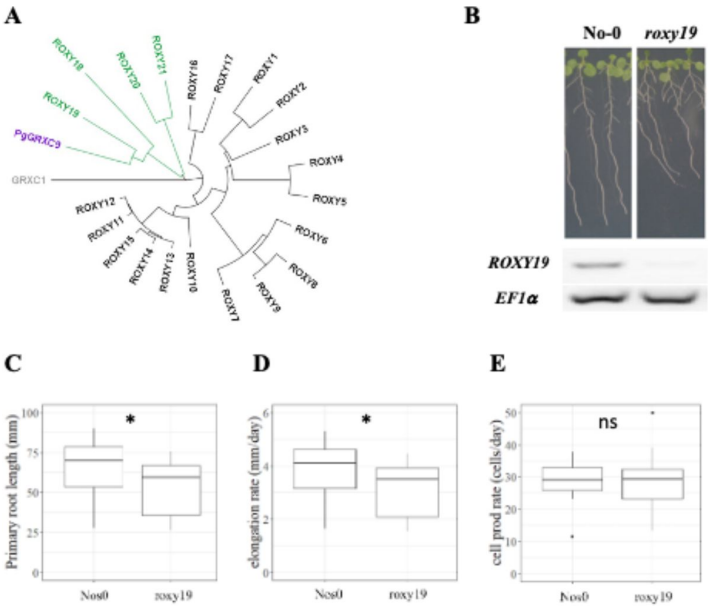

Figure 4.

The Arabidopsis homolog of PgGRXC9 regulates root growth in Arabidopsis. (A) Phylogenetic tree of ROXYs protein sequences. This tree has been obtained from pairwise alignments of all whole protein sequence pairs, using NeighborJoining method and Jukes-Cantor distance matπx. GRXC1 (grey), a member of Class I GRX, is used as the tree root. Arabidopsis ROXY 18-21 are represented in green, and PgGRXC9 is represented in purple. (B) Contrasted primary root phenotype in NosO and *roxyl9* in 17 days old seedlings grown in agar plates. (C) Primary root length of NosO (N=27) and *roxyl9* (N=25). (D) Cell elongation rate. (E) Estimation of the cell production rate assuming a steady root grow th rate. * *p*-value < 0.01, ns: not significant.

Transcriptomic data indicate that *ROXY19* is expressed in root tissues, with the strongest expression detected in the columella and stele of the elongation and maturation zone and some expression in the ground tissue and epidermis (Belin et al., 2015). Given this expression profile was similar to *PgGRXC9* in pearl millet, we exploited a *roxy19* null mutant available in the *Nossen* (No-0) background [19] to study its function. Strikingly, we observed that *roxy19* had reduced primary root growth compared to its wild-type ecotype (No-0; Figure 4B, C). Closer examination revealed that the defect in *roxy19* root growth was due to a reduction in cell elongation (Figure 4D), whereas cell production rate was similar in the mutant and wild type (Figure 4E), thus mimicking the phenotype observed in pearl millet. Hence, our functional studies reveal that *ROXY19*, the closest homolog of *PgGRXC9* in *A. thaliana*, is a positive regulator of root growth through modulation of cell elongation.

Discussion

Drylands, defined as regions where precipitation is lower than atmospheric water demand, cover around 40% of the land surface and host about 2 billion people (Wang et al., 2022). They are key regions for global food security as it is estimated that they are responsible for about 60% of global food production (Wang et al., 2022). They also play an important role for the global carbon budget (Wang et al., 2022). Climate change is expected to have a negative impact on agriculture in drylands with direct consequences for the livelihood of about 178 million people by 2050 under a 1.5°C temperature increase scenario (Wang et al., 2022). There is therefore an urgent need to devise new agricultural practices and crop varieties to address this challenge. This is particularly critical in the Sahel, the dryland region stretching

across Africa and delimited by the Sahara to the North and the Sudanian savanna to the South, where agriculture is mainly rainfed with limited access to fertilizers and irrigation (Ndoye et al., 2022). Pearl millet was domesticated in the Sahel about 4,500 years ago (Burgarella et al., 2018) and it is a key crop for food security in that region (Debieu et al., 2017; Varshney et al., 2017). In the Sahel, drought stress is a major factor limiting crop yield. The semi-arid tropical climate is characterized by a long dry season and a short rainy season where most of the agriculture occurs. Pearl millet is traditionally sowed before or right after the first rain so that the water from this first rain is used for germination and seedling establishment. However, the precipitation pattern is irregular and varies from season to season and these intra- and interannual variability are expected to increase with future climate (Sultan and Gaetani, 2016). To devise strategies to adapt agriculture to future climate, it is important to identify the stress patterns faced by crops. In this study, we used meteorological data together with a crop model to estimate the water stress patterns faced by pearl millet in the 2000-2020 period. This revealed 3 main types of patterns, early drought stress, terminal drought stress and no stress. Early drought stress, corresponding to rain pause during crop establishment, was found to occur roughly one fourth of the years and to have a large impact on both grain and biomass (an important source of fodder) production. Indeed, we found that lapse between the first rain and subsequent significant rain were occurring frequently, and current models predict that such gaps are going to be more frequent in future climate (Sultan and Gaetani, 2016). This indicates that early drought stress after germination is a major constraint for crop growth in the Sahelian agrosystems.

The embryonic root system makes most of the root system for the first weeks of the seedlings life and is therefore important for crop establishment. Interestingly, we previously reported that early root system development in pearl millet is characterized by a unique fast growing primary root (Passot et al., 2016). There are no seminal roots, and post-embryonic root system branching (formation of lateral and crown roots) only starts 6 days after germination (Passot et al., 2016). We hypothesized that this could be beneficial for early establishment and access to deep resources (water and nutrients) as an adaptation to the Sahelian climate and, in particular, to face early drought stress events. We used the natural variability for primary root growth in pearl millet to test this hypothesis in two years of field trials set up to mimic early rain pause episodes after germination. We observed that pearl millet lines with faster primary root growth had better tolerance to this stress thus indicating that indeed fast primary root growth was beneficial to cope with post-germination drought stress.

Early primary root growth showed a high heritability. We therefore studied the genetic bases of this useful trait using a combination of association genetics (GWAS) and QTL analysis (BSA). We are confident our genetic analysis targeted specifically early primary root growth rather than seed reserves or seedling vigor because 1) we previously showed that primary root growth was not correlated to seed weight in our experimental set up (Passot et al., 2016) and 2) we selected parents with very contrasted root growth but similar shoot biomass to generate the bi-parental population used for QTL analysis. Moreover, the lines used for QTL analyses showed significant differences in primary root growth in different root phenotyping systems (including soil columns) thus suggesting that the loci we identified are robust and relevant for primary root growth *in naturae*. Our genetic analysis revealed a limited number of loci controlling early primary root growth.

We focused our analysis on the most significant marker-trait association for GWAS that was co-localizing with a BSA QTL on chromosome 1. Re-sequencing and re-annotation of the corresponding genomic region revealed a new gene close to the most significant SNP. This gene, *PgGRXC9*, encodes a potential glutaredoxin protein. The gene is more expressed in the root tip of the line with the allele associated with higher root growth. We found no polymorphism in the *PgGRXC9* coding region in the two parents of the QTL population. We showed that the closest homolog in *A. thaliana*, *AtROXY19*, has a similar expression pattern

and that it regulates primary root growth. Interestingly, the root growth phenotypes observed in contrasted pearl millet lines and in the *roxy19* mutant indicate that, in both cases, regulation of root growth occurs at the cell elongation level. Although the link between PgGRXC9/AtROXY19 and root growth elongation is novel, previous studies have revealed connections between root redox status and growth. In Arabidopsis, other members of the ROXY family have been shown to regulate root growth elongation in response to nitrate (Ota et al., 2020; Patterson et al., 2016). More generally, redox homeostasis has been previously reported to regulate root meristem organization and functioning in Arabidopsis (e.g., (Bashandy et al., 2010); (Tsukagoshi, 2016); (Tsukagoshi et al., 2010); (Vernoux et al., 2000)) including regulation of cell elongation (Mabuchi et al., 2018; Tsukagoshi, 2016). The mechanism and the actors of the redox regulation of root growth elongation will need further investigation.

Based on our results, we propose that redox regulation in the root meristem is responsible for a root growth QTL in pearl millet. Indeed, our data suggest that changes in *PgGRXC9* expression level due to polymorphisms in the promoter or 5'UTR region of the gene level might cause differences in root cell elongation and ultimately root growth that are important for adaptation to post-embryonic drought stress. Further work will be needed to validate this hypothesis. Pearl millet is an orphan crop and no functional genomics tools are currently available. Future work will first target the development of an efficient gene editing protocol in this species.

Ideas and Speculation

Pearl millet evolved and was domesticated in the Sahel. Its seeds are small (8 mg on average, about 5 and 20 times lighter than wheat or maize seeds respectively for example) with limited reserves available for early seedling growth. It invests the available seed reserves towards the growth of a unique primary root to rapidly colonize deeper soil layers rather than forming more root axes (seminal roots for example) as seen in other cereals. Based on our results, we speculate that this specific early root development strategy was selected during evolution to cope with the specific rain pattern encountered in the Sahel.

Material and methods

Plant materials

The panel of pearl millet inbred lines derived from West and Central African landraces (open-pollinated varieties) used in this study has been previously described (Debieu et al., 2018). Nine lines from this panel that were contrasting for root length were selected for field trials (Table S6).

Field trials

Field experiments were performed at the CNRA station (Centre National de Recherche Agronomique) of the Institut Sénégalais des Recherches Agricoles (ISRA) in Bambey, Senegal (14.42°N, 16.28°W), during the dry season of 2018 and 2020 to fully control irrigation. Fields are composed of deep sandy soil with low levels of clay and silt (12%) and organic matter (0.4%). Clay and silt content increase with soil depth from 10.2% in the 0 to 0.2 m layer to 13.3% in the 0.8 to 1.2 m layer. Experiments were set up using a complete randomized block design with 4 plots per variety, each composed of 6 rows of 6.3 m long with 0.9 m between plants and 0.9 m between rows (42 plants/plot). Irrigation was provided after sowing (30 mm

of water) to allow seeds to germinate and was followed by a period of 42 days of water withholding to impose seedling drought stress. Thinning was performed 15 days after sowing to conserve a single plant per planting hole. Fertilization (NPK) following standard recommendation of 150 kg ha^{-1} NPK (15-15-15) was applied to the entire trial after sowing and before irrigation. Fields were maintained free of weeds. Plant height was measured at 42 days after sowing. Stay-green trait expressed as the percentage of green leaves compared to the total number of leaves was estimated on 3 plants per plot at 42 days after sowing. Survival rate was measured as the percentage of surviving plants at 42 days after sowing in each plot compared to the initial number of plants that had emerged. Photosynthesis parameters (FvFm: maximum quantum efficiency of photosystem II and PI: performance index of photosynthesis) were measured on three plants per plot at 32 days after sowing in both 2018 and 2020 using a Handy Pea chlorophyll fluorometer (Hansatech Instruments Ltd.).

Identification of water stress pattern

Long-term weather data (2000-2021) in CNRA (Bambey, Senegal) were gathered and analyzed to evaluate how the rainfall gap affects crop growth. An adapted version of the Simple Simulation Model (SSM-iCrop, (Soltani et al., 2013; Soltani and Sinclair, 2012)) was used to simulate the crop growth of a common West African pearl millet genotype (Souna3) and dynamic of water in the soil. To test the effect of water limitation alone, the model was run in water-limited potential mode with 3.7 plants per m^{-2} density and no fertilizer limitation. From April 10th, the model began simulating soil water balance with a quarter-saturated profile. Sowing date was defined by the first significant rain of the year (actual transpirable soil water superior or equal to 10 mm). Clustering was done based on the trend of the fraction of transpirable soil water (FTSW) from sowing date to maturity in different years to group years into different stress patterns and the effect on the yield and biomass. The NbClust Package (Pašiaková et al., 2013) was used to determine the optimal number of clusters and the dynamic time warping method to cluster the daily simulated FTSWs in different years.

Root growth phenotyping

For high-throughput experiments (association genetics and bulk segregant analysis), plants were phenotyped for primary root growth with a paper-based hydroponic system as previously described (Passot et al., 2016). Seeds were surface-sterilized and pre-germinated in Petri dishes, transferred into pouches 24 hours after germination at a density of 3 seeds per paper and then maintained in a growth room with a 14 hour photoperiod (28°C during day and 24°C during night). Pictures of the root systems were taken 6 days after germination with a D5100 DSLR camera (Nikon) at a resolution of 16 M pixels. The camera was fixed on a holder to maintain the same distance between the lens and each root system. Primary root lengths were measured using RootNav (Pound et al., 2013). Rhizotron experiments were performed as previously described (Passot et al., 2018). For X-ray tomography, seeds were sterilized with 20% bleach for 5 minutes, then washed with sterilized water five times. Sterilized seeds were pre- germinated on moist sterilized filter paper for 36 hours at 28°C in a plant growth chamber (12-hour photoperiod and 300 µmol/m^2/s light with 70% relative humidity). Equally germinated pearl millet seedlings (1cm radicle length) were gently placed in loamy sand soil in CT columns (30 cm height x 5cm diameter). Loamy sand soil collected from the University of Nottingham farm at Bunny, Nottinghamshire, UK (52·52 °N, 1·07 °W) was crushed thoroughly and sieved through 2 mm mesh size. These columns were saturated with water and then drained to field capacity. Five replicates of each SL2 and ICML-IS 11155 pearl millet seedlings were grown for 10 days for the CT experiment in a growth chamber maintained at a 12-hour photoperiod at 25°C and 250 µmol/m^2/s light with 60% relative

humidity. The root systems of 10-day old pearl millet lines (ICML-IS 11155 and SL 2) were imaged non-destructively using a GE Phoenix v|tome|x M 240 kV X-ray tomography system (GE Inspection Technologies, Wunstorf, Germany). Scans were acquired by collecting 3433 projection images at 140 kV X-ray energy, 200 µA current and 131 ms detector exposure time at scan resolution of 45 µm in FAST mode (8-minute total scan time). Three-dimensional image reconstruction was performed using Datos|REC software (GE Inspection Technologies, Wunstorf, Germany) and root length was measured using the polyline tool in VGStudioMax (Volume Graphics GmbH, Germany).

For Arabidopsis experiments, seeds were surface-sterilized and placed on plates containing half-strength Murashige and Skoog (1/2 MS) medium with 0.5 $g.l^{-1}$ MES and 0.8% (w/v) plant agar without sucrose. All plates were incubated vertically at 20 °C with 160 µE m^{-2} s^{-1} light intensity and a 16h light / 8h dark regime. The primary root elongation rate was quantified between day 8 and day 17. Lengths were quantified from pictures using the public domain image analysis program ImageJ 1.52i (https://imagej.nih.gov/ ij/) and its NeuronJ plugin.

Heritability

Broad sense heritability was computed with the following formula:

$$H^2 = \frac{\text{Var(line)}}{\text{Var(line)} + \frac{\text{Var(res)}}{n_{\text{plant/line}}}},$$

where

- $n_{\text{plant/line}}$ is the average number of plants measured per line,
- Var(line) is the variance associated with lines,
- Var(res) is the residual variance.

Both variances are parameters of the following linear mixed model:

$$Length = \mu + \alpha_{line} + \varepsilon_{res},$$

where μ is the overall mean length, α_{line} is the random effect attached to the lines with α_{line} ~ N(0, Var(line)) and ε_{res} is the error term with ε_{res} ~ N(0, Var(res)).

Genome wide association mapping

Genotyping by sequencing of the panel of inbred lines was reported in previous work (Debieu et al., 2018). In order to conduct association mapping, we first estimated population structure based on the ancestry coefficients estimated with the R package LEA v2.0. Then, GWAS was performed using latent factor mixed model (LFMM 2.0) which corrects for unobserved population confounders and considers ridge estimates (Caye et al., 2019). Given the reduced number of lines, GWAS was performed using four other methods for association analysis: analysis of variance (*i.e.*, ANOVA), Efficient Mixed Model Association or EMMA (Kang et al., 2008), Mixed Linear Model or MLM (Yu et al., 2006) and a previous version of LFMM (Frichot et al., 2013).

Bulk segregant analysis

Root growth in F2 seedlings derived from the cross between ICML-IS 11155 and SL-2 (low and high primary root growth respectively) was characterised in the paper phenotyping system as described above. The 10% extreme lines in the tails of the distribution were selected to form the bulks of contrasted lines. Leaf discs (1.5 mm diameter) were sampled for each line during the phenotyping experiment and stored at -80°C. Leaf discs from selected lines were pooled together to make the high root growth (H) and low root growth (L) bulks for DNA extraction. Genomic DNA was isolated for each bulk using the MATAB method as previously described (Mariac et al., 2006). DNA libraries were constructed from genomic DNA fragmented by acoustic shearing (Bioruptor®) with a peak fragment target size of 200 – 300 bp. Sheared DNA was end-repaired using a T4 polymerase (End Repair NEB®) and bound with the P5 and PE- P7 sequencing adaptors (Rohland and Reich, 2012). A combination of unique oligonucleotides barcode sequences was ligated to the P5 adaptor to index the DNA libraries derived from each bulk (H and L) and from the parental lines of the cross. Then, equimolar amounts of each DNA library were combined in the genomic DNA bank for the cross. Subsequently, the DNA bank library was hybridized with biotinylated RNA probes or 'baits' (myBaits®) targeting the first 500 bp of the 32,100 pearl millet predicted genes. Finally, high-throughput sequencing of the enriched DNA library was performed on an Illumina HiSeq sequencer by Novogene Company Limited (HK). Initial sequencing quality checks using FastQC version 0.11.5 (Andrews, 2010) were followed by trimming and quality filter steps on which adaptors, barcode sequences and low-quality reads (< 35 bp) were removed. Filtered reads were aligned to the pearl millet reference genome (Varshney et al., 2017) using BWA MEM algorithm (BWA version 0.7.17 - r1188 (Li and Durbin, 2009)). Reads mapping at the target enriched regions were used for SNP calling using the UnifiedGenotyper algorithm from GATK 3.7 (McKenna et al., 2010) with the parameter down-sampling limit (dcov) set at 9000. Multi-allelic sites and those with low total allele frequency (AF<0.25) were removed. In addition, sites with either low or high total sequencing depth (below the 25th and above the 95th percentiles respectively) were removed.

Finally, SNPs with more than 50% missing data and minor allele frequency under 5% were excluded.

For bulk segregant study, only biallelic SNP variants of the bulks that were present in the parental lines of the cross were kept. The line ICML-IS 11155 (low primary root growth) was used as the reference genome for the cross to designate the alternate and reference SNP variants in the bulks. Out of the range of statistical approaches for measuring the differences in allele frequency in bulk segregant analysis, Euclidean distance-based statistics as suggested by (Hill et al. 2013) was selected based on a preliminary study on which we tested the efficiency of the methods for QTL detection using simulations (de la Fuente Cantó and Vigouroux, 2022). The Euclidean distance between allele frequencies of the bulks at each marker position (*EDm*) was calculated as follows:

$$EDm = \sqrt{(faL - fAL)^2 + (faH - fAH)^2}$$

Where *fa* and *fA* correspond to the allele frequency of the alternate and reference allele in the low bulk (L) and the high bulk (H) respectively. Then, to reduce the effect of sequencing noise and increase the signal of the differences in allele frequency we calculated the fourth power of the cumulative *EDm* value in windows of 100 consecutive markers (Omboki et al., 2018; Zhang et al., 2019). The confidence interval of the statistic was determined using simulations as described (de la Fuente Cantó and Vigouroux, 2022).

RNAseq

Seeds were surface-sterilized and germinated in Petri dishes containing wet filter paper for 24 hours in the dark at 27°C. After two days, plants were transferred to hydroponic tanks containing 1/4 Hoagland solution and grown for 15 days at 27°C. RNA was extracted from the root tip (2 cm apex) of the primary root using the RNeasy Plant Mini Kit (QIAGEN). RNA-seq was performed by the Montpellier GenomiX Platform (MGX, https://www.mgx.cnrs.fr/).

Sequencing was performed on an Illumina HiSeq 2500. Analyses were performed as previously described (de la Fuente Cantó et al., 2022). Three different statistical tests were used to identify differentially expressed genes: EdgeR (McCarthy et al., 2012; Robinson et al., 2010), DESeq (Anders and Huber, 2010) and DESeq2 (Love et al., 2014). GO terms enrichment was performed in the 1778 genes that were significantly differentially expressed between the slow growth and fast growth lines according to the three statistical tests using the TopGO package in R. Briefly, overrepresentation of GO terms in the list of differentially expressed genes (1032 of the 1778 with GO annotations) was investigated in relation to the list of annotated pearl millet genes with GO annotations (16620 genes with GO annotations and 47234 GO terms in total; (Varshney et al., 2017)) using a Fischer test. Each GO categories were tested independently or considering hierarchical links between GO terms. GO terms showing *p*-values below 0.01 were further considered for enrichment analysis.

Cellular analysis of root meristems

Root meristem phenotype of lines with contrasted primary root length was characterized using confocal microscopy. Lines ICML-IS 11155 and SL-2 (low and high primary root growth respectively) were grown in paper rolls under controlled conditions in a growth room. In brief, pre-germinated seeds were sown along the long side of germination paper (Anchor Paper Company, USA) rolled on itself and imbibed in ¼ strength Hoagland solution (Hoagland and Arnon, 1950). Each paper roll was placed in an Erlenmeyer flask containing 200 ml of nutrient solution, a volume maintained constant throughout the experiment. Primary root length was measured, and 2 cm length were sampled from the tip of one-week old seedlings. Root tips were fixed in FAA solution for 24 hours. Then, root tips were washed twice in PBS solution and moved to the ClearSee clearing (Kurihara et al., 2015) solution for a minimum of 48 hours. Before imaging, root tips were stained for 30 minutes in 0.1% Calcofluor White and washed in ClearSee^{TM} for other 30 minutes (protocol adapted from (Ursache et al. 2018)). Root tip images were obtained using a Leica SP8 confocal microscope equipped with a 20 x /0.70 dry objective at a detection range of 420-485 nm. Images were analyzed using the Broadly Applicable Routines for ImageJ (Ferreira et al., 2015). Cell walls from the meta-xylem vessel were used to estimate cell length along the axial axis of the root. The “find peaks” option was used to determine the coordinates of the cell walls along a segmented line traced from the quiescent center to the mature zone where the first root hairs were observed, and maximum cell length was reached. Consecutive data points defined the cell length along the root axis and a logistic function was fitted to the data to characterize axial root growth (Morris and Silk, 1992). Elongation rate was estimated as the root length reached per day of experiment. This value divided by the maximum cell elongation defined per sample was used to approximate the cell production value or number of cells produced in the meristem per day assuming steady-state growth (Beemster et al., 2002).

Re-annotation of QTL region using long reads data

Long reads were used to reannotate the QTL region as in (Grondin et al. 2020) (Genbank accessions MT474864 and MT474865). For identification of Nanopore contigs corresponding to the QTL region, a 1MB sequence located around the most significant GWAS SNP was extracted from the reference genome and aligned to the long read genome using the nucmer tool (MUMmer version 4.0.0beta2, - -mum option (Marçais et al., 2018)) with a minimum aligned sequence length of 300 bp. We pre-selected contigs alignments if at least five regions of the same contig were aligned successively to the QTL region in a span shorter than 20kb and covering at least 3% of the QTL sequence. Contigs were considered as valid if the alignment covered at least 40% of the contig length and 20% of the QTL length. For annotation, a *de novo* transposable elements (TEs) library was generated from the long reads with RepeatModeler2 (version 2.0.1, options -engine ncbi (Flynn et al., 2020)). TEs were detected and removed using RepeatMasker (version 4.1.0 (Tarailo-Graovac and Chen, 2009)) with the *de novo* TEs library. Annotation of the genome was performed with MAKER2 (version 2.31.9 (Holt and Yandell, 2011)) using all ESTs sequences downloaded from the NCBI (organisms: *P. glaucum*, *Oryza sativa*, *Zea mays*, *Sorghum bicolor*, *P. miliaceum*, *Setaria italica*), all protein sequences of *P. glaucum* available on the NCBI (July 2020), all protein sequences of annotated genes on the reference genome (http://gigadb.org/dataset/100192) and the Uniprot-Swiss-Prot protein database (section viridiplantae, release-2020_06). RNAseq data mapping was performed with TOGGLe (v3 (Tranchant-Dubreuil et al., 2018)). Reads were aligned to the long-read sequences with HISAT2 (version 2.0.1 (Kim et al., 2015)) and an annotation file was produced with Stringtie (version 1.3.4 (Pertea et al., 2015)). This file was used as input of MAKER2 (default parameters, the SNAP HMM *O. sativa* file model). Predicted protein sequences were aligned to the Uniprot-Swiss-Prot protein database (section viridiplantae) using blastx (Altschul et al., 1990). Genes with protein domain signatures were recovered using Pfam database and InterProScan (version 5.19-58.0, -appl pfam -dp -f TSV -goterms -iprlookup -pa -t p (Mulder and Apweiler, 2007)).

In situ hybridization

Pearl millet root tip fixation, embedding, and sectioning step were performed as described (Mounier et al., 2020). Briefly, 7 days-old millet primary root tip (1,5 cm) were hand-dissected and the tip were immediately aligned between two biopsy foam (M476-1, Simport, Canada), and transferred in a cassette (1,267,796 Thermo Scientific, USA) in a 3:1 ethanol:acetic acid fixative solution. The samples were then placed in a fresh fixative solution and a 5 minute vacuum was applied two times. The solution was then replaced by a fresh fixative solution and samples were stored over-night at 4°C. The samples were then subjected to several 5 minutes baths with increasing ethanol concentrations (75, 80, 85, 90, 95 and 100%), one bath in an ethanol/butanol (1:1) solution and one bath in absolute butanol on ice. The samples were transferred to a water bath at 54 °C inside of a histology microwave oven (Histos 5 Rapid Tissue Processor, Milestone, Italy). The samples were then subjected to a bath in butanol/paraffin (1:1) solution at 54 °C and 300 W and then two baths in paraffin at 54 °C and 250 W. Prior to the embedding step, the root bundles were rapidly removed from the cassettes while the paraffin was still liquid and transferred to a cold RNase-free surface. The bundles were subsequently transferred vertically and placed upside down in a molding tray (E70182, EMS, USA). The paraffin blocks were maintained at 4 °C and protected from light. Transversal sections with a thickness of 8µm were cut on an RNase-free microtome (RM2255, Leica, Germany) and mounted on a cut edge frosted glass slide (VWR, 631-1551) prewarmed at 45°C with drops of RNase-free water. Slides where then baked at 60°C until the section was well fixed on the slide (around 20 minutes) prior to RNAscope.

The RNAscope assay was performed by Be More Specific. Probes against *PgGRXC9* were custom-designed by ACD and are available in the ACD catalogue as Came-GRXC9-C1 (Ref. 1187801-C1). The probes were designed based on the *PgGRXC9* re-annotated sequence and were complementary to nucleotides at positions 71 to 671, excluding the 398 to 510 positions. The negative probe was provided by ACD (Accession # EF191515). The *in-situ* hybridization assay was performed using the ACD RNAscope® 2.5 HD Detection Reagent-RED kit (cat. no. 322360) using the provided protocol. (http://www.acdbio.com/technical-support/user-manuals). Imaging of tissue sections was performed using a Nikon Eclipse NI-E (Nikon Corporation, Tokyo, Japan) with a 40X Plan Apo λ 0.95 NA objectives. Images were processed using imageJ contrast enhancement tool to 0,001% of saturated pixel.

Statistical methods

Statistical analyses were performed using R version 4.0.2 5 ((R core team, 2018).). Principal component analyses were performed using the prcomp() function. Pearson's correlation analyses were performed using the corr() function within the ggcorrplot package. The variance of each variable was partitioned into components attributable to the genotypic (line) and year in interaction with block as additional factor using an analysis of variance (aov() function in the agricolae package). Adjusted means of the variables for the different lines across the two experiments were further calculated using the least-squares means lsmeans() function (lsmeans package).

Data availability

Genomic data are available at the National Center for Biotechnology Information (NCBI). Genotyping (GBS) data are available in genbank under reference number PRJNA492967 (GWAS) and PRJNA769524 (BSA). RNAseq data are available in the Gene Expression Omnibus (GEO) under reference GSE185517.

Oxford Nanopore long reads are available on the European Nucleotide Archive (ENA) under reference ERR10627707.

Field trials data are available at Dryad under reference doi:10.5061/dryad.qv9s4mwk2.

Source data legends

Figure 4 source data. *ROXY19* and *EF1a* (control gene) expression detected by RT-qPCR in different Arabidopsis lines. No ROXY19 expression was detected in the roxy19 mutant in contrast to the corresponding wild-type background.

Acknowledgements

We dedicate this article to the memory of our colleague Yann Guédon (CIRAD). This work was supported by the French Institute for Sustainable Development (IRD), the French Ministry for Research and Higher Education (PhD grant to SP), the Agence National pour la Recherche (RootAdapt grant n° ANR-17-CE20-0022 to LL), the Agropolis Fondation (NewPearl grant n° AF 1301-015 in the frame of the CERES initiative and ValoRoot grant n°2202-002 to LL and Flagship Project CalClim grant no. 1802-002 to JPR) as part of the "Investissement d'avenir" (ANR-l0-LABX-0001-0l), under the frame of I-SITE MUSE (ANR-16-IDEX-0006), by the Fondazione Cariplo (n° FC 2013-0891) and by the CGIAR Research Programme on Grain Legumes and Dryland Cereals (GLDC). Financial support by the Access to Research

Infrastructures activity in the Horizon 2020 Programme of the EU (EPPN2020 Grant Agreement 731013) is gratefully acknowledged. The authors acknowledge support from the iTrop High-performance computing platform (member of the South Green Platform) at IRD Montpellier.

Competing interests

The authors declare no competing interests.

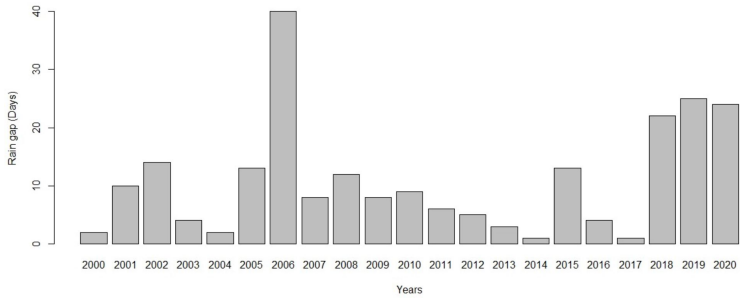

Supplementary Figure 1.

Lapse between the first and the second significant rainfall.

Significant rainfall was considered as more than 10 mm rainfall per day. Data from the Bambey experimental station.

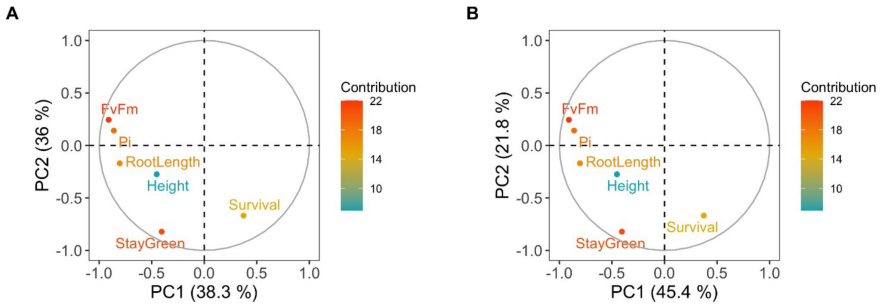

Supplementary Figure 2.

Covariation of root length, plant height and drought related traits including maximum quantum efficiency of photosystem II (FvFm) and performance index of photosynthesis (PI) measured at 32 days after sowing, and stay-green and plant survival measured at 42 days after sowing.

Mean values measured in 2018 (A) and 2020 (B) field trials were used for Principal Component Analysis (PCA). The contribution of each PCA axis (PC1 and PC2) is indicated on the graph.

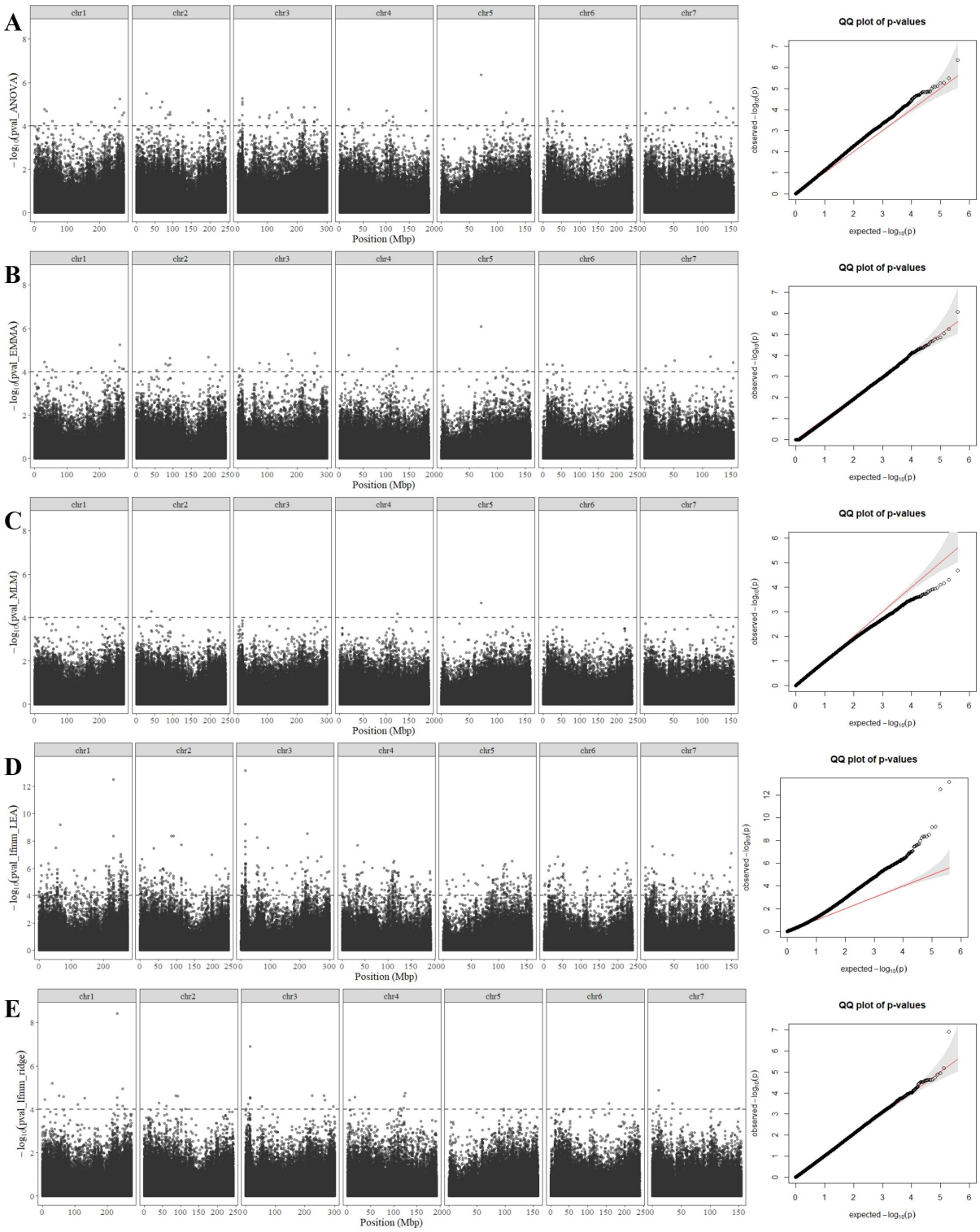

Figure S3.

GWAS Manhattan plot and *p*-values QQ plots obtained with five methods. (A) Analysis of variance or ANOVA, (B) Efficient Mixed Model Association or EMMA, (C) Mixed lineal model or MLM, (D) Latent Factor Mixed Model using an stochastic algorithm (MCMC), or LFMM_LEA, (E) Latent Factor Mixed Model using the ridge algorithm or LFMM_ridge.

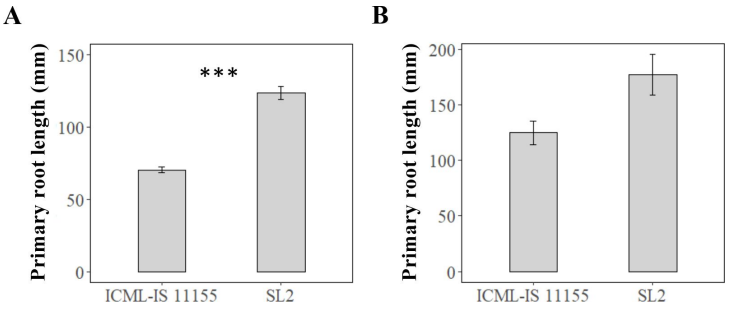

Figure S4.

Contrasted primary root length of lines ICML-IS 11155 and SL2.

(A) on paper roll 7 days after germination ($N_{ICML\text{-}IS\ 11155}$ = 32, N_{SL2} = 34) and (B) soil column using by X-ray tomography 10 days after germination ($N_{ICML\text{-}IS\ 11155}$ = 4, N_{SL2} = 5, *P*-value= 0.058).

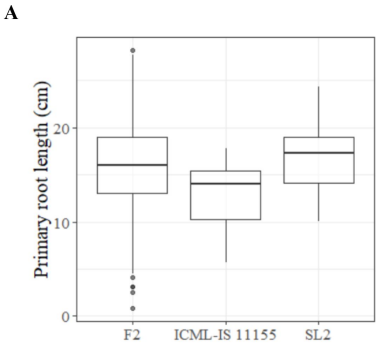

B

	F2s	ICML-IS 11155	SL2
Number of individuals	737	33	30
RL Mean (cm) ± SE	15.98 ± 0.17	13 ± 0.52	16.74 ± 0.68
RL Min – Max (cm)	0.81 - 28.26	5.71 – 17.83	10.07 – 24.37

Figure S5.

Distribution phenotypes F2 and parents ICML-IS 11155 and SL2.

(A) Distribution of the phenotype parents vs F2 (histogram or box-plot). (B) Table of averages.

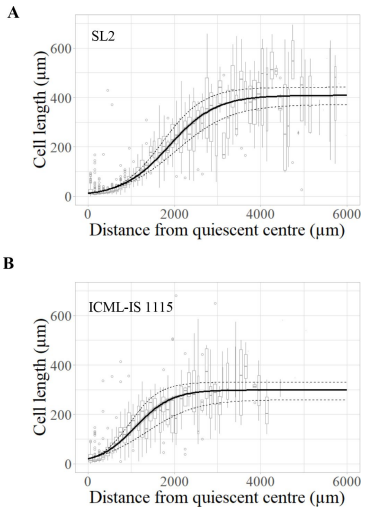

Figure S6.

Cell length profile in the root meristem of (A) SL2 and (B) ICML-IS 11155.

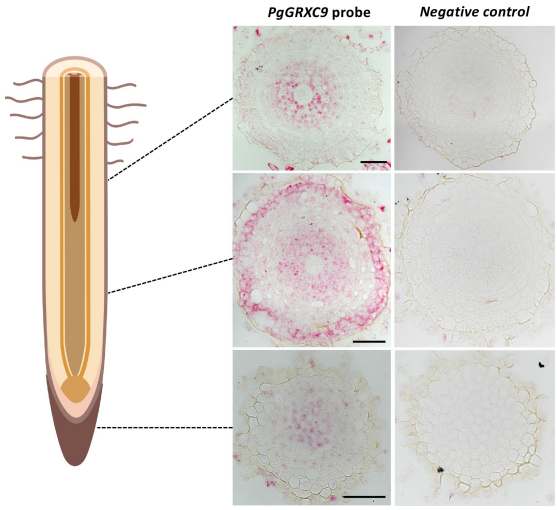

Figure S7.

Expression pattern of *PgGRXC9* in the root tip as revealed by RNAscope.

Transversal sections in the root cap, elongation zone and mature zone of the root. Scalebars: 50 µM. Drawing created with BioRender.com

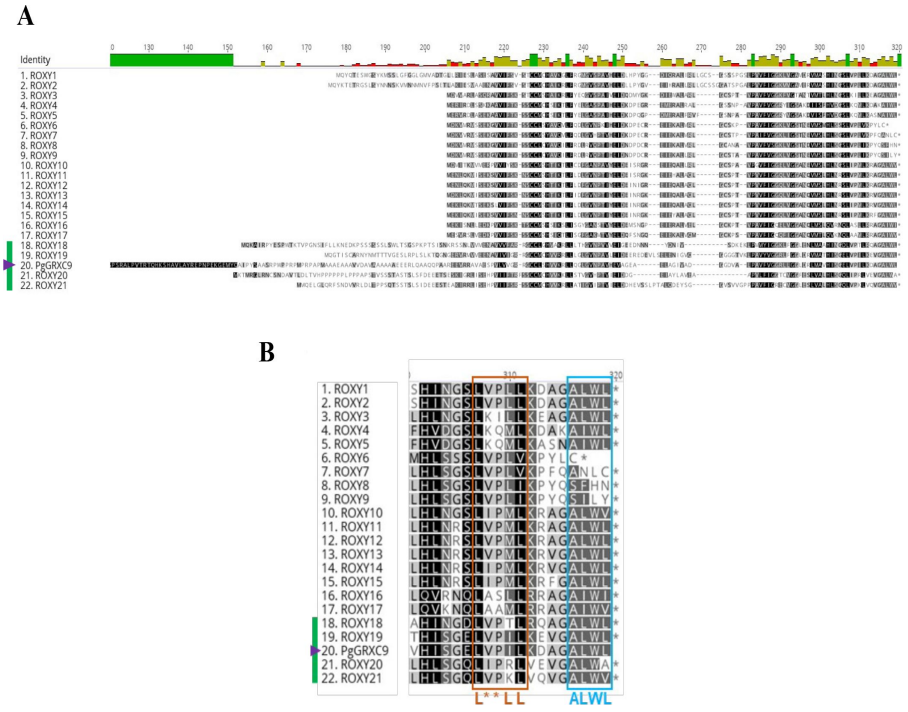

Figure S8.

Protein alignment of PgGRXC9 and Arabidopsis ROXY members.

(A) Whole sequence alignment of PgGRXC9 and the 21 ROXY from *Arabidopsis thaliana*. The first 120 N-terminal amino acids of PgGRXC9 are not represented in this alignment. (B) C-terminus alignment of ROXY proteins. This alignment displays the L**LL (orange) and the ALWL (light blue) C-terminal motifs, important for binding to TGA and TPL/TPR. The green bar and purple triangle mark the ROXY18-21 Arabidopsis subclass and the PgGRXC9, respectively.

Table S1.

Drought-tolerance related traits in selected inbred lines grown in field conditions in 2018 and 2020.

After sowing, seeds were irrigated with 30 mm of water to allow germination and plants grew for 42 days without any further irrigation. Plant height, stay-green and survival were measured at 42 days after sowing while photosynthesis related traits (FvFm: maximum quantum efficiency of photosystem II; PI: performance index of photosynthesis) were measured at 32 days after sowing. Root length was measured 6 days after germination on a paper-based hydroponic system in growth chamber. Numbers indicate mean ± se.

	Line	Height (cm)	Stay-Green (%)	Survival (%)	FvFm	PI	Root length (mm)
2018	1	16.33 ± 2.62	39.37 ± 2.43	28.67 ± 14.76	0.76 ± 0.03	0.82 ± 0.04	61.05 ± 20.12
	69	23.88 ± 7.25	40.97 ± 6.52	10.48 ± 5.50	0.64 ± 0.19	0.99 ± 0.04	75.65 ± 21.39
	127	17.11 ± 2.97	40.80 ± 4.29	37.83 ± 15.58	0.69 ± 0 .00	0.95 ± 0.08	74.53 ± 16.13
	241	21.97 ± 0.90	41.18 ± 3.40	23.35 ± 18.57	0.73 ± 0.03	0.95 ± 0.26	
	249	17.35 ± 4.98	38.36 ± 8.38	28.29 ± 17.29	0.76 ± 0.02	1.25 ± 0.27	66.35 ± 14.60
	263	41.37 ± 5.41	35.61 ± 2.67	58.94 ± 21.17	0.76 ± 0.01	1.07 ± 0.07	107.21 ± 10.89
	337	27.94 ± 5.57	43.37 ± 6.29	47.23 ± 13.94	0.77 ± 0.01	1.33 ± 0.20	149.30 ± 10.04
	343	35.10 ± 6.65	40.40 ± 1.03	22.53 ± 13.75	0.77 ± 0.01	1.16 ± 0.27	79.91 ± 20.59
	344	26.69 ± 5.90	46.21 ± 9.23	31.48 ± 11.94	0.70 ± 0.08	1.32 ± 0.30	167.57 ± 12.92
2020	3	28.67 ± 5.75	60.87 ± 4.66	64.48 ± 9.21	0.74 ± 0.01	2.95 ± 0.55	58.94
	55	31.54 ± 8.64	56.53 ± 7.22	58.07 ± 13.18	0.74 ± 0.02	3.97 ± 0.79	61.21 ± 12.75
	69	19.58 ± 4.14	51.92 ± 7.28	76.11 ± 18.93	0.73 ± 0.01	3.21 ± 0.33	75.65 ± 21.39
	81	24.28 ± 1.37	54.20 ± 9.02	41.40 ± 8.83	0.76 ± 0.01	4.55 ± 1.29	136.53 ± 21.19
	132	28.67 ± 2.23	56.15 ± 2.01	66.93 ± 5.03	0.72 ± 0.02	3.34 ± 0.22	68.70 ± 12.99
	249	19.83 ± 4.09	56.08 ± 6.79	70.43 ± 18.91	0.72 ± 0.03	2.85 ± 1.12	66.35 ± 14.60
	263	24.42 ± 4.31	61.88 ± 4.94	70.83 ± 15.35	0.74 ± 0.01	4.04 ± 0.56	107.21 ± 10.89
	337	30.63 ± 4.54	61.65 ± 2.70	59.53 ± 10.56	0.74 ± 0.01	3.44 ± 0.27	149.30 ± 10.04
	343	30.67 ± 6.38	56.27 ± 4.95	58.75 ± 4.93	0.74 ± 0.01	3.68 ± 0.67	79.91 ± 20.59
	344	27.42 ± 4.06	60.18 ± 4.10	81.51 ± 14.29	0.75 ± 0.01	4.76 ± 0.51	167.57 ± 12.92
p-values	*Line*	*	*0.84*	*0.64*	*0.54*	*0.29*	***
	Year	*0.31*	***	***	*0.86*	***	*0.73*
	Line x Year	*0.27*	*0.88*	*0.28*	*0.34*	*0.28*	*0.98*
lsmeans	69	21.8	46	43.3	0.693	2.19	75.7
	249	18.6	47.2	49.4	0.741	2.05	66.3
	263	33.1	49.3	64.9	0.755	2.58	107.2
	337	29.3	52.5	53.4	0.754	2.36	149.3
	343	32.9	49.1	40.6	0.759	2.52	79.9
	344	27.1	53.2	56.5	0.729	3.04	167.6

Table S2.

GWAS p-values for the significant SNP markers identified through LFMM (ridge) using four other GWAS methods

Chr.	Position (Mbp)	Allele Freq REF	Allele Freq ALT	GWAS p-values[1]				
				ANOVA	EMMA	MLM	LFMM (LEA)	LFMM (ridge)
1	7.848	0.828	0.172	ns	ns	ns	***	***
1	30.561	0.910	0.090	***	***	**	**	***
1	52.188	0.730	0.270	**	**	**	***	***
1	65.933	0.475	0.525	ns	ns	ns	***	***
1	109.737	0.893	0.107	*	*	*	**	***
1	130.348	0.934	0.066	*	*	*	**	***
1	231.244	0.754	0.246	*	*	*	***	***
1	231.246	0.672	0.328	*	*	*	***	***
1	231.265	0.295	0.705	*	ns	*	***	***
1	247.636	0.836	0.164	***	***	**	***	***
1	247.637	0.852	0.148	**	**	**	***	***
1	253.567	0.648	0.352	**	*	*	***	***
2	40.574	0.164	0.836	***	ns	***	***	***
2	60.654	0.926	0.074	**	**	**	*	***
2	85.902	0.656	0.344	***	***	**	***	***
2	92.005	0.689	0.311	*	*	ns	***	***
2	113.747	0.631	0.369	*	*	*	***	***
3	1.657	0.934	0.066	**	*	*	*	***
3	8.847	0.951	0.049	**	**	**	ns	***
3	14.107	0.484	0.516	***	ns	**	***	***
3	14.107	0.459	0.541	**	ns	**	***	***
3	14.124	0.254	0.746	***	ns	**	***	***
3	14.192	0.164	0.836	ns	ns	ns	***	***
3	14.602	0.672	0.328	**	*	*	***	***
3	53.909	0.566	0.434	**	**	*	***	***
3	224.557	0.443	0.557	***	ns	*	***	***
3	225.059	0.762	0.238	*	*	ns	***	***
3	264.082	0.934	0.066	*	*	*	*	***
3	267.439	0.918	0.082	***	***	**	**	***
3	294.825	0.041	0.959	**	ns	**	ns	***
4	4.566	0.230	0.770	**	ns	*	***	***
4	16.258	0.861	0.139	ns	ns	ns	***	***
4	45.631	0.869	0.131	*	**	**	**	***
4	113.503	0.770	0.230	*	**	*	***	***
4	121.206	0.787	0.213	*	**	**	***	***
4	122.223	0.820	0.180	***	***	**	***	***
4	124.508	0.893	0.107	**	***	***	**	***
5	97.383	0.836	0.164	*	*	*	***	***
6	36.876	0.713	0.287	***	**	**	***	***
6	52.098	0.713	0.287	***	***	**	***	***
6	157.606	0.082	0.918	*	ns	ns	**	***
7	10.770	0.787	0.213	ns	*	*	***	***
7	10.819	0.918	0.082	**	**	*	**	***
7	34.533	0.967	0.033	*	*	*	ns	***
7	149.890	0.697	0.303	**	**	*	***	***

[1] Analysis of variance (ANOVA), Efficient Mixed Model Analysis (EMMA), Mixed Linear Model (MLM) and Latent Factor Mixed Model using the algorithm MCMC (LFMM LEA). *** P-value ≤ 0.0001, ** P-value ≤ 0.001, * P-value ≤ 0.01, *ns* not significant

Table S3.

Significant genomic regions identified by Bulk Segregant Analysis (BSA) for primary root length at the 95% confidence interval.

	Chr.	Peak position[1] (Mbp)	Region range[2] (Mbp)	Region length (Mbp)	Number sig SNPs
RL1.1	1	52.57	31.21 – 60.57	29.36	7
RL1.2	1	176.47	165.42 – 195.36	29.94	71
RL1.3	1	215.85	196.38 – 239.10	42.72	185
RL6.1	6	89.99	4.55 – 101.68	97.13	695
RL6.2	6	116.91	108.03 – 125.64	17.61	37
RL6.3	6	201.08	176.52 – 240.48	65.79	290

[1] Position of the most significant SNP in the region range
[2] Limits of the significant region considering the overlapping confidence interval of significant markers in the region

Table S4.

Common GWAS and BSA Marker trait associations for primary root length.

Chr.	Position (Mbp)	Allele Freq REF	Allele Freq ALT	GWAS -$\log_{10}$ (*pvalue*)	BSA sig region (95% CI)
1	52.188	0.730	0.270	4.623	*RL1.1*
1	231.244	0.754	0.246	4.200	*RL1.3*
1	231.246	0.672	0.328	4.531	
1	231.265	0.295	0.705	8.413	
6	36.876	0.713	0.287	4.020	*RL6.1*
6	52.098	0.713	0.287	4.018	

Table S5.

Top ten GO enriched terms in the differentially expressed genes between contrasting lines for root growth. Annotated: number of genes annotated with the corresponding GO term in the pearl millet genome; Significant: number of genes annotated in the differentially expressed genes with the corresponding GO term; Expected: number of corresponding GO term expected in the differentially expressed genes; Rank: rank of p-value in the classic Fisher test; p-value: p-value of the classic Fischer test; Weight01: weight01 in the Fischer test taking into account hierarchical links between GO terms.

GO term	Annotation	Ontology	Annotated	Significant	Expected	Rank	*p*-value	Weight01
GO:0043531	ADP binding	Molecular interaction	357	82	22.24	1	8.10E-26	8.10E-26
GO:0009045	xylose isomerase activity	Enzymatic reactions	5	3	0.31	13	0.0022	0.0022
GO:0005230	extracellular ligand-gated ion channel activity	Transporters	17	4	1.06	26	0.0185	0.0039
GO:0004497	monooxygenase activity	Enzymatic reactions	69	10	4.3	21	0.01	0.0055
GO:0004930	G protein-coupled receptor activity	Signal transduction	7	3	0.44	17	0.007	0.007
GO:0016765	transferase activity, transferring alkyl or aryl groups	Enzymatic reactions	46	8	2.87	16	0.0069	0.0079
GO:0046873	metal ion transmembrane transporter activity	Transporters	91	10	5.67	55	0.0563	0.0094
GO:0030170	pyridoxal phosphate binding	Molecular interaction	112	14	6.98	19	0.0097	0.0097
GO:0042626	ATPase activity, coupled to transmembrane	Transporters	134	14	8.35	46	0.0396	0.0103
GO:0016841	ammonia-lyase activity	Enzymatic reactions	9	3	0.56	23	0.0152	0.0152

Table S6.

Lines selected for field trials. Average root length represent the value observed in paper growth system in the original phenotyping performed for GWAS/

Line	Average Root Growth
ICML-IS 11001	61.05
ICML-IS 11002	59.94
ICML-IS 11047	75.65
ICML-IS 11108	172.18
ICML-IS 11155	66.35
ICML-IS 11165	107.21
SL 2	149.3
SL 4	79.91
SL 5	167.57

References

1. Altschul SF , Gish W , Miller W , Myers EW , Lipman DJ (1990) **Basic local alignment search tool** *J Mol Biol* **215**:403–410
https://doi.org/10.1016/S0022-2836(05)80360-2

2. Anders S , Huber W (2010) **Differential expression analysis for sequence count data** *Genome Biol* **11**
https://doi.org/10.1186/gb-2010-11-10-r106

3. Andrews S. (2010) **FastQC: a quality control tool for high throughput sequence data**

4. Bashandy T , Guilleminot J , Vernoux T , Caparros-Ruiz D , Ljung K , Meyer Y , Reichheld JP (2010) **Interplay between the NADP-linked thioredoxin and glutathione systems in Arabidopsis auxin signaling** *Plant Cell* **22**:376–391
https://doi.org/10.1105/tpc.109.071225

5. Beemster GTS , De Vusser K , De Tavernier E , De Bock K , Inze D (2002) **Variation in Growth Rate between Arabidopsis Ecotypes Is Correlated with Cell Division and A- Type Cyclin-Dependent Kinase Activity** *Plant Physiol* **129**:854–864
https://doi.org/10.1104/pp.002923.854

6. Belin C , Bashandy T , Cela J , Delorme-Hinoux V , Riondet C , Reichheld JP (2015) **A comprehensive study of thiol reduction gene expression under stress conditions in Arabidopsis thaliana** *Plant, Cell Environ* **38**:299–314
https://doi.org/10.1111/pce.12276

7. Burgarella C , Cubry P , Kane NA , Varshney RK , Mariac C , Liu X , Shi C , Thudi M , Couderc M , Xu X , Chitikineni A , Scarcelli N , Barnaud A , Rhoné B , Dupuy C , François O , Berthouly-Salazar C , Vigouroux Y (2018) **A western Sahara centre of domestication inferred from pearl millet genomes** *Nat Ecol Evol* **2**:1377–1380
https://doi.org/10.1038/s41559-018-0643-y

8. Caye K , Jumentier B , Lepeule J , François O (2019) **LFMM 2: Fast and accurate inference of gene-environment associations in genome-wide studies** *Mol Biol Evol* **36**:852–860
https://doi.org/10.1093/molbev/msz008

9. Cantó C de la Fuente , Diouf MN , Ndour PMS , Debieu M , Grondin A , Passot S , Champion A , Barrachina C , Pratlong M , Gantet P , Assigbetsé K , Kane N , Cubry P , Diedhiou AG , Heulin T , Achouak W , Vigouroux Y , Cournac L , Laplaze L. (2022) **Genetic control of rhizosheath formation in pearl millet** *Sci Rep* **12**:9205
https://doi.org/10.1038/s41598-022-13234-w

10. Cantó C de la Fuente , Vigouroux Y. (2022) **Evaluation of nine statistics to identify QTLs in bulk segregant analysis using next generation sequencing approaches** *BMC Genomics* **23**:490
https://doi.org/10.1186/s12864-022-08718-y

11. Debieu M , Kanfany G , Laplaze L (2017) **Pearl Millet Genome: Lessons from a Tough Crop** *Trends Plant Sci* **22**:911–913
https://doi.org/10.1016/j.tplants.2017.09.006

12. Debieu M , Sine B , Passot S , Grondin A , Akata E , Gangashetty P , Vadez V , Gantet P , Fonceka D , Cournac L , Hash CT , Kane N , Vigouroux Y , Laplaze L (2018) **Response to early drought stress and identification of QTLs controlling biomass production under drought in pearl millet** *PLoS One* **13**
https://doi.org/10.1101/373233

13. Herder G Den , Van Isterdael G , Beeckman T , De Smet I. (2010) **The roots of a new green revolution** *Trends Plant Sci* **15**:600–607
https://doi.org/10.1016/j.tplants.2010.08.009

14. Ferreira T , Miura K , Bitdeli C , Eglinger J (2015) **Scripts: Bar 1.1.6** *Zenodo*
https://doi.org/10.5281/ZENODO.28838

15. Flynn JM. , Hubley R , Goubert C , Rosen J , Clark A. . , Feschotte C , Smit A. . (2020) **RepeatModeler2 for automated genomic discovery of transposable element families** *Proc Natl Acad Sci* **117**:9451–9457
https://doi.org/10.1073/pnas.1921046117

16. Frichot E , Schoville SD , Bouchard G , François O (2013) **Testing for associations between loci and environmental gradients using latent factor mixed models** *Mol Biol Evol* **30**:1687–1699
https://doi.org/10.1093/molbev/mst063

17. Grondin A , Affortit P , Tranchant-Dubreuil C , de la F Cantó C , Mariac C , Gantet P , Vadez V , Vigouroux Y (2020) **Aquaporins are main contributors of root hydraulic conductivity in pearl millet [Pennisetum glaucum (L) R. Br.]** *PLoS One* **15**
https://doi.org/10.1101/2020.05.13.094094

18. Hill JT , Demarest BL , Bisgrove BW , Gorsi B , Su YC , Yost HJ (2013) **MMAPPR: Mutation Mapping Analysis Pipeline for Pooled RNA-seq** *Genome Res* **23**:687–697
https://doi.org/10.1101/gr.146936.112

19. Hoagland D , Arnon D (1950) **The water-culture method for growing plants without soil** *Calif Agr Expt Sta Circ* **347**:1–32

20. Holt C , Yandell M (2011) **MAKER2: an annotation pipeline and genome-database management tool for second-generation genome projects** *BMC Bioinformatics* **12**:491
https://doi.org/10.1186/1471-2105-12-491

21. Kang HM , Zaitlen NA , Wade CM , Kirby A , Heckerman D , Daly MJ , Eskin E (2008) **Efficient Control of Population Structure in Model Organism Association** *Mapping* **1723**:1709–1723
https://doi.org/10.1534/genetics.107.080101

22. Kim D , Langmead B , Salzberg SL (2015) **HISAT: a fast spliced aligner with low memory requirements** *Nat Methods* **12**:357–360
https://doi.org/10.1038/NMETH.3317

23. Kurihara D , Mizuta Y , Sato Y , Higashiyama T (2015) **ClearSee: a rapid optical clearing reagent for whole-plant fluorescence imaging** *Development* **142**:4168–79
https://doi.org/10.1242/dev.127613

24. Li H , Durbin R (2009) **Fast and accurate short read alignment with burrows-wheeler transform** *Bioinformatics* **25**:1754–1760
https://doi.org/10.1093/bioinformatics/btp324

25. Love MI , Huber W , Anders S (2014) **Moderated estimation of fold change and dispersion for RNA-seq data with DESeq2** *Genome Biol* **15**
https://doi.org/10.1186/s13059-014-0550-8

26. Lynch JP (2019) **Root phenotypes for improved nutrient capture: an underexploited opportunity for global agriculture** *New Phytol* **223**:548–564
https://doi.org/10.1111/nph.15738

27. Lynch JP (2007) **Roots of the second green revolution** *Aust J Bot* **55**:493–512
https://doi.org/10.1071/BT06118

28. Mabuchi K , Maki H , Itaya T , Suzuki T , Nomoto M , Sakaoka S , Morikami A , Higashiyama T , Tada Y , Busch W , Tsukagoshi H (2018) **MYB30 links ROS signaling, root cell elongation, and plant immune responses** *Proc Natl Acad Sci U S A* **115**
https://doi.org/10.1073/pnas.1804233115

29. Marçais G , Delcher AL , Phillippy AM , Coston R , Salzberg SL , Zimin A (2018) **MUMmer4: A fast and versatile genome alignment system** *PLoS Comput Biol* **14**
https://doi.org/10.1371/journal.pcbi.1005944

30. Mariac C , Luong V , Kapran I , Mamadou A , Sagnard F , Deu M , Chantereau J , Gerard B , Ndjeunga J , Bezançon G , Pham JL , Vigouroux Y (2006) **Diversity of wild and cultivated pearl millet accessions (Pennisetum glaucum [L** *R. Br.) in Niger assessed by microsatellite markers. Theor Appl Genet* **114**:49–58
https://doi.org/10.1007/s00122-006-0409-9

31. McCarthy DJ , Chen Y , Smyth GK (2012) **Differential expression analysis of multifactor RNA-Seq experiments with respect to biological variation** *Nucleic Acids Res* **40**:4288–4297
https://doi.org/10.1093/nar/gks042

32. McKenna A , Hanna M , Banks E , Sivachenko A , Cibulskis K , Kernytsky A , Garimella K , Altshuler D , Gabriel S , Daly M , DePristo MA (2010) **The Genome Analysis Toolkit: A MapReduce framework for analyzing next-generation DNA sequencing data** *Genome Res* **20**:1297–1303
https://doi.org/10.1101/gr.107524.110

33. Meyer Y , Belin C , Delorme-Hinoux Valérie Reichheld , Riondet C Jean-Philippe (2012) **Thioredoxin and Glutaredoxin Systems in Plants: Molecular Mechanisms, Crosstalks, and Functional Significance** *Antioxid Redox Signal* **17**:1124–1160
https://doi.org/10.1089/ars.2011.4327

34. Meyer Y , Buchanan BB , Vignols F , Reichheld J-P (2009) **Thioredoxins and Glutaredoxins: Unifying Elements in Redox Biology** *Annu Rev Genet* **43**:335–367
https://doi.org/10.1146/annurev-genet-102108-134201

35. Morris AK , Silk WK (1992) **Use of a flexible logistic function to describe axial growth of plants** *Bull Math Biol* **54**:1069–1081

36. Mounier T , Navarro-Sanz S , Bureau C , Antoine L , Varoquaux F , Durandet F , Périn C (2020) **A fast, efficient and high-throughput procedure involving laser microdissection and RT droplet digital PCR for tissue-specific expression profiling of rice roots** *BMC Mol Cell Biol* **21**:92
https://doi.org/10.1186/s12860-020-00312-y

37. Mulder N , Apweiler R (2007) **InterPro and InterProScan: tools for protein sequence classification and comparison** *Methods Mol Biol* **396**:59–70

38. Ndoye MS , Burridge J , Bhosale R , Grondin A , Laplaze L (2022) **Root traits for low input agroecosystems in Africa: Lessons from three case studies** *Plant Cell Environ* **45**:637–649
https://doi.org/10.1111/pce.14256

39. Olodo K. , Barnaud A , Kane AK , Mariac C , Faye A , Couderc M , Zekraoui L , Dequincey A , Diouf D , Vigouroux Y , Berthouly-Salazar C (2020) **Abandonment of pearl millet cropping and homogenization of its diversity over a 40 year period in Senegal** *PLoS One* **15**
https://doi.org/10.1371/journal.pone.0239123

40. Omboki RB , Zheng Y , Chen Z , Guan H , Tang W , Huang L , Xie X , Wu W (2018) **Pooled mapping of quantitative trait loci conferring male sterility - conditioned glume split in rice (Oryza sativa)** *Plant Breed* **137**:848–856
https://doi.org/10.1111/pbr.12643

41. Ota R , Ohkubo Y , Yamashita Y , Ogawa-Ohnishi M , Matsubayashi Y (2020) **Shoot-to-root mobile CEPD-like 2 integrates shoot nitrogen status to systemically regulate nitrate uptake in Arabidopsis** *Nat Commun* **11**:1–9
https://doi.org/10.1038/s41467-020-14440-8

42. Pašiaková M , Gajdoš V , Bučová J , Brixová B , Bielik M (2013) **NbClust: An R Package for Determining the Relevant Number of Clusters in a Data Set** *Acta Geol Slovaca* **5**:45–54

43. Passot S , Gnacko F , Moukouanga D , Lucas M , Guyomarc'h S , Ortega BM , Atkinson JA , Belko MN , Bennett MJ , Gantet P , Wells DM , Guédon Y , Vigouroux Y , Verdeil J-L , Muller B , Laplaze L (2016) **Characterization of Pearl Millet Root Architecture and Anatomy Reveals Three Types of Lateral Roots** *Front Plant Sci* **7**:1–11
https://doi.org/10.3389/fpls.2016.00829

44. Passot S , Moreno-Ortega B , Moukouanga D , Balsera C , Guyomarc'h S , Lucas M , Lobet G , Laplaze L , Muller B , Guédon Y (2018) **A New Phenotyping Pipeline Reveals Three Types of Lateral Roots and a Random Branching Pattern in Two Cereals** *Plant Physiol* **177**:896–910
https://doi.org/10.1104/pp.17.01648

45. Patterson K , Walters LA , Cooper AM , Olvera JG , Rosas MA , Rasmusson AG , Escobar MA (2016) **Nitrate-regulated glutaredoxins control arabidopsis primary root growth** *Plant Physiol* **170**:989–999
https://doi.org/10.1104/pp.15.01776

46. Pertea M , Pertea GM , Antonescu CM , Chang T-C , Mendell JT , Salzberg SL (2015) **StringTie enables improved reconstruction of a transcriptome from RNA-seq reads** *Nat Biotechnol* **33**:290–295
https://doi.org/10.1038/nbt.3122

47. Peter R , Eschholz TW , Stamp P , Liedgens M (2009) **Early growth of flint maize landraces under cool conditions** *Crop Sci* **49**:169–178
https://doi.org/10.2135/cropsci2007.10.0538

48. Pound MP , French a P , Atkinson J a. , Wells DM , Bennett MJ , Pridmore T. (2013) **RootNav: Navigating Images of Complex Root Architectures** *Plant Physiol* **162**:1802–1814
https://doi.org/10.1104/pp.113.221531

49. Robinson MD , McCarthy DJ , Smyth GK (2010) **edgeR : a Bioconductor package for differential expression analysis of digital gene expression data** *Bioinformatics* **26**:139–140
https://doi.org/10.1093/bioinformatics/btp616

50. Rohland N , Reich D (2012) **Cost-effective, high-throughput DNA sequencing libraries for multiplexed target capture** *Genome Res* **22**:939–946
https://doi.org/10.1101/gr.128124.111

51. Soltani A , Madah V , Sinclair TR (2013) **SSM-Wheat: a simulation model for wheat development, growth and yield** *Int J Plant Prod* **7**:711–740

52. Soltani A , Sinclair TR (2012) **Modeling physiology of crop development, growth and yield, Modeling Physiology of Crop Development** *Growth and Yield*
https://doi.org/10.1079/9781845939700.0000

53. Sultan B , Gaetani M (2016) **Agriculture in West Africa in the twenty-first century: Climate change and impacts scenarios, and potential for adaptation** *Front Plant Sci* **7**:1262
https://doi.org/10.3389/fpls.2016.01262

54. Tarailo-Graovac M , Chen N (2009) **Using RepeatMasker to identify repetitive elements in genomic sequences** *Curr Protoc Bioinfo*
https://doi.org/10.1002/0471250953.bi0410s25

55. R core Team (2018) **R: A Language and Environment for Statistical Computing**

56. Tranchant-Dubreuil C , Ravel S , Monat C , Sarah G , Diallo A , Helou L A. D , Orjuela-Bounio J , Sabot F (2018) **TOGGLe, a flexible framework for easily building complex workflows and performing robust large-scale NGS analyses** *bioRxiv*
https://doi.org/10.1101/245480

57. Tsukagoshi H (2016) **Control of root growth and development by reactive oxygen species** *Curr Opin Plant Biol* **29**:57–63
https://doi.org/10.1016/j.pbi.2015.10.012

58. Tsukagoshi H , Busch W , Benfey PN (2010) **Transcriptional regulation of ROS controls transition from proliferation to differentiation in the root** *Cell* **143**:606–616
https://doi.org/10.1016/j.cell.2010.10.020

59. Uhrig JF , Huang LJ , Barghahn S , Willmer M , Thurow C , Gatz C (2017) **CC-type glutaredoxins recruit the transcriptional co-repressor TOPLESS to TGA-dependent target promoters in Arabidopsis thaliana** *Biochim Biophys Acta - Gene Regul Mech* **1860**:218–226
https://doi.org/10.1016/j.bbagrm.2016.11.001

60. Ursache R , Andersen TG , Marhavý P , Geldner N (2018) **A protocol for combining fluorescent proteins with histological stains for diverse cell wall components** *Plant J* **93**:399–412
https://doi.org/10.1111/tpj.13784

61. van der Bom FJT , Williams A , Bell MJ. (2020) **Root architecture for improved resource capture: Trade-offs in complex environments** *J Exp Bot* **71**:5752–5763
https://doi.org/10.1093/jxb/eraa324

62. Varshney RK , Shi C , Thudi M , Mariac C , Wallace J , Qi P , Zhang H , Zhao Y , Wang X , Rathore A , Srivastava RK , Chitikineni A , Fan G , Bajaj P , Punnuri S , Gupta SK , Wang H , Jiang Y , Couderc M , Katta MAVSK , Paudel DR , Mungra KD , Chen W , Harris-Shultz KR , Garg V , Desai N , Doddamani D , Kane NA , Conner JA , Ghatak A , Chaturvedi P , Subramaniam S , Yadav OP , Berthouly-Salazar C , Hamidou F , Jianping Wang , Liang X , Clotault J , Upadhyaya HD , Cubry P , Rhoné B , Gueye MC , Sunkar R , Dupuy C , Sparvoli F , Cheng S , Mahala RS , Singh B , Yadav RS , Lyons E , Datta SK , Tom Hash C , Devos KM , Buckler E , Bennetzen JL , Paterson AH , Ozias-Akins P , Grando S , Jun Wang , Mohapatra T , Weckwerth W , Reif JC , Liu X , Vigouroux Y , Xu X (2017) **Pearl millet genome sequence provides a resource to improve agronomic traits in arid environments** *Nat Biotechnol* **35**:969–976
https://doi.org/10.1038/nbt.3943

63. Vernoux T , Wilson RC , Seeley KA , Reichheld J , Muroy S , Brown S , Maughan SC , Cobbett CS , Van Montagu M , Inzé D , May MJ , Sung ZR (2000) **The ROOT MERISTEMLESS1/CADMIUM SENSITIVE2 gene defines a glutathione-dependent pathway involved in initiation and maintenance of cell division during post- embryonic root development** *Curr Opin Plant Biol* **3**:97–109
https://doi.org/10.1016/s1369-5266(00)80035-7

64. Wang L , Jiao W , MacBean N , Rulli MC , Manzoni S , Vico G , D'Odorico P (2022) **Dryland productivity under a changing climate** *Nat Clim Chang* **12**:981–994
https://doi.org/10.1038/s41558-022-01499-y

65. Yu J , Pressoir G , Briggs WH , Vroh Bi I , Yamasaki M J.F. D , McMullen MD , Gaut BS , Nielsen DM , Holland JB , Kresovich S , Buckler ES (2006) **A unified mixed-model method for association mapping that accounts for multiple levels of relatedness** *Nat Genet* **38**:203–208

66. Yuan Y , Bayer PE , Batley J , Edwards D (2017) **Improvements in Genomic Technologies: Application to Crop Genomics** *Trends Biotechnol* **35**:547–558
https://doi.org/10.1016/j.tibtech.2017.02.009

67. Zhang H , Wang X , Pan Q , Li P , Yunjun Liu , Lu X , Zhong W , Li M , Han L , Li J , Wang P , Li D , Yan Liu , Li Q , Yang F , Zhang YM , Wang G , Li L (2019) **QTG-Seq Accelerates QTL Fine Mapping through QTL Partitioning and Whole-Genome Sequencing of Bulked Segregant Samples** *Mol Plant* **12**:426–437
https://doi.org/10.1016/j.molp.2018.12.018

Author information

Carla de la Fuente
DIADE, Université de Montpellier, IRD, CIRAD, Montpellier, France

Alexandre Grondin
DIADE, Université de Montpellier, IRD, CIRAD, Montpellier, France, LMI LAPSE, Dakar, Senegal, CERAAS, ISRA, Thies, Senegal

Bassirou Sine
LMI LAPSE, Dakar, Senegal, CERAAS, ISRA, Thies, Senegal

Marilyne Debieu
DIADE, Université de Montpellier, IRD, CIRAD, Montpellier, France

Christophe Belin
LGDP, Université de Perpignan, Perpignan, France
ORCID iD: 0000-0003-2129-5349

Amir Hajjarpoor
DIADE, Université de Montpellier, IRD, CIRAD, Montpellier, France

Jonathan A. Atkinson
School of Biosciences, University of Nottingham, Sutton Bonington, UK

Sixtine Passot
DIADE, Université de Montpellier, IRD, CIRAD, Montpellier, France

Marine Salson
DIADE, Université de Montpellier, IRD, CIRAD, Montpellier, France

Julie Orjuela
DIADE, Université de Montpellier, IRD, CIRAD, Montpellier, France
ORCID iD: 0000-0001-8387-2266

Christine Tranchant-Dubreuil
DIADE, Université de Montpellier, IRD, CIRAD, Montpellier, France

Jean-Rémy Brossier
DIADE, Université de Montpellier, IRD, CIRAD, Montpellier, France

Maxime Steffen
DIADE, Université de Montpellier, IRD, CIRAD, Montpellier, France

Charlotte Morgado
DIADE, Université de Montpellier, IRD, CIRAD, Montpellier, France

Hang Ngan Dinh
DIADE, Université de Montpellier, IRD, CIRAD, Montpellier, France

Bipin K. Pandey
School of Biosciences, University of Nottingham, Sutton Bonington, UK
ORCID iD: 0000-0002-9614-1347

Julie Darmau
DIADE, Université de Montpellier, IRD, CIRAD, Montpellier, France

Antony Champion
DIADE, Université de Montpellier, IRD, CIRAD, Montpellier, France
ORCID iD: 0000-0002-3731-1510

Anne- Sophie Petitot
DIADE, Université de Montpellier, IRD, CIRAD, Montpellier, France

Celia Barrachina
Montpellier GenomiX, Montpellier, France

Marine Pratlong
Montpellier GenomiX, Montpellier, France

Thibault Mounier
Be More Specific, Montpellier, France

Pascal Gantet
DIADE, Université de Montpellier, IRD, CIRAD, Montpellier, France
ORCID iD: 0000-0003-1314-0187

Prakash Gangashetty
ICRISAT, Hyderabad, India

Yann Guédon
AGAPi, Université de Montpellier, CIRAD, INRAE, SupAgroM, Montpellier, France

Vincent Vadez
DIADE, Université de Montpellier, IRD, CIRAD, Montpellier, France, LMI LAPSE, Dakar, Senegal, CERAAS, ISRA, Thies, Senegal
ORCID iD: 0000-0003-2014-0281

Jean-Philippe Reichheld
LGDP, CNRS, Perpignan, France

Malcolm J. Bennett
School of Biosciences, University of Nottingham, Sutton Bonington, UK

Ndjido Kane
LMI LAPSE, Dakar, Senegal, CERAAS, ISRA, Thies, Senegal
ORCID iD: 0000-0002-1879-019X

Soazig Guyomarc'h
DIADE, Université de Montpellier, IRD, CIRAD, Montpellier, France

Darren M. Wells
School of Biosciences, University of Nottingham, Sutton Bonington, UK
ORCID iD: 0000-0002-4246-4909

Yves Vigouroux
DIADE, Université de Montpellier, IRD, CIRAD, Montpellier, France

Laurent Laplaze
DIADE, Université de Montpellier, IRD, CIRAD, Montpellier, France, LMI LAPSE, Dakar, Senegal
For correspondence: laurent.laplaze@ird.fr
ORCID iD: 0000-0002-6568-6504

Editors

Reviewing Editor
Magnus Nordborg
Gregor Mendel Institute, Austria

Senior Editor
Jürgen Kleine-Vehn
University of Freiburg, Germany

Reviewer #1 (Public Review):

The authors use a combination of crop modeling and field experiments to argue that drought during seedling establishment likely severely impacts the yield of pearl millet, an important but understudied cereal crop, and that rapid seedling root elongation could play a major role in mitigating this. They further argue that this trait has a strong genetic basis and that major polymorphisms in candidate genes can be identified using standard methods from modern genetics and genomics. Finally, they use homology with the model plant

Arabidopsis thaliana to argue that the function of one putatively causal gene is to regulate root cell elongation.

The major strength of this paper is that it convincingly demonstrates how modern methods from plant breeding and model organisms can be combined to address questions of great practical importance in important but poorly understood crops. The notion that it is possible to connect single-locus polymorphism and cellular biology to drought tolerance and crop yield in pearl millet is not a trivial one.

The weakness is obvious: while the argument made is convincing, it must be recognized that the strength of the evidence is by no means of the level expected in a model organism. Conclusions could easily be wrong, and there is no direct evidence that regulatory variation in PgGRXC9 leads to higher crop yield via cell elongation and seedling drought tolerance. However, generating such evidence in a poorly studied crop would be a monumental undertaking, and should probably not be the priority of people working on pearl millet!

The utility of this work is that it suggests that it is practicable to gain valuable insight into crop adaptation by clever use of modern methods from a variety of sources.

Reviewer #2 (Public Review):

Carla de la Fuente et al., utilize a diversity of approaches to understand which plant traits contribute to the stress resilience of pearl millet in the Sahelian desert environment. By comparing data resulting from crop modeling of pearl millet growth and meteorological data from a span of 20 years, the authors clearly determined that early season drought resilience is contributed by accelerated growth of the seedling primary root, which confirms a hypothesis generated in a previous study, Passot et al., 2016. To determine the genetic basis for this trait, they performed a combination of GWAS, QTL analysis, and RNA sequencing and identified a previously unannotated coding sequence of a glutaredoxin C9-like protein, PgGRXC9, as the strongest candidate. Phenotypic analysis using a mutant of the closest Arabidopsis homolog AtROXY19 suggests the broad conservation of this pathway. Comparisons between the transcript of PgGRXC9 by in situ hybridization (this work) and AtROXY19 pattern expression (Belin et al., 2014) support the hypothesis that this pathway acts in the elongation zone of the root. Additional analysis of cell production and elongation rates in root apex in both pearl millet and A. thaliana suggests that PgGRXC9 specifically regulates primary root through the promotion of cell elongation. While several studies have established the connection between redox status of cells and root growth, the current study represents an important contribution to the field because of the agricultural importance of the plant studied, and the connection made between this developmental trait and stress resilience in a specific and stressful environmental context of the Sahelian desert.

While the study presents a compelling narrative that is based on a diverse range of approaches, some aspects require further refinement to be fully convincing.

First, while it is appreciated that working with pearl millet presents certain technical challenges regarding genetic characterization, and the authors have done outstanding work by combing the power of GWAS and QTL mapping to reproducibly identify genetic loci associated with root growth, the related work in Arabidopsis is not fully substantiated. In particular, only one mutant allele was utilized to test the function of this gene in root growth. The lack of a second characterized allele or evidence of genetic complementation makes it difficult to definitively contribute the root developmental defects to the characterized mutation in ROXY19.

The role of redox status in contributing to root growth differences between accessions was not directly tested here. The manuscript is not able to mechanistically link the molecular function of ROXY19 to the change in root growth rate, however, this limitation of the study was not clearly described in the text.

The authors state the use of cell elongation rate (Morris and Silk, 1992) as a parameter to estimate the difference in root growth between contrasted pearl millet lines and *A. thaliana* roxy19 mutant versus wild type; however, there are inconsistencies in what data are presented. First, in Figure 2E, regarding the comparison between different genotypes of pearl millet lines, they use the parameter of maximum cell length but when authors compare cell elongation between *A. thaliana* genotypes, in Figure 4D, they use the elongation rate parameter. Second, while the cell elongation rate is based exclusively on the cell length data of the "elongation only" zone (Morris and Silk, 1992), the authors profile the cell length in the whole root apex, from the quiescent center to the beginning of the differentiation zone and it is not clear how they discriminate between each developmental zone and what data was used to estimate elongation rate.